Departement für Chemie

Universität Freiburg (Schweiz)

Synthesis of novel alkyl- and perfluoroalkyl-substituted polycondensed aromatic hydrocarbons for molecular electronics

INAUGURAL-DISSERTATION

zur Erlangung der Würde eines *Doctor rerum naturalium* der Mathematisch-Naturwissenschaftlichen Fakultät der Universität Freiburg (Schweiz)

vorgelegt von

Mauro K. Schindler

aus

Röthenbach im Emmental (BE)

Dissertation Nr. 1670

Uniprint

2010

Von der Mathematisch-Naturwissenschaftlichen Fakultät der Universität Freiburg (Schweiz) angenommen, auf Antrag von:

Prof. Dr. Christian Bochet, Präsident der Jury

Prof. Dr. Titus A. Jenny, Dissertationsleiter

Prof. Dr. Peter Belser, interner Gutachter

Prof. Dr. Bernd Giese (Universität Basel), externer Gutachter

Fribourg, 23.06.2010

Dissertationsleiter und Dekan

Prof. Dr. Titus A. Jenny

Vizedekan

Prof. Dr. Rolf Ingold

Für Roger Lebet (1923 – 1984)

There are those that look at things the way they are, and ask "why"?
I dream of things that never were, and ask "why not"?

Viele sehen die Welt, so wie sie ist und fragen „warum"?
Ich träume von einer Welt, die noch nie da war und frage „warum nicht"?

Robert F. Kennedy (1925-1968) /
George Bernard Shaw (1856-1950)

Acknowledgements

This work has been realized under the supervision of Prof. Dr. Titus A. Jenny in the period of August 2006 to May 2010 at the Department of Chemistry, University of Fribourg, Switzerland.

I would like to express my profound gratitude to Prof. Jenny for accepting me in his group and leading me through the obstacles of my thesis. His guidance as well as the great autonomy he has given me have been a great motivation.

I also would like to gratefully thank my two experts, namely Prof. Dr. Bernd Giese (Uni Basel) and Prof. Dr. Peter Belser (UNIFR) for their valuable feedbacks and comments.

Prof. Christian Bochet is acknowledged as president of the chemistry department and of the Jury. I would like to thank PD Dr. Norbert Engel for accepting me as a teaching assistant for the second year students. Thanks go also to Prof. Jenny who gave me the opportunity to teach second year students in instrumental analytics. He also invited me into the Analytics – Group of the chemistry department which gave me a great and valuable insight in analytical methods. Special thanks go to Helsinn Advanced Synthesis, who provided me with very challenging projects which gave me an insight into the private sector.

My appreciation goes also to persons exterior to the University of Fribourg:
Prof. Dr. Stefan Grimme and Dr. Jens Anthony (University of Münster, Germany) for the theoretical calculations of the dimers.

Many thanks go to the analytical service, namely Felix Fehr (NMR spectra), Fredy Nydegger (mass spectra), Inge Müller (general support) and Michel Piccand (IT, posters).

All the former and present members of the Jenny – Group, especially Dr. Olivier Aebischer, Dr. Bassam Alameddine, Dr. Daniela Bossi, Nicolas Fragnière, Dr. Deborah Gusmeroli, Sofia Martín Caba, Dr. Roger Mafua and Patrick Tondo are thanked for their friendship and the great time we had.

Very special thanks go to Anne Schuwey and the whole central lab, including Emmanuel and the apprentices who provided me with precious precursors in big quantity and great quality.

All the collaborators of the central services and administration, namely Verena Schwalm, Emerith Brügger (secretaries), Olivier Graber (engineer), Xavier Hanselmann, Lucienne Rouiller, Noëlle Chassot, Hubert Favre and Nicolas Hoyler.

All the other collaborators of the Chemistry Department are thanked, namely Prof. Katharina Fromm, Prof. Michael Allan, Prof. Thomas Bally, Prof. Claude Daul, Prof. Alke Fink, Prof. Werner Hug and all the postdocs and assistants.

I'd like to thank Priscilla Brunetto, Aurélien Crochet, Laurent Mirolo and Dr. Olivier May for their friendship all over these years.

I also want to express my gratitude to my closest friends Charles, Marc and Antoine from Luxemburg as well as Alexandra and Desiree for their deep friendship and support.

The most special thanks go to my wife Noémie, who supported me morally all these years during euphoric and less euphoric times and sharing the passion of music. I also would like to thank my parents Susanne and Kurt for the moral and financial support during the many years in school and university. Thank you for having given me the opportunity to choose the career I wanted.
A big thank goes to the Paroz-family who accepted me in their midst.
Thanks also to my grand parents Frieda and Albrecht Schindler, Olga and especially my late grandfather Roger Lebet, to whom this thesis is dedicated. His values and his words have given me strength all over my life.

The thesis was financially supported by the Swiss National Science Foundation and the Canton of Fribourg.

Table of Contents

List of abbreviations

AIBN	2,2’-azobis(2-methylpropionitrile)
Alq	aluminum quinoxalate
BBTO	benzo[*o*]bistriphenyleno-ovalene
BTACl	benzyltriethylammonium chloride
BTF	α,α,α-benzotrifluoride
CIE	commission internationale de l’eclairage
Cp	cyclopentadienone
CRT	cathode ray tube
Cryo-SEM	cryogenic-scanning electron microscope
CVD	chemical vapor deposition
dba	dibenzylideneacetone
DBN	1,5-diazabicyclo[4.3.0]non-5-ene
DBPH	dibenzo-phenanthro-heptaphenes
DBPO	dibenzoylperoxide
DCM	dichloromethane
DCTB	(*E*)-2-(3-(4-(tert-butyl)phenyl)-2-methylallylidene)malononitrile
DDQ	2,3-dichloro-5,6-dicyano-1,4-benzochinone
DMF	N,N-dimethylformamide
DMSO	dimethylsulfoxide
dppf	1,1’-bis(diphenylphosphine)ferrocene
EI	electron impact
EML	emissive layer
ESI	electron spray ionization
ETL	electron transport layer
FAB	fast atomic bombardment
HBC	hexa-*peri*-hexabenzocoronene
HFB	hexafluorobenzene
HOMO	highest occupied molecular orbital
HOPG	highly ordered pyrolytic graphite
HTL	hole transport layer
IR	infrared
ITO	indium tin oxide

LASER	Light Amplification by Stimulated Emission of Radiation
LCD	liquid crystal display
LUMO	lowest unoccupied molecular orbital
LWC	low work function cathode
LWE	low work function electrode
MALDI-ICR	matrix assisted laser desorption ionization – ion cyclotron resonance
MALDI-TOF	matrix assisted laser desorption ionization – time of flight
NBS	N-bromosuccinimide
NMR	nuclear magnetic resonance
OFET	organic field effect transistor
OLED	organic light emitting diode
PAH	polycondensed aromatic hydrocarbon
PFO	poly(9,9-dioctylfluorene)
PVD	physical vapor deposition
RFID	radio frequency identification
$Rf_{n,m}$	abbreviation for linear semi-perfluorinated chains: n indicating the number of alkyl carbons, m indicating the number of perfluorinated carbons
RT	room temperature
SEM	scanning electron microscopy
TCB	1,2,4-trichlorobenzene
TCNQ	7,7,8,8-tetracyanoquinodimethane
TCO	transparent conducting oxide
TEA	triethylamine
TFA	trifluoroacetic acid
THF	tetrahydrofurane
TLC	thin layer chromatography
TMS	tetramethylsilane / trimethylsilane
TMSA	trimethylsilylacetylene
Tol	tolane / toluene
UV	ultraviolet
VIS	visible

Summary

The demand for electronic devices has exploded in the last few years. They are all around us and we use them everyday; TV, mobile phones, computers, etc. Most people could not imagine living without them. The presence of these devices has increased the consumption of electrical power and other resources such as silicon and petrol derivatives.

This increase has itself created a demand for electronic devices that are environmentally friendly and less power consuming. In the last decade, research has focused on this goal and scientists have come up with a lot of new concepts and ideas.

This is where this thesis takes up. We would like to synthesize new compounds that can be used in flat panel displays or microchips. The electronic devices containing our molecules should consume less power and be environmentally friendly as they are made of organic materials.

In this thesis we will focus on the synthesis of new polycondensed aromatic hydrocarbons (PAH) which bear alkyl- and perfluoroalkyl sidechains. The PAH we will try to synthesize have the shape of a halfmoon and a triangle. The sidechains are necessary to allow the processability of our compounds, which should be deposited on surfaces using different methods such as physical vapor deposition (PVD), spin coating or printing.

We will discuss the synthesis of a new class of PAH, the half-moon shaped tribenzopentaphene (TBP) derivatives substituted by octyl sidechains. We also designed a synthesis for the elongated version of the TBP, the so-called dibenzo-phenanthro-heptaphenes (DBPH) as well as for the triangular shaped benzo-bistriphenyleno-ovalene (BBTO). These aromatic cores will be substituted by alkyl or perfluoroalkyl-sidechains which consist of an important challenge in this thesis.

The synthesis has been designed in such a way that the part bearing the perfluorinated sidechain can be used for building both the BBTO and the DBPH derivatives.

Zusammenfassung

Die Nachfrage nach elektronischen Geräten, wie z.B. Fernseher, Computer oder Mobiltelefone ist in den letzten Jahren extrem gestiegen. Diese Geräte sind überall vorhanden und können aus dem Alltag fast nicht mehr herausgedacht werden. Die vermehre Benutzung dieser Geräte führt nach und nach zu einer immer grösseren Verbrauch von Strom, fossilen Brennstoffen oder anderen Ressourcen.

Dieser erhöhte Verbrauch führt selbst zu einer Nachfrage an Strom sparenden und umweltfreundlichen Geräten. Während den letzten Jahrzehnten hat sich die Forschung im Elektroniksektor auf diese Schwerpunkte konzentriert; viele Konzepte und neue Materialien sind entstanden.

Diese Dissertation setzt an diesen Punkten an. Wir möchten neue Moleküle synthetisieren, welche in Flachbildschirmen oder Mikrochips verwenden werden können um sie damit Strom sparender oder effizienter zu machen.

In dieser Dissertation werden wir polycyclische aromatische Kohlenwasserstoffe (PAK) synthetisieren, welche alkyl- oder perfluoroalkyl-Ketten tragen. Die Seitenketten dienen dazu, die unlöslichen PAK-Kerne in organischen Lösungsmitteln zu lösen. Dies erlaubt, sie mit verschiedenen Verfahren, wie z.B. durch physikalische Gasphasenabscheidung (engl.: Physical Vapor Deposition, PVD), Rotationsbeschichtung (engl.: spin-coating) oder Drucken (engl.: printing) auf Oberflächen aufzutragen.

Die PAK, welche wir synthetisieren wollen, sind tribenzo-pentaphen (TBP) und dibenzo-phenanthro-heptaphene (DBPH) welche grob gesehen die Form eines Halbmondes haben. Ein dritter PAK, welchen wir in dieser Dissertation behandeln ist das dreieckige benzo-bistriphenyleno-ovalen (BBTO). Die drei Derivate werden mit alkyl- und perfluoroalkyl-Ketten ausgestattet.

Die Synthese wurde so gestaltet, dass die perfluorierten Seitenketten für beide DBPH und BBTO Derivate verwendet werden können.

I. INTRODUCTION

1.1 General considerations

During the last two decades, computers and other electronic devices have taken an important part in our life. The fabrication processes of these devices become more and more complicated and the technology is reaching the limits of the physical possibilities.
Indeed, modern circuits for example are made using a technique called lithography which uses light to etch the circuits into silicon wafers. The newest processors contain 731 millions transistors on a surface of 263 mm^2 [1].
The evolution of the calculation power of computer chips follows Moore's Law [2] which states that the number of transistors on a wafer, or one could say the calculation power doubles every 20 months.
To achieve such a high density, the processors are fabricated using 45 nm technology, which correspond to the average half-pitch of a memory cell. Considering that visible light has a wavelength of 400 – 700 nm, we can see that the electronic parts are much smaller than the wavelength of light. The processors are fabricated using "deep" UV light of 193 nm or 248 nm.

In the future computer chips will become even smaller, hence also the wavelength of the "etching" light will have to be shorter and soon hit physical limitations.
It is therefore necessary to introduce new concepts for fabricating such electronic parts. One distinguishes between "top-down" and "bottom-up" approaches.
The "top-down" approach breaks down bigger architectures into small blocks. Macroscopic objects are treated with macroscopic tools to form smaller and smaller objects. An example of this approach is lithography as discussed above.
The "bottom-up" approach assembles small building blocks, such as molecules, to build bigger architectures. In chemistry we apply this principle by designing molecules that will assemble in solution to form objects such as layers or rods. This is where the concept of "molecular self assembly" comes in place. Certain types of molecules have the tendency to aggregate together.

A possibility is to design molecules in such a way that they will stack one on top of another in solution, in a solid state or upon deposition on a surface by chemical or physical vapor deposition (CVD / PVD), hence applying the "bottom-up" approach.

In a near future such molecules could potentially replace the existing electronic parts of a computer or make better computer displays, everywhere we can use the self-assembling properties to form molecular stacks or rods. Possible applications of molecular assembling are organic field effect transistors (OFET) or organic light emitting diodes (OLED).

1.2 Organic Field Effect Transistors (OFET)

1.2.1 Principles and Structure

Semiconducting materials based on organic materials have been much investigated in the last 50 years [3], [4]. Compared to the inorganic semiconductors such as silica (Si) or germanium (Ge), the solid state structure is based on dipole / dipole and van der Waals interactions, the so-called weak interactions, between the different molecules that form the substrate.
Si and Ge have a bulk band structure. In molecules, the band structure is created by their orientation. To apply as candidates for organic electronics, these molecules must carry charges, which means that they have to be able to be oxidized or reduced without damaging the molecule itself.
The concept of organic field effect transistor has been introduced by Tsumura, Koezuka and Ando in 1986 [5].
Until now, many classes of semiconductors have been discovered and synthesized. Organic molecules made of polyaromatic hydrocarbons are capable of transporting charges and can replace classical inorganic semiconductors as we know them today.

The currently used metal oxide semiconductor field effect transistors (MOSFET) based on inorganic materials are the crucial and substantial building blocks in the electronics industry [6]. These devices are highly efficient and reliable. For the moment the OFET are not able to compete with the modern Si/GaAs technologies but could be used in niche applications such as low performance radio frequency [7], sensors [8], [9], light emission [10] as well as on integrated optoelectronic devices such as pixel drives and switching elements in displays [11], [12].

The advantages of these organic systems are clear: they can be fabricated using vapor- or solution – phase depositions and can be printed on flexible plastic substrates [13], [14], [15] or structurally tailored [16], [17], [18].
All these trends are pushed forward by the demand of large area, flexible and cheap devices which can be processed at much lower temperatures than standard Si – chips.

OFET consist principally of three electrodes called the source- (S), drain- (D) and gate- (G) electrode. Besides this they are made of an insulator and a semiconductor and the whole is deposited on a substrate.

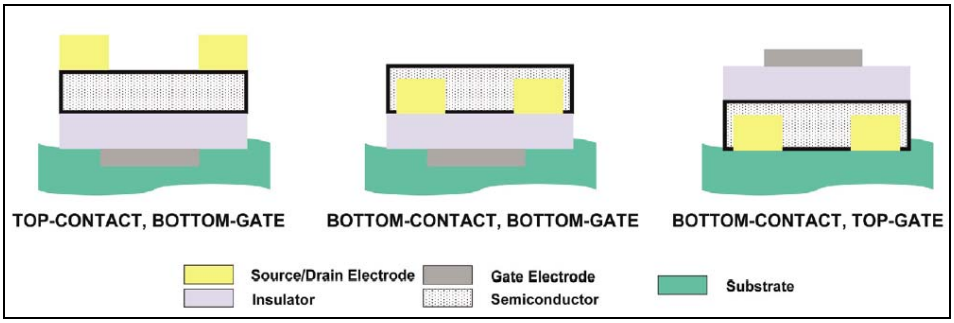

Fig. 1: The most common setups for OFET devices, top-contact / bottom-gate (left), bottom-contact / bottom-gate (middle) and bottom-contact / top-gate (right) [19]

We differentiate three kinds of OFET constructions. The most common setups consist of a film of organic semiconductor deposited on the top of a dielectric with an underlying gate electrode.

The charge injecting source / drain electrodes which provide the contact are either on top of the organic film (top contact) or on the surface of the FET substrate deposited before the semiconducting film (bottom contact).

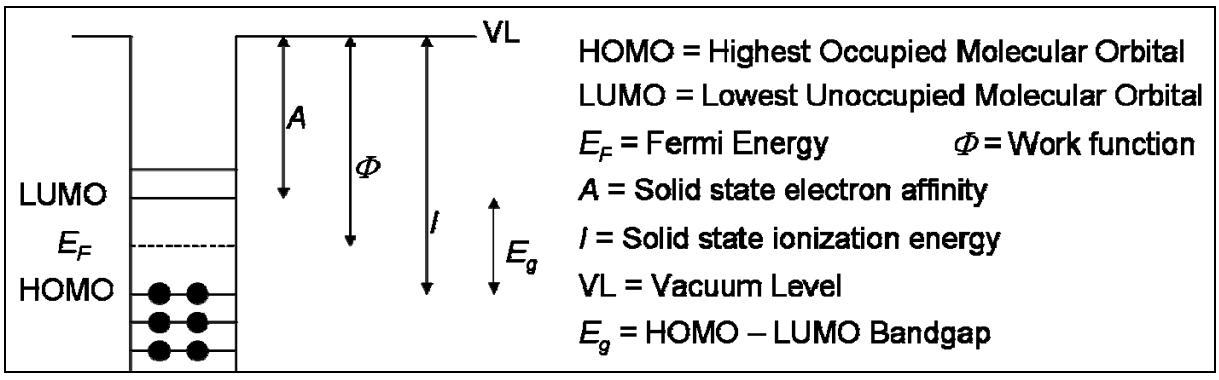

Fig. 2: Electronic structure of an organic solid represented with potential wells and definitions of the most common terms [20]

The minimum current between the S and D electrodes is measured when no potential is applied between the S and G electrode. This is called the "*off-state*". When a voltage is applied to the gate, electrons (n-channel, positive voltage) or holes (p-channel, negative voltage) can be induced at the surface between the semiconductor and the dielectric and the S-D current increases to what is called the "*on-state*" (see next figure).

The application of a positive gate voltage produces a large electric field at the interface of the organic semiconductor and the insulator. This electric field causes the HOMO (highest occupied molecular orbital) and LUMO (lowest unoccupied molecular orbital) lower in energy (shift down) with respect to the Fermi – Levels of the metal electrodes.

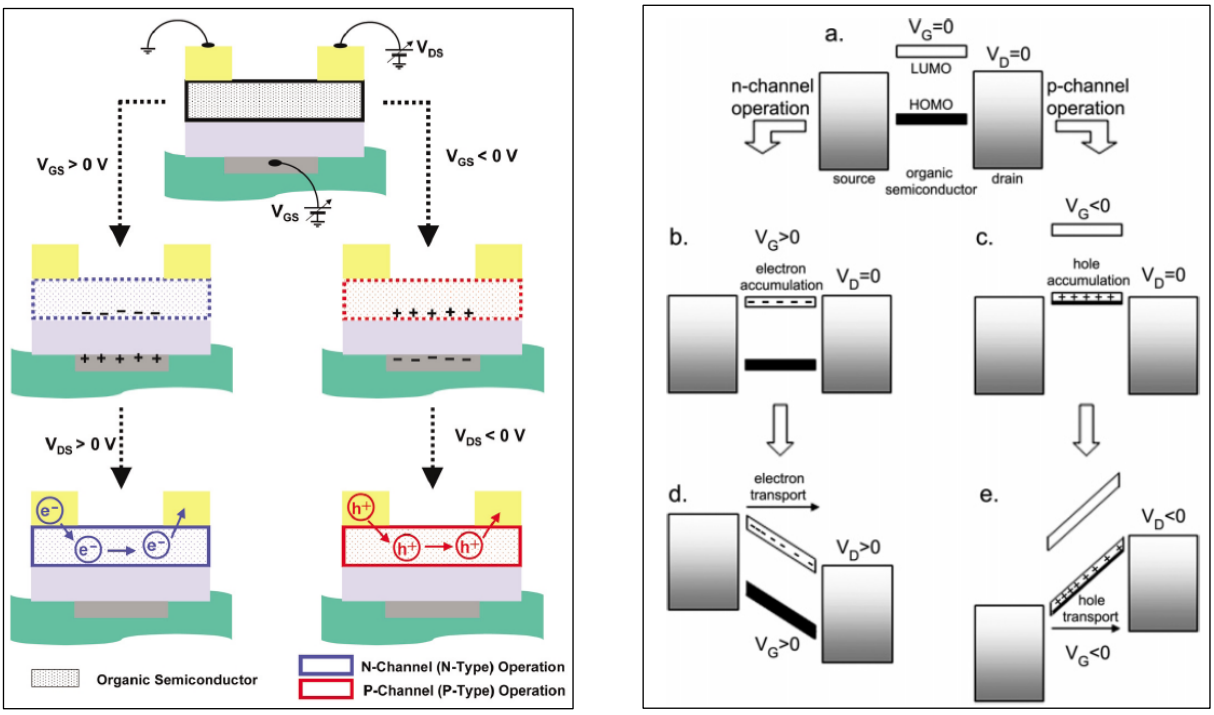

Fig. 3: Scheme of the two thin layer transistor operations (left) [19], idealized energy level diagrams of an OFET (right) [21]

There are two basic relationships which describe the OFET drain currents [19]:

$$(I_{SD})_{lin} = \left(\frac{W}{L}\right)\mu C_i\left(V_{SG} - V_T - \frac{V_{SD}}{2}\right)V_{SD} \qquad (1)$$

$$(I_{SD})_{sat} = \left(\frac{W}{2L}\right)\mu C_i (V_{SG} - V_T)^2 \qquad (2)$$

where μ is the field-effect carrier mobility of the semiconductor, W the channel with, L the channel length, C_i the capacitance per unit area of the insulator layer, V_T the threshold voltage, V_{SD} the source – drain voltage, V_{SG} the source-gate voltage.

If one increases V_{SD} and V_{SG}, a linear current regime can be observed at low drain voltages ($V_{SD} < V_{SG}$) which is followed by a saturation regime when the drain voltage exceeds the gate voltage.

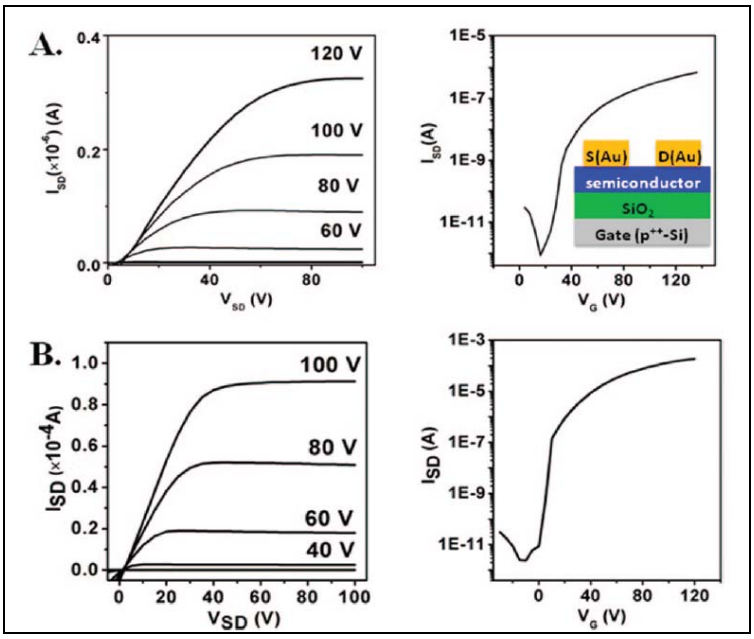

Fig. 4: Typical OFET I/V output (left) and transfer (right, at V_{SD} = 100 V) diagrams [22]

It has to be noted that the OFETs mostly work in accumulation mode ($V_{SG} < 0$) where an increase of V_{SG} enhances the channel conductivity in contrast to normal silicon transistors. There are two other modes called the inversion mode and the depletion mode where $V_{SG} > 0$.

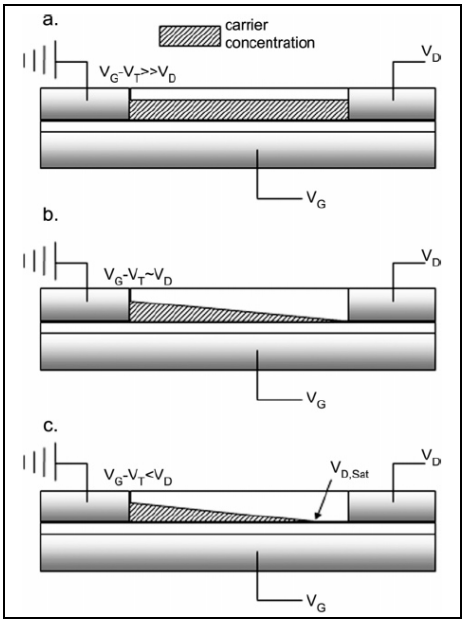

Fig. 5: (a) Carrier concentration profile of OFET in the linear regime, (b) pinch-off occurs when $V_D \approx V_G - V_T$, (c) Carrier concentration profile of OFET in the saturation regime [21]

In order to achieve an acceptable performance of the OFET, the organic semiconductors must satisfy general criteria regarding both the injection and current-carrying characteristics in particular:

- The HOMO/LUMO energies of the single molecules must be at levels where the holes or electrons can be induced at accessible applied electric fields
- The semiconducting solid has to be extremely pure since impurities act as charge carrier traps [23]
- The molecules should be preferentially oriented with the long axes parallel to the OFET substrate since the most efficient charge transport occurs along the direction of the intramolecular π-π stacking
- The thickness of the semiconducting layer influences the contact resistance between electrode and substrate. Increasing the thickness of the layer reduces both electron and hole current [24]. On the other side, by reducing the thickness too much (below 20 nm), the contact resistance increases exponentially [25]. Sirringhaus and coworkers have argued that the optimal thickness of the semiconductor would be around 80 nm [25].

As already mentioned above, the organic material is said to be *p-channel* type as holes are the major charge carriers upon the application of a negative source gate voltage V_{SG}. On the contrary if a positive source - drain current is observed under application of a positive V_{SG} and V_{SD} the semiconductor is called *n-channel*, since the electrons are mobile.

In some cases, the OFET can be operated by both V_{SG} and V_{SD} polarities and the semiconductor is said to be *ambipolar* [26], [27].

1.2.2 P-channel organic semiconductors

We will now focus on p-channel organic semiconductors. The most prominent candidate is pentacene (P5) [28], [29], [30], although the first experiments were done on anthracene and tetracene [31].

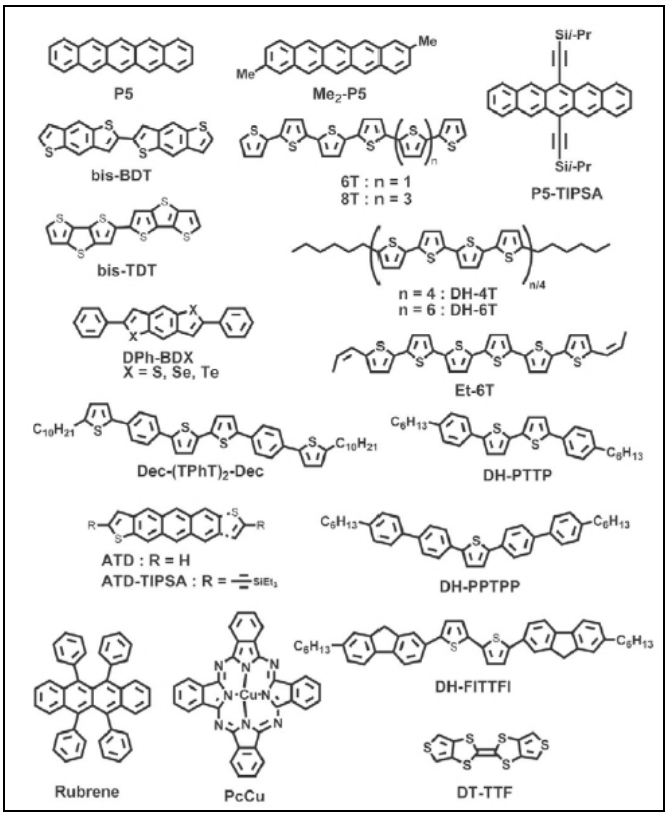

Fig. 6: Some prominent p-channel organic semiconductor molecules

In the past years many papers focused also on rubrene - based transistors [32], [33], [34], [35]. The efforts on acene semiconductors have been reviewed by Würthner and Schmidt [36].

One of the highest charge carrier mobility known today is the one of pentacene, which is commercially available and has a charge carrier mobility μ of 1.5 cm^2/Vs and an on/off current ratio (I_{on}/I_{off}) of > 10^8 as reported by Lin et al. [37]. Using polymer dielectrics one can obtain a μ of 3.0 cm^2/Vs [38]. Highly pure pentacene single crystals prepared from the vapor phase in a stream of nitrogen or hydrogen [39].

The major drawback of pentacene is that it is quite insoluble even in organic solvents, as well as unstable to oxygen and light. Studies have been made concerning its stability in a standard atmosphere [40].
Addition of methyl-groups (Me_2-P5 in **Fig. 6**) [41] can help solubilizing the pentacene core but influences strongly the charge carrier mobility (μ = 0.3 cm^2/Vs). Addition of TIPSA-groups solubilizes the core, reduces the air-sensitivity and keeps the mobility at 1.0 cm^2/Vs [42], [43].

When optimizing the performance of OFET (namely the charge transport capabilities) one has also to tune the quality of the interface between the insulator and the semiconductor [44], [45], [46]. The interface can be functionalized [47], [48], [49], [50], the substrate deposition-rate and -temperature changed [51] etc.

One has also to mention the case of rubrene [32] which exhibits a charge carrier mobility of up to 20 cm^2/Vs, which is almost a ten-fold increase as compared to pentacene but the drawback is that the on/off ratio of 20 is very low as compared to the performance of pentacene (on/off ratio 10^8).

Another class of p-channel semiconducting molecules are the electron-rich thiophene-based derivatives. OFETs using these derivatives have first been intensively studied by Garnier [52]. The problem of thiophenes or oligothiophenes is that they oxidize rapidly on contact with atmospheric oxygen because of their high HOMO energy levels. They can be lowered by replacing some of the thiophenes by phenyl rings [53].

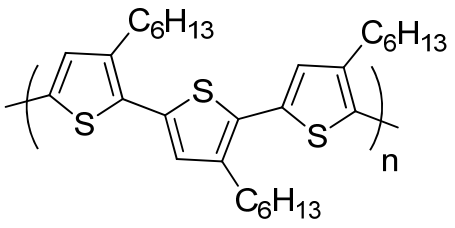

P3HT

Fig. 7: Poly(3-hexylthiophene) **P3HT**

To be complete, it is necessary to mention the polymeric n-channel semiconductors. Poly(3-substituted thiophene)s are one of the most investigated polymer family for molecular electronic applications [54] due to their good solubility and processability.

The P3HT derivative was the first solution-processed polymer for OFET [55], it can also be deposited using the Langmuir - Blodgett (LB) technique [56].
Looking at the dielectric material used for OFET, mostly SiO_2 [57], [58] is used but also Al_2O_3 [59], [60], [61], Ta_2O_5 [62], TiO_2 [63] or other high-*k* metal oxides [64] (*k* being the dielectric constant).
The substrate on which the OFET is built can be flexible such as PET or more rigid like in the case of indium-tin-oxide ITO [65].

The molecules discussed in this chapter form mostly amorphous materials. In order to achieve high charge carrier mobilities, the charges have to be transported from one molecule to another efficiently. The orbital overlap of the single molecules influences the mobility; the better the overlap, the better the charge carrier mobility.
Semiconducting substrates with high order have the best charge carrier mobility. On the lower end of order we have totally amorphous materials. Polymers and liquid crystalline materials possess areas of high order and areas that are less ordered; hence the charge carrier mobilities are larger than in amorphous organic materials. Single crystals exhibit the highest possible order and exhibit therefore the highest mobility.
A drawback is that these single crystals are difficult to obtain and have to be of high purity. Even small impurities or crystal defects can trap charges hence reduce the carrier mobility. [25]

Polycondensed aromatic hydrocarbons (PAH) such as the target molecules within this thesis stack together due to weak interactions such as π-π-stacking. They form columnar structures in solution or after deposition on surfaces. These molecules are ordered in stacks; the stacks can carry charges along their longitudinal axis due to the overlap of the orbitals. The charge carrier mobilities of such single-stranded stacks range between 10^{-4} and 1 cm^2/Vs [67].
A detailed section at the end of this chapter is devoted to PAH and π-π-stacking.

1.2.3 N-channel organic semiconductors

Depicted below are some examples for n-channel semiconducting molecules.

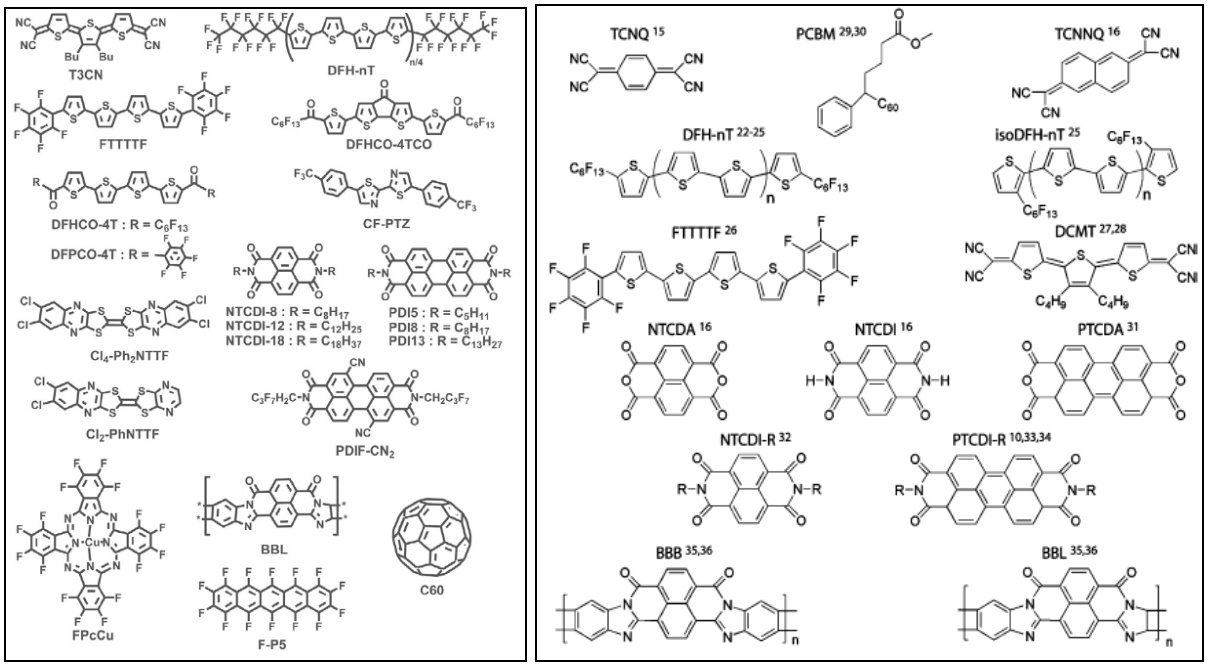

Fig. 8: Some n-channel organic semiconductors [19], [21]

There are many reasons why the n-channel materials are less investigated than their p-channel counterparts. One of them is that the metals used for the electrodes (Au, Ag and other noble metals) have work functions that would rather allow the injection of holes into the HOMO than electrons into the LUMO for organic semiconductors. Metals with low work-functions such as Mg, Al or Ca have lower electron injection barriers but oxidize easily and form reactive complexes with the organic semiconducting materials present in the OFET [56].

Another reason is that oligothiophenes and oligoacenes have quite small electron affinities (2.8 eV for solid pentacene [3]). These molecules have to be decorated by electron withdrawing groups to stabilize the anionic forms of the molecules and allow them to efficiently transport positive charges. These molecules still have the disadvantage that they react with water and oxygen present in the atmosphere [68]. This affinity can lead to the formation of electron traps or the degradation of the transport properties.

When treating n-channel semiconductors one has to maximize the charge carrier mobility of these materials while minimizing the deterioration of their electronic properties over the time of their application.

There are two strategies to get efficient OFET electron conductivity. One is based on reducing the molecule / polymer frontier molecular orbitals by substitution with strong electron-withdrawing groups so that the electron injection and transport prevail. Another strategy is to modify the insulator surface properties in order to eliminate electron trapping sites. When following this approach, electron transport has been observed for many polymeric semiconductors previously thought to be only p-channel conductors [69], as well as an enhancement of the electron mobilities of known n-channel materials [70].

Many n-channel semiconducting molecules are based on oligothiophenes in which the HOMO-LUMO levels have been tuned by addition of cyano- or perfluoro-alkyl groups. Facchetti and coworkers describe the synthesis and characterization of perfluorohexyl-substituted thiophene oligomers with charge carrier mobilities of up to 0.24 cm^2/Vs [71], [72]. The mechanism of electron carrier stabilization is not yet fully clear and probably reflects an interplay of effects other than LUMO energy reductions.

An important class of electron conductors can be based on fused acenes such as naphthalene and perylene [73], [74]. The energy levels of pentacene- [75] and phthalocyanine- [76] derivatives can also be tuned by substitution of electron withdrawing groups.

A fullerene mixture (C_{60}:C_{70} - 9:1) was first used in an OFET by Kastner and coworkers [77]. The C_{60} fullerene forms isotropic solids so the films do not require particular attention to control the molecular orientation on the surface of the substrate as in other organic materials. Haddon et al. [78] deposited C_{60} films in ultrahigh vacuum and reported mobilities up to 0.08 cm^2/Vs with an on/off ration of 10^6. Solution processable C_{60}- [79] and C_{80}-functionalized [80] materials have been reported as well.

Recent progress has been made on the synthesis and investigation of air stable n-channel polymers based on phenacyl-thiophene and quinine [81] with mobilities up to 0.3 cm^2/Vs.

1.2.4 OFET device applications

On the pictures below one can find the newest applications of OFET in devices that are used in our life every day.

Flexible OFETs are used as drive devices in TV-screens and computers, RFID (radio frequency identification) tags are used as transponders in the logistics industry to track or identify parcels or other packages during their transportation.

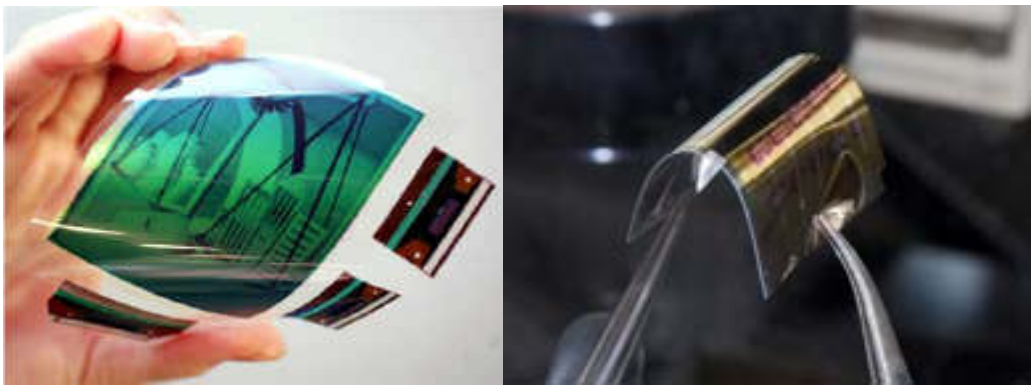

Image 1: Flexible OFET made by Merck (left) [82] and by Kippelen and Marder at Georgia Tech (right) [83]

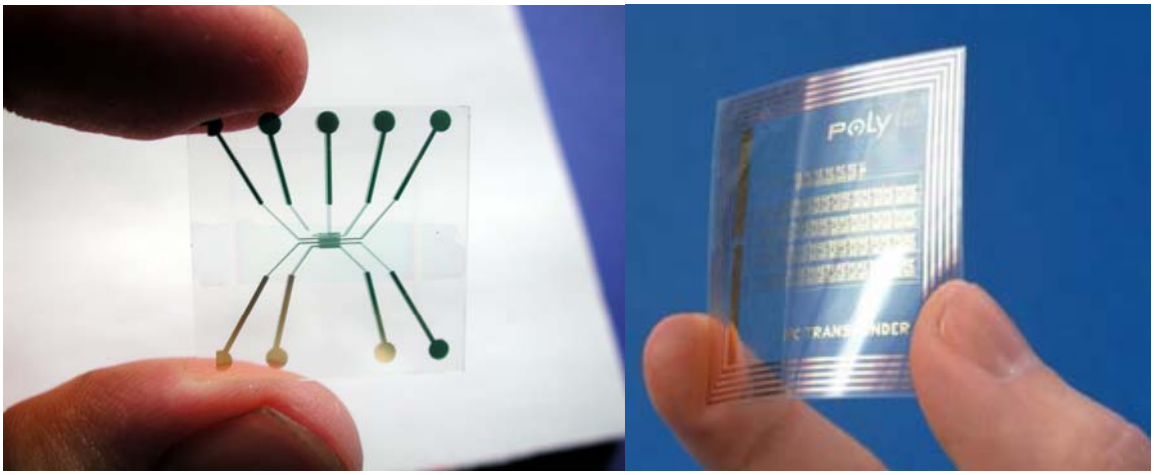

Image 2: OFET made by the Sokolowski-group at the University of Bonn [84] (left) and an organic RF-ID tag made by Polyic Ltd.® [85] (right)

1.3 Organic light emitting diodes (OLED)

1.3.1 Principles and structure

The first observation of organic electroluminescence has been made by Helfrich, Schneider and Pope in the early 1960's [86], [87] in anthracene single crystals. The field of organic light emitting diodes has been marked over the years by the discovery of efficient emission from amorphous small molecule-derived multilayer structures by Tang and coworkers [88] in the mid 1980's, the discovery of emission of polymeric materials by Friend et al. [89] to the triplet phosphorescent devices [90].

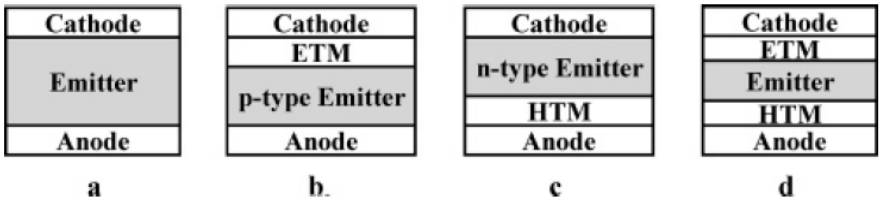

Fig. 9: OLED architectures with a hole-transport material (HTM) and an electron-transporting material (ETM) [91]

In **figure 9** above, the diagram *b* shows an OLED that carries an oxidative stable emission material topped by an electron transporting material. Diagram *c* shows the HTM on top of the anode and topped by an n-type emitter which is stable to reduction. The figure on the right with a HTM an ETM and an emissive layer in the middle is the most common architecture for OLEDs today. [91]
The multilayer architecture of the OLED allows the individual optimization of the different layers. Single emissive layers such as shown in diagram *a* are quite difficult to achieve as the emissive layer has to be both an n-type and p-type emitter. On top of that, this architecture yields only poor efficiencies and brightness [88].

Compared to conventional cathode ray tube and liquid crystal displays, OLEDs have many advantages and are predicted to revolutionize the display industry. OLED provide superior brightness and color purity, lower drive voltages as well as increased viewing angles.

Depicted below is a scheme of an organic light emitting diode in its most common architecture using two different HTL and ETL materials.

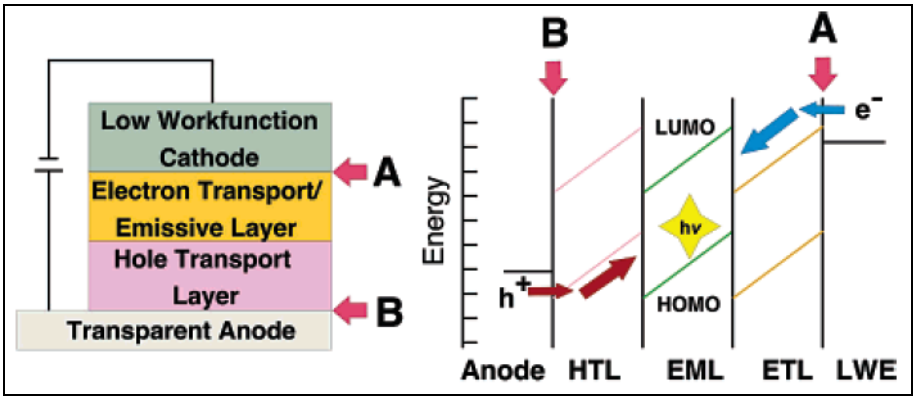

Fig. 10: Scheme of a heterostructure OLED (left), energy diagram of a multilayer OLED (right) [89]

A classical OLED is made of a transparent conducting oxide anode (TCO), a hole transport layer (HTL), an emissive layer (EML), an electron transport layer (ETL) and a metallic low work function electrode (LWE or LWC) as cathode.
For most working devices the ETL and EML are made of aluminum quinoxalate (Alq) and poly(9,9-dioctylfluorene) (PFO), the transparent anode is mostly made of indium tin oxide (ITO).

The mechanism of an OLED works as follows: under forward bias the HTL is oxidized as holes are injected (or electrons extracted) from the anode into its HOMO. The ETL is reduced as electrons are injected from the cathode into its LUMO. The charge carriers migrate under the applied electrical field and recombine to form singlet and triplet excitons (bound excited-state electron-hole pairs) within the EML.
These excited-state species can return to the ground state via radiative or non-radiative decay pathways. Energy levels offsets on the anode and cathode work functions from the HTL HOMO and ETL LUMO energies strongly influence the intrinsic carrier injection barriers [20].

One can distinguish three key electronic processes in OLED: charge injection, charge transport and charge recombination.

An approach regarding the optimization of charge recombination would be to maximize the productive electron-hole combination using dopants that emit from the triplet state. This enhances the quantum efficiency by taking in advantage the 1:3 exciton singlet/triplet ratio [93]. This process is also called “triplet harvesting” [90].

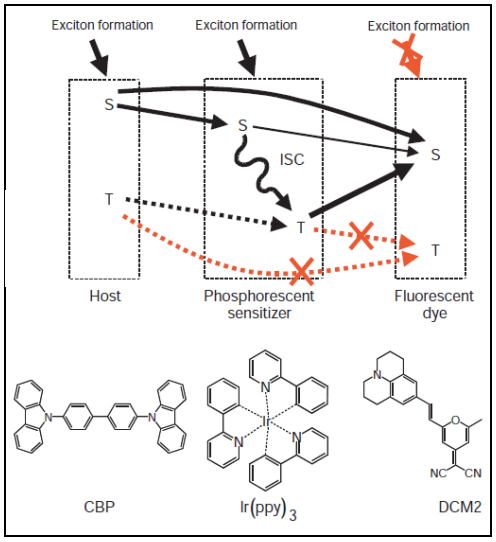

Fig. 11: Energy transfer mechanisms in phosphorescent sensitized OLED: Förster process (solid line) and Dexter mechanism (dotted line) [90]

In the example above, 4,4’-N,N’-dicarbazole-biphenyl (CBP) is used as the donor and host material [94], *fac*-tris(2-phenylpyridine)iridium ($Ir(ppy)_3$) [95] as green emitting phosphorescent sensitizer and [2-methyl-6-[2-(2,3,6,7-tetrahydro-1*H*,5*H*-benzo[*ij*]quinolizin-9-yl)ethenyl]-4*H*-pyran-4-ylidene]propane-dinitrile (DCM2) [96] as red fluorescent dye.

Förster transfers are drawn by solid and Dexter type transfers by dotted lines. The recombination of electrons and holes create singlet (S) and triplet (T) excitons in the host material. Charge trapping could also be responsible for exciton formation in the other materials. A direct transfer into the singlet state of the fluorescent dye by a Förster – type process is also possible, as well as a Dexter transfer into the triplet state. Singlet excitons can transfer into triplets by intersystem crossing (ISC).

The triplets can then dipole – dipole couple with the singlet state of the fluorescent dye or Dexter transfer to the triplet by a loss mechanism. The direct triplet formation in the fluorescent dye is also a path to loss. [90]

1.3.2 Hole transport materials (HTM) and electron transport materials (ETM)

This chapter will give a small overview of the electron- and hole-transport materials that are currently used in OLED devices. The target molecules in this thesis may be an alternative to these materials.

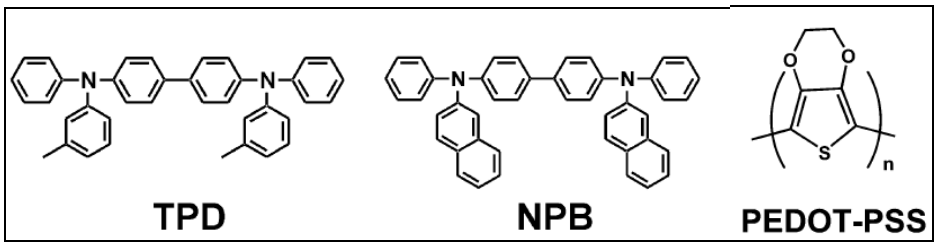

Fig. 12: Typical OLED hole-transport materials: TPD (1,4-bis(phenyl-*m*-tolylamino) biphenyl), NPB (1,4-bis(1-naphthylphenylamino)biphenyl) and PEDOT-PSS (poly-3,4-ethylenedioxythiophene-polystyrene sulfonate)

An important goal in OLED science is to maximize carrier – transport and –mobility. This can be done by tailoring the chemical structures of the compounds. The electronic properties of organic molecules are typically characterized by preferential hole transport and low charge carrier mobilities. Therefore exciton formation is frequently limited by low electron fluence. These characteristics combined with bigger hole currents significantly lowers the OLED light output and external quantum efficiency.

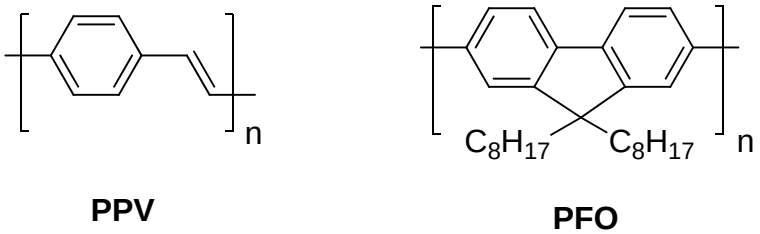

Fig. 13: Typical OLED electron-transport materials: PPV (poly(p-phenylene vinylene) and PFO (poly(9,9-dioctylfluorene)

One can summarize the following important properties an electron transport material should have in order to enhance OLED performance [91]:

- A reversible electrochemical reduction with a sufficiently high reduction potential. This facilitates electron transport which can be thought of as a series of redox processes within the organic film. [3] [97 - 111]
- Suitable EA and IP values relative to the p-type emitter, thereby allowing minimization of the barrier for electron injection, reduction of turn-on/operating voltage and effective hole blocking. If the EA is too high (e.g., 4.0 eV) relative to that of the p-type emitter such as **1a** or **1b** (EA = 2.7 - 3.0 eV), EL can be significantly or even completely quenched due to efficient exciton dissociation [102], [103]. To also serve as an efficient hole blocker, the material should have a wide band gap energy with a high IP value (>6.0 eV) and an EA value closely aligned with that of the p-type emitter.
- High electron mobility, to move the charge recombination zone away from near the cathode and improve the exciton generation rate. An electron mobility in the ETM comparable to the hole mobility in the p-type emitter would be ideal, however, electron mobilities in organic materials can be several orders of magnitude less than hole mobilities [104]
- High glass transition temperatures and thermal stability to withstand inevitable Joule heating encountered during OLED operation, especially at higher electric fields and current densities
- Processability to uniform, pinhole-free, thin films either by vacuum evaporation (low molar mass ETM) or by spin casting, printing, and related techniques (soluble polymeric ETM)
- Amorphous morphology, which prevents light scattering and crystallization-induced degradation.

1.3.3 OLED device applications

There are many practical applications for OLED devices. The demand for high-resolution and low power consumption devices has been steadily increasing over the last few years.
Judging from the examples below, one can see that these devices are totally transparent and highly flexible and the TV screens made with this technique are very flat and exhibit a very large viewing angle (c.f. side view, below at the right).

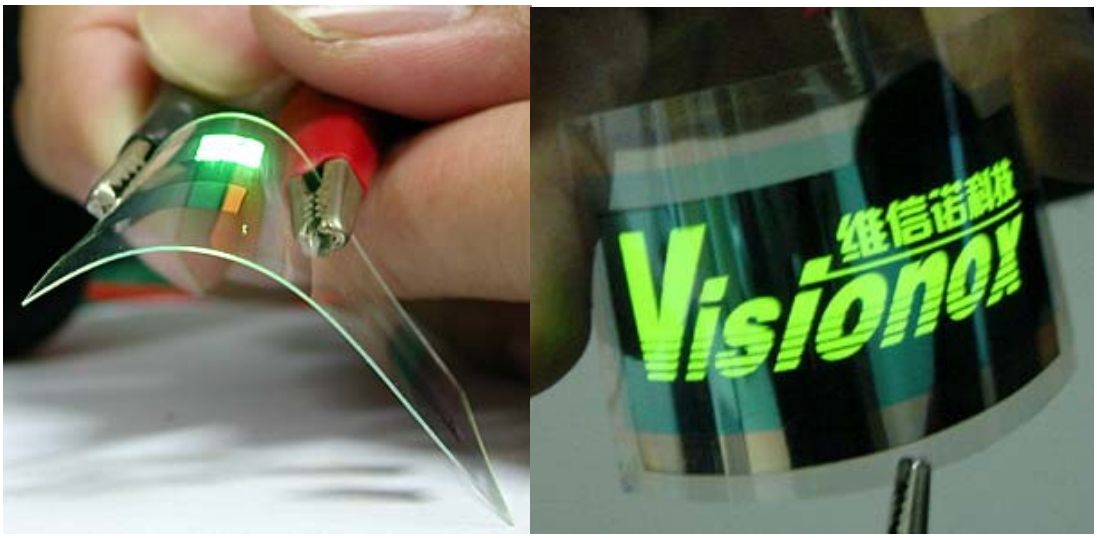

Image 3: Flexible OLED panels made by Samsung® and Visionox® [105, 106]

Image 4: 40-inch OLED-TV made by Samsung® [105] and a 13-inch OLED screen produced by Sony® [107]

1.4 Molecular self-assembly

Polycyclic aromatic hydrocarbons (PAH) are known to form molecular columnar stacks by interacting with one another through weak forces such as electrostatic- or Van-der-Waals interactions [108]. As non-covalent interactions can be also highly directional, molecules can arrange on a substrate to form structures such as layers, crystals or fibrils upon solvent evaporation [109].

The processability of PAH can be improved by attaching substituents such as alkyl chains at the molecular periphery in order to increase their solubility in organic solvents [110].
The self-assembly behavior can be modified by varying for example the shape of the aromatic core or by tuning the length, the amount or the type of sidechains attached to the core [111].
Changing the nature of the solvent can as well influence the way the molecules behave in solution or upon deposition on a substrate [112].

Optimal self-assembly is obtained by a compromise between three different interactions:

- If the interaction between the single molecules is too strong, the molecules will be only poorly soluble in the solvent [113]
- If the interactions between the molecule and the substrate are too strong, the molecules will be trapped kinetically on surfaces instead of forming supramolecular stacks [114]
- If the molecule-solvent interactions are dominant, the interaction between the molecules will be shielded and only amorphous structures will be obtained.

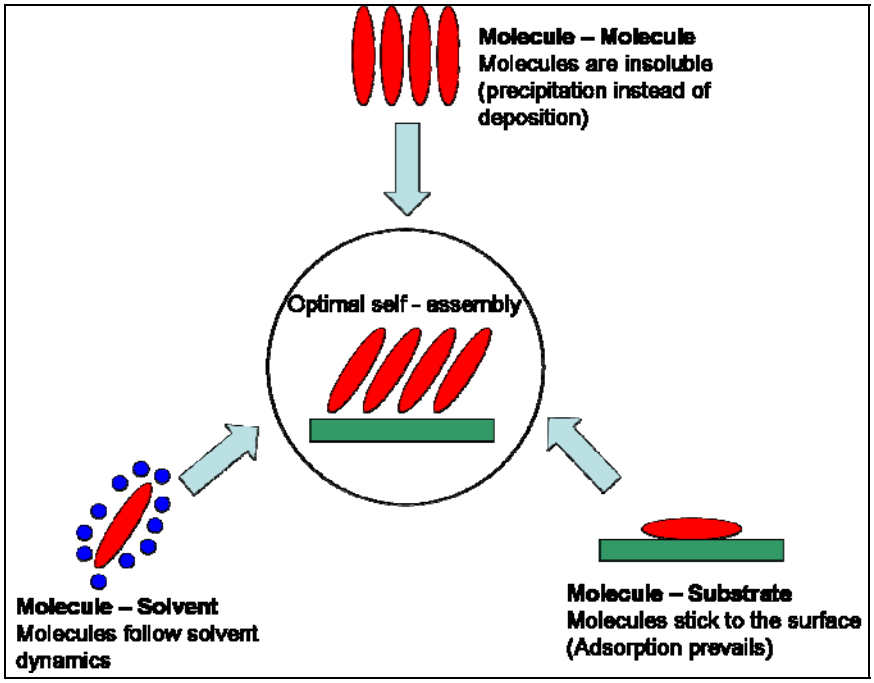

Fig. 14: Schematic representation of the major interaction types playing a role during solvent-assisted deposition [108]

PAH stack preferably in "herringbone" structures or in columnar stacks as depicted in the figure below.

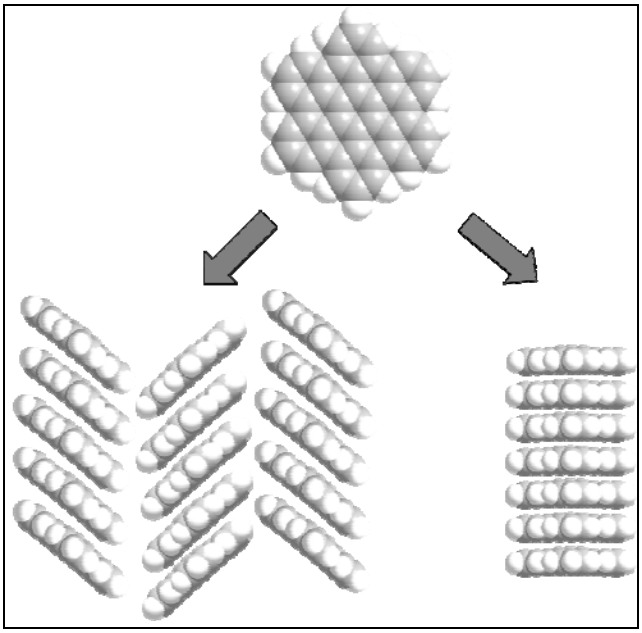

Fig. 15: Schematic PAH stacking into herringbone- (left) or cofacial columnar architectures (right)

Müllen and coworkers have synthesized a wide range of PAHs bearing mainly alkyl sidechains [110]. Linear, branched and also chiral sidechains have been attached to hexa-peri-hexabenzocoronenes (HBC) in order to study their aggregation behavior in solution as well as upon solvent-assisted deposition on solid substrates.

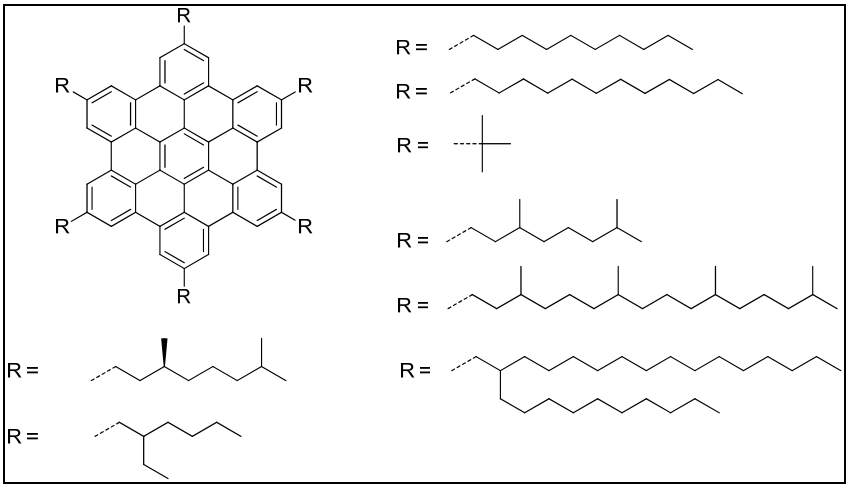

Fig. 16: Some HBC bearing alkyl sidechains synthesized by Müllen and coworkers [115 - 118]

The HBCs bearing alkyl chains have however some drawbacks, since the molecular stacks tend to aggregate laterally. Upon heating these crystalline alkane domains melt and arrange the remaining columnar stacks in a hexagonal lattice [119].

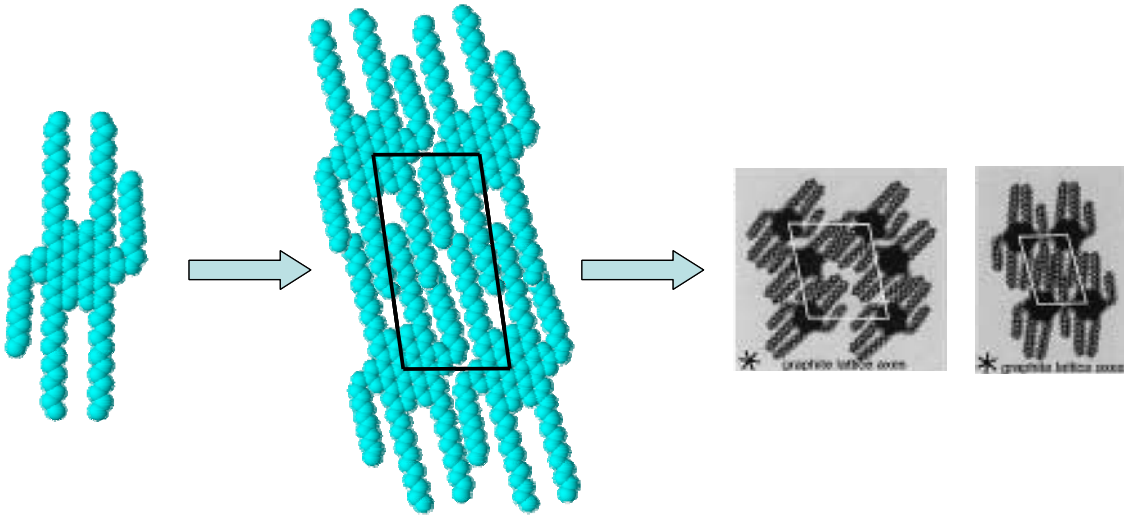

Fig. 17: Aggregation of alkyl-chain bearing HBC at room temperature [119]

The Jenny group therefore introduced HBCs bearing perfluoroalkyl chains of different length to prevent or reduce lateral aggregation between the single stacks [111], [120].
Aebischer has synthesized many C_6-symmetric HBC derivatives bearing linear and branched perfluoroalkyl chains [111]. Depicted below are some of the synthesized derivatives.

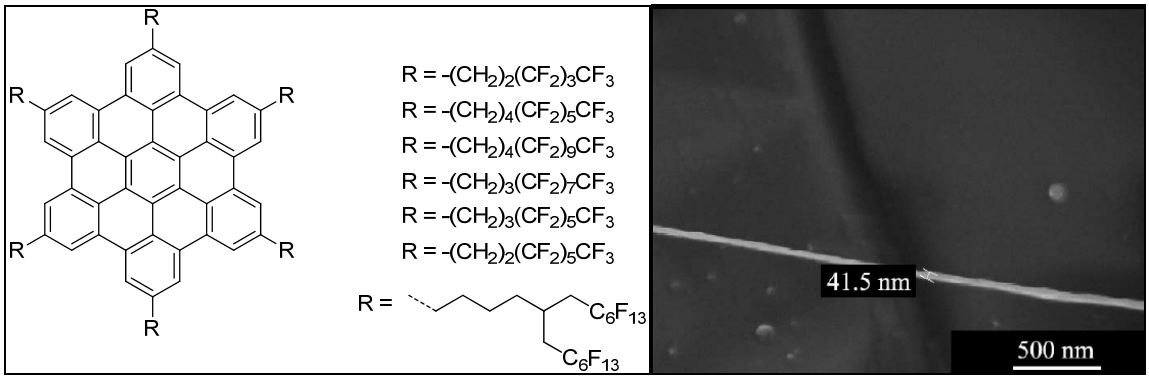

Fig. 18: Some of the perfluoroalkyl – chain bearing HBC synthesized by Aebischer (left), cryo-SEM image of a single perfluoroalkylated HBC strand shaded by 20 nm of platinum (right) [111]

These chains act like a Teflon® mantle around the core and hinder therefore the lateral aggregation of the molecular strands. The alkyl spacer is necessary for synthetic reasons, the minimum length are two alkyl CH_2 – groups as spacer, but in addition has been shown to positively influence the fluorous effect of the perfluorinated tails[120].

1.5 Aim of the thesis

Symmetrically substituted hexa-*peri*-hexabenzocoronenes (HBC) exhibit a six-fold symmetry and have thoroughly been investigated in our research group in the past [111], [120]. Perfluorinated sidechains of different lengths have been attached and their influence on the aggregation properties studied.

The aim of this thesis is to synthesize polycondensed aromatic hydrocarbons (PAH) which are not C_6 symmetric and could be used in the field of molecular electronics such as OLEDs and OFETs as discussed in the preceding chapters.

These molecules should bear alkyl or perfluoroalkyl sidechains in order to ease their handling and the solubility in common organic solvents. The ultimate goal is to study their stacking behaviour in solution as well as on solid surfaces after deposition by PVD, CVD, spin coating or printing.

The work should also include a computational study for calculating HOMO – LUMO gaps, predicting the stacking abilities and other electronic properties of differently shaped PAHs, and finally to synthesize a selection of promising candidates.

This calls for design of new PAH derivatives and developing methods to introduce two perfluoroalkylated sidechains in ortho-positions on aromatic synthons.

II. RESULTS AND DISCUSSION

2.1 General aspects

Polycondensed aromatic hydrocarbons (PAH) especially C_6 symmetric hexa-peri-hexabenzocoronenes have been investigated thoroughly in our research Group by Alameddine and Aebischer [120], [111].

Our main idea of this thesis was to screen for possible alternative PAH which do not exhibit C_6 symmetry and that could be used in molecular electronics or as organic semiconductors.

We soon discovered a paper by Y. Ruiz-Morales [121] that had calculated HOMO-LUMO gaps for different PAH. One of the optimal results regarding ideal HOMO – LUMO gaps indicated by that paper was the tribenzopentaphene family, which have the shape of a halfmoon and roughly consist of a half-HBC.

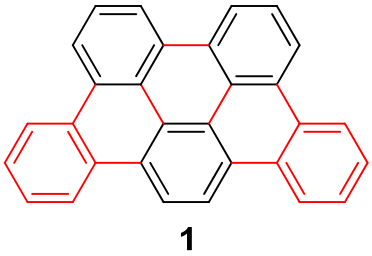

1

Fig. 19: tribenzopentaphene (**1**)

Ruiz-Morales gives a H-L gap of 478 nm (2.59 eV) for the TBP. It is quite similar to the 475 nm of HBC [122].

We picked the TBP family for synthesis because it could theoretically stack edge-on onto surfaces and not flat-on such as HBC. This could lead to ribbon – like structures on surfaces. As the current passes through the molecular stacks, it would pass parallel to the surface and therefore be an ideal substrate for field effect transistors (see chapter 1).

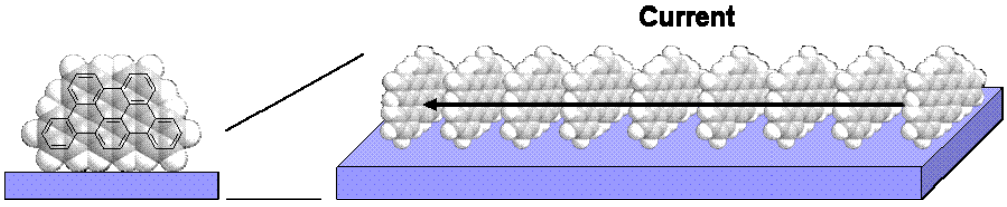

Fig. 20: Theoretical edge-on stacking of FET on a surface (sidechains omitted for clarity)

We also wanted to know if the positions of the sidechains influence the stacking on the surface. This is why we synthesized different derivatives bearing alkyl sidechains.

2.2 Halfmoon-shaped polycondensed hydrocarbons (Tribenzopentaphenes, TBP)

2.2.1 Strategy

Tribenzopentaphenes (TBP) (**1**) are a completely new class of compounds. We developed the following retrosynthetic strategy involving the known Scholl reaction [123] using $FeCl_3$ in nitromethane, Knoevenagel and Diels-Alder type reactions.

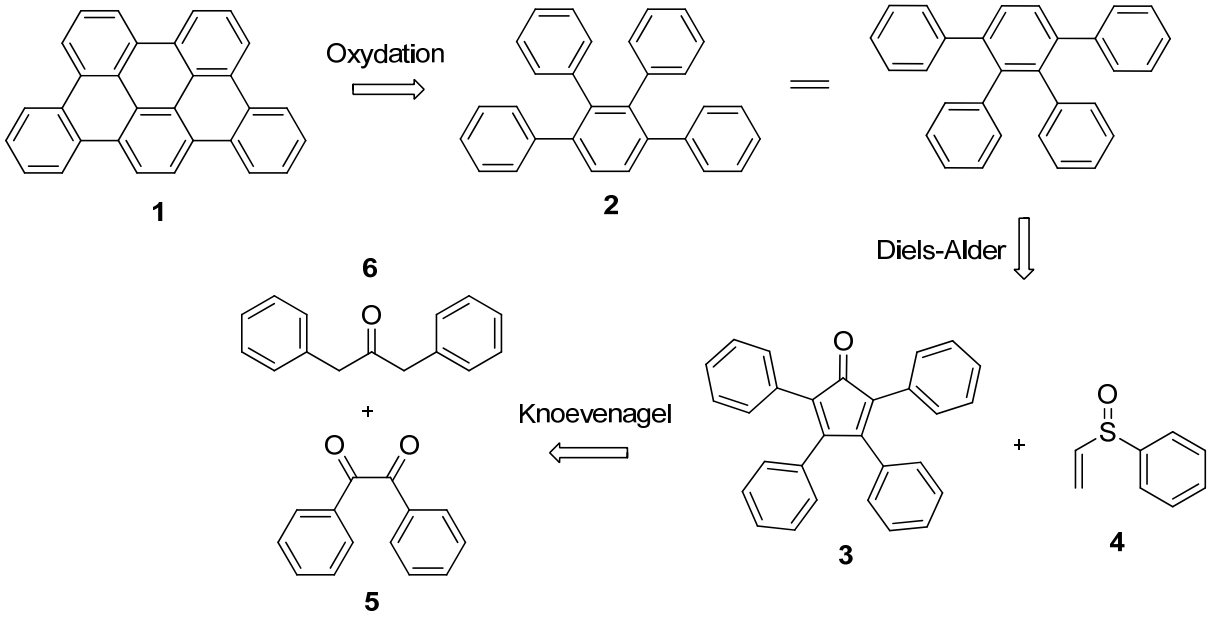

Fig. 21: General retrosynthetic strategy

The Diels – Alder type reaction involved in this strategy uses tetraphenylcyclopentadienone **3** or its derivatives, which act as an acceptor and phenylvinylsulfoxide **4** which is the acetylene-equivalent. The reaction liberates HSO and CO via a syn-elmination.

This strategy has the great advantage of being straightforward, involving only three steps and using many commercial substances (**4**, **5** and **6**) As we wanted to synthesize various derivatives of **1** bearing sidechains on different positions, we had to use different functionalized starting compounds.

Both starting materials **6** and **7** are commercial. Using a similar idea as above in **Fig. 21** one can easily deduce the steps to the other derivatives.

2.2.2 6,9-Dioctyltribenzo[*fg,ij,rst*]pentaphene

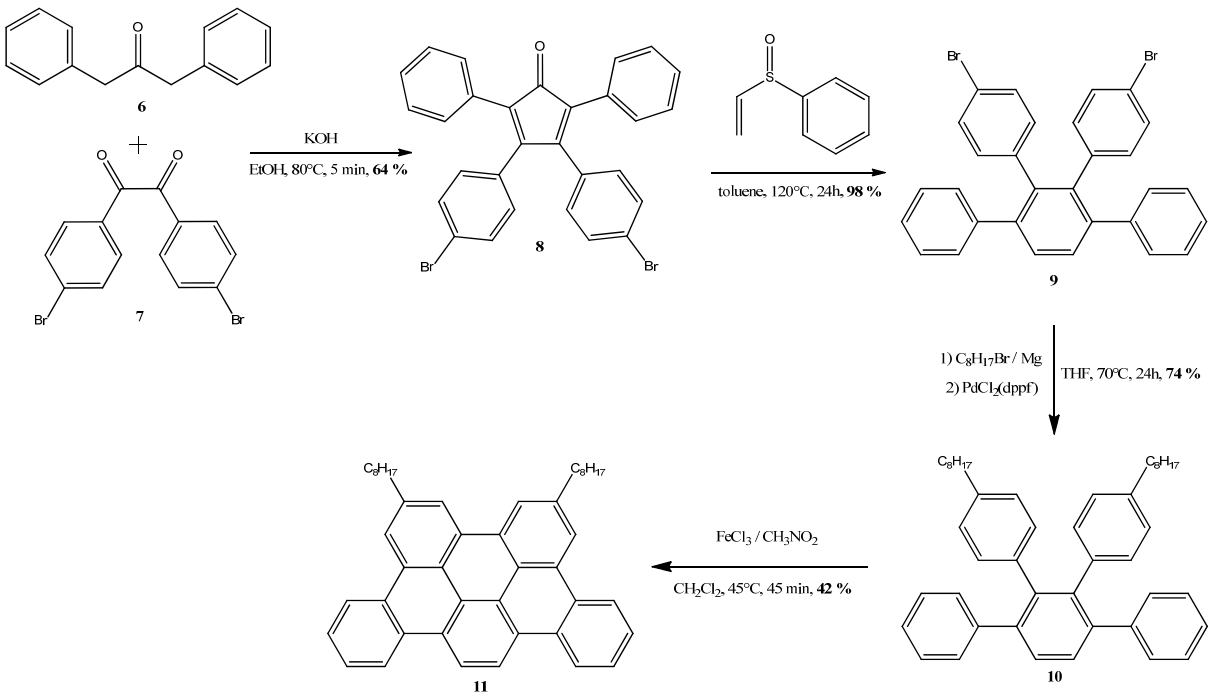

Fig. 22: Synthesis of 6,9-dioctyltribenzopentaphene **11**

The synthesis of the first derivative bearing two octyl sidechains on positions 6 and 9 is quite straightforward. We begin with a double Knoevenagel reaction using potassium hydroxide as base and ethanol as solvent. The choice of the solvent and base has not been optimized, because the yield of 64 % was judged sufficient for this first step.

We can observe a color change from colorless to purple as soon as one adds the base to the mixture. The reaction time is quite short (5 min) at refluxing temperature. After extraction with DCM and water, the mixture is filtered over a short silica – gel plug to yield the pure product **8** as a purple powder in good yield (64 %). The structure is confirmed by NMR and EI-MS. The ^{13}C-NMR exhibits the typical C=O signal at 200.02 ppm and the two quaternary cyclopentadienone signals at 152.55 and 130.18 ppm.

The next step involves a Diels – Alder type reaction on **8** using phenylvinylsulfoxide as reactant in refluxing toluene. The progress of the reaction is evident by its color change since the starting material is deep purple and the desired product colorless. As the reaction evolves, the color gets first darker and then slowly disappears. The purification is done by column chromatography using a mixture of ethyl acetate and hexanes as eluent. The yield is excellent (98 %) and one obtains the desired compound **9** as a white powder. The structure is confirmed by NMR and EI-MS.

The sidechains are installed by a double Kumada crosscoupling reaction. The sidechain has to be long enough to help solubilizing the final products once they were oxidized. We therefore chose to use octyl sidechains as bromooctane is very cheap and the Grignard reagent can be obtained easily. A solution of bromooctane in THF is added dropwise onto dry magnesium turnings. The slurry containing the magnesium bromide is then transferred by syringe onto the substrate **9**. Using a palladium catalyst ($PdCl_2$(dppf)) in dry THF the mixture is heated for 24 h at reflux. After column chromatography using a mixture of pentane and DCM as eluent, the desired compound **10** is recovered as a white powder in good yield (74 %) and its structure was confirmed by NMR and MS.

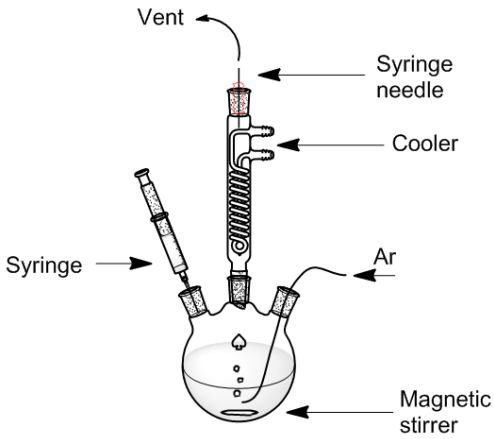

Fig. 23: Apparatus for the Scholl - Reaction

The final step is the oxidation using iron(III)-chloride and nitromethane in DCM. This reaction requires special preparations. All the solvents have to be sparged with argon. The $FeCl_3$ is dissolved in nitromethane and the solution was also sparged with argon. The reaction apparatus consists of a three – necked flask topped by a cooler and sealed by septums with a cannula at the top as pressure relief. A slow stream of argon is bubbled continuously through the reaction mixture using a Teflon® tube in order to evacuate the HCl formed during the reaction. The solution containing the substrate is heated to 45°C while bubbling with argon.

The iron-chloride containing nitromethane is then added dropwise to the reaction which turns yellow, green and then brown. The mixture is refluxed for 2 h and then cooled to RT. Precipitation of a brown powder is induced with methanol. The residue is filtered off through a Millipore® filter (1 µm pore size). This process (dissolution in DCM, precipitation by ethanol and filtration) is repeated until the compound is pure as indicated by his yellow color. The desired product **11** is obtained in 42 % yield. The structure of the compound was confirmed by NMR and EI-MS. The MS spectrum shows the loss of the two octyl sidechains beside the main peak of the desired compound.

The UV / VIS and fluorescence spectrum of **11** is dominated by a very strong absorption band at 307 nm. There are also two smaller absorption bands at 356 nm and 375 nm. The fluorescence was therefore measured by exciting the 307 nm UV-band.

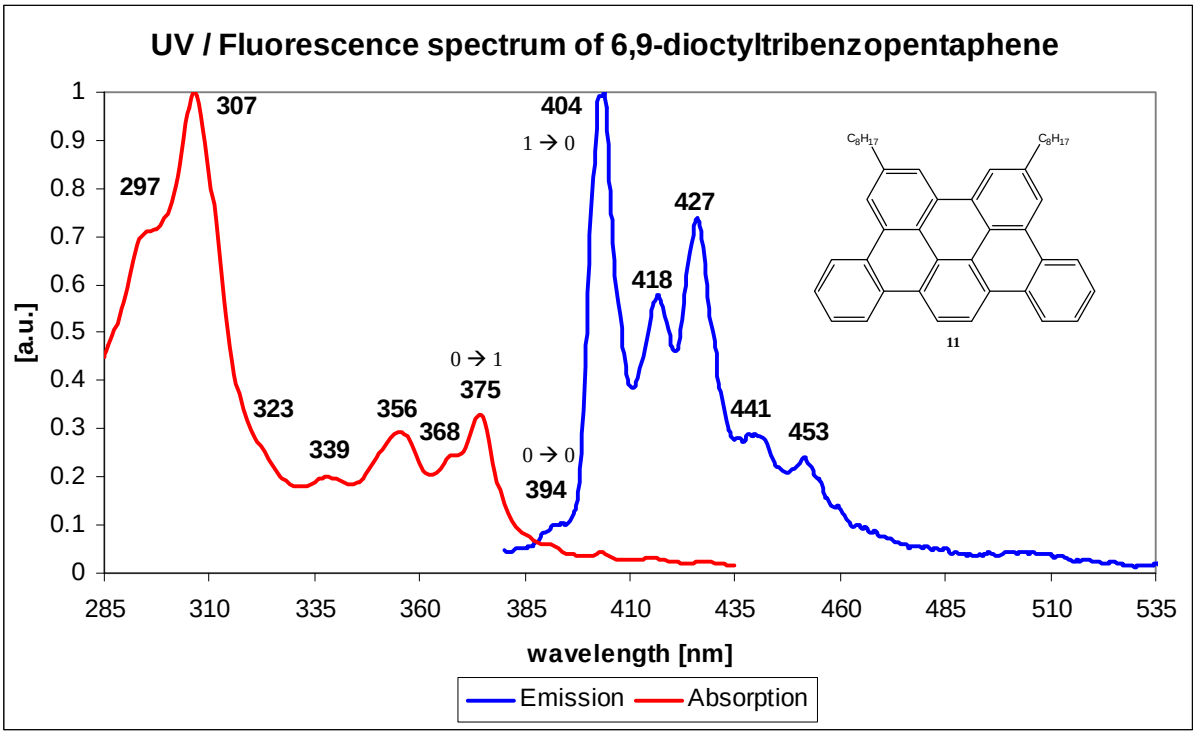

Fig. 24: UV/VIS and fluorescence spectrum (λ_{ex} = 307 nm) of **11**.

The HOMO – LUMO gap of compound **11** can roughly be estimated at 385 – 395 nm which corresponds to energies of 3.14 to 3.22 eV. The gap corresponds to the 0 → 0 transition which is forbidden due to symmetry reasons. These values are too high in energy to be used in our envisioned application such as field effect transistors. The values should be around 2.5 – 2.8 eV to apply as successful candidate for our application.

2.2.3 3,12-Dioctyltribenzopentaphene

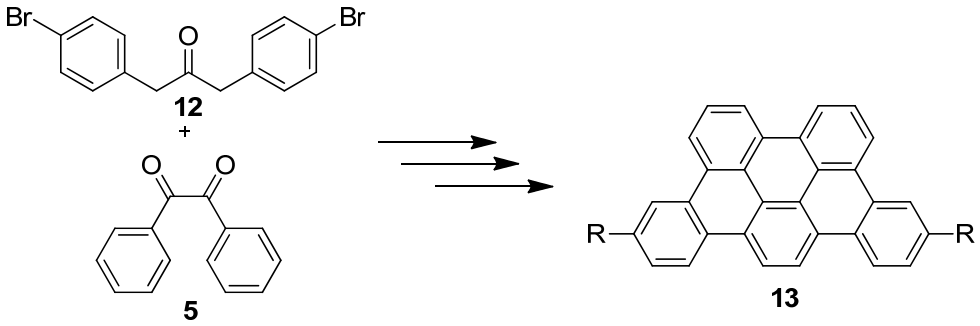

Fig. 25: Path to the derivatives bearing sidechains

Compound **12** is not commercial but has been synthesized in gram-scale by condensing 4-bromophenylacetic acid using DCC and DMAP following a known procedure. In order to check the feasibility of the compounds and to investigate their properties we chose to attach octyl sidechains on the different positions.

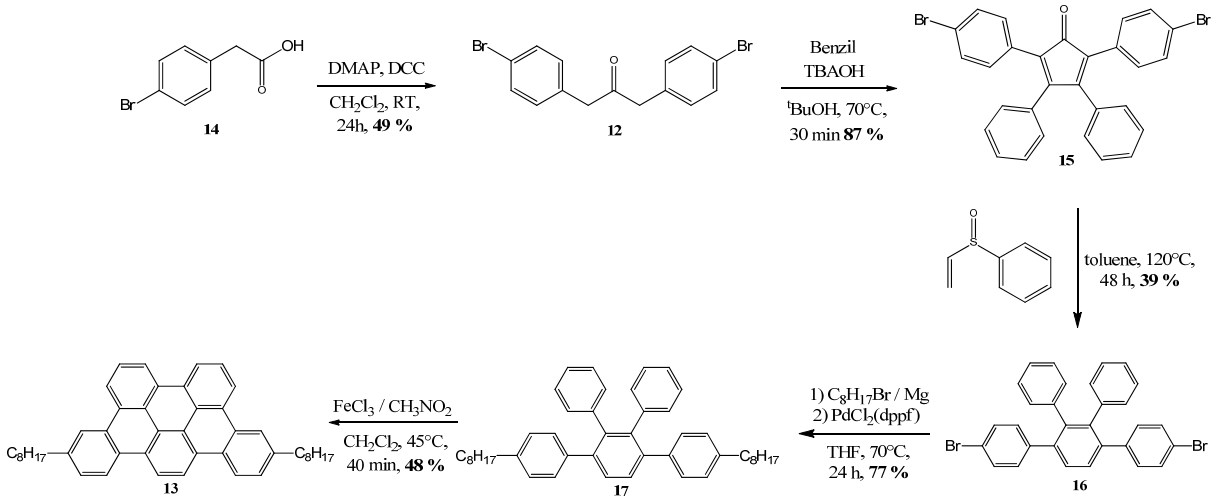

Fig. 26: Synthetic pathway to 3,12-dioctyltribenzopentaphene **13**

The synthesis of the TBP derivative bearing two octyl sidechains in the 3 and 12 positions begins with the dimerization of 4-bromophenylacetic acid using DCC and DMAP. A solution of DCC and DMAP is treated with the substrate **14** and stirred at room temperature for 24 h. After removing an undesired precipitate (mostly dicyclohexyl urea) by filtration, we precipitate the desired product by adding methanol to the solution. After recrystallization, the desired compound **12** is obtained in reasonable yield (49 %) as a white powder; the structure was confirmed by NMR (C=O signal at 204.19 ppm) and EI-MS.

The following step is again a double Knoevenagel with the commercial benzil as dicetone component. We optimized this reaction using different solvents and bases (see table 1 below). A 1M tetrabutylammonium hydroxide solution in methanol as base and *tert*-butanol as solvent turned out to be best in our hands. It is worth mentioning that Oda and coworkers [124] have developed a method for Knoevenagel reactions using KOH, EtOH and 18-crown-6 in benzene, giving similar yields as in the conditions developed above.
Once again a color change from colorless to deep purple was observed. The reaction time was 30 min in the refluxing solvent. Purification consists of three successive flash chromatographies using DCM as eluent. We obtain the desired tetraphenylcyclopentanone derivative in very good yield (87 %) as a purple powder; the structure of the compound was again confirmed by NMR and EI-MS. The ^{13}C-NMR shows the typical signals of C=O at 199.94 ppm and those of the cyclopentadienone ring at 155.40 and 129.89 ppm.

Entry	**12** [mmol]	Benzil [eq]	Base, [eq]	Solvent	Temp. [°C]	Time [min]	Yield [%]
2.2.3.1	1.00	1.00	NaOH, 1.0	MeOH	70	60	**49**
2.2.3.2	1.00	1.00	KOH, 1.0	EtOH	80	60	**64**
2.2.3.3	1.00	1.00	TBAOH, 1.0	*t*-BuOH	85	30	**87**

Table 1: Knoevenagel reaction on **12** using different solvents and bases

Looking at the table we can conclude that TBAOH is the best base in this case because it is fully miscible in organic solvents. The *tert*-butanol is also the solvent which is the most organic.

The following Diels-Alder reaction of **15** with phenylvinyl sulfoxide in dry refluxing toluene took 48 h until all the purple color disappeared. Column chromatography in DCM / pentane 1:1 afforded the desired product **16** in 39 % yield. The structure was confirmed by NMR and EI-MS.

As before, the octyl sidechains were attached by a double Kumada reaction with the Grignard reagent obtained from bromooctane. After extraction and recrystallization from a mixture of DCM and ethanol we obtained the terphenyl derivative **17** as a white powder in good yield (77 %). Confirmation of the structure was made by NMR and MALDI-MS.

The final oxidation was done in DCM under similar conditions described above in section 2.2.2. Precipitation and three successive filtrations on Millipore® filters (1 μm pore size) lead to compound **13** in moderate yield (48 %). The structure was confirmed by NMR and MALDI-MS in a DCTB matrix.
UV / VIS and fluorescence measurements gave very similar results as compared to **11**. However, while the UV spectra superimpose perfectly, the emission spectra differ considerably.

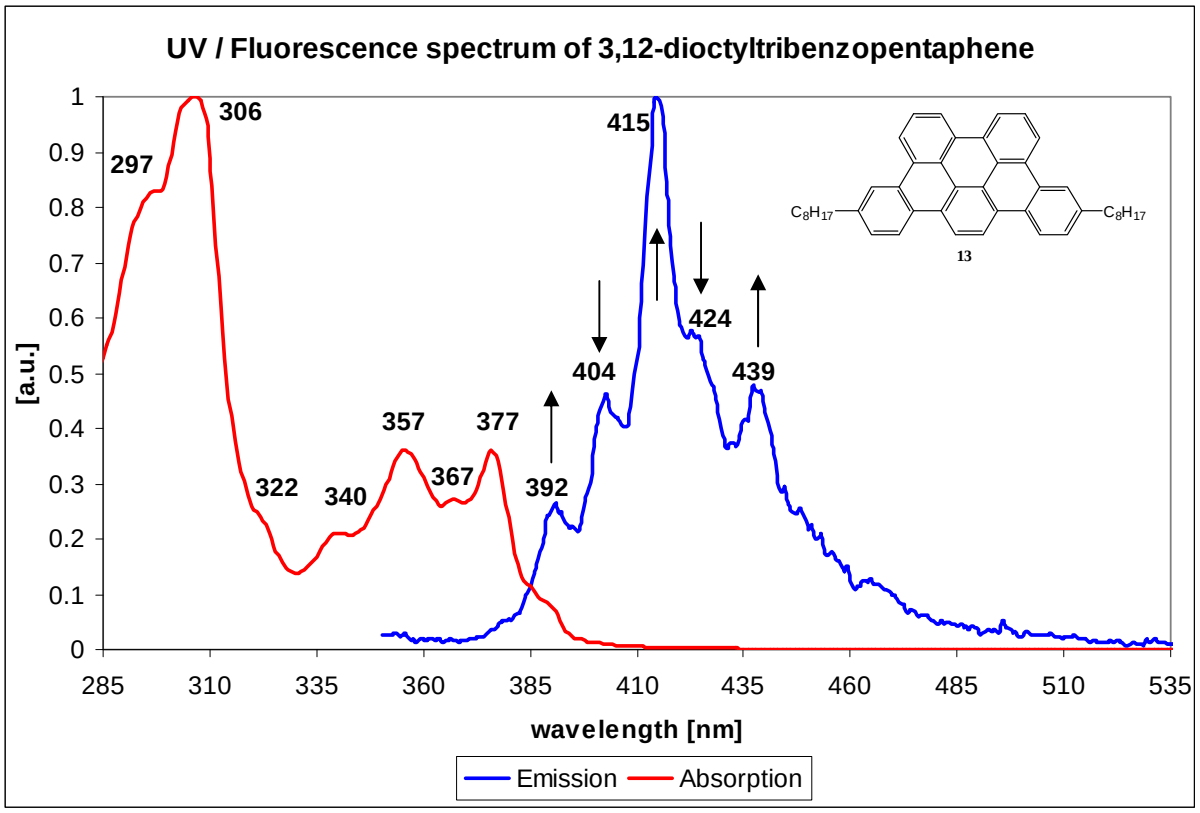

Fig. 27: UV/VIS and fluorescence spectrum (λ_{ex} = 306 nm) of **13**.

The transitions have almost the same energies but their intensities differ considerably. The bands at 392, 415 and 439 nm increase with respect to the same bands for **11**. In contrary the 404 and 424 nm bands decrease in intensity compared to the spectrum of **11**. The aromatic core is the same for both derivatives but the sidechains influence the coefficients in a non-negligible manner.

2.2.4 3,6,9,12-Tetraoctyltribenzopentaphene

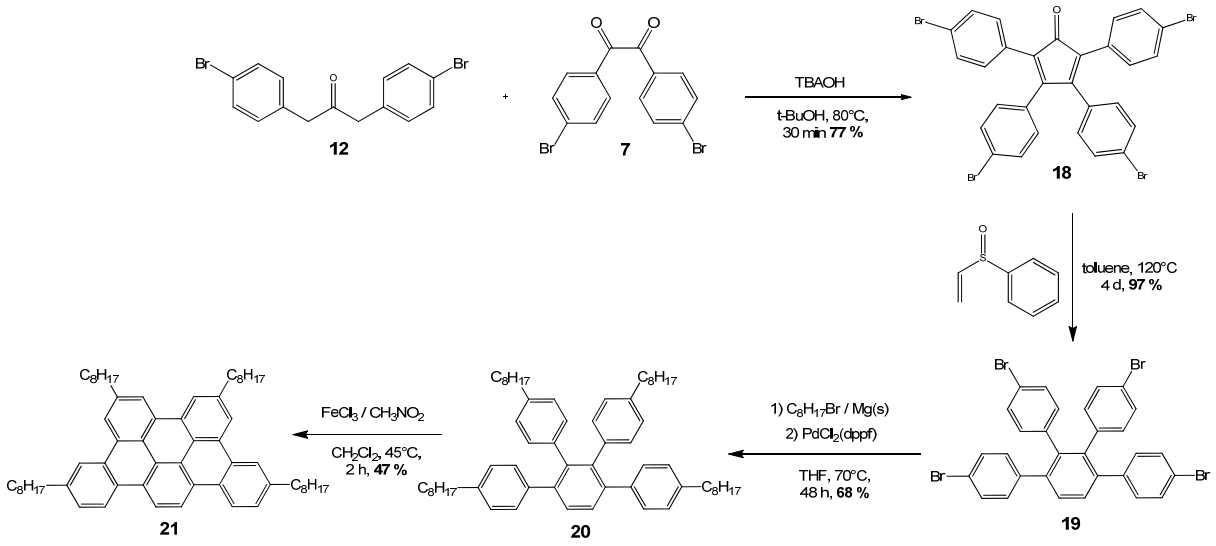

Fig. 28: Synthetic pathway to 3,6,9,12-dioctyltribenzopentaphene

For the first step we react the commercial 4,4'-dibromobenzil **7** with the 1,3-bis(4-bromophenyl)propan-2-one **12,** which was synthesized according to the method described in section 2.2.3. The double Knoevenagel condensation was done again in tert-butanol with tetrabutylammonium hydroxide in methanol as base. The color changes from colorless to dark red. After 30 min of reaction time, the mixture is quenched with water. After extraction the organic layer is purified by flash chromatography. One obtains the purple tetraphenylcyclopentanone derivative **18** in good yield (77 %); structure confirmation was obtained by NMR and EI-MS. The typical quaternary signals of C=O and the cyclopentadienone can be found at 198.92, 153.19 and 131.25 ppm respectively.

The Diels – Alder reaction follows the method previously described. The tetraphenylcyclopentanone derivative **18** was heated with phenylvinylsulfoxide in toluene for 4 days until all the starting material had reacted. After extraction and column chromatography one obtains the desired white terphenyl derivative **19** in nearly quantitative yield (97 %). The structure was confirmed by NMR and EI-MS as well as MALDI-MS. In the EI-MS one obtains the molecular peak of the target compound at 697.9 m/z, in the MALDI-MS, only the Na-adduct peak is found at 716.79 m/z.

Again the sidechains were introduced by a fourfold Kumada crosscoupling following the method described previously. The octyl – Grignard substrate and $PdCl_2$(dppf) were reacted in refluxing THF. The realized yield (68 %) corresponds to an excellent 91 % average yield per coupling step; structure confirmation was obtained by NMR and EI-MS.

The final oxidation step is done as described before. After purification, the TBP derivative **21** bearing four sidechains is obtained as an orange powder in 47 % yield; the structure was confirmed by MALDI-MS.

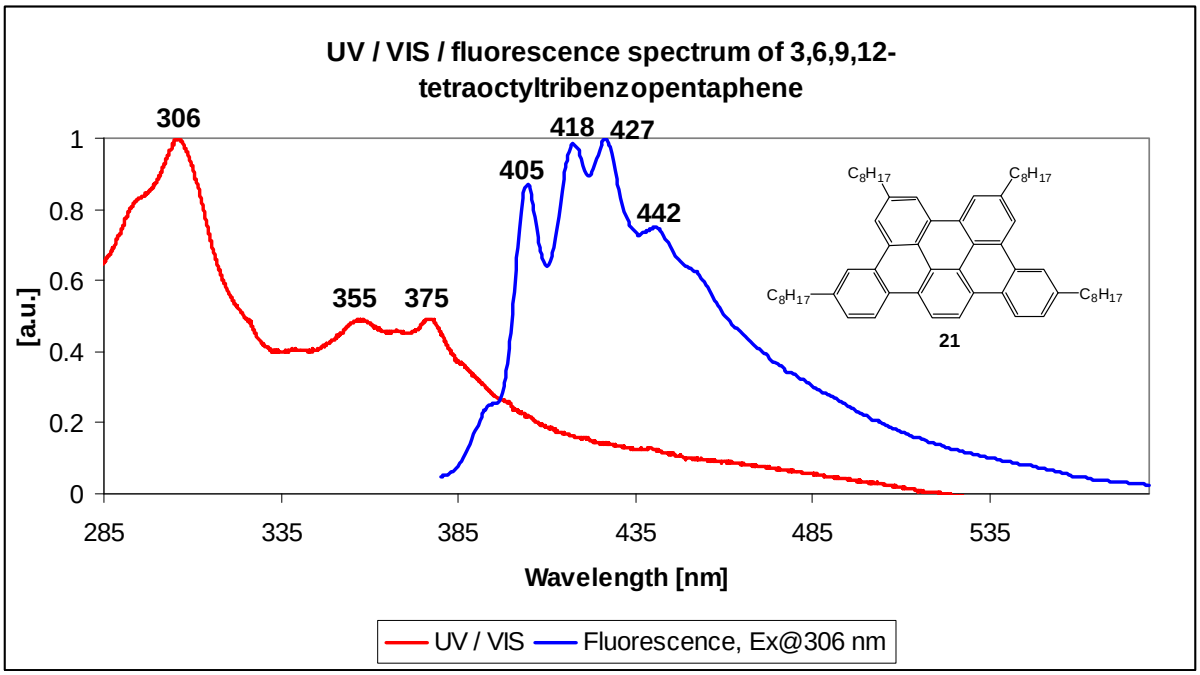

Fig. 29: UV and fluorescence spectrum of **21**

The less resolved UV spectrum of **21** does not differ from the ones for **11** and **13** as it reveals four distinct absorption peaks at 293, 306, 356 and 375 nm. The emission spectrum shows the same bands as in the case of **11** and **13** but with the intensities about halfway between the two other compounds.

The MALDI – MS spectrum has its main peak at 824.63 m/z which corresponds to **21** with a calculated mass of 824.6260. The slow decrease of the UV curve after 390 nm indicates a small impurity in the desired product.

This is confirmed by a small MALDI – peak at 858.59 of an unknown product which could not be removed completely by standard purification methods.

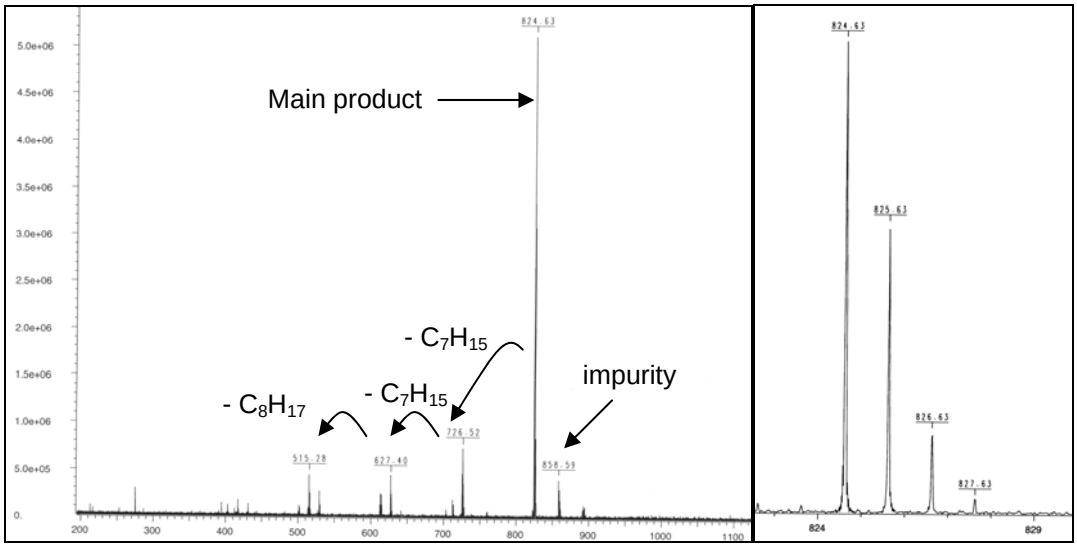

Image 5: MALDI-MS of the final product (left), zoom on the main peak of **21** (right)

2.2.5 15,16-Diheptyltribenzopentaphene

One last derivative was synthesized by modifying a reagent for the Diels-Alder reaction, namely hexadec-8-yne instead of phenylvinylsulfoxide. This leads to the attachment of two heptyl chains at the “bottom” of the halfmoon. We chose heptyl chains because the alkyne starting material was commercially available and their length is similar to the octyl ones.

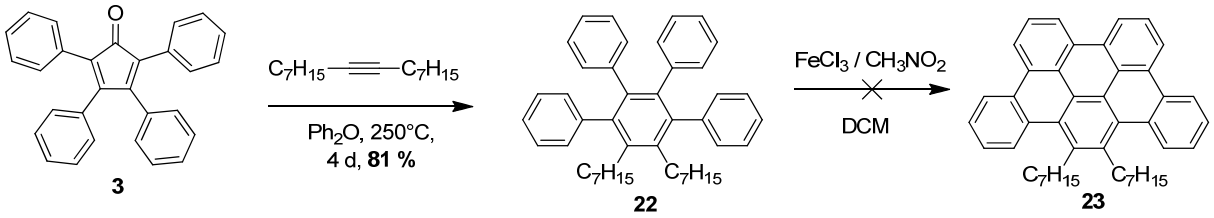

Fig. 30: Synthetic pathway to 15,16-diheptyltribenzopentaphene **23**

Reaction of the commercial tetraphenylcyclopentanone with the commercially available alkyne 8-hexadecyne as reactant requires a high temperature since the chosen alkyne is less reactive than phenylvinylsulfoxide.

After 4 days at 250°C, the red color had disappeared. The diphenylether was removed by distillation using a turbomolecular pump. After extraction and column chromatography using a 4:1 mixture of pentane and DCM, we obtained the desired product **22** in very good yield (81 %) as a bright white powder; structure confirmation was achieved by NMR and EI-MS.

Oxidation of **22** using $FeCl_3$ (see preceding sections) followed by precipitation with methanol, filtration on Millipore® (1 μm pore size) yielded an orange powder which emits a green fluorescence in solution. This green fluorescence does not correspond to the blue emission observed in the case of the other TBP derivatives.

The MALDI-MS spectrum of the material hints to a mixture of compounds. The main peak at 770.20 m/z does clearly not correspond to the expected target molecule of mass 572.344.

As the sidechains are attached in the bay-region of the aromatic core, one could expect that this compound behaves differently from the other three derivatives. These chains probably interfere with the normal course of the oxidation reaction and therefore produce unknown compounds.

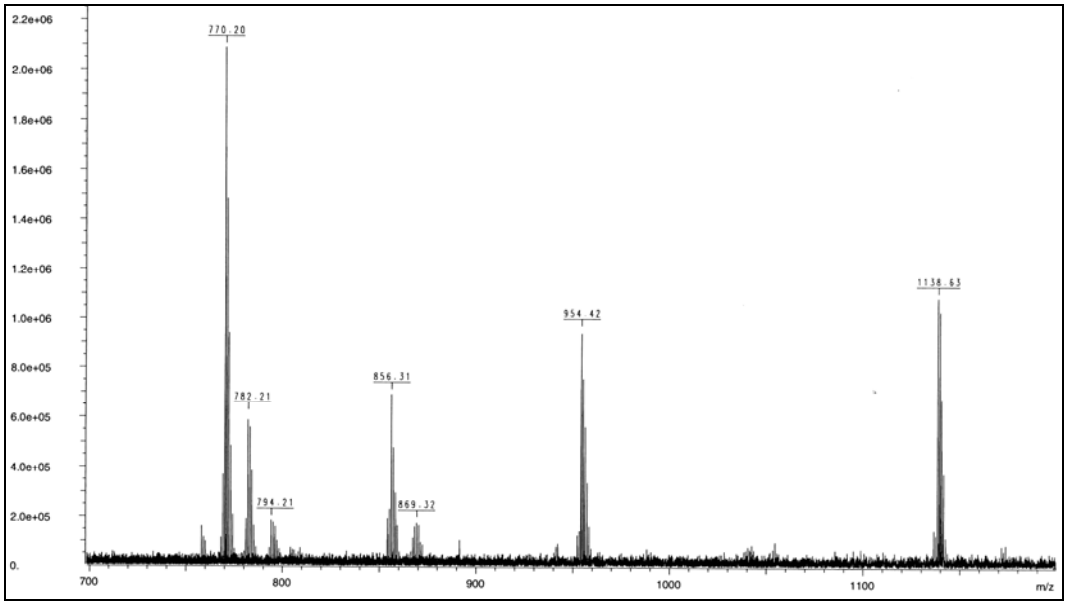

Image 6: MALDI-MS of the mixture after oxidation of **22**

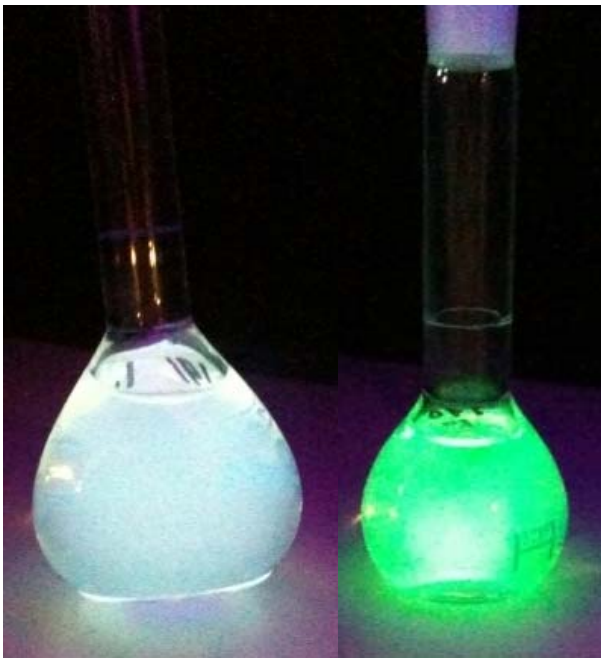

Image 7: Typical blue-white fluorescence of TBP derivatives (**21**, left) and green fluorescence of the mixture after oxidation of **22**

2.2.6 Tribenzopentaphene

In order to get a complete series of derivatives we decided to synthesize the unsubstituted aromatic core. The straightforward synthesis is displayed below.

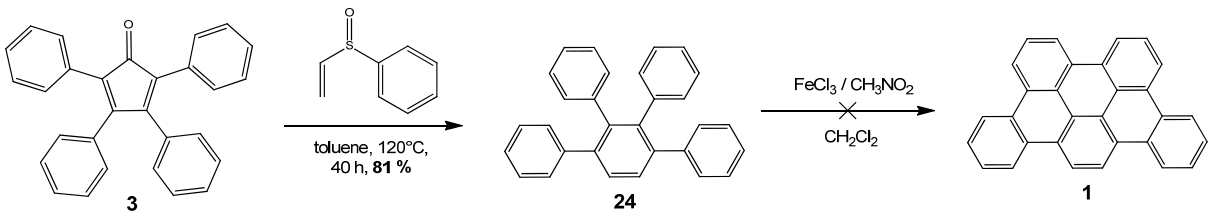

Fig. 31: Synthetic pathway to tribenzopentaphene

Reaction of commercially available tetraphenylcyclopentadienone **3** and phenylvinylsulfoxide in refluxing toluene for 40 h yields after extraction and column chromatography using a 1:1 mixture of pentane and DCM pure 1,2,3,4-tetraphenylbenzene **24** in good yield (81 %); NMR and EI-MS confirmed the structure of the target substance.

The oxidation step involves the same conditions as before, however immediately after the addition of the first drops of iron(III)chloride in nitromethane an insoluble material sticks to the wall of the reactor.

After complete addition (2 h) the solvents were removed by rotary evaporation. The resulting black material is insoluble in common solvents like DCM, ether, acetone, chloroform, ethyl acetate, etc. Even hot sulfuric acid was not able to dissolve any of the material.

A sublimation attempt was likewise unsuccessful as nothing sublimed even at 10^{-5} mbar (turbomolecular pump) and 250°C (oven limit).

2.2.7 Conclusions on the halfmoon shaped derivatives & conformational studies

Looking at the UV and fluorescence spectra we can conclude the following:

- The HOMO-LUMO gap can be estimated roughly at 385 nm which corresponds to 3.22 eV.
- These values do not correspond to the value of 478 nm (2.59 eV) calculated by Ruiz-Morales [121].
- Therefore our TBP derivatives are not suitable for our applications such as FET, because the HOMO – LUMO gap is too high in energy.

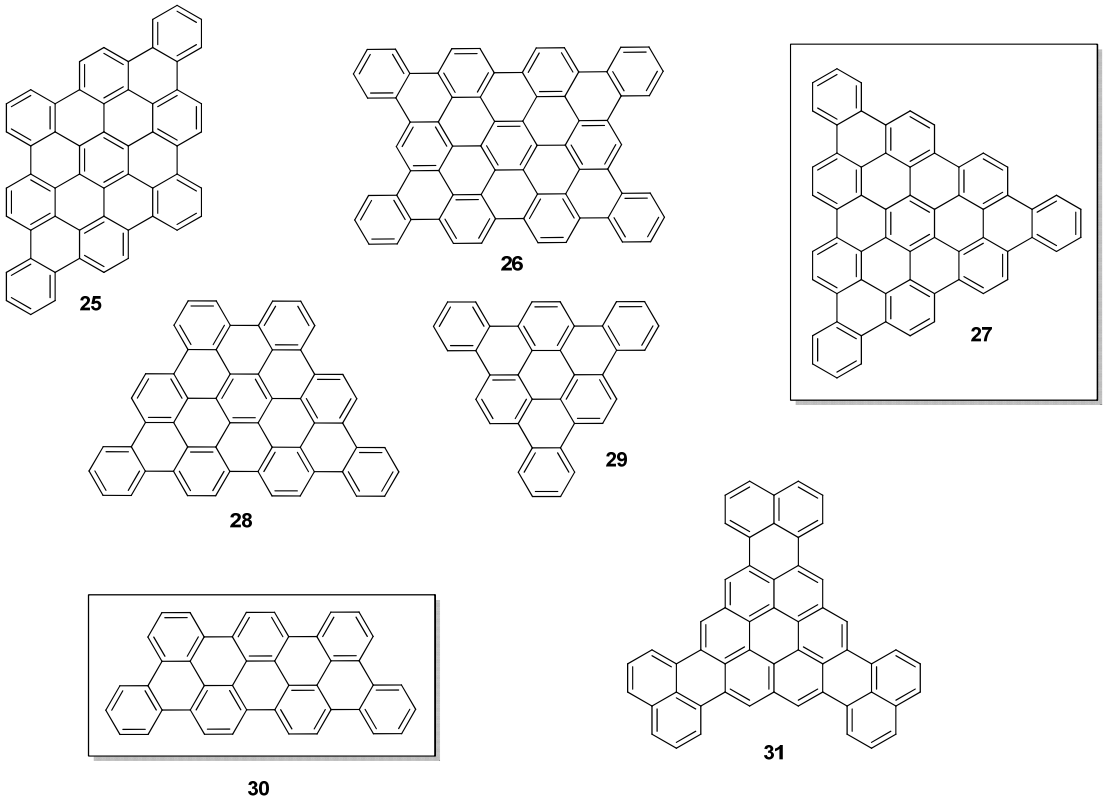

Fig. 32: Some of the possible PAHs. Our selected candidates are highlighted.

One therefore needs other molecules that meet the requirements set at the start of the work. We concluded that the ideal core must have at least the same number of aromatic rings as HBC but with a lower symmetry than HBC.

This is why we initiated a theoretical study of possible shapes for new PAH cores. In collaboration with Prof. Dr. Stefan Grimme at the University of Münster (Germany) a number of compounds were screened in a computational study (c.f. Annex).

The dispersion-corrected density functional theory (DFT-D) [125] has been used to optimize the geometries and calculate the energies of the compounds. After the geometry optimization the potential energy surface of the dimer has been calculated, keeping the monomers rigid. The energies were calculated after modifying the interplanar distance as well as the horizontal displacement. The structures corresponding to the local minima of the energy potential surface were fully energy minimized.
The results of those calculations are described below.

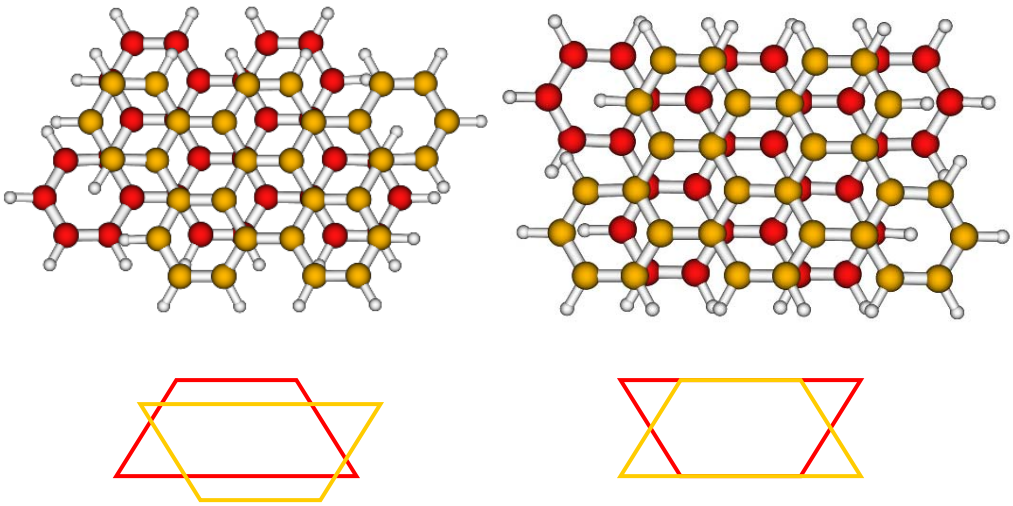

Fig. 33: The two most stable dimers of TBP

One can see that the most stable dimer of TBP and DBPH is the one where both molecules are turned by 180° with respect to the other, one is slightly laterally shifted, in the other dimer both molecules are almost aligned.

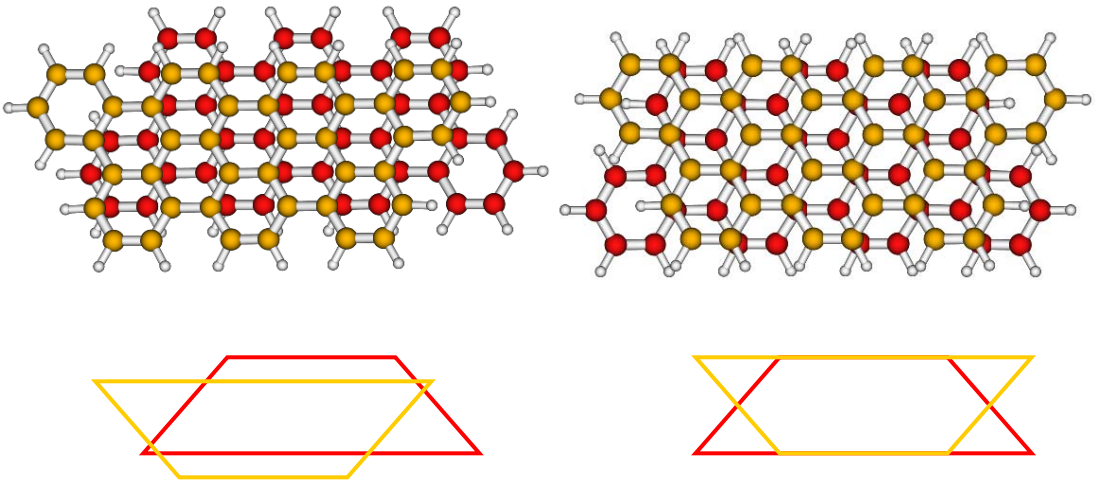

Fig. 34: The two most stable dimers of dibenzo-phenanthro-heptaphenes (DBPH)

Figure 34 shows that the most stable dimers for the elongated halfmoon shaped molecule are almost the same as the ones of the TBP. On one dimer the molecules are shifted laterally and on the second one, they are almost aligned.

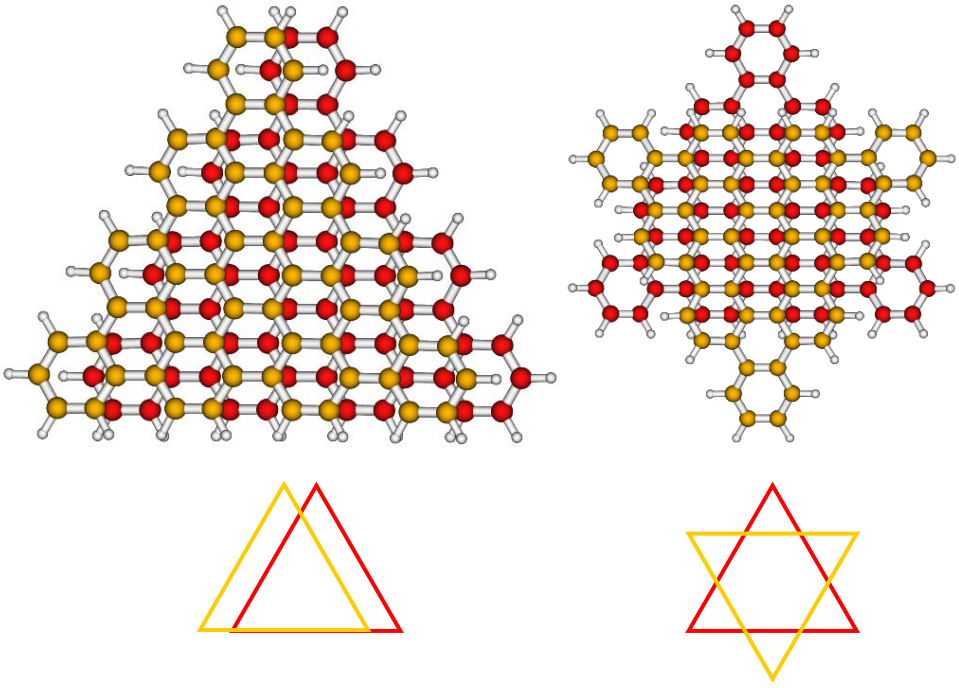

Fig. 35: The two most stable dimers of benzo[*o*]bistriphenyleno-ovalene (BBTO)

The two most stable dimers of the triangular BBTO cores are those who are slightly shifted laterally and the one which is turned by 60° with respect to the neighboring molecule.

For the continuation of our work we focused on two main candidates for a next generation core. The first consists of an “elongated” half moon shaped core which contains the same number of rings as HBC but could behave like TBP and stack edge-on onto a surface. The second candidate is a triangular shaped core structure, which according to the predictions by Feng and coworkers [126], should excel HBC as a charge carrier.

In parallel, P. Tondo from our group focuses on the synthesis of alkyl- and perfluoroalkyl chain bearing “meso-naphtho-trianthrones”, which can be seen as an aromatic core in rectangular shape [127].

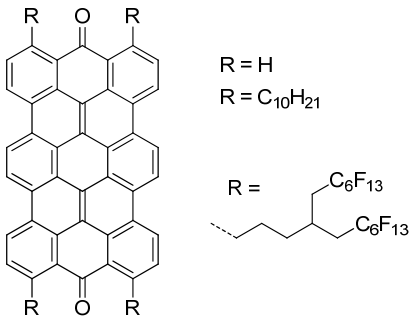

Fig. 36: Derivatives made by Tondo [127]

To influence their stacking, these core structures need sidechains. As seen in the thesis of Aebischer [111], perfluorinated sidechains favorably influence the stacking of the monomers. The best results were obtained using a mixed chain with 4 alkyl spacers and a 6 perfluorinated carbon tail ([core]-$(CH_2)_4$-$(CF_2)_6F$).

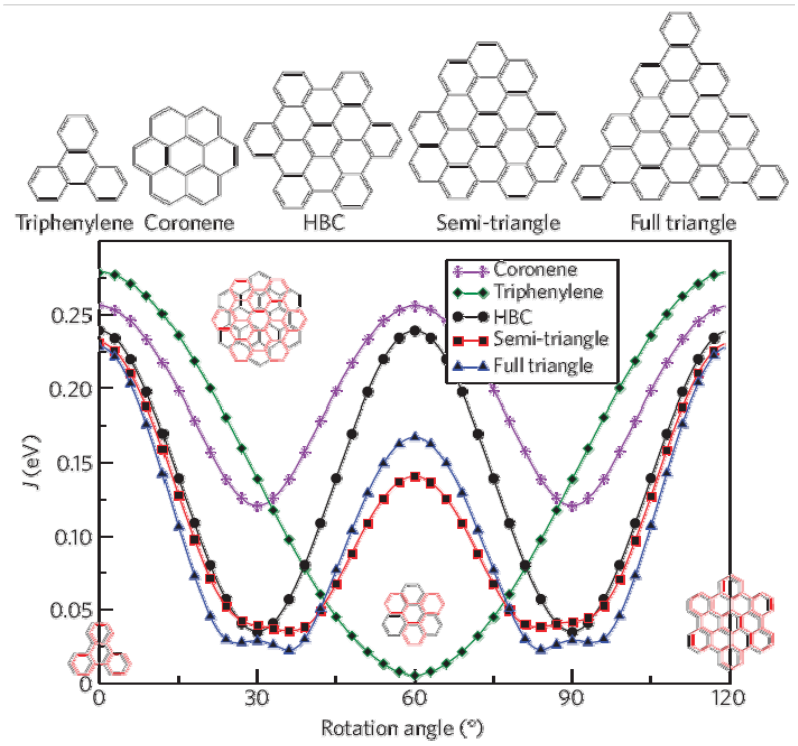

Fig. 37: Absolute value of the transfer integral *J* as a function of the azimuthal rotation angle. The distance between the dimers is fixed [126]

Since the space required by these chains exceeds the thickness of the core, these HBCs stack with a 30° angle in respect to each other. According to the predictions of Feng and coworkers [126], this arrangement lowers the charge carrier mobility (c.f. Fig. 37). On the other hand the perfluorinated sidechains are shown to prevent lateral aggregation much more than aliphatic sidechains.

As evident from figure 37, the *J* value for the full triangle (blue line) excels at 60° rotation all other structures which are forced by the sidechain interaction to stack at 30° like HBC.

In the next figure 38 the perfluoroalkylated sidechains are placed in ideal positions for the two new core structures. In these positions they should not influence the stacking of the cores (c.f. theoretical calculations).

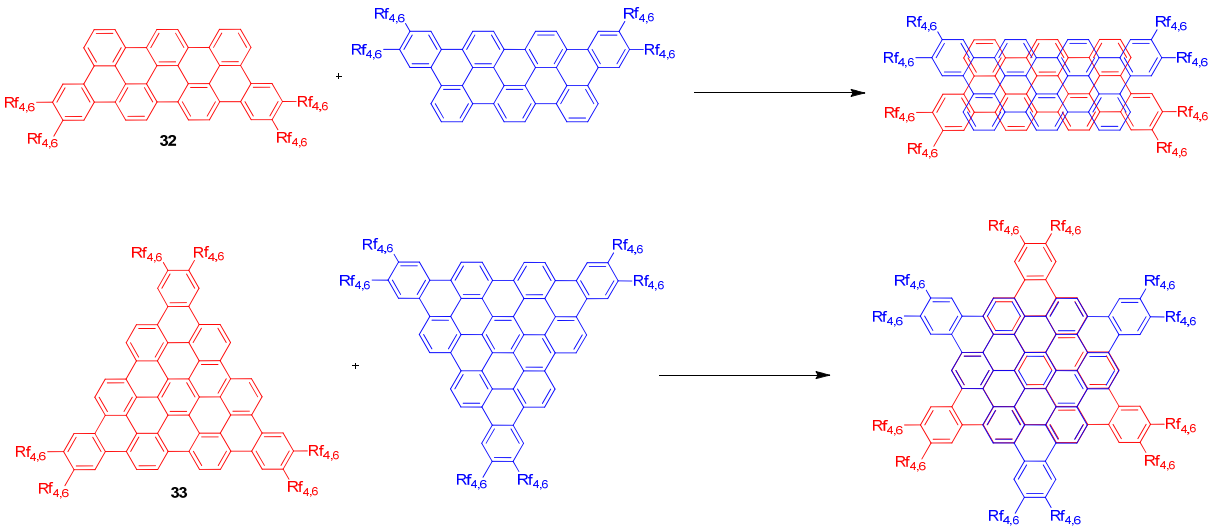

Fig. 38: Possible stacking pattern of perfluoroalkylated PAHs

The stacks of the triangular molecules should be interesting because the sidechains are farther away from each other. The sidechains force the stacks into a 60° rotated position which enhances the charge – carrier mobility as it can be seen on the following graph [126].

A possible strategy for synthesizing these target molecules involves the three synthons in figure 39.

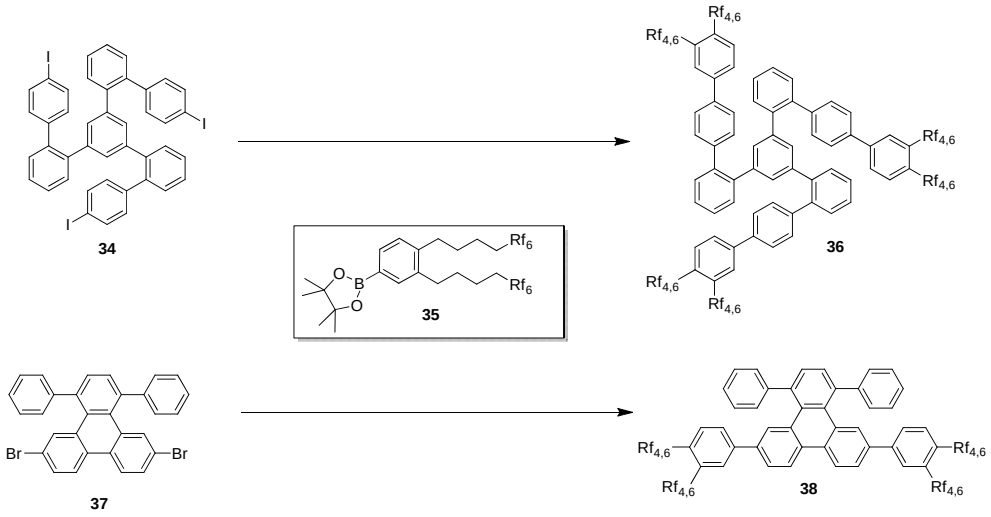

Fig. 39: Coupling of the sidechain bearing synthon **35** to the cores

2.3 Elongated halfmoon-shaped dibenzo-phenanthro-heptaphenes (DBPH)

2.3.1 Synthetic strategies

Route 1 would require a precursor with *ortho*-disubstituted aromatic cores. Two general routes could be envisioned for the synthesis of the DBPH structure. Besides the known synthetic problems expected for the repeated ortho-disubstitution, the compound **39** suffers from too many degrees of rotation since it can rotate around the C-C bonds and hence create rotamers which would give different core shapes upon oxidation (ring closing dehydrogenation).

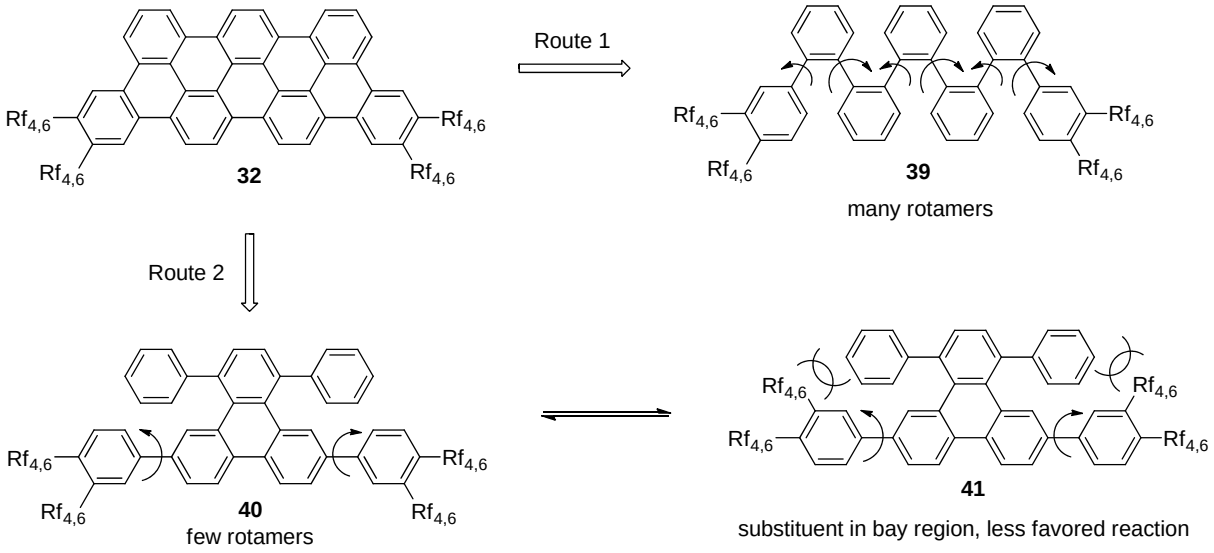

Fig. 40: Retrosynthesis for the oxidation – step

Route 2 involves a rigidified precursor on which the possible rotamers where the substituents are turned in the bay region are not expected to oxidize. We therefore concentrate on a strategy involving route 2.

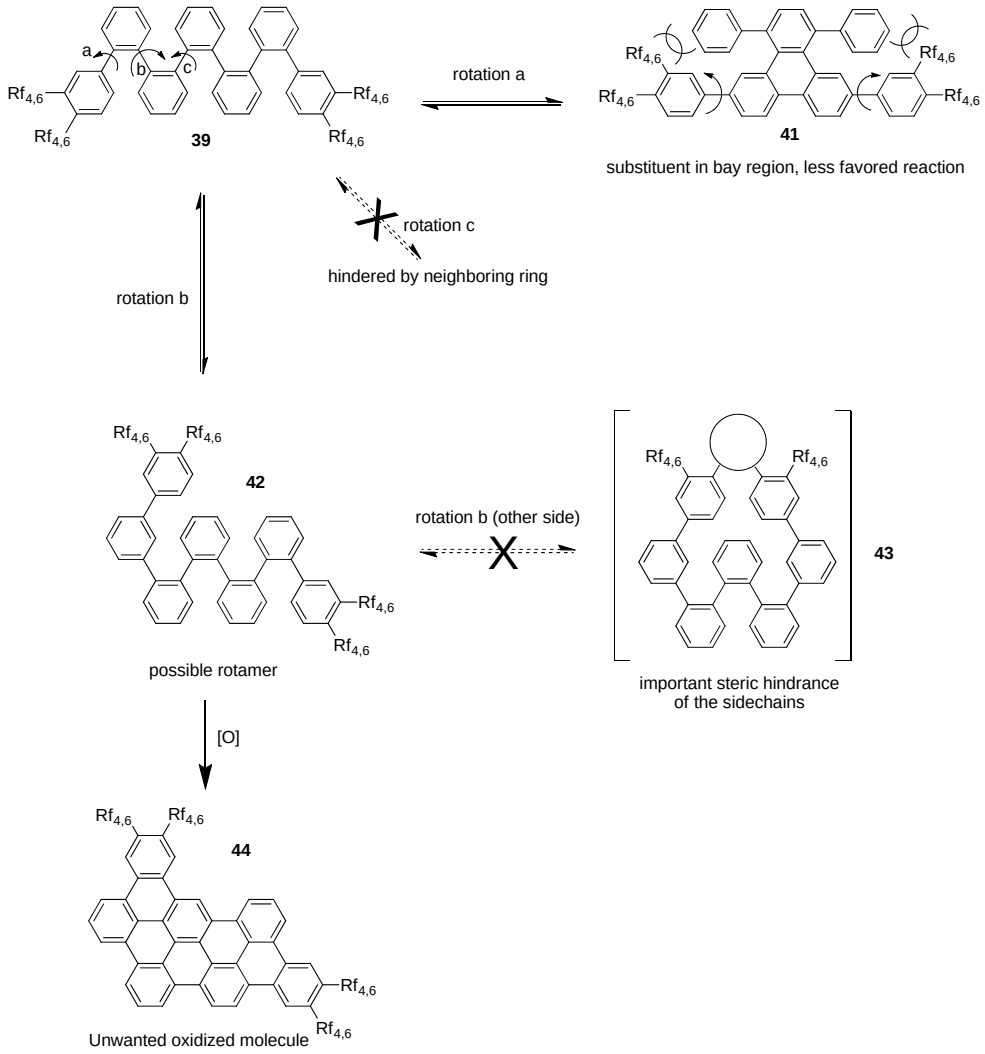

Fig. 41: Detailed study of the possible rotamers of **39**.

Figure 41 shows the possible rotamers of compound **39**. One can distinguish 3 different rotations marked “a”, “b” and “c”. Rotation “a” leads to the same compound as in figure 40 where the substituents are turned in the bay region.

Rotation “b” yields a possible rotamer **42** which can be oxidized to the unwanted compound **44**. From rotamer **42** two “a”-type rotations are possible but would not lead to an oxidized product due to the issue discussed before.

A rotation of type “c” is not possible due to the presence of an aromatic ring in *ortho*-position.

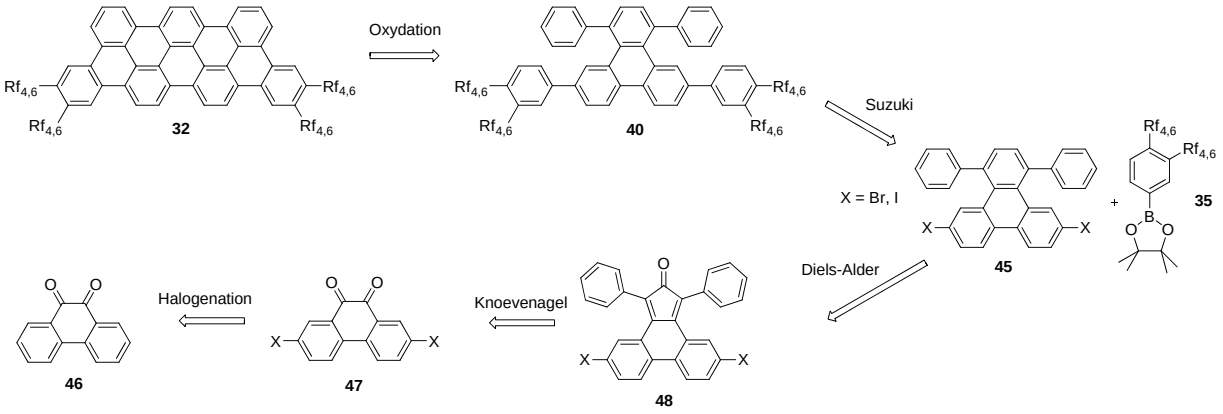

Fig. 42: Proposed retrosynthesis for the DBPH derivative. The synthon **35** bearing the sidechain will be treated later in the thesis.

The straightforward retrosynthesis points to the halogenated phenanthrenequinone **47** as starting material. This known compound is obtained by halogenation of 9,10-phenanthrenequinone **46**.

One could also consider synthesizing a simpler compound bearing only one alkyl or perfluoroalkyl sidechain on each side. The aromatic core precursor **45** would be coupled to a synthon consisting of an alkyl para-substituted phenylboronic acid. A simple alkyl chain would suffice as proof-of-concept.

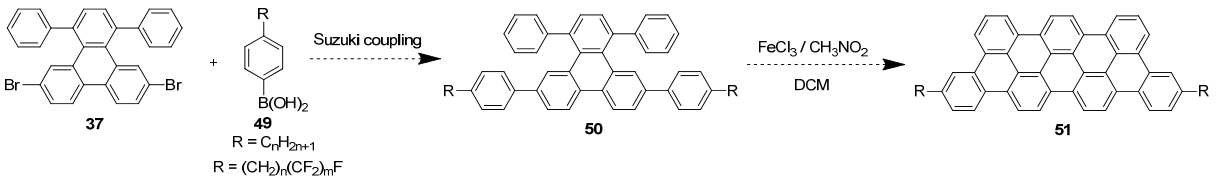

Fig. 43: Alternative strategy for a substrate bearing only two sidechains

It has to be shown that two sidechains are sufficient to increase the solubility in common organic solvents. The advantage of the oxidation step from **50** to **51** is that only one product will be formed due to the absence of possible rotamers.

2.3.2 Core synthesis

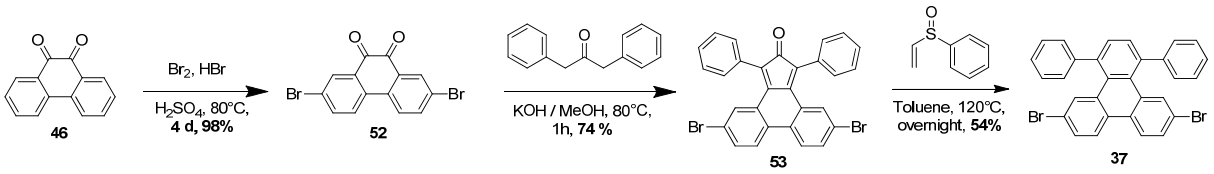

Fig. 44: Detailed synthesis of 6,11-dibromo-1,4-diphenyltriphenylene

This halogenation of phenanthrenequinone **46**, not well described in literature, requires very harsh conditions due to the high stability of the starting material. The following table summarizes the various tested conditions.

Entry	**46** [mmol]	Reactants	Solvent	Reaction time [h]	Temp. [°C]	Yield [%]
2.3.2.1	0.72	ICl (3.0 eq)	$CHCl_3$	24	RT	*
2.3.2.2	0.72	ICl (3.0 eq)	$CHCl_3$	24	60	*
2.3.2.3	0.72	I_2 (3.0 eq)	HNO_3	24	RT	*
2.3.2.4	0.72	I_2 (3.0 eq)	HNO_3	24	60	*
2.3.2.5	0.72	KI/KIO_3/HCl	MeOH/H_2O	24	RT	*
2.3.2.6	0.72	KI/KIO_3/HCl	MeOH/H_2O	24	60	*
2.3.2.7	0.72	$AlCl_3$/ICl	$CHCl_3$	24	RT	*
2.3.2.8	0.72	$AlCl_3$/ICl	$CHCl_3$	24	60	*
2.3.2.9	0.72	$AlBr_3$/Br_2	CH_2Cl_2	24	RT	*
2.3.2.10	0.72	$AlBr_3$/Br_2	CH_2Cl_2	24	60	*
2.3.2.11	0.72	NBS (2.3 eq)	H_2SO_4	24	RT	*
2.3.2.12	0.72	NBS (2.3 eq)	H_2SO_4/HBr	24	RT	*
2.3.2.13	0.72	Br (cat.)	H_2SO_4/HBr	24	RT	**~10**
2.3.2.14	0.72	Br (cat.)	H_2SO_4/HBr	24	80	**85**
2.3.2.15	11.0	Br (cat.)	H_2SO_4/HBr	24	80	**92**
2.3.2.16	24.0	Br (cat.)	H_2SO_4/HBr	96	80	**98**

* Only starting material was recovered

Table 2: Halogenation reactions on **46** using different solvents and reactants

Initially different iodination reactions (entries 2.3.2.1 – 2.3.2.8) based on known general aromatic halogenation procedures, not designed for phenanthrenequinone were tried [128]. Since they were unsuccessful even at higher temperatures we turned our attention to the bromination (entries 2.3.2.9 – 2.3.2.12) [129 - 131]. These methods proved also to be not successful and we only recovered the starting materials.

Finally a patent [132] covering a similar reaction gave a hint for the conditions involving catalytical amounts of Br_2. A low conversion was observed at RT, but at higher temperatures a conversion of up to 98 % was achieved.

The ideal conditions proved to be a 1:1 mixture of sulfuric acid and HBr at 80°C. Since the reactants are very aggressive, we a heavy walled glass reaction container capped by Teflon® security seals.

As the reaction progresses, a dark orange precipitate appears at the walls of the tubes. The reaction vessel has to be cooled down and shaken every 5 hours in order to homogenize the mixture. After a total of 4 days reaction time, the reaction mixture was poured on ice. After extraction with DCM and washing with $NaHCO_3$ and water, one obtains the brominated compound **52** in excellent yield (98 %).

The following double Knoevenagel condensation step analogous to the one developed for the TBP in chapter 2.2 required some optimization, since the standard conditions failed to produce the expected product (c.f. table 3).

Entry	**52** [mmol]	Base	Solvent	Reaction time [h]	Temp. [°C]	Yield [%]
2.3.2.17	0.41	KOH (1.0 eq)	EtOH	0.2	80	*****
2.3.2.18	0.40	KOH (1.0 eq)	EtOH	0.6	80	**~10**
2.3.2.19	0.40	KOH (1.0 eq)	EtOH	1	80	**~10**
2.3.2.20	0.40	KOH (1.0 eq)	EtOH	6	80	**~15**
2.3.2.21	0.40	KOH (1.0 eq)	MeOH	0.2	80	**60**
2.3.2.22	3.55	KOH (1.0 eq)	MeOH	1	80	**74**

* Only starting material was recovered

Table 3: Knoevenagel condensations on **52** using different solvents and bases

As we show in table 3 the combination of methanol and potassium hydroxide is best for these reactants. The reaction is complete after 1 h, the product precipitates from the reaction mixture upon cooling. Filtration over Büchner yields the desired product as a green powder in good yield (74 %). The structure of the target compound was confirmed by NMR and MALDI-MS. The ^{13}C-NMR shows the quaternary carbon signals at 196.08 ppm for the C=O, 148.46 and 126.24 ppm for the carbons in the cyclopentadienone ring. Interestingly, the peak of the decarbonylated compound ($[M\text{-}CO]^{\bullet+}$) was found in the MALDI spectrum besides the peak of the target compound.

The next step is a Diels – Alder reaction, again similar to the one investigated for the TBP case. It involves phenylvinyl sulfoxide in toluene for 14 hours under inert atmosphere and under light exclusion. The reaction is followed by the disappearance of the green color.
It appears that the starting material is thermally unstable. This requires a compromise between the reaction time and the temperature. The results are shown in table 4.

Entry	**53** [mmol]	Phenylvinyl sulfoxide [eq]	Solvent	Reaction time [h]	Temp. [°C]	Yield [%]
2.3.2.23	0.19	1.5	Toluene	24	80	*
2.3.2.24	0.19	1.5	Toluene	96	80	*
2.3.2.25	0.19	1.5	Toluene	24	120	**51**
2.3.2.26	1.85	1.5	Toluene	14	120	**54**

* starting material decomposed, traces of target product detected

Table 4: Diels - Alder conditions with **53** at different temperatures and reaction times

As the reaction is done under inert atmosphere and under light protection, decomposition of the starting material **53** by atmospheric oxygen or light can be excluded. Dennis and coworkers have shown that an analogue to **53** is heat sensitive and begins to decompose above 70°C [133].
There seems to be a concurrence between the decomposition reaction of the starting material and the Diels-Alder reaction itself. Increasing the temperature accelerates the decomposition process. The DA reaction needs a higher temperature than 80°C to be initiated.

Heating at a too high temperature would decompose the starting material faster than the reaction could happen. Doing the reaction at a lower temperature will decompose the starting material before it can react with the dienophile.
This is why a temperature of 120°C has to be chosen for this reaction leading to a yield of around 55 %. The small yield difference of 3 % in the last two entries could be explained by the fact that the last entry was made on a larger scale and less product was lost during the workup.
The structure of compound **37** was confirmed by NMR and MALDI-MS.

2.3.3 Suzuki coupling reactions and oxidation

With the core in hand a Suzuki cross – coupling test reaction of the core **37** with phenylboronic acid was done. The standard conditions involve tetrakis-triphenylphosphine palladium(0) as catalyst, K_2CO_3 as base and a mixture of water, ethanol and toluene as solvent. The reaction mixture is stirred at reflux for 3 days. After extraction with water one obtains the desired product in excellent yield (92 %). Again, the structure was confirmed by NMR and MALDI-MS.

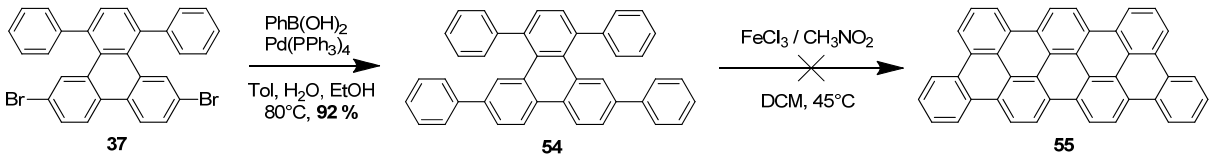

Fig. 45: Test reactions on **37**

Oxidation of **54** using the standard conditions involving $FeCl_3$ in nitromethane and DCM under a constant argon flow yielded a black powder, insoluble in common organic solvents, similar to the case of TBP reported previously. Neither an NMR nor an MS spectrum could be measured.

The coupling of the core precursor **37** to a newly commercially available boronic acid bearing one alkyl chain was then tested. The Suzuki crosscoupling was done under the same conditions as developed above. The starting materials were dissolved in a Schlenk vessel in a 5:1:1 mixture of toluene, water and ethanol. Tetrakis-triphenylphosphine-palladium(0) was used as catalyst and potassium carbonate as base.

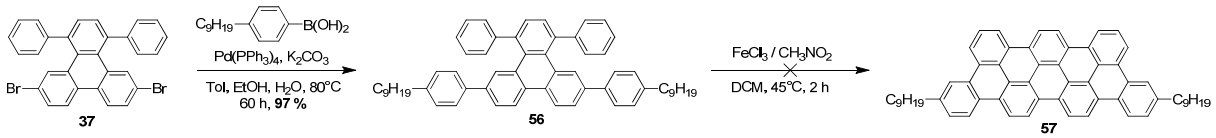

Fig. 46: Coupling of an alkyl chain bearing synthon on **37** and the subsequent oxidation

The mixture was then refluxed for 2.5 days. After washing of the mixture using water, the organic phases were dried and reduced *in vacuo*. The mixture was then poured over a short silica gel plug using a 9:1 pentane / DCM mixture. The target product was obtained in excellent yield (97 %) as colorless viscous oil, which exhibits blue fluorescence. The structure was confirmed by NMR and MALDI-ICR-MS.

The subsequent oxidation was carried out in a similar way as described in the chapters before. The starting material **56** was dissolved in DCM and treated with iron(III)chloride in nitromethane at 45°C. After cooling and quenching with methanol, a brown precipitate was observed which was then filtered several times on a Millipore® filter (1 µm pore size).

MALDI-ICR-MS measurements indicate that a partially oxidized compound is formed. The peak of the main compound has a mass of 780.49 which is 4 m/z more than the desired compound. The main peak designates a compound where only 2 of the 4 C-C bonds have been formed and the molecule was only oxidized partially.
When looking closely at the spectrum, also a small amount of a compound (mass 778.48 m/z) can be found. This corresponds to the molecule which was oxidized one step further than **58** but which is still not fully oxidized.

Resubmitting the mixture containing compound **58** to the same conditions as well as increasing the amount of iron(III)-chloride did not yield the desired product. It has to be seen in a future work if the addition of perfluorinated chains to the precursor molecule **56** influences the oxidation.
No valid NMR spectrum could be obtained due to the low solubility of the compound in common organic solvents.

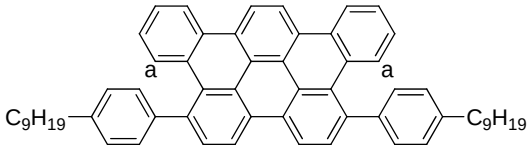

58

Fig. 47: Probable structure of the compound obtained by oxidation of **56**

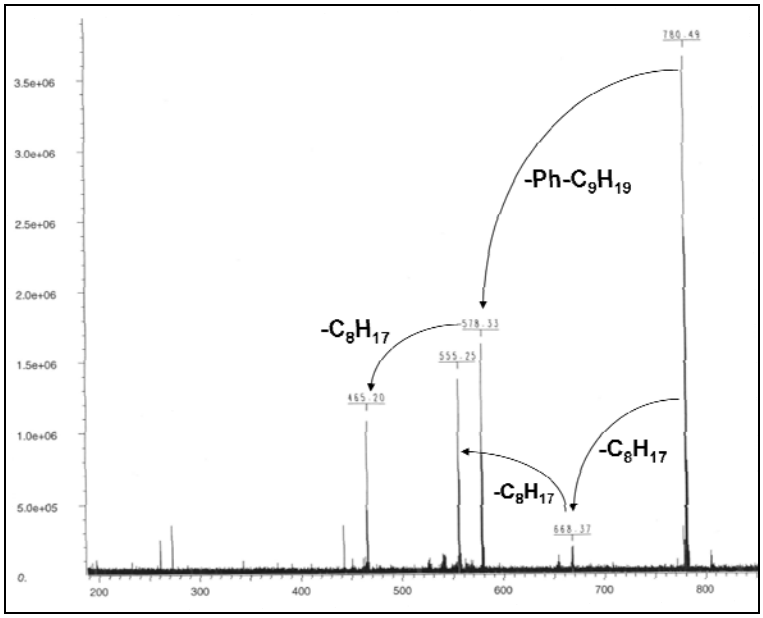

Fig. 48: MALDI-MS spectrum of the partially oxidized compound **58**

The MALDI-MS spectrum indicates that the main product loses parts of the alkyl sidechain as well as a phenyl ring upon MALDI-ionization.

Another indication for the structure of the partially oxidized compound is that its UV spectrum is similar to the ones of the TBP derivatives, characterized by absorption peaks at 310, 352 and 372 nm. At a closer look, compound **58** is a TBP derivative bearing two supplementary phenyl groups at positions 5 and 10.

The NMR spectra were not conclusive, the hydrogen labeled (a) (c.f. Fig. 47) should have a displacement around 5 ppm due to the shielding of the aromatic ring below but could not be found on the ^{1}H-NMR spectrum, but the MALDI spectrum strongly suggests that product **58** is formed.

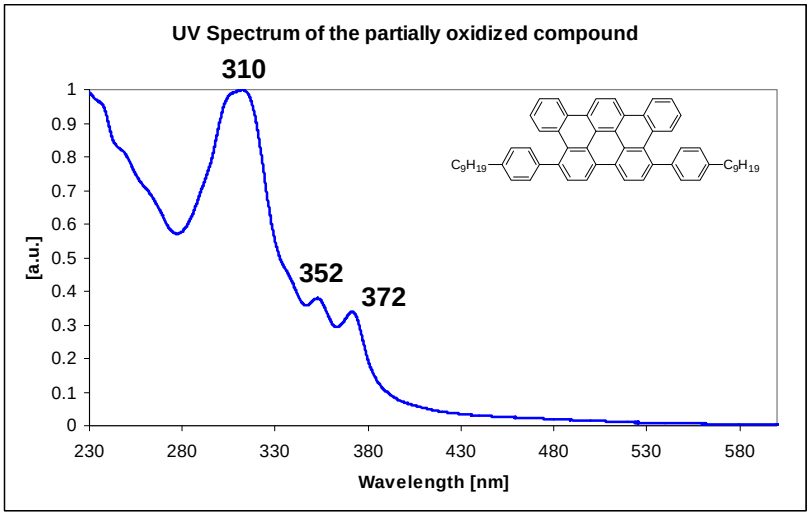

Fig. 49: UV / VIS spectrum of the partially oxidized compound **58**

2.4 Triangular shaped benzo[*o*]bistriphenyleno-ovalene (BBTO)

This section focuses on the synthesis of a triangular shaped polycondensed aromatic hydrocarbon. First we will analyze the problem by retrosynthesis and then discuss the steps of the chosen synthesis.

2.4.1 Strategy studies

The last step in any synthesis is the oxidation step. At a first glance we can identify three possible precursors. As the target molecule is C_3 symmetric we take this into consideration in the analysis. All HBC and related structures were formed so far by ring closing cyclodehydrogenation of a suitable network of linked oligophenyl derivatives.

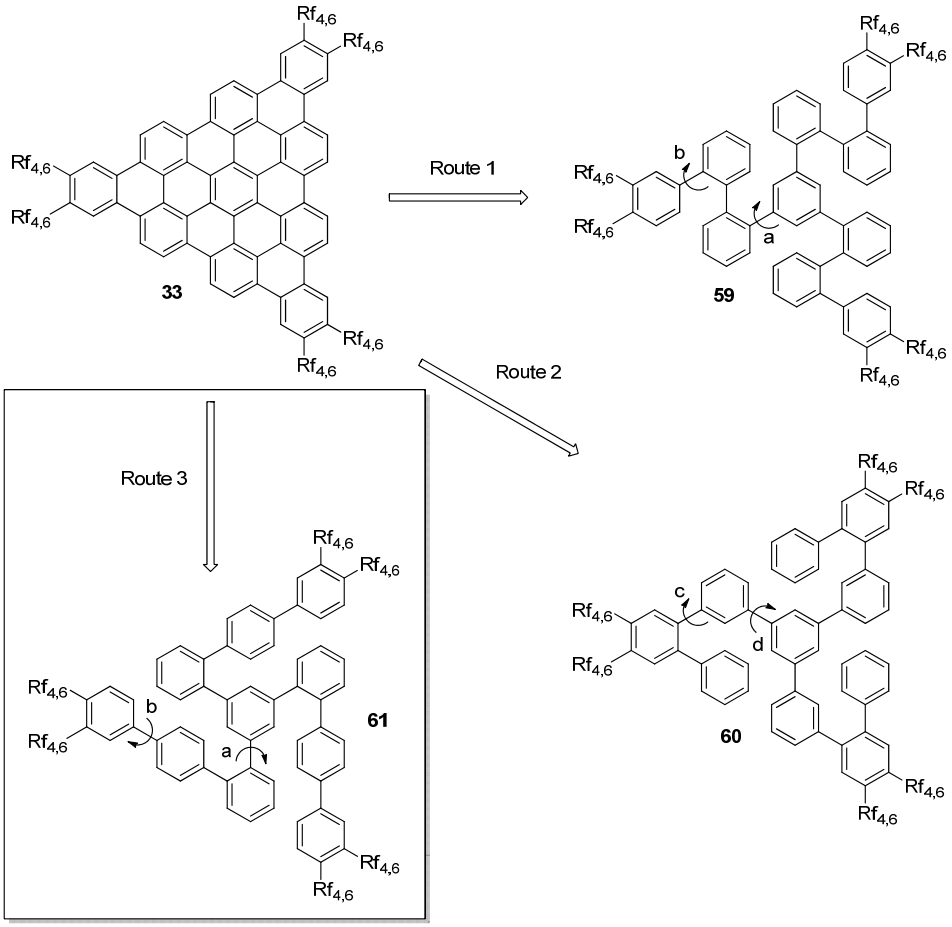

Fig. 50: First step of the retrosynthesis for the triangular derivative with the C-C bond rotation axis

At the oligophenyl stage, the aromatic rings can freely rotate around the Ar-Ar bonds, as depicted in figure 50.

The rotations labeled “a” are not critical, since the first bond forming reaction in **59** or **61** freezes this type of rotation in the two remaining branches in the central benzene ring.
The rotations labeled “b” are not critical either, since only the depicted orientation could lead to an aryl-aryl connection, since the other rotamer would force one of the two sidechains in a bay position similar to the TBPH case discussed earlier (c.f. Fig. 52 structure **33a**).
The rotation of type “c” in **60**, however, presents a problem since it could lead to an intermediate which is no longer capable of further connecting the three wings on the central benzene ring.

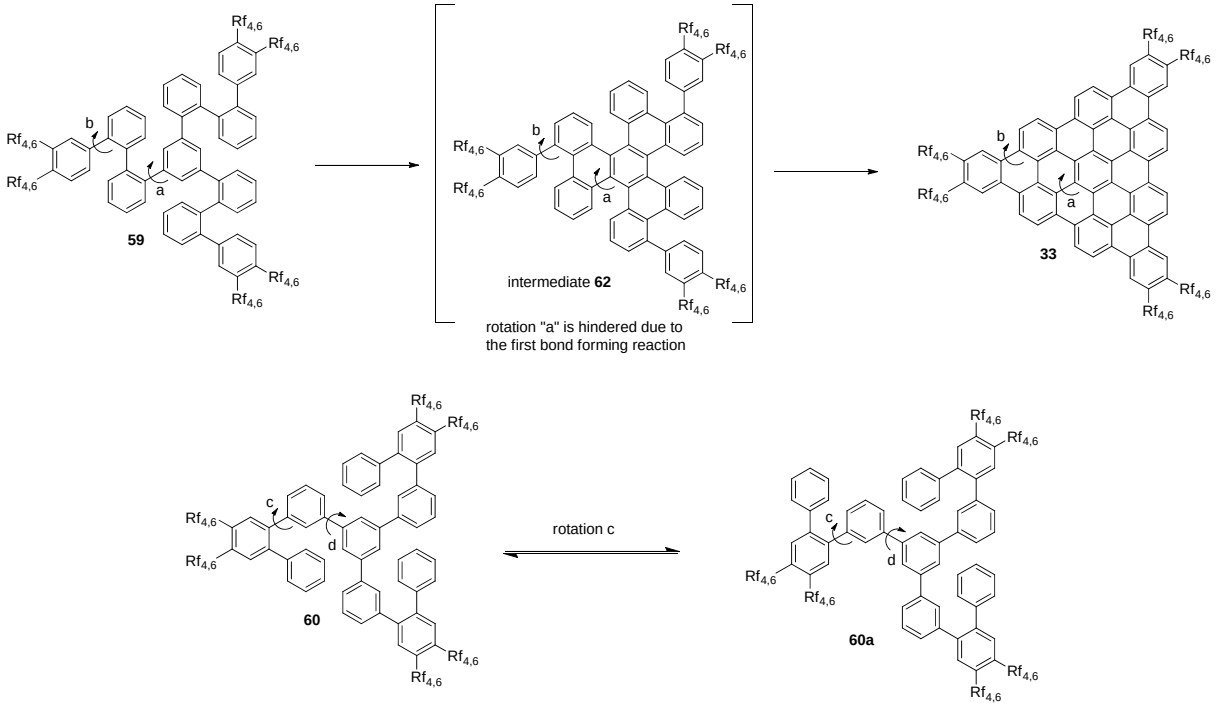

Fig. 51: Detailed description of some rotamers of **59** and **60**

Rotation “d” finally is again not critical, since it would only come into play at a stage where the rings are already internally connected. These considerations rule out route 2.

All these routes require a 1,3,5-trisubstituted central ring. Routes 1 and 3 in addition call for an *ortho*-disubstitution, which is known to present problems. Since route 1 requires a second *o*-disubstitution in each wing, we will therefore choose the route 3 for our strategy.

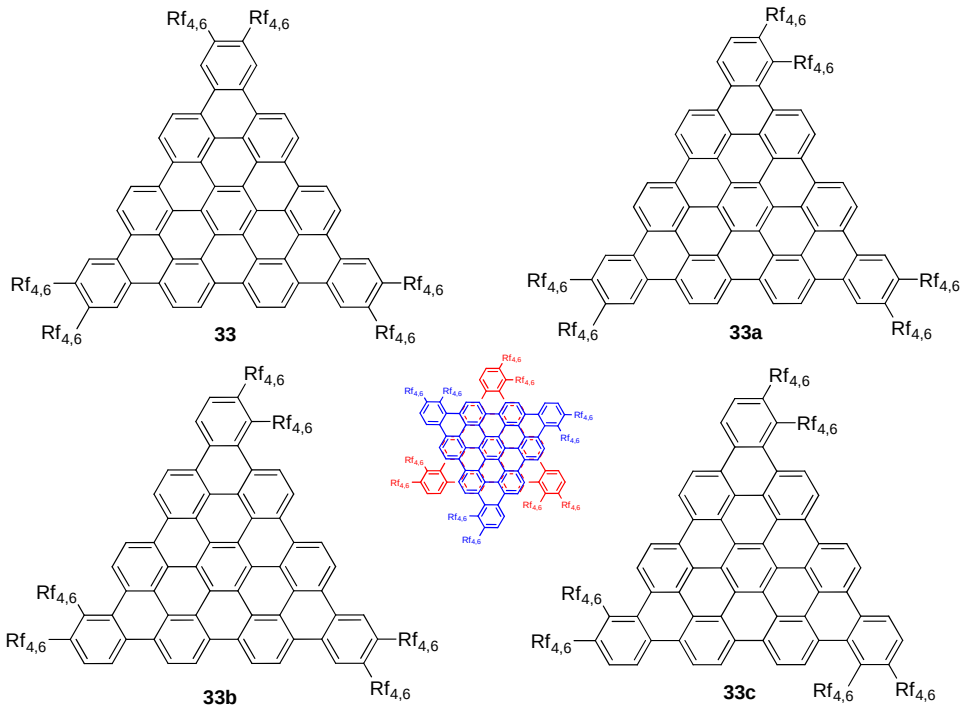

Fig. 52: Possible rotamers of the triangular derivative **33** using route 3

Considering that we take the synthetic route 3 we can now design the rest of the strategy of the derivative. We will design it in a way that the sidechain bearing synthon **35** can be used on both cores, the one of the elongated halfmoon and of the triangular derivative.

For simplicity reasons we will consider that only the target molecule **33** is formed and omit the possibility of rotamers.

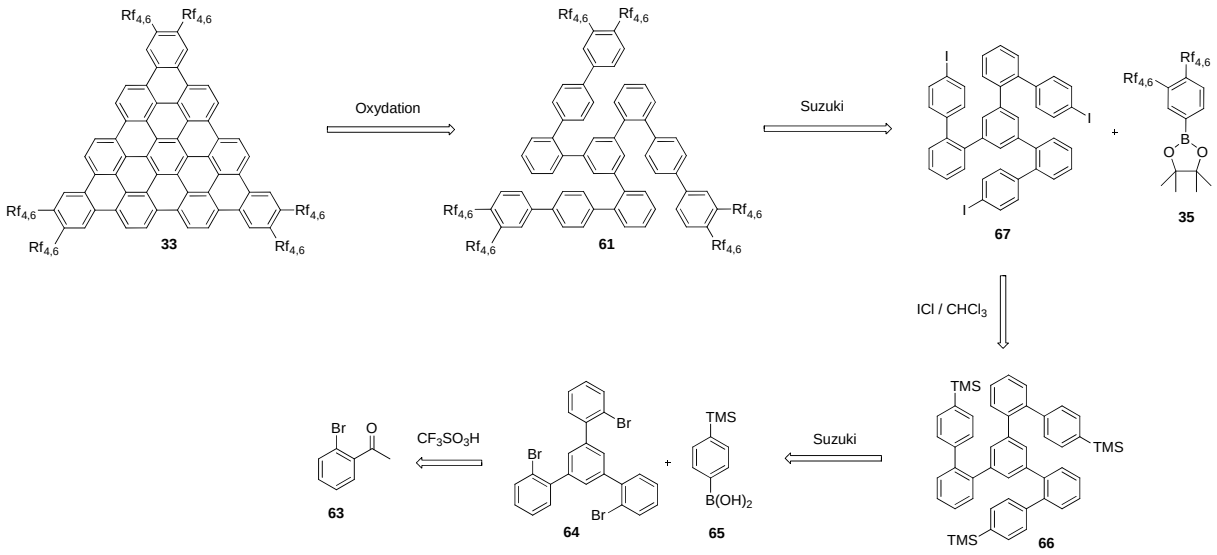

Fig. 53: Retrosynthesis for the triangular BBTO derivative

As one can see on the preceding figure the synthesis involves an acidic trimerization of 2'-bromoacetophenone **63**, followed by a Suzuki crosscoupling reaction at the hindered *ortho* position. A TMS-halogen exchange introduces iodine on the three aromatic *para*-positions which will allow inserting the sidechain bearing synthon. The final step will be the oxidation using iron(III)chloride.

2.4.2 Core synthesis for the triangular derivative

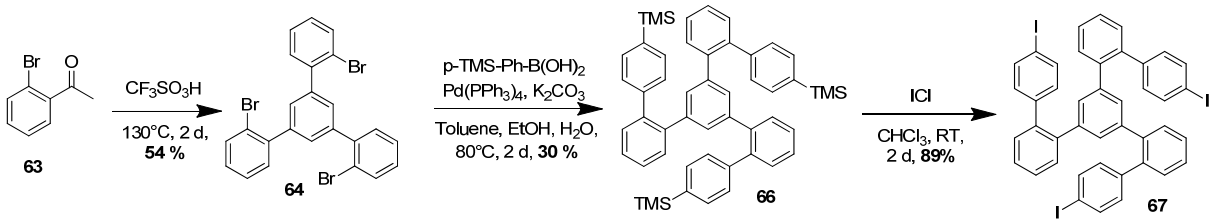

Fig. 54: Final synthesis for the core **67** of the triangular BBTO

The trimerization of 2'-bromoacetophenone **63** [134] is achieved by reacting 2'-bromoacetophenone with trifluoromethanesulfonic acid catalysis over 2 days at 130°C. After extraction from the black reaction mixture with DCM, washing with water and brine and purification by column chromatography using a 9:1 mixture of pentane and DCM, we obtain the desired trimer as a white powder.

The structure of the trimer is confirmed by NMR, EI-MS as well as X-ray diffraction. The ^{1}H-NMR signal of the protons on the inner ring of **64** form a singlet of integral 3 at 7.51 ppm.

The yield is not quite satisfactory (54 %) since the work-up is impeded by a black, polymeric substance which is not soluble in common organic solvents such as DCM, ether or acetone. This product sticks on silica and can be separated quite easily from our desired compound.
Trials in a microwave reactor were not successful due to the decomposition of the triflic acid.
An x-ray crystal structure of compound **64** was obtained and is shown below.

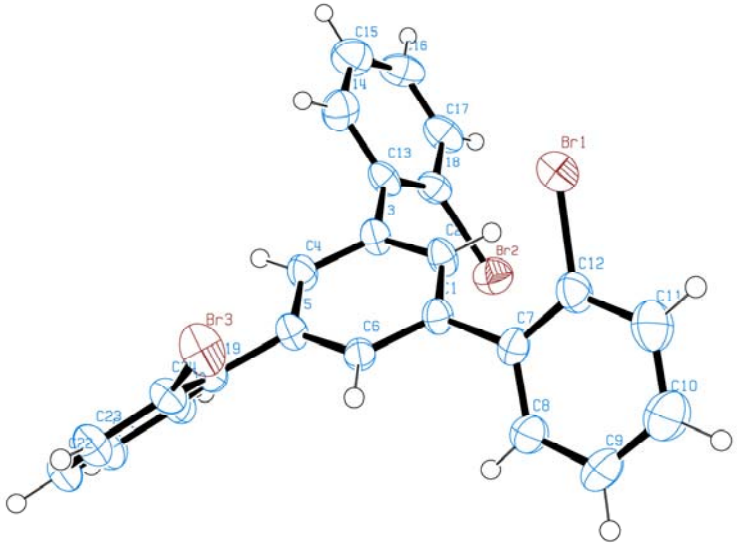

Fig. 55: X-Ray structure (ORTEP) of the trimer **64**

Compound **64** forms white triclinic crystals. The outer rings are twisted by 50 – 60° with respect to the center ring, the C-Br bond lengths are approximately 1.90 Å. The detailed crystallographic data is shown in the experimental part of this thesis.
The subsequent Suzuki crosscoupling reaction was the greatest challenge in this part of the synthesis. The bromine substituents are positioned *ortho* to the next aromatic ring, which hinders the insertion of the palladium catalyst.

In table 5, the principal efforts invested into this step are listed. For all preliminary trials phenylboronic acid was used as reactant.

Entry	**64** [mmol]	$PhB(OH)_2$ [eq]	Cat. [mol%]	Base [eq]	Solvent	Time [h]	Temp. [°C]	Yield [%]
2.4.2.1	0.25	3.6	$Pd(PPh_3)_4$ [0.03]	K_2CO_3 [10.0]	toluene	24	80	*
2.4.2.2	0.20	3.6	$Pd(PPh_3)_4$ [0.03]	K_2CO_3 [10.0]	toluene	24	120	*
2.4.2.3	0.20	3.6	$Pd(PPh_3)_4$ [0.03]	K_2CO_3 [10.0]	tol/H_2O	24	100	*
2.4.2.4	0.27	3.6	$Pd(PPh_3)_4$ [0.03]	K_2CO_3 [10.0]	tol/H_2O/EtOH	12	80	**25**
2.4.2.5	0.20	3.6	$Pd(PPh_3)_4$ [0.03]	K_2CO_3 [10.0]	tol/H_2O/EtOH	24	80	**30**
2.4.2.6	0.20	3.6	$Pd(PPh_3)_4$ [0.03]	K_2CO_3 [10.0]	tol/H_2O/EtOH	48	80	**30**
2.4.2.7	0.20	3.6	$Pd(PPh_3)_4$ [0.03]	K_2CO_3 [10.0]	tol/EtOH	24	80	*

* only starting material recovered

Table 5: Suzuki coupling on **64** using different solvents

As seen from these results the solvent mixture is crucial to this reaction. Using only toluene will not dissolve the inorganic base and therefore prevent any reaction. Adding water to the mixture and stirring the mixture vigorously dissolves the base but only the starting material is recovered.

Only upon the addition of ethanol to the mixture, a successful Suzuki coupling is observed. The low yield of 25 – 30 % is not ideal but sufficient for a test reaction. It seems that ethanol acts like a phase transfer agent for the base.
Longer reaction times did not increase the yield. After evaporation of the solvents, no other products were detected. We suppose that the boronic acid decomposes due to its sensitivity to water before it could react.

As the decomposition products are volatile, they evaporate as soon as the volume of the solvents is reduced *in vacuo*. No mono- or di-coupled product was recovered, so we assume that the reaction happens easily on all the positions.

After the successful test reaction we repeated the reaction using the commercial para-trimethylsilyl-phenylboronic acid under the conditions used in entry 2.4.2.6. Again a similar yield of around 30 % was obtained. Using $PdCl_2(PPh_3)_2$ as catalyst and NaOH as base did not improve the yield. Due to time constraints the conditions were not optimized further because the boronic acid is commercially available. Despite the low yield, we could rapidly obtain gram-scale batches of pure product **66**. The structure of the target compound was confirmed by NMR and EI-MS.

The Suzuki reaction using the same conditions as above also works in slightly better yields for meta-trimethylsilyl-phenylboronic acid. This gives access to C_3 - symmetric hexabenzocoronenes bearing three sidechains, a goal previously attempted by Aebischer in his thesis [111].

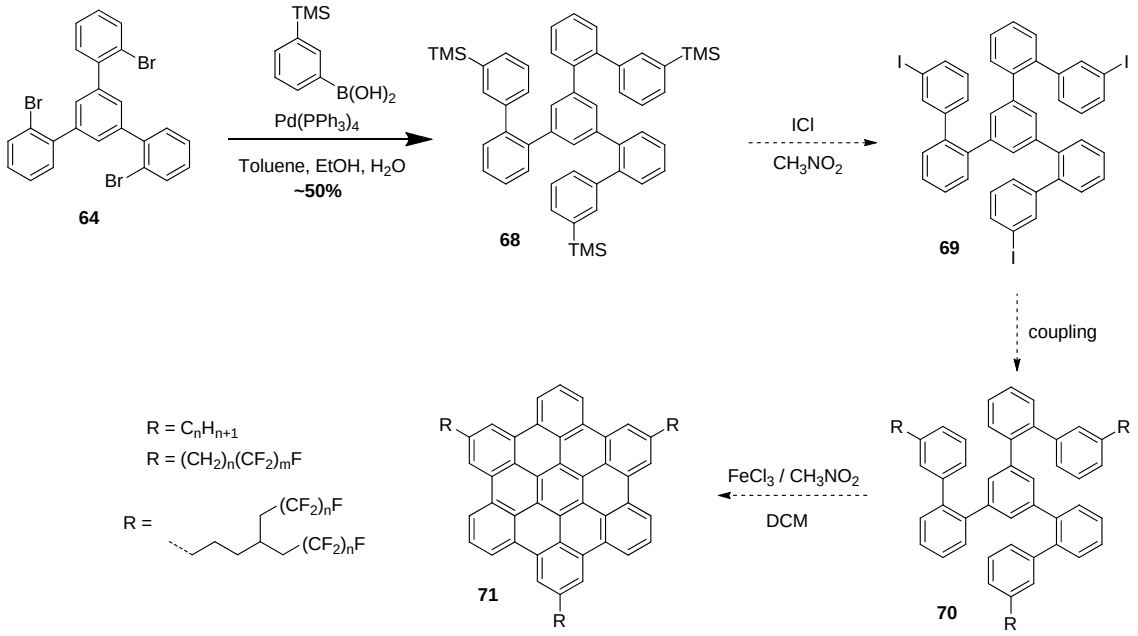

Fig. 56: Suzuki test-reaction on **64** giving access to C_3-symmetric HBC **71**

C_3-symmetric HBC bearing alkyl or perfluoroalkyl sidechains would be an alternative to the classical C_6-symmetric HBC **71**. A challenge in this synthesis would be the coupling step of the sidechains to the core [127]. As this is not a target molecule of our thesis, we will not pursue this synthetic path.

The next step is the halogen exchange of the three TMS groups into iodine in order to prepare the core for the coupling with the sidechain bearing synthon. The reaction conditions are quite straightforward. The *para* substituted tri-TMS core **66** is dissolved in chloroform and treated with iodine chloride and stirred at room temperature overnight. Extraction with water and precipitation by methanol gives the desired product in high yield (89 %), as confirmed by NMR and EI-MS. The previously mentioned ^{1}H-NMR singlet signal of the three protons of the inner ring can now be observed at around 6.7 ppm. Replacing the neighboring bromines by phenyl rings has induced an upfield signal shift.

2.4.3 Suzuki coupling reactions and oxidation

We also did a successful test coupling-reaction on the triiodo-compound **67** using phenylboronic acid as model compound for the sidechain bearing synthon. The oxidation of compound **72**, however, yielded only black insoluble material, comparable to the DBPH analogue.

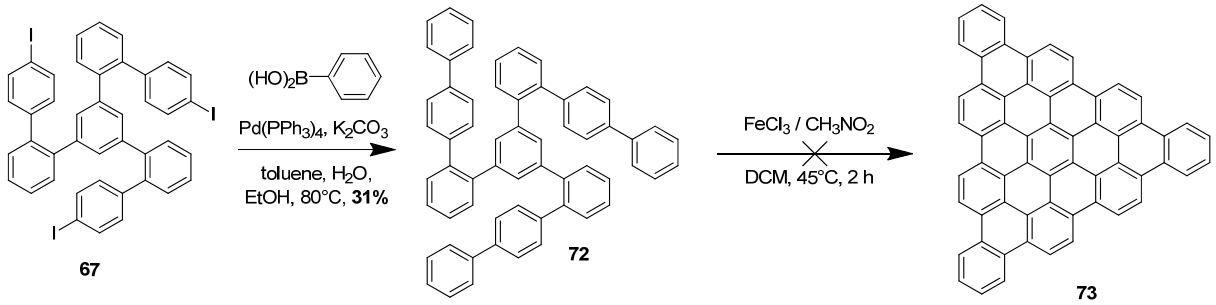

Fig. 57: Test-reactions on **67**

Judging from this test result we can predict that the coupling of a sidechain bearing synthon would probably work.

A possible alternative for obtaining soluble BBTO derivatives would be the use of a *para*-alkyl-substituted phenylboronic acid, similar to the one proposed for the DBPH derivative. A Suzuki crosscoupling reaction on **67** followed by an oxidation using iron(III)chloride would yield a single BBTO derivative **76** bearing three sidechains.

The specialty of this derivative **76** is that it has two enantiotopic faces. This could lead to interesting stacking properties as the single molecules can stack in a more or less orderly fashion. As face “A” is different from face “B”, the molecules could form stacks where all molecules have face “A” turned upwards. One could also imagine stacks where the faces alternate, e.g. ABABABA. A third type of stacks could form where there is no particular order like AABABBAABABBBAB. It has to be seen if those three types of stacks inherit different properties.

Therefore a Suzuki crosscoupling involving the commercial (4-nonylphenyl)boronic acid was carried out using the previously developed method. The starting materials as well as the $Pd(PPh_3)_4$ catalyst and the base (K_2CO_3) were dissolved in a 5:1:1 - mixture of toluene, water and ethanol. The reaction was refluxed at 80°C for 4 days. After washing with water and drying over $MgSO_4$, the organic phase was reduced *in vacuo*. The crude mixture was poured over a short silica gel plug using a pentane / DCM 9:1 mixture, giving the desired compound **75** in high yield (92 %) as colorless viscous oil, as confirmed by NMR and MALDI-MS.

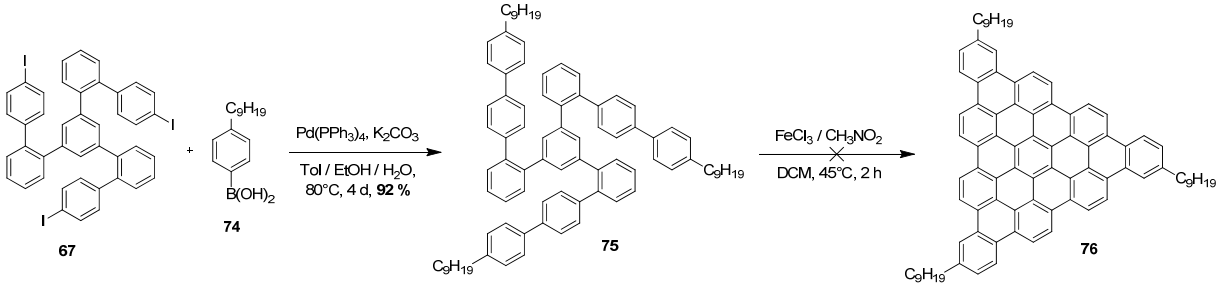

Fig. 58: Alternative pathway to a BBTO derivative

The following oxidation was carried out using the same conditions as described in the preceding chapters. The starting material **75** was dissolved in dry DCM. In a separate flask, $FeCl_3$ was dissolved in nitromethane and sparged with argon. This mixture was added dropwise to the solution containing the starting material at 45°C under a positive stream of argon. After stirring at this temperature for 2 h, the mixture is cooled down, quenched with methanol and stored in the fridge overnight. The brownish precipitate was filtered off by Millipore® (1 μm pore size).

Due to its low solubility, the precipitate was dissolved in a large amount (~1 L) of DCM and washed with water. The combined organic layers were reduced in vacuo giving 299 mg (44 %) of a brown powder. The MALDI-MS spectrum gives the main peak at 1122.61 m/z which corresponds to the fully oxidized compound. The compound exhibits a pale green-yellow fluorescence under a 366 nm UV-lamp (c.f. image 8 below).

Despite its three alkyl chains, the oxidized molecule is quite insoluble in common organic solvents (roughly $5 \cdot 10^{-4}$ M in DCM). Increasing the length of the sidechains would probably also increase the solubility. No NMR could be obtained due to the low solubility of the derivative.

Image 8: Fluorescence of a 10^{-4}M solution of supposed **76** in DCM under a 366 nm UV lamp

UV / VIS as well as fluorescence spectra were obtained from the supposed compound **76** and are shown below. The UV spectrum is characterized by a broad peak at 393 nm.

The fluorescence spectrum which was measured using an excitation wavelength of 393 nm corresponding to the UV absorption peak, shows distinct peaks at 450, 498 and 515 nm.

Due to the quite bad quality of the UV spectrum which could not be improved (broad bands as well as a hump around 470 nm), it is difficult to conclude any observations concerning the HOMO – LUMO gap of the compound. Rough estimations, if we assume that the UV and fluorescence spectra are valid, would put the gap around 420 nm (2.95 eV) which is similar to the one of Aebischer's HBC [111]. This value however, has to be considered carefully.

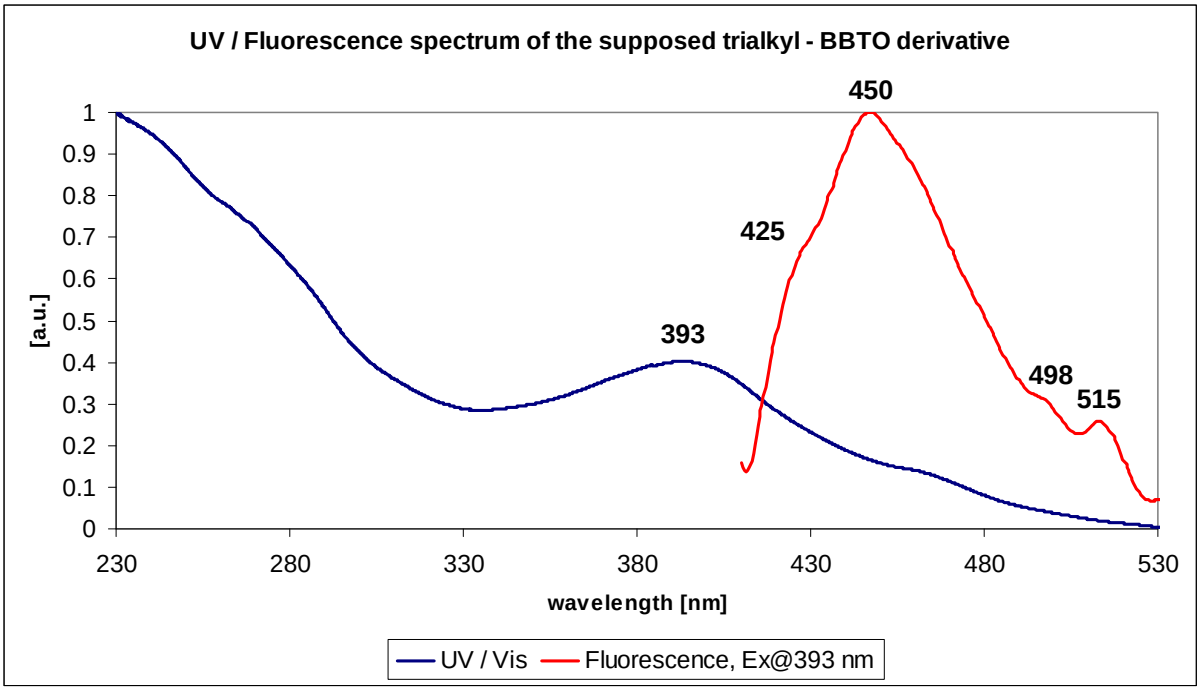

Fig. 59: UV / VIS and fluorescence spectrum of the supposed compound **76**, excitation wavelength 393 nm

A possible structure of the supposed compound **77** can be found below. If only 6 of the desired 9 C-C bonds have been formed, the compound would resemble to a HBC substituted by three alkyl rings. This structure would support the fact of the supposed HOMO – LUMO gap being similar to HBC.

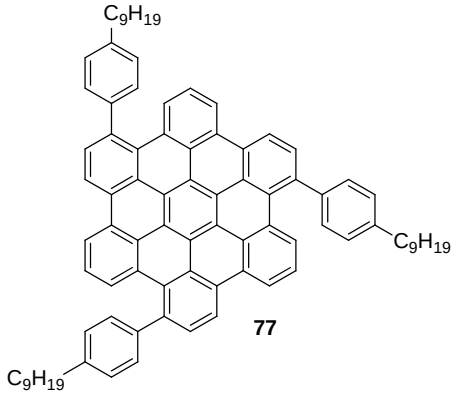

Fig. 60: possible structure of the obtained partially oxidized compound **77**

The correct mass indicated by the MALDI spectrum (c.f. chapter IV) could be explained by the fact that the ionization energy of the LASER beam of the instrument is sufficiently high to oxidize the molecule completely. No valid NMR spectrum could be obtained, also the UV spectrum is not well resolved. The final structure of the obtained compound remains therefore unknown.

Sadly the desired fully oxidized compound could not be obtained. The encountered problem of the incomplete oxidation of the BBTO- as well as of the DBPH-derivatives could possibly be resolved by using different oxidation methods. These issues have not been investigated in this work due to time constraints but could be addressed in future work on this subject.

2.5 Attempted synthesis of the sidechain-bearing synthon

2.5.1 Two linear perfluoroalkylated sidechains versus one branched sidechain

Aebischer first discussed in his thesis [111] the synthesis of branched perfluoroalkylated sidechains. The synthesis of these branched sidechains is more complicated and their coupling to the core is not straightforward.

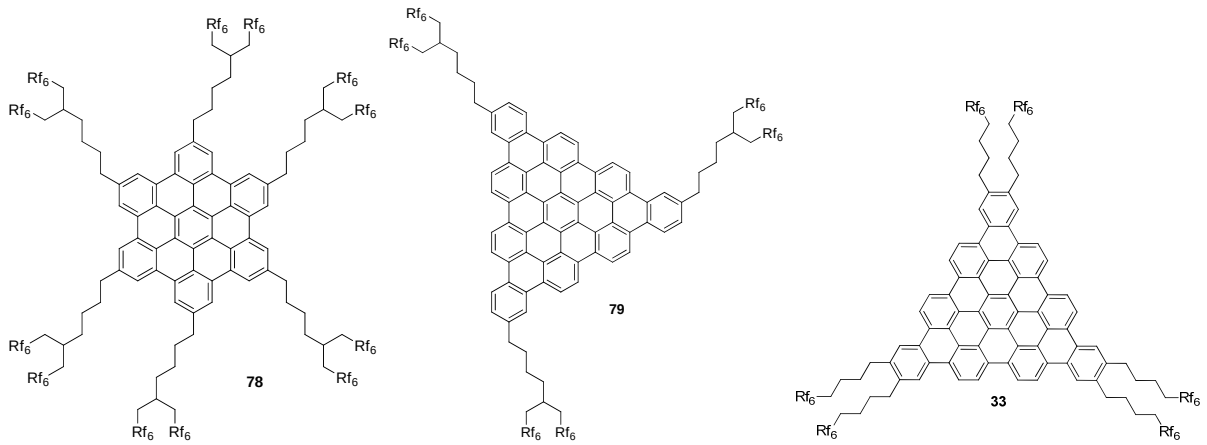

Fig. 61: HBC derivative bearing branched sidechains synthesized by Aebischer [111] (left), triangular derivative bearing branched (middle) and linear (right) sidechains.

As one can easily see that two branched sidechains side-to-side would be too cumbersome for the molecules. Regarding the stacking we can see that three branched sidechains would probably not be enough to induce the 60° twist in stacking between the neighboring molecules.

The solution using two linear sidechains instead seems the most favorable as the triangular derivative bearing branched sidechains **79** has two enantiotopic faces. The stacking was not calculated for derivatives bearing sidechains because the molecule would have been too big and would have required too large calculation times.

However an MM2 Energy minimization was calculated on the triangular derivatives using the Chem3D® program, the results are shown below.

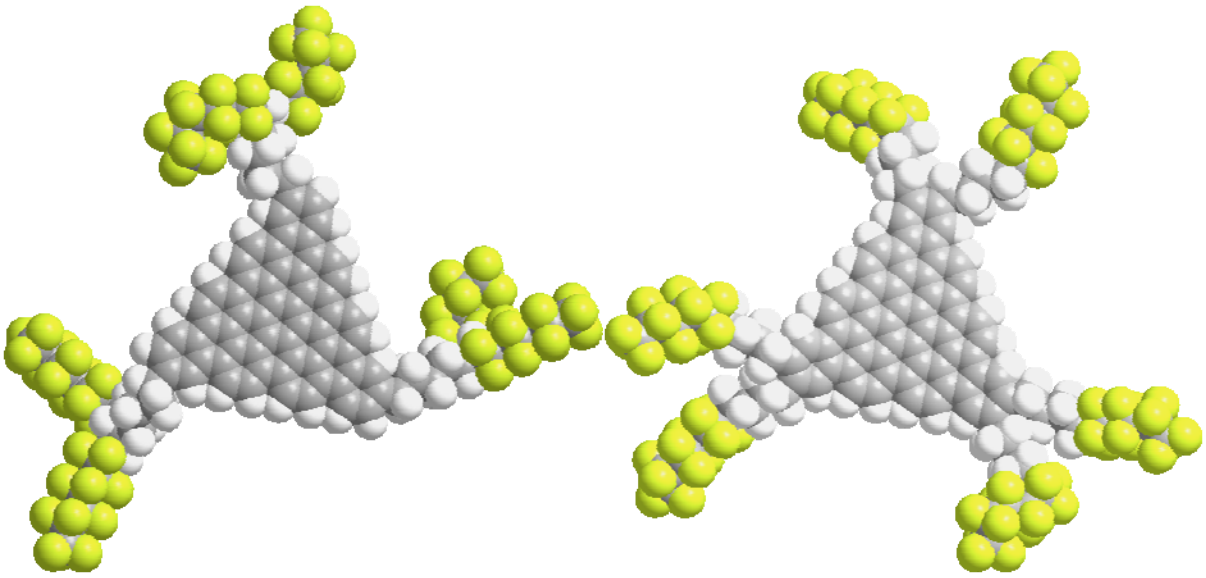

Fig. 62: MM2 energy optimized space – filling models (top view) of triangular BBTO derivatives bearing three branched **79** (left) and six linear perfluoroalkyl sidechains **33** (right)

One can observe from the figure above, that the perfluorinated parts of the chains (yellow) for the branched derivative are pushed away from one another in an angle greater that 90°.

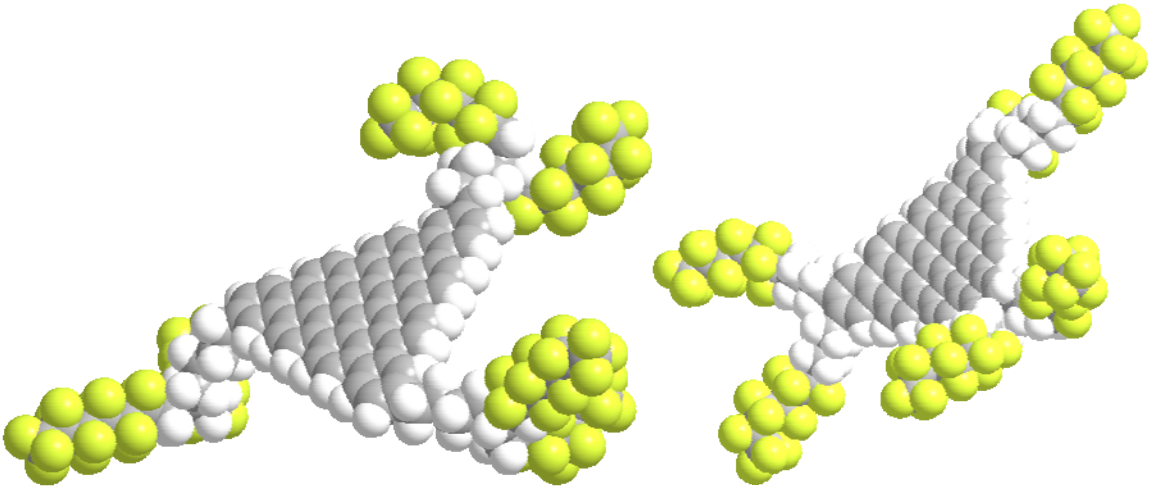

Fig. 62: MM2 energy optimized space – filling models (side view) of triangular BBTO derivatives bearing three branched **79** (left) and six linear perfluoroalkyl sidechains **33** (right)

From the side view one can see that the branched sidechains are more “out-of-plane” than the linear ones.

It is difficult to say *a priori* whether one or the other derivative has more optimal stacking. It has to be shown experimentally which one of these derivatives is most suitable for molecular electronics applications.

We chose to consider the derivative **33** bearing six linear sidechains which exhibits the higher symmetry than derivative **79** bearing three branched sidechains.

2.5.2 First strategy

The triangular core structure very much limits the number of carbon atoms at which solubilizing side chains could be attached without interference with the core structure and / or the π-π stacking.

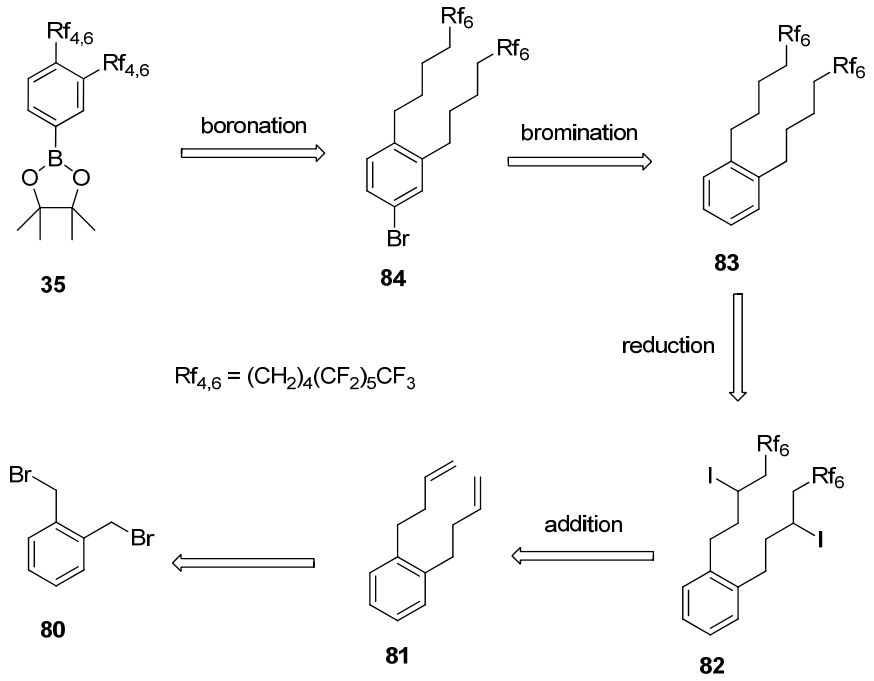

Fig. 64: Initial retrosynthesis of the sidechain-synthon

This plan requires the synthesis of a 1,2,4-trisubstituted benzene derivative with two sidechains in ortho – position. Since the core structure synthon carries halogen functions (c.f. chapters 2.3 and 2.4), the sidechain synthon should exhibit a boronic acid or ester, as the most reliable coupling reaction was found to be the Suzuki coupling (c.f. chapters 2.3 and 2.4).

The boronic ester is transformed using *n*-BuLi and 2-isopropoxy-4,4,5,5-tetramethyl-1,3,2-dioxaborolane. The next sequence of steps is similar to the one designed by Aebischer in his thesis [111]. The novelty of our strategy is that it is done on two sidechains simultaneously. The last respectively the first step of the synthesis is the attachment of allyl sidechains on α,α'-bromo-*o*-xylene **80** which is achieved by adding allylmagnesium bromide in diethyl ether.

The bromine on the aromatic ring has to be introduced after the reduction step using $LiAlH_4$ because not only the iodine on the sidechains would be removed but also the halogen on the aromatic ring upon reduction.

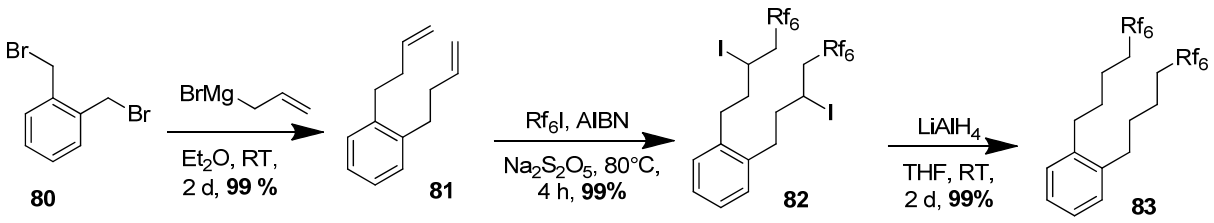

Fig. 65: First steps of the synthesis for the sidechain-synthon

The synthesis starts by attaching two allyl sidechains on an aromatic core. To achieve this, we added a 1M solution of allylmagnesium bromide in ether to a solution of the α-α'-dibromo-*o*-xylene in diethyl ether. After the end of the addition period the reaction mixture was stirred for 2 days while monitoring it by GC/MS. After acidic hydrolysis of the excess Grignard reagent and extraction with diethyl ether one recovers the desired product **81** as yellowish, transparent oil in almost quantitative yield, as confirmed by NMR and EI-MS. As the product was sufficiently pure it was used without further purification.
Trials were done by adding α,α'-bromo-*o*-xylene **80** onto the allylmagnesium bromide as reported by Lindner et al. [135] but this type of addition gave only a maximum of 50 % yield.

The following step is the addition of the perfluorinated part. The method is similar to the one of Aebischer [111] but on two sites simultaneously. The starting material **81** was treated with perfluorohexyliodide, sodium metabisulfite and AIBN at 80°C. Due to the short half – life of AIBN at 80°C one adds AIBN portionwise until the reaction is complete. The reaction was followed using ^{1}H-NMR and stopped as soon as all the starting material has been consumed.

The reaction is quenched by addition of water. After extraction with diethyl ether, the final product **82** is retrieved in almost quantitative yield. The structure was confirmed by NMR and EI-MS.
This product (as well as the following ones) has an extremely high vapor pressure and evaporates rapidly at room temperature. It seems to form azeotropic mixtures with non-polar solvents such as pentane or hexane. It coevaporates even while carefully distilling off these solvents. All these solvents have therefore to be avoided when handling or purifying these compounds.

Reductive removal of the iodines on the sidechains, a left over of the previous radical addition of perfluorohexyliodide is done by adding a solution of starting material **82** in THF dropwise onto a slurry of $LiAlH_4$, again followed by ^{1}H-NMR. After 2 days at room temperature, the mixture was quenched with water and NaOH. After extraction with diethyl ether, one obtains the desired compound **83** in almost quantitative yield; the structure was confirmed by NMR and EI-MS.
This product has a high vapor pressure too and should be treated with the same precaution as the compound of the previous step.

Parallel to the synthesis described before, we developed a method for brominating 1,2- alkyl – substituted aromatic rings. As a model – compound we chose the commercial 1,2-diethylbenzene. We discovered a method developed by Steele et al. [136] which uses elementary bromine in trimethylphosphate (TMP) on similar compounds. The challenge is just to add one bromine in the “4” position of the aromatic ring. Many methods will brominate the first position of the allyl sidechain (e.g. using NBS [137]) or install two or more bromines (e.g. with $AlBr_3$). This soft method has worked on our model compound after a few adjustments such as reaction temperature and time and we achieved yields reaching up to 91 %.

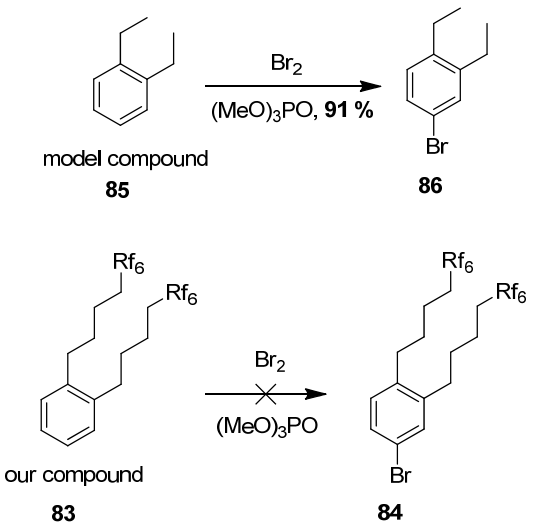

Fig. 66: Bromination of 1,2-substituted aromatic cores

As we transferred the conditions on the perfluorinated compound **83**, no bromination was achieved. We tried increasing the reaction temperature and time, the amount of bromine, heating by classical methods or by microwave, heating while sonicating using an ultrasonic bath.

We also tested the addition of perfluorinated co-solvents such as hexafluorobenzene (HFB) or α,α,α-trifluorotoluene (BTF). We could not achieve any bromination on the aromatic ring.

The table below lists the principal efforts made to brominate compound **83**.

Entry	**83** [mmol]	Reactants	Solvent	Time [h]	Temp. [°C]	Heating method	Yield [%]
2.5.2.1	0.73	Br_2	TMP	16 – 48	70 – 95	classical	*
2.5.2.2	0.73	Br_2	TMP	12 – 48	70 – 95	ultrasound	*
2.5.2.3	0.73	Br_2 / HFB	TMP	48	70 – 100	classical	*
2.5.2.4	0.73	Br_2 / TFT	TMP	48	70 – 120	classical	*
2.5.2.5	0.73	Br_2	TMP	1	70 – 120	μw	*
2.5.2.6	0.73	Br_2 / HFB	TMP	1	70 – 120	μw	*
2.5.2.7	0.73	Br_2 / TFT	TMP	1	70 – 120	μw	*
2.5.2.8	0.73	Br_2 / $ZnBr_2$	hexane	1 - 24	RT – 50	classical	*
2.5.2.9	0.73	Br_2 / $ZnBr_2(SiO_2)$	hexane	1 - 24	RT – 50	classical	*
2.5.2.10	0.24	Br_2 / $AlBr_3$	CCl_4	1 - 48	RT – 50	classical	*
2.5.2.11	0.24	Br_2 / $AlCl_3$	CCl_4	1 - 48	RT – 50	classical	*
2.5.2.11	0.24	NBS/AcOH	DCM	1 - 72	RT – 50	classical	*

* only starting material recovered

Table 6: Bromination trials on **83** using different conditions

We have unsuccessfully tried the method developed by Tovar [138] using NBS in acetic acid which enhances the ionic character of NBS. Classical methods involving $AlBr_3$ or $AlCl_3$ were also used without success.

This puzzling result needs a theory to explain these findings. When looking at our compound **83** we can divide it into two parts, on one end the perfluorinated part and on the other end the aromatic ring. These molecules could aggregate like benzene crystals; the aromatic parts stacked in the centre and the perfluoroalkyl chains pointing out.

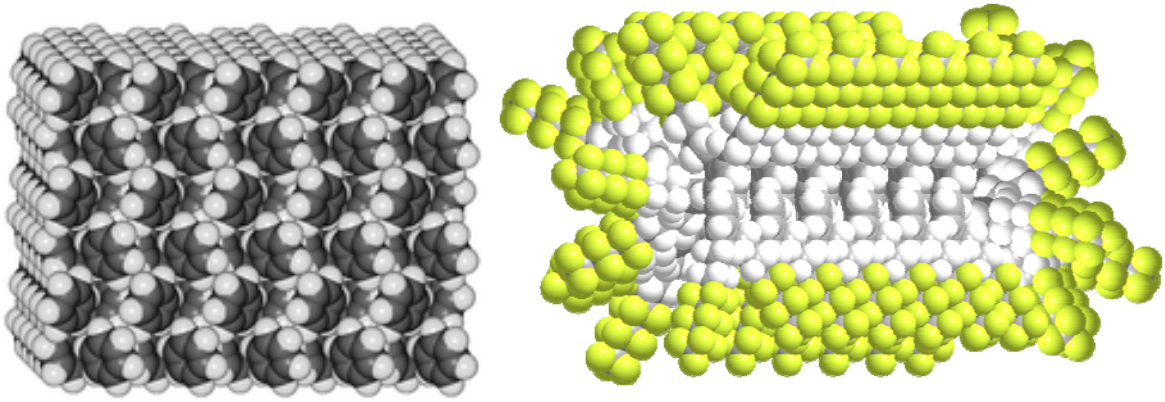

Fig. 67: Benzene crystal (left) [139], possible aggregation structure of **83** (right). Fluorine atoms are colored yellow, hydrogen white and carbon atoms grey.

Looking at the figure above we can see that the molecules aggregate and therefore could change the reactivity of the molecules.
We tried to break the “particles” using ultrasonic baths but were not successful. We also added perfluorinated solvents to the mixture but the reactivity remained unchanged. Even heating did not resolve the problem.

If we shine a laser beam trough a quartz container containing pure **83**, as well as in solution in DCM or BTF, we observe light scattering which can be seen at a 90°angle with respect to the beam direction. The beam is more scattered when shined through the pure compound as in the mixtures with organic solvents. This is a proof that we have particles in the liquid but they are smaller than half the wavelength of the laser. Neutron scattering could reveal the size of these particles but as this method needs a synchrotron like the one which is available at the Paul Scherrer Institute at which we have only rarely access to.

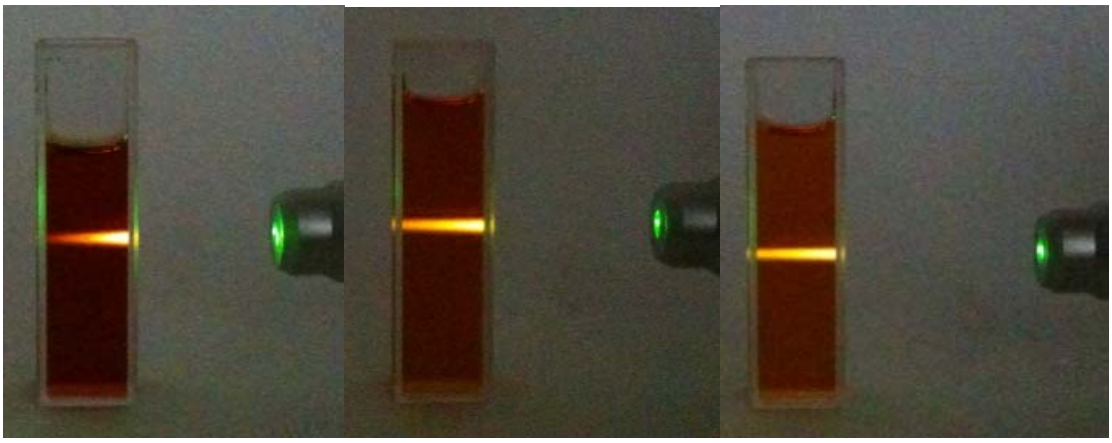

Image 9: Scattering of a laser beam of pure compound **83** (left), in DCM (middle), in BTF (right), 90° viewing angle with respect to the beam

As we were not able to brominate our compound we had to design a new strategy. We would have to introduce the aromatic bromine at the beginning of the synthesis. The problem would still be to remove the iodines on the sidechain without touching the bromine on the aromatic ring.

At this time Nicolas Fragnière from our research group discovered a soft method for removing the iodines using Zinc powder and heating by microwave. We have tuned this method and have been able to use this synthetic method successfully.
We will discuss this new strategy in the next chapter.

2.5.3 Second strategy

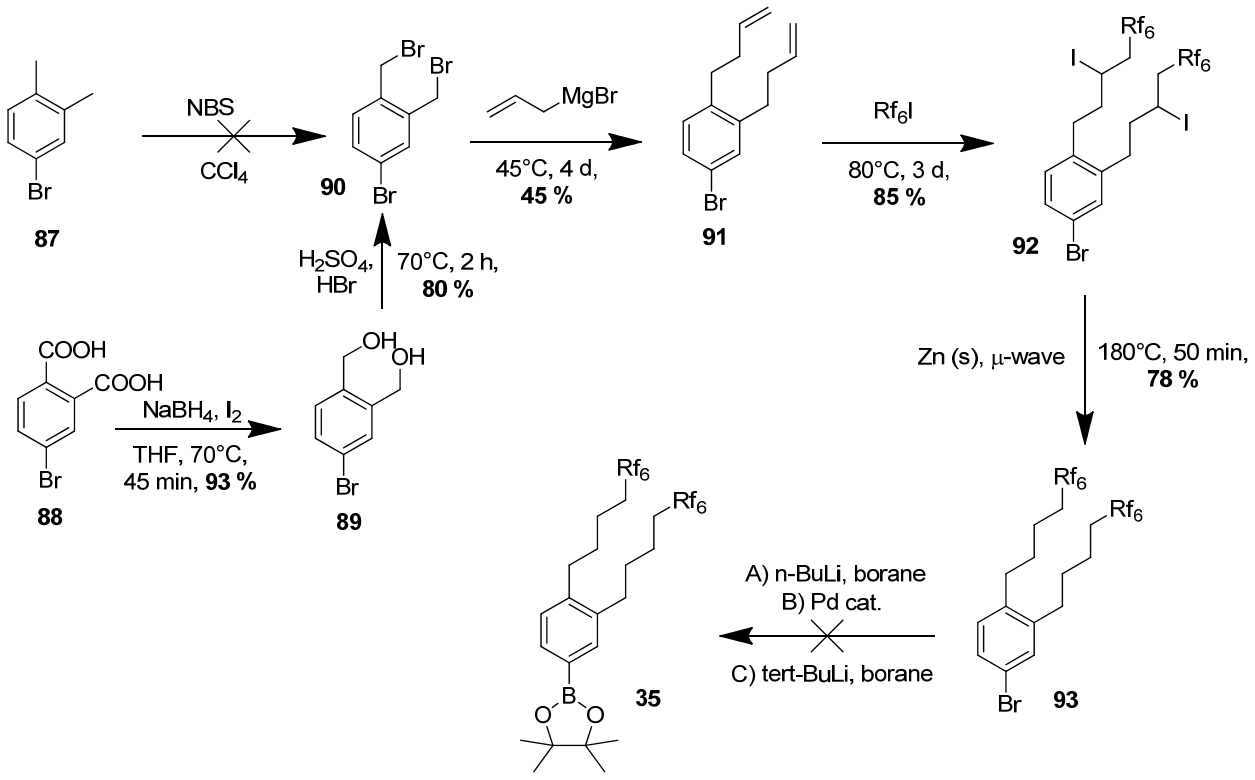

Fig. 68: Reaction steps for the bromine bearing sidechain – synthon

For the second pathway we based ourselves on the first one. The challenge was to get the 4-bromo-1,2-bis(bromomethyl)benzene **90** which is only commercially available in Canada for a price of around 400 CHF / g (January 2010). This was therefore not an option to buy it there also for time constraints.

The first attempt was to brominate 4-bromo-*o*-xylene using NBS and benzoyl peroxide following a patent by Yatsunami et al. [140]. These reaction steps only lead to an inseparable mixture of mono-, di- and polybrominated products.

An alternative route was then developed starting from 4-bromophthalic acid **88**. The carboxylic acids are reduced to alcohols using sodium borohydride and iodine. The starting material is dissolved in THF and added dropwise onto a slurry of $NaBH_4$ in THF. The elementary iodine is also dissolved in THF and added last. After refluxing the mixture during 45 minutes, the volatiles were removed by distillation yielding a white solid.

After a series of extractions using 10 % aqueous NaOH, 2M HCl and ethyl acetate followed by evaporation of the remaining solvents the dialcohol **89** was obtained in high yield which can be used without further purification. The structure of the target compound was confirmed by NMR and EI-MS. One can easily observe the loss of the bromines in the MS spectrum.

The alcoholic functional groups are then exchanged into bromine with sulfuric and hydrobromic acid by heating at 70°C for 2 hours yielding the desired 4-bromo-1,2-bis(bromomethyl)benzene **90** in excellent overall yields. Again, the structure was confirmed by NMR and EI-MS. In the MS spectrum one can observe the loss of a bromine as well as one of the sidechains.

The following steps are similar to the ones described before. The attachment of two allyl sidechains using the allyl-Grignard reagent was achieved. The 1M solution of Grignard reagent is added slowly (2 mL/h) on a solution of the brominated compound in ether and then stirred for 5 days. After hydrolysis and extraction with diethyl ether, we obtained the allyl compound **91** in medium yield.
If the resulting product is not pure, it has to be separated by chromatography. It has to be considered that the compound forms an azeotropic mixture with pentane and hexane and decomposes in contact with silica (c.f. chapter 2.5.1). The structures of the target compound **91** was confirmed by NMR.

The following addition step of perfluorohexyliodide was achieved by adding 6 portions of AIBN at 80°C over 2 days, similarly to the method used in the previous chapter for the derivative without the aromatic bromine. Extraction with diethyl ether and careful evaporation of the excessive solvents yielded the desired sidechain bearing product **92** in good yield; NMR and EI-MS confirmed the structure of the compound.

The novelty of the next step is that we used zinc powder in a mixture of THF and water. The starting material **92** is dissolved in THF in a microwave reactor and zinc powder was added. After putting the reactor under inert atmosphere, water was added. The mixture was heated to 180°C for 50 minutes. After washing with a 10 % solution of sodium thiosulfate and evaporation of the solvent we obtained the desired product **92** in good yield as confirmed by NMR and EI-MS measurements.

Being in possession of the sidechain synthon bearing bromine **93** on the aromatic core, we had circumvented the problem of brominating the aromatic ring. The next step was to transform the bromine into a boronic ester. Boronic esters are more stable and less sensitive to moisture than their corresponding acid.

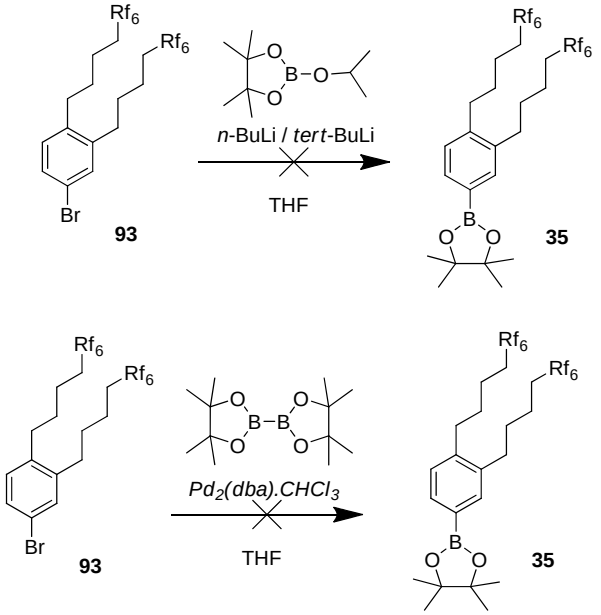

Fig. 69: The unsuccessful boronation - steps

The following table illustrates the principal efforts invested into this transformation.

Entry	**93** [mmol]	Reactants	Solvent	Time [h]	Temp. [°C]	Yield [%]
2.5.3.1	2.34	*n*-BuLi/borane	THF	1 – 12	-78 → RT	*
2.5.3.2	2.34	*tert*-BuLi/borane	THF	1 – 12	-78 → RT	*
2.5.3.3	5.83	cat./diborane	THF	18	70	*

* only starting material recovered

Table 6: Boronation trials on **93** using different conditions

We can see that the transformation of the bromine into borane could not be achieved. We therefore tried to invert the problem. We would have to boronate the other part of the molecule, in this case the cores **37** and **67**. Before we did that we had to be sure that the Suzuki crosscoupling will work in our sidechain bearing part **93** so we designed a test reaction using phenylboronic acid as analogue for the core.

We did these reactions under the same conditions as for the previous couplings using $Pd(PPh_3)_4$ and a mixture of toluene, water and ethanol.

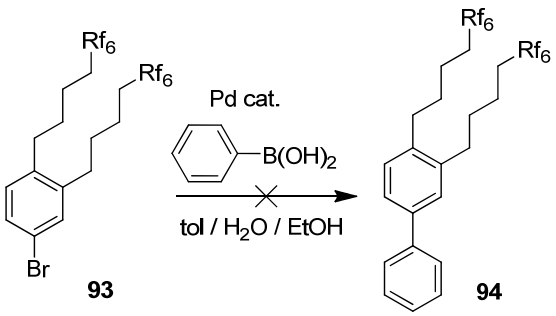

Fig. 70: Suzuki crosscoupling test reaction

Entry	**93** [mmol]	Cat	Base	Solvent	Time [h]	Temp. [°C]	Yield [%]
2.5.3.4	0.30	$Pd(PPh_3)_4$	K_2CO_3	tol/H_2O/EtOH	24 – 72	80	*
2.5.3.5	0.30	$Pd_2(PPh_3)_2$	K_2CO_3	tol/H_2O/EtOH	24 - 72	80	*

* only starting material recovered

Table 7: Suzuki trials on **93** using different conditions

Looking at these findings we can resume the following:

- The compounds with and without bromine **93** and **83** exhibit similar properties in respect to their very low reactivity.
- The compound **93** also forms particles which scatter LASER beams the same way as **83**
- The coupling of the sidechain bearing synthon is presently not possible or only with important future investigative work by other coworkers.

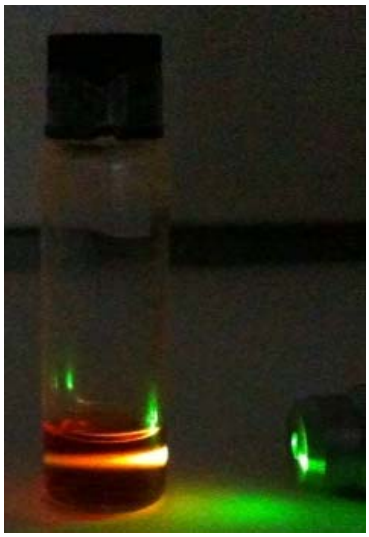

Image 10: Scattering of a laser beam of pure compound **93**, 90° viewing angle with respect to the beam

Due to the many difficulties encountered in all these previous steps, the synthesis of an alternative synthon bearing one branched sidechain instead of two linear ones should be considered for a future work.

III. CONCLUSIONS AND OUTLOOKS

We have successfully synthesized four derivatives of a new class of substances: tribenzopentaphenes (TBP) which have the shape of a halfmoon. These derivatives bear alkyl sidechains on different positions of their aromatic core.
Their synthesis is straightforward, atom-efficient and comprises a maximum of five steps with an overall yield of around 10 – 12 %. All the products have been characterized. Sadly the predicted value for the HOMO – LUMO gaps of these tribenzopentaphenes did not correspond to the ones we determined at the beginning of this work.

We have designed strategies for the synthesis of two different classes of polycondensed aromatic hydrocarbons bearing perfluorinated sidechains. The elongated version of the previously synthesized tribenzopentaphene, dibenzo-phenanthro-heptaphenes (DBPH) and the triangular shaped benzo-bistriphenyleno-ovalene (BBTO).

We have achieved the synthesis of partially oxidized precursors of alkyl-chain bearing DBPH- and BBTO-derivatives. Precursors of a synthon, bearing linear perfluoroalkylated sidechains bearing were also synthesized. The final target synthons as well as their coupling to the aromatic core precursors were not synthesized successfully due to unexpected effects of the perfluoroalkyl chains on the properties of the molecules.
For future work, the synthesis of synthons bearing branched instead of linear perfluoroalkyl sidechains as well as the research for suitable oxidation techniques of the DBPH and BBTO cores should be considered.

This thesis can be seen as a feasibility study for new shapes of aromatic cores. Hexabenzocoronene cores can roughly be described as round shaped; TBP and DPH as halfmoon shaped or half disks and BBTO as triangles, substituted on their edges by sidechains of different nature. We have shown that different core shapes can be accessed using straightforward strategies.
We have found a straightforward way to produce C_3-symmetric HBC by synthesizing a novel aromatic core precursor.

We have also initiated a calculation of dimers of some polycondensed aromatic hydrocarbons with a research group of the University of Münster (D). The results can be found in the annex section of this thesis.

As future work one can imagine depositing our TBP molecules on surfaces such as highly ordered pyrolytic graphite (HOPG) or gold surfaces to study their stacking. It would be interesting to know if the positions of the sidechains influence their alignment on the surface.

After the successful coupling and oxidation to the fully aromatic derivatives one could imagine depositing the derivatives on different surfaces and study their aggregation in solution by cryo-SEM or by SAXS (solution small angle x-ray scattering) measurements.

The target molecules should also be deposited on surfaces to test their ability to serve as organic light emitting diodes, field effect transistors or similar molecular electronics applications.

Another possibility would be to investigate the path to C_3-symmetric HBC and compare their properties and aggregation behaviour to their classical C_6-symmetric derivatives.

IV. EXPERIMENTAL PART

General considerations

All chemicals were used without further purification as purchased from Acros, Aldrich, Fluka, Fluorochem, Merck, Riedel-de-Haën, Strem and TCI unless otherwise notified. All the reactions were done under a protective atmosphere using dry nitrogen (45) or argon (48) purchased from Carbagas unless otherwise stated. The solvents, namely dichloromethane, ether, pentane, tetrahydrofurane and toluene were dried and deoxygenated by passing them over molecular sieves using a similar system as proposed by Grubbs [141]. All solvents were saturated with argon or nitrogen prior to use.

Column chromatography was carried out with silica gel 60, 0.04 - 0.06, from Merck or Brunschwig.

Thin layer chromatography was performed on aluminum sheets coated with silica gel 60 F_{254} and revealed by a UV lamp or a solution of $KMnO_4$.

Mass spectra were recorded on the following spectrometers: EI spectra were recorded on a HP5988A Quadrupol spectrometer, ESI on a Bruker HCT Esquire Ion Trap spectrometer in positive and/or negative mode. The samples were directly injected into the apparatus using a flow rate of 250 μL / h. MALDI-ICR spectra were recorded on a FT/ICR Bruker 4.7 T BioApex II spectrometer. All MALDI spectra used DCTB or TNCQ as matrix with a 337 nm nitrogen laser. The most volatile compounds were measured on a ThermoQuest TraceGC 2000/Voyager GC/MS or a ThermoScientific TraceGC Ultra DSQII spectrometer.

NMR spectra were recorded on the following spectrometers: either on a Bruker Advance DRX 500 (^{1}H: 500 MHz, ^{13}C: 125.77 MHz), a Bruker Advance DPX 360 MHz (^{1}H: 360 MHz, ^{13}C: 90.55 MHz) using $CDCl_3$, DMSO-*d6*, DCM-*d2* or D_2O as solvent. Chemical shifts (δ) are given in ppm, coupling constants (*J*) in Hz and are referred to tetramethylsilane TMS.

4.1 Halfmoon shaped TBP derivatives

4.1.1 3,4-bis(4-bromophenyl)-2,5-diphenylcyclopenta-2,4-dienone

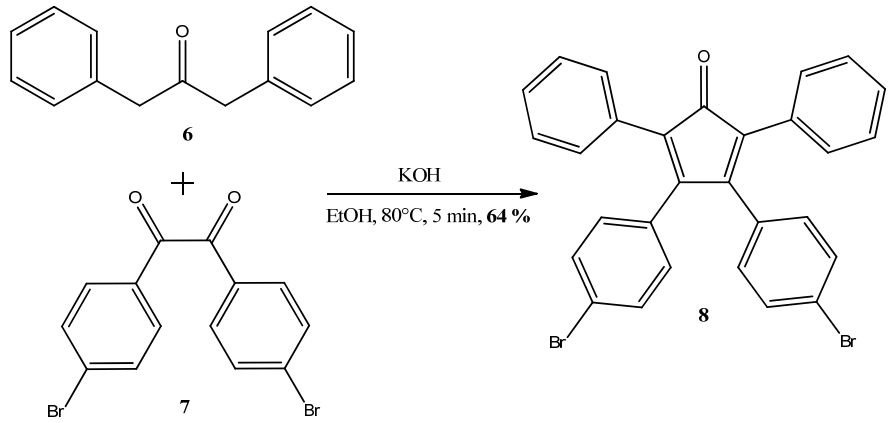

Method A. A solution of KOH (293 mg) in EtOH (2 mL) was added to a refluxing mixture of diphenylacetone **6** (1.0 g, 4.75 mmol) and 4,4'-dibromobenzil **7** (1.92 g, 5.22 mmol) in EtOH (9 mL). After 5 min the reaction was cooled to 0°C and the resulting brown mixture was extracted with CH_2Cl_2 and H_2O. The combined organic layers were dried over Na_2SO_4, filtered over a short silica gel plug using CH_2Cl_2 as eluent and the remaining solvents evaporated *in vacuo*. One obtained 1.65 g (64 %) of the desired compound **8** as a purple solid.

^{1}H-NMR: (360 MHz, $CDCl_3$): δ 7.32 – 7.37 (*d*, 4H, $^3J_{HH}$ = 8.6 Hz, Ph), 7.24 – 7.29 (*m*, 6H, Ph), 7.17 – 7.22 (*m*, 4H, Ph), 6.77 – 6.82 (*d*, 4H, $^3J_{HH}$ = 8.2 Hz, Ph).
^{13}C-NMR: (90.55 MHz, $CDCl_3$): δ 200.02 (C=O), 152.55 (Cp), 131.64 (Ph), 131.50 (Ph), 130.94 (Ph), 130.18 (Cp), 130.07 (Ph), 128.23 (Ph), 127.84 (Ph), 125.89 (Ph), 123.12 (Ph).
EI-MS: m/z (% int): 542.1 ($M^{\bullet+}$, 100 %), 462.0 ($[M\text{-}Br]^{\bullet+}$, 10 %), 382.2 ($[M\text{-}Br_2]^{\bullet+}$, 30 %).

4.1.2 2',3'-bis(4-bromophenyl)-1,1':4',1''-terphenyl

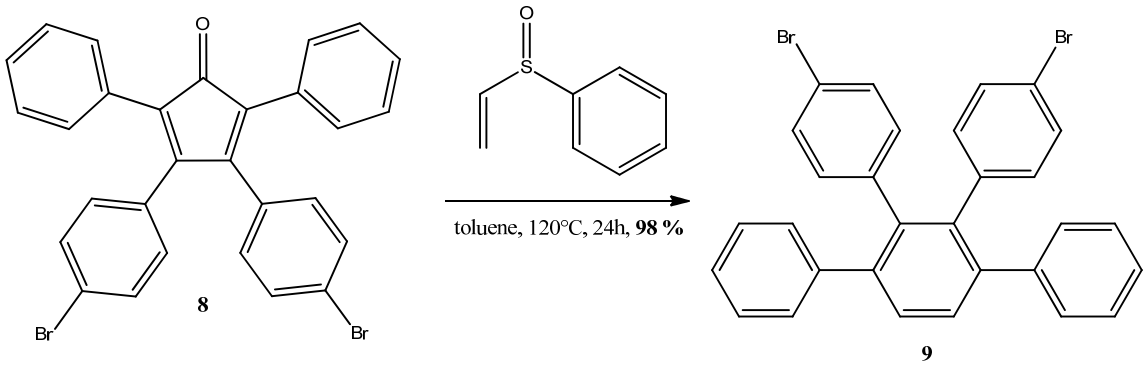

Method B. A mixture of **8** (27.45 g, 50.62 mmol) and phenylvinylsulfoxide (11.55 g, 75.93 mmol) in toluene were refluxed for 24 hrs. After cooling down to RT, the mixture was poured over a short silica gel plug and the remaining solvents were evaporated *in vacuo*. The residue was purified by column chromatography using hexanes: EtOAc / 10:1. One obtained 25.91 g (98 %) of compound **9** as a white solid.

^{1}H-NMR: (360 MHz, $CDCl_3$): δ 7.50 (*s*, 2H, Ph), 7.15 – 7.23 (*m*, 6H, Ph), 7.03 – 7.12 (*m*, 8H, Ph), 6.62 – 6.69 (*d*, 4H, $^{3}J_{HH}$ = 8.6 Hz, Ph).
^{13}C-NMR: (90.55 MHz, $CDCl_3$): δ 141.47 (2C, Ph), 141.17 (2C, Ph), 138.97 (2C, Ph), 138.76 (2C, Ph), 133.22 (4C, Ph), 130.52 (4C, Ph), 129.98 (2C, Ph), 129.95 (4C, Ph), 127.94 (4C, Ph), 126.63 (2C, Ph), 120.30 (2C, Ph).
EI-MS: m/z (% int): 540 ($M^{\bullet+}$, 100 %), 460 ($[M\text{-}Br]^{\bullet+}$, 5 %), 380 ($[M\text{-}Br_2]^{\bullet+}$, 30 %), 302 ($[M\text{-}Br_2\text{-}Ph]^{\bullet+}$, 30 %).

4.1.3 2',3'-bis(4-octylphenyl)-1,1':4',1''terphenyl

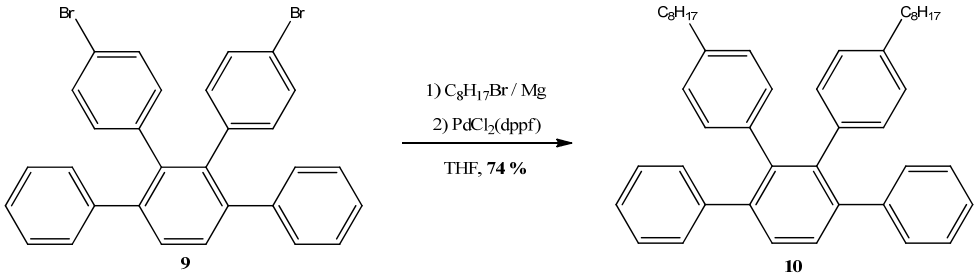

9 **10**

Method C. A solution of bromooctane (773 mg, 4.0 mmol) in THF (3 mL) was added dropwise on magnesium turnings (100 mg, 4.0 mmol). After the complete consumption of the magnesium turnings the Grignard reagent was added to a mixture of **9** (540 mg, 1.0 mmol) and $PdCl_2$(dppf) (110 mg, 0.15 mmol) in THF (7 mL). The resulting mixture was refluxed over 24 hrs. After cooling down, the reaction mixture was extracted with saturated NH_4Cl, CH_2Cl_2 and water. The combined organic layers were dried and reduced in vacuo. The resulting mixture was separated by column chromatography (pentane / CH_2Cl_2, 1:1). One obtained 450 mg of the desired product **10** as a white powder (74 %).

^{1}H-NMR: (360 MHz, $CDCl_3$): δ 7.46 (*s*, 2H, Ph), 7.07 – 7.14 (*m*, 10H, Ph), 6.65 – 6.70 (*d*, 4H, $^3J_{HH}$ = 7.9 Hz, Ph), 6.61 – 6.65 (*d*, 4H, $^3J_{HH}$ = 7.9 Hz, Ph), 2.37 (*t*, 4H, $^3J_{HH}$ = 7.4 Hz, Ar-C*H*$_2$-C_7H_{15}), 1.35 – 1.46 (*m*, 4H, Ar-CH_2-C*H*$_2$-C_6H_{13}), 1.05 – 1.30 (*m*, 20H, Ar-C_2H_4-C_5*H*$_{10}$-CH_3), 0.80 – 0.90 (*t*, 6H, $^3J_{HH}$ = 6.7 Hz, Ar-C_7H_{14}-C*H*$_3$).

^{13}C-NMR: (90.55 MHz, $CDCl_3$): δ 144.21 (2C, Ph), 141.70 (2C, Ph), 140.98 (2C, Ph), 139.21 (2C, Ph), 139.13 (2C, Ph), 130.88 (4C, Ph), 130.44 (4C, Ph), 129.91 (2C, Ph), 129.12 (4C, Ph), 128.08 (4C, Ph), 126.79 (2C, Ph), 35.70 (2C, Ar-*C*H_2-C_7H_{15}), 31.99 (2C, Ar-C_5H_{10}-*C*H_2-C_2H_5), 31.41 (2C, Ar-CH_2-*C*H_2-C_6H_{13}), 29.54 (2C, Ar-C_2H_4-*C*$_3H_6$-C_3H_7), 29.41 (2C, Ar-C_2H_4-*C*$_3H_6$-C_3H_7), 29.12 (2C, Ar-C_2H_4-*C*$_3H_6$-C_3H_7), 22.57 (2C, Ar-C_6H_{12}-*C*H_2-CH_3), 14.02 (2C, Ar-C_7H_{14}-*C*H_3).

EI-MS: m/z (% int): 606.2 ($M^{\bullet+}$, 100 %).

4.1.4 6,9-dioctyltribenzo[*fg,ij,rst*]pentaphene

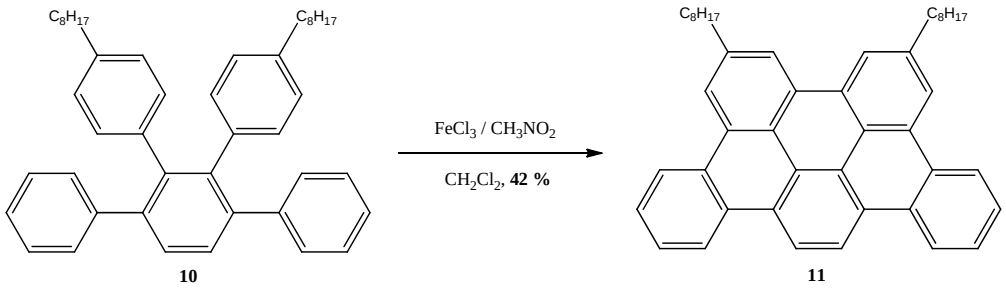

10 **11**

Method D. $FeCl_3$ (960 mg, 5.93 mmol, 3 eq. per H to be removed) was dissolved in CH_3NO_2 (3.5 mL) and cleaned with argon over 20 min. A solution of **10** (200 mg, 0.33 mmol) in dichloromethane (20 mL) was bubbled with argon over 30 min and then heated to 45°C. The $FeCl_3$ solution was added dropwise over 20 min and the reaction color turned from slight yellow over green to brown. After 40 min reaction time, the mixture was cooled down to RT and quenched with methanol. A brown substance precipitates. The mixture was cooled in the fridge overnight and filtered several times over Millipore.

The resulting black powder was extracted with dichloromethane and water. The volume of the combined organic layers was reduced to 5 mL and poured over a short silica pad using dichloromethane as eluent. One obtained 83 mg of **11** (42 %) as an orange powder.

^{1}H-NMR: (360 MHz, $CDCl_3$): δ 8.97 (*br s*, 2H, Ph), 8.75 – 8.82 (*m*, 4H, Ph), 8.72 (*br s*, 2H, Ph), 8.66 (*br s*, 2H, Ph), 7.66 – 7.72 (*m*, 4H, Ph), 3.09 (t, 4H, $^3J_{HH}$ = 7.7 Hz, Ar-C*H*$_2$-C_7H_{15}), 1.88 – 1.98 (*tt*, 4H, $^3J_{HH}$ = 7.7 Hz, $^3J_{HH}$ = 7.7 Hz, Ar-CH_2-C*H*$_2$-C_6H_{13}), 1.27 – 1.59 (*m*, 20H, Ar-C_2H_4-C_5H_{10}-CH_3), 0.85 – 0.93 (*t*, 6H, $^3J_{HH}$ = 6.4 Hz, Ar-C_7H_{14}-C*H*$_3$)

^{13}C-NMR: (90.55 MHz, $CDCl_3$): δ 141.04 (Ph), 130.32 (Ph), 130.14 (Ph), 130.12 (Ph), 129.92 (Ph), 127.44 (Ph), 127.32 (Ph), 127.12 (Ph), 123.81 (Ph), 123.73 (Ph), 123.43 (Ph), 122.93 (Ph), 122.01 (Ph), 121.69 (Ph), 120.56 (Ph), 37.30 (Ar-*C*H_2-C_7H_{15}), 32.44 (Ar-C_5H_{10}-*C*H_2-C_2H_5), 32.10 (Ar-CH_2-*C*H_2-C_6H_{13}), 29.86 (2C, Ar-C_2H_4-*C*$_3H_6$-C_3H_7), 29.81 (2C, Ar-C_2H_4-*C*$_3H_6$-C_3H_7), 29.53 (2C, Ar-C_2H_4-*C*$_3H_6$-C_3H_7), 22.86 (2C, Ar-C_6H_{12}-*C*H_2-CH_3), 14.29 (2C, Ar-C_7H_{14}-*C*H_3).

EI-MS: m/z (% int): 599.9 ($M^{\bullet+}$, 100 %), 488.0 ([M-C_8H_{17}]$^{\bullet+}$, 10 %), 376.1 ([M - 2 x C_8H_{17}]$^{\bullet+}$, 5 %).

UV/VIS: (DCM, 10^{-5} M), λ_{max} [nm] = 297, 307, 356, 375.

4.1.5 1,3-bis(4-bromophenyl)propan-2-one

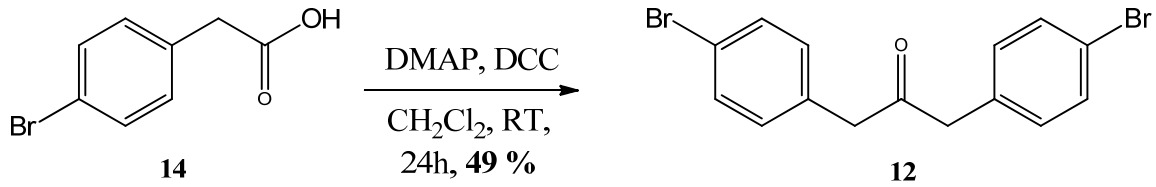

14 **12**

Method E. A solution of dicyclohexylcarbodiimide (29.76 g, 120.0 mmol) and 4-(dimethylamino)pyridine (3.67 g, 30.0 mmol) in CH_2Cl_2 (225 mL) was stirred at RT under argon and treated dropwise with a solution of 4-bromophenylacetic acid **14** (25.0 g, 120.0 mmol) in CH_2Cl_2 (75 mL). The resulting mixture was stirred at RT for 24 hrs and the precipitated solid was filtered off. The filtrate volume was reduced to 5 mL and precipitated by ethanol. Filtration and recrystallization in CH_2Cl_2/ethanol gave 21.5 g of **12** (49 %).

^{1}H-NMR: (360 MHz, $CDCl_3$): δ 7.45 (*d*, 4H, $^3J_{HH}$ = 8.3 Hz, Ph), 7.01 (*d*, 4H, $^3J_{HH}$ = 8.3 Hz, Ph), 3.69 (*s*, 4H, C*H*$_2$).

^{13}C-NMR: (90.55 MHz, $CDCl_3$): δ 204.19 (C=O), 133.25 (2C, Ph), 131.30 (4C, Ph), 130.51 (4C, Ph), 121.20 (2C, Ph), 48.42 (4C, *C*H_2).

EI-MS: m/z (% int): 368 ($M^{\bullet+}$, 10 %), 170 ([M-Br-Ph-CO-CH_2]$^{\bullet+}$, 100%), 90.1 ([C7H7]$^{\bullet+}$, 50%).

4.1.6 2,5-bis(4-bromophenyl)-3,4-diphenylcyclopenta-2,4-dienone

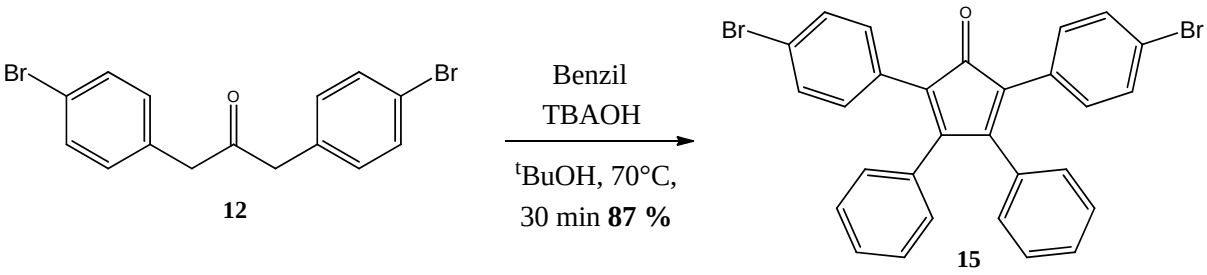

Method F. The compounds **12** (0.64 g, 3.0 mmol) and benzil (1.1 g, 3.0 mmol) were dissolved in *t*-BuOH (8 mL) at 85°C. Tetrabutylammoniumhydroxide 1 M solution in MeOH (3 mL, 3.0 mmol) was then added and the reaction mixture was stirred for 30 min. The reaction mixture was quenched with 15 mL H_2O. The mixture was then extracted with H_2O, dried and adsorbed on silica gel to be eluted over a short silica gel plug using CH_2Cl_2 as eluent. One obtains 1.41 g (87 %) of product **15** as a red powder.

^{1}H-NMR: (360 MHz, $CDCl_3$): δ 7.37 (*d*, 4H, $^3J_{HH}$ = 7.2 Hz, Ph), 7.25 – 7.30 (*m*, 2H, Ph), 7.15 – 7.11 (*dd*, 4H, $^3J_{HH}$ = 7.2 Hz, $^3J_{HH}$ = 7.2 Hz, Ph) 7.06 – 7.14 (*m*, 4H, Ph), 6.90 (*d*, 4H, $^3J_{HH}$ = 7.2 Hz, Ph).

^{13}C-NMR: (90.55 MHz, $CDCl_3$): δ 199.94 (C=O), 155.40 (2C, Cp), 132.96 (2C, Ph), 132.02 (4C, Ph), 131.73 (2C, Ph), 129.89 (2C, Cp), 129.56 (4C, Ph), 129.28 (2C, Ph), 128.61 (4C, Ph), 124.77 (2C, Ph), 122.39 (2C, Ph).

EI-MS: m/z (% int): 542 ($M^{\bullet+}$, 100 %), 462 ($[M\text{-}Br]^{\bullet+}$, 5 %), 382 ($[M\text{-}Br_2]^{\bullet+}$, 5 %), 256 ([Br-Ph-CH=CH-Ph]$^{\bullet+}$, 50%), 176 (40 %).

4.1.7 3',6'-bis(4-bromophenyl)-1,1':2',1''-terphenyl

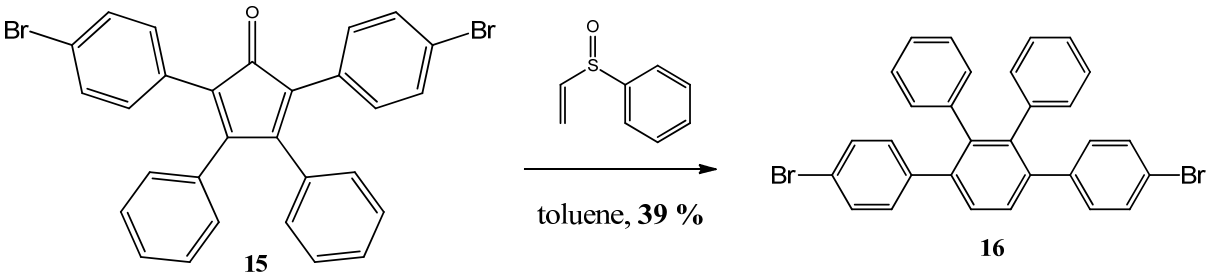

This reaction was performed following method B. Compound **15** (1.3 g, 2.4 mmol) and phenylvinylsulfoxide (547 mg, 3.6 mmol) were dissolved in toluene (10 mL) and refluxed under argon over 48 hrs. After cooling down to RT, the mixture was separated by column chromatography (pentane: CH_2Cl_2 / 1:1). One obtained 500 mg of **16** as a white solid (39 %).

^{1}H-NMR: (360 MHz, $CDCl_3$): δ 7.46 (*s*, 2H, Ph), 7.24 – 7.32 (*m*, 6H, Ph), 6.92 – 6.99 (*m*, 8H, Ph), 6.75 – 6.82 (*d*, 4H, $^3J_{HH}$ = 8.6 Hz, Ph).

^{13}C-NMR: (90.55 MHz, $CDCl_3$): δ 140.81 (2C, Ph), 140.60 (2C, Ph), 140.12 (2C, Ph), 139.49 (2C, Ph), 131.60 (4C, Ph), 131.53 (4C, Ph), 130.91 (4C, Ph), 129.43 (2C, Ph), 127.31 (4C, Ph), 126.08 (4C, Ph), 120.76 (2C, Ph).

EI-MS: m/z (% int): 540 ($M^{\bullet+}$, 100 %), 460 ([M-Br]$^{\bullet+}$, 5 %), 380 ([M-Br_2]$^{\bullet+}$, 10 %), 302 ([M-Br_2-Ph]$^{\bullet+}$, 20 %).

4.1.8 3',6'-bis(4-octylphenyl)-1,1':2',1''-terphenyl

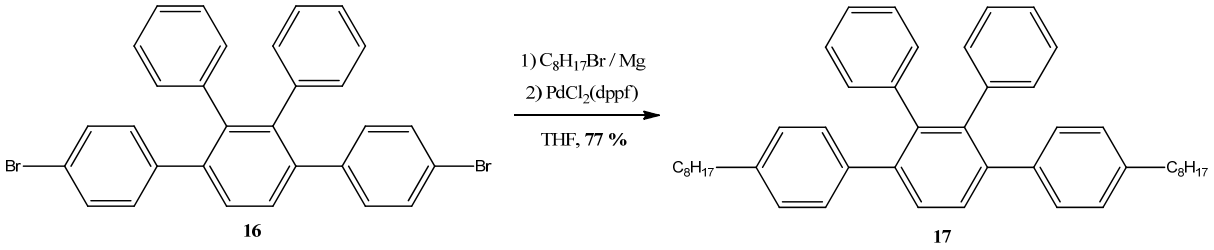

16 17

This Kumada crosscoupling was performed following method C. A solution of bromooctane (428 mg, 2.2 mmol) in THF (2 mL) was added dropwise on magnesium turnings (55 mg, 2.2 mmol). After the complete consumption of the magnesium turnings the Grignard reagent was added to a mixture of **16** (300 mg, 0.55 mmol) and $PdCl_2$(dppf) (61 mg, $8.33 \cdot 10^{-5}$ mol) in THF (4 mL). The resulting mixture was refluxed over 24 hrs. After cooling down, the reaction mixture was extracted with saturated NH_4Cl, CH_2Cl_2 and water. The combined organic layers were dried and reduced *in vacuo* to 5 mL and precipitated by EtOH. The product was recrystallized several times in CH_2Cl_2 / EtOH. One obtained 258 mg of **17** (77 %) as a white solid.

^{1}H-NMR: (360 MHz, $CDCl_3$): δ 7.49 (*br s*, 2H, Ph), 7.00 (*d*, 4H, $^3J_{HH}$ = 7.7 Hz, Ph), 6.95 (*d*, 4H, $^3J_{HH}$ = 7.7 Hz, Ph), 6.87 – 6.93 (*m*, 6H, Ph), 6.76 – 6.84 (*m*, 4H, Ph), 2.51 (*t*, 4H, $^3J_{HH}$ = 7.7 Hz, Ar-C*H*$_2$-C_7H_{15}), 1.49 – 1.61 (*m*, 4H, Ar-CH_2-C*H*$_2$-C_6H_{13}), 1.18 – 1.35 (*m*, 20H, Ar-C_2H_4-C_5*H*$_{10}$-CH_3), 0.88 (*t*, 6H, $^3J_{HH}$ = 6.8 Hz, Ar-C_7H_{14}-C*H*$_3$).

^{13}C-NMR: (90.55 MHz, $CDCl_3$): δ 140.69 (2C, Ph), 140.67 (2C, Ph), 140.24 (2C, Ph), 140.13 (2C, Ph), 139.11 (2C, Ph), 131.59 (4C, Ph), 129.72 (4C, Ph), 129.37 (2C, Ph), 127.52 (4C, Ph), 126.80 (4C, Ph), 125.42 (2C, Ph), 35.49 (2C, Ar-*C*H_2-C_7H_{15}), 31.87 (2C, Ar-C_5H_{10}-*C*H_2-C_2H_5), 31.26 (2C, Ar-CH_2-*C*H_2-C_6H_{13}), 29.45 (2C, Ar-C_2H_4-*C*$_3$$H_6$-$C_3H_7$), 29.27 (2C, Ar-$C_2H_4$-*C*$_3$$H_6$-$C_3H_7$), 29.26 (2C, Ar-$C_2H_4$-*C*$_3$$H_6$-$C_3H_7$), 22.68 (2C, Ar-$C_6H_{12}$-*C*$H_2$-$CH_3$), 14.11 (2C, Ar-$C_7H_{14}$-*C*$H_3$).

MALDI-ICR-MS (DCTB): m/z (% int): 606.42 ($M^{\bullet+}$, 100 %).

4.1.9 Synthesis of 3,12-dioctyltribenzo[*fg,ij,rst*]pentaphene

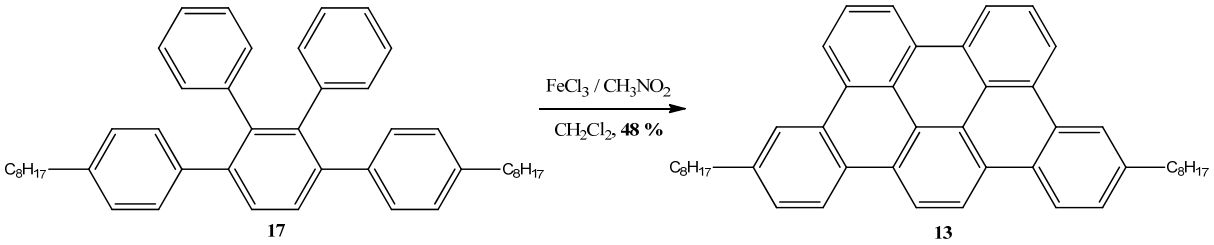

17 **13**

This oxidation reaction was performed following method D. $FeCl_3$ (817 mg, 5.04 mmol, 18 eq) was dissolved in CH_3NO_2 (2.5 mL) and cleaned with argon over 20 min. A solution of **17** (170 mg, 0.28 mmol) in dichloromethane (20 mL) was bubbled with argon over 30 min and then heated to 45°C. The $FeCl_3$ solution was added dropwise over 20 min and the reaction color turned from slight yellow over green to brown opaque. After 40 min of reaction time, the mixture was cooled down to RT and quenched with MeOH. An orange substance precipitated. The mixture was cooled in the fridge overnight and filtered several times over Millipore.

The resulting brown powder was extracted with dichloromethane and water. The volume of the combined organic layers was reduced to 5 mL and poured over a short silica pad using dichloromethane as eluent. The organic layers were reduced again and the product was recrystallized several times with CH_2Cl_2 / EtOH and filtered by Millipore.

One obtained 80 mg of **13** (48 %) as a dark yellow solid.

^{1}H-NMR: (360 MHz, $CDCl_3$): δ 9.11 (*s*, 1H, Ph), 9.02 (*d*, 2H, $^3J_{HH}$ = 7.7 Hz, Ph), 8.95 (*d*, 2H, $^3J_{HH}$ = 7.7 Hz, Ph), 8.80 (*d*, 2H, $^3J_{HH}$ = 8.2 Hz, Ph), 8.62 (*s*, 2H, Ph), 8.06 (*dd*, 2H, $^3J_{HH}$ = 7.7 Hz, $^3J_{HH}$ = 7.7 Hz), 7.60 (*d*, 2H, $^3J_{HH}$ = 8.2 Hz, Ph), 2.94 (*t*, 4H, $^3J_{HH}$ = 7.7 Hz, Ar-C*H*$_2$-C_7H_{15}), 1.78 – 1.91 (*m*, 4H, Ar-CH_2-C*H*$_2$-C_6H_{13}), 1.18 – 1.67 (*m*, 20H, Ar-C_2H_4-C_5H_{10}-CH_3), 0.89 (*t*, 6H, $^3J_{HH}$ = 6.4 Hz, Ar-C_7H_{14}-C*H*$_3$).

^{13}C-NMR: (90.55 MHz, $CDCl_3$): δ 142.29 (2C, Ph), 130.39 (2C, Ph), 130.08 (2C, Ph), 130.07 (2C, Ph), 128.58 (2C, Ph), 128.27 (2C, Ph), 127.51 (2C, Ph), 126.51 (2C, Ph), 124.89 (2C, Ph), 123.82 (2C, Ph), 123.36 (2C, Ph), 123.20 (2C, Ph), 121.71 (2C, Ph), 121.66 (2C, Ph), 121.02 (2C, Ph), 36.60 (2C, Ar-*C*H_2-C_7H_{15}), 32.08 (2C, Ar-C_5H_{10}-*C*H_2-C_2H_5), 31.90 (2C, Ar-CH_2-*C*H_2-C_6H_{13}), 29.75 (2C, Ar-C_2H_4-*C*$_3H_6$-C_3H_7), 29.66 (2C, Ar-C_2H_4-*C*$_3H_6$-C_3H_7), 29.48 (2C, Ar-C_2H_4-*C*$_3H_6$-C_3H_7), 22.85 (2C, Ar-C_6H_{12}-*C*H_2-CH_3), 14.28 (2C, Ar-C_7H_{14}-*C*H_3).

MALDI-ICR-MS (DCTB): m/z (% int): 600.38 ($M^{\bullet+}$, 100 %).

EI-MS: m/z (% int): 600.2 ($M^{\bullet+}$, 100 %), 488.0 ($[M\text{-}C_8H_{17}]^{\bullet+}$, 60 %), 376.1 ($[M - 2 \times C_8H_{17}]^{\bullet+}$, 5 %)

UV/VIS: (DCM, 10^{-5} M), λ_{max} [nm] = 297, 306, 355, 376.

4.1.10 2,3,4,5-tetrakis(4-bromophenyl)cyclopenta-2,4-dienone

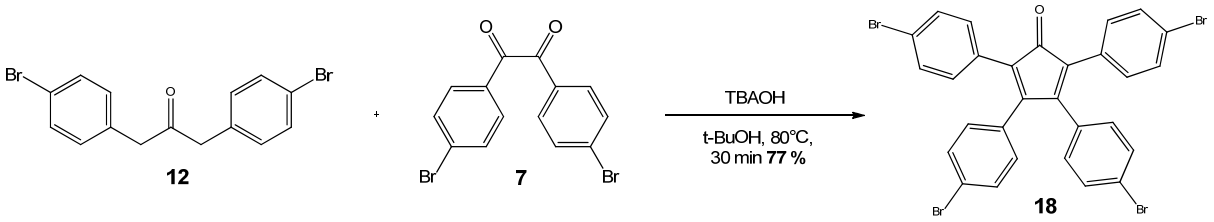

This reaction was performed following method F. 1,3-bis(4-bromophenyl)propan-2-one **12** (997 mg, 2.71 mmol) and 1,2-bis(4-bromophenyl)ethane-1,2-dione **7** (997 mg, 2.71 mmol) were suspended in tert-butanol (8 mL) and heated to 80°C. A solution of tetrabutylammoniumhydroxide (2.71 mL, 1 eq, 1 M) in methanol was added dropwise over 30 min.

The solution turned from colorless over yellow to dark red. After 30 min of reaction time, the mixture was cooled down to room temperature and quenched with water. The mixture was then extracted with water, dried and adsorbed on silica gel to be eluted over a short silica gel plug using CH_2Cl_2 as eluent. One obtained 1.46 g (77 %) of desired product **18** as a dark red powder in good yield.

^{1}H-NMR: (360 MHz, $CDCl_3$): δ 7.40 (*d*, 4H, $^3J_{HH}$ = 8.6 Hz, Ph), 7.37 (*d*, 4H, $^3J_{HH}$ = 8.6 Hz, Ph), 7.06 (*d*, 4H, $^3J_{HH}$ = 8.2 Hz, Ph), 6.77 (*d*, 4H, $^3J_{HH}$ = 8.2 Hz, Ph).

^{13}C-NMR: (90.55 MHz, $CDCl_3$): δ 198.92 (1C, C=O), 153.19 (2C, Cp), 131.89 (2C, Ph), 131.70 (2C, Ph), 131.69 (2C, Ph), 131.25 (2C, Cp), 130.90 (2C, Ph), 129.05 (2C, Ph), 125.07 (2C, Ph), 123.72 (2C, Ph), 122.58 (2C, Ph).

EI-MS: m/z (% int): 700.2 ($M^{\bullet+}$, 100 %), 316 (80 %).

4.1.11 4,4''-dibromo-3',4'-bis(4-bromophenyl)-1,1':2',1''-terphenyl

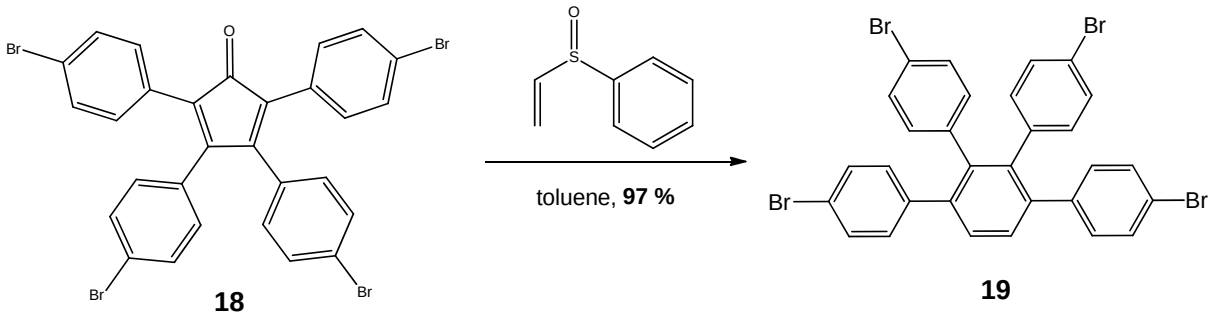

This reaction was performed following method B. 2,3,4,5-tetrakis(4-bromophenyl)cyclopenta-2,4-dienone **18** (1.44 g, 2.06 mmol) and phenylvinylsulfoxide (407 µl, 470 mg, 1.5 eq) were dissolved in toluene (10 mL) and refluxed under argon over 4 days. After cooling down to RT, the mixture was separated by column chromatography using pentane/DCM 1:1 as eluent.

One obtained 1.39 g (97 %) compound **19** as a white powder.

^{1}H-NMR: (360 MHz, $CDCl_3$): δ 7.45 (*s*, 2H, Ph), 7.32 (*d*, 4H, $^{3}J_{HH}$ = 8.2 Hz, Ph), 7.12 (*d*, 4H, $^{3}J_{HH}$ = 8.6 Hz, Ph), 6.92 (*d*, 4H, $^{3}J_{HH}$ = 8.2 Hz, Ph), 6.63 (*d*, 4H, $^{3}J_{HH}$ = 8.6 Hz, Ph).

^{13}C-NMR: (90.55 MHz, $CDCl_3$): δ → 140.24 (2C, Ph), 140.23 (2C, Ph), 130.09 (2C, Ph), 138.19 (2C, Ph), 133.04 (4C, Ph), 131.48 (4C, Ph), 131.18 (4C, Ph), 130.80 (4C, Ph), 129.91 (2C, Ph), 121.12 (2C, Ph), 120.67 (2C, Ph).

EI-MS: m/z (% int): 697.9 ($M^{\bullet+}$, 100 %), 617.9 ($[M\text{-}Br]^{\bullet+}$, 5 %), 537.9 ($[M\text{-}Br_2]^{\bullet+}$, 20 %).

MALDI-ICR-MS (DCTB): 716.79 ($[M+Na]^{\bullet+}$, 100 %).

4.1.12 4,4''-dioctyl-3',4'-bis(4-octylphenyl)-1,1':2',1''terphenyl

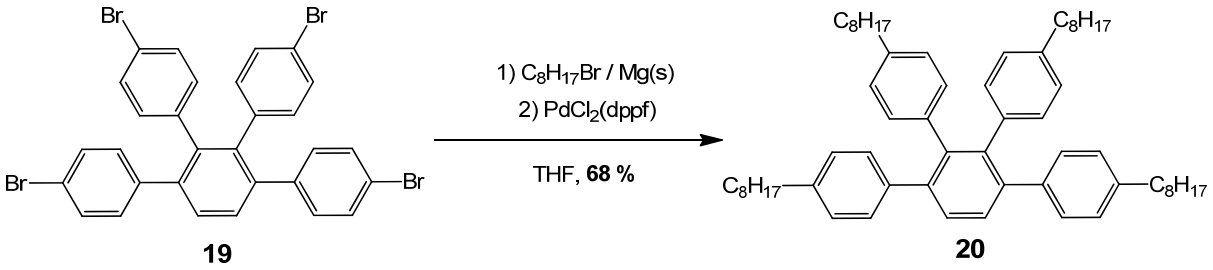

19 **20**

This reaction was performed following method C. A solution of bromooctane (2.12 mL, 3.07 g, 15.9 mmol) in THF (50 mL) was added dropwise on magnesium turnings (387 mg, 15.9 mmol). After the complete consumption of the magnesium turnings, the Grignard reagent was added to a mixture of 4,4''-dibromo-3',4'-bis(4-bromophenyl)-1,1':2',1''-terphenyl **19** (1.39 g, 20.0 mmol) and $PdCl_2$(dppf) (407 mg, 0.53 mmol, 28 %mol) in THF (50 mL). The resulting mixture was refluxed over 48 hrs. After cooling down, the reaction mixture was extracted with saturated NH_4Cl, CH_2Cl_2 and water. The combined organic layers were dried and reduced to 10 mL and precipitated by EtOH. The product was recrystallized several times in CH_2Cl_2 / EtOH. One obtained 1.12 g (68 %) of compound **20** as a white powder.

^{1}H-NMR: (360 MHz, $CDCl_3$): δ 7.47 (*s*, 2H, Ph), 6.99 (*d*, 4H, $^3J_{HH}$ = 7.7 Hz, Ph), 6.93 (*d*, 4H, $^3J_{HH}$ = 7.7 Hz, Ph), 6.69 (*d*, 4H, $^3J_{HH}$ = 8.2 Hz, Ph), 6.65 (*d*, 4H, $^3J_{HH}$ = 8.2 Hz, Ph), 2.51 (*t*, 4H, $^3J_{HH}$ = 8.2 Hz, Ar-C*H*$_2$-C_7H_{15}), 2.40 (*t*, 4H, $^3J_{HH}$ = 8.2 Hz, Ar-C*H*$_2$-C_7H_{15}), 1.55 (*tt*, 4H, $^3J_{HH}$ = 7.3 Hz, Ar-CH_2-C*H*$_2$-C_6H_{13}), 1.44 (*tt*, 4H, $^3J_{HH}$ = 7.3 Hz, Ar-CH_2-C*H*$_2$-C_6H_{13}), 1.10 – 1.35 (*m*, 40H, Ar-C_2H_4-C_5*H*$_{10}$-CH_3), 0.88 (*t*, 12H, $^3J_{HH}$ = 7.5 Hz, Ar-C_7H_{14}-C*H*$_3$).

^{13}C-NMR: (90.55 MHz, $CDCl_3$): δ 140.79 (2C, Ph), 140.66 (2C, Ph), 140.61 (2C, Ph), 139.81 (2C, Ph), 139.50 (2C, Ph), 137.51 (2C, Ph), 131.57 (4C, Ph), 129.92 (4C, Ph), 129.29 (2C, Ph), 127.59 (4C, Ph), 127.01 (4C, Ph), 35.69 (2C, Alk), 35.54 (2C, Alk), 32.12 (2C, Alk), 32.07 (2C, Alk), 31.47 (2C, Alk), 31.42 (2C, Alk), 29.68 (2C, Alk), 29.65 (2C, Alk), 29.53 (2C, Alk), 29.46 (2C, Alk), 29.00 (4C, Alk), 22.85 (4C, Ar-C_6H_{12}-*C*H_2-CH_3), 14.28 (4C, Ar-C_7H_{14}-*C*H_3).

EI-MS: m/z (% int): 830.4 ($M^{\bullet+}$, 100 %), 718.2 ($[M\text{-}C_7H_{15}]^{\bullet+}$, 30 %).

4.1.13 3,6,9,12-tetraoctyltribenzo[*fg,ij,rst*]pentaphene

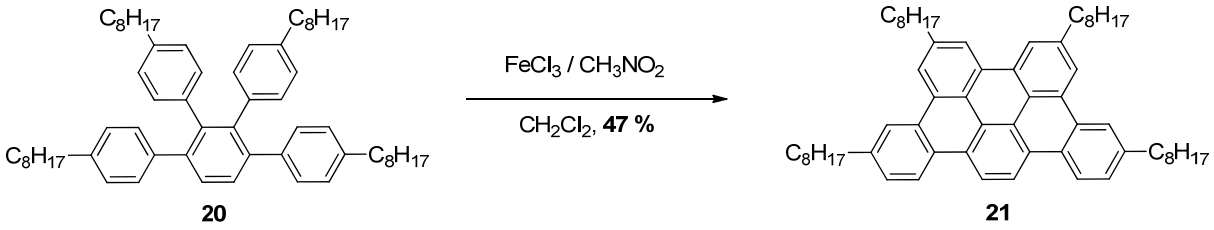

20 **21**

This reaction was performed following method D. $FeCl_3$ (7.02 g, 43.3 mmol) was dissolved in CH_3NO_2 (20 mL) and cleaned with argon over 40 min. A solution of **20** (2.00 g, 2.41 mmol) in dichloromethane (160 mL) was bubbled with argon over 30 min and then heated to 45°C. The $FeCl_3$ solution was added dropwise over 20 min and the reaction color turned from slight yellow over green to brown. After 2 h of reaction time, the mixture was cooled down to RT and quenched with MeOH. A brown substance precipitated. The mixture was cooled in the fridge overnight and filtered several times over Millipore. One obtains 933 mg (47 %) of the desired compound **21** as a yellow powder.

MALDI-MS (DCTB): m/z (% int): 824.63 ($M^{\bullet+}$, 100 %), 726.52 ($[M\text{-}C_7H_{15}]^{\bullet+}$, 20 %), 627.40 ($[M\text{- }2 \times C_7H_{15}]^{\bullet+}$, 15 %), 516.71 ($[M\text{- }2 \times C_7H_{15} - C_8H_{17}]^{\bullet+}$, 15 %).
UV/VIS: (DCM, 10^{-6} M), λ_{max} [nm] = 293, 305, 356, 375.

4.1.14 3',4'-diheptyl-5',6'-diphenyl-1,1':2',1''-terphenyl

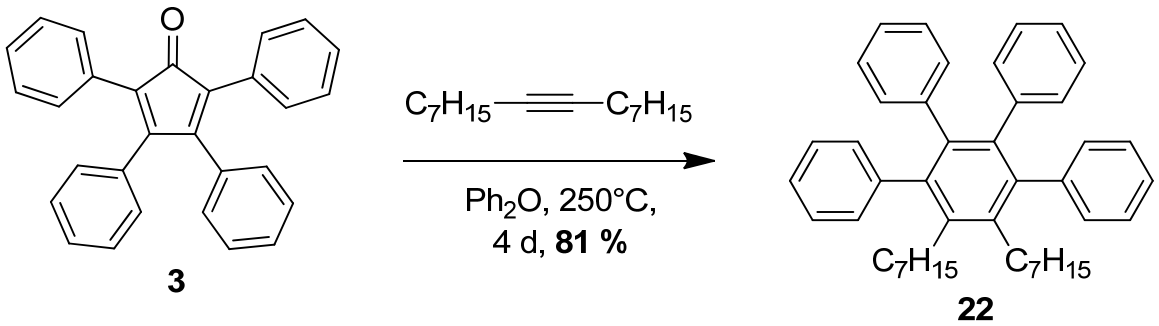

3 **22**

Method G. Tetraphenylcyclopentadienone **3** (1.02 g, 2.6 mmol) and 8-hexadecyne (880 mg, 3.9 mmol, 1.5 eq.) were dissolved in diphenylether (22 mL) and heated to 250°C over 4 days. The reaction mixture turned from dark red to pale yellow as an indication of the evolving reaction.

The diphenylether was distilled off by turbomolecular pump. The resulting mixture was separated by column chromatography using pentane/DCM 8:2 as eluent to give 2.56 g (81 %) of **22** as a white powder.

^{1}H-NMR: (360 MHz, $CDCl_3$): δ 7.02 – 7.16 (*m*, 10H, Ph), 6.70 – 6.80 (*m*, 10H, Ph), 2.51 (*t*, 4H, $^{3}J_{HH}$ = 8.3 Hz, Ar-C*H*$_2$-C_6H_{13}), 1.38 – 1.48 (*m*, 4H, Ar-CH_2-C*H*$_2$-C_5H_{11}), 1.08 – 1.24 (*m*, 16H, Ar-C_2H_4-C_4*H*$_8$-CH_3), 0.83 (*t*, 6H, $^{3}J_{HH}$ = 7.6 Hz, Ar-C_6H_{12}-C*H*$_3$).

^{13}C-NMR: (90.55 MHz, $CDCl_3$): δ 141.37 (2C, Ph), 141.11 (2C, Ph), 141.07 (2C, Ph), 138.83 (2C, Ph), 138.51 (2C, Ph), 131.36 (4C, Ph), 130.77 (4C, Ph), 127.19 (4C, Ph), 126.40 (4C, Ph), 125.90 (2C, Ph), 124.95 (2C, Ph), 31.72 (2C, Alk), 31.25 (2C, Alk), 30.89 (2C, Alk), 30.21 (2C, Alk), 28.72 (2C, Alk), 22.74 (Ar-C_5H_{10}-*C*H_2-CH_3), 14.22 (Ar-C_6H_{12}-*C*H_3).

EI-MS: m/z (% int): 578.5 ($M^{\bullet+}$, 100 %), 478.2 ([M-C_7H_{15}]$^{\bullet+}$, 5 %), 382.5 ([M - 2 x C_7H_{15}]$^{\bullet+}$, 80 %).

4.1.15 3',6'-diphenyl-1,1':2',1''-terphenyl

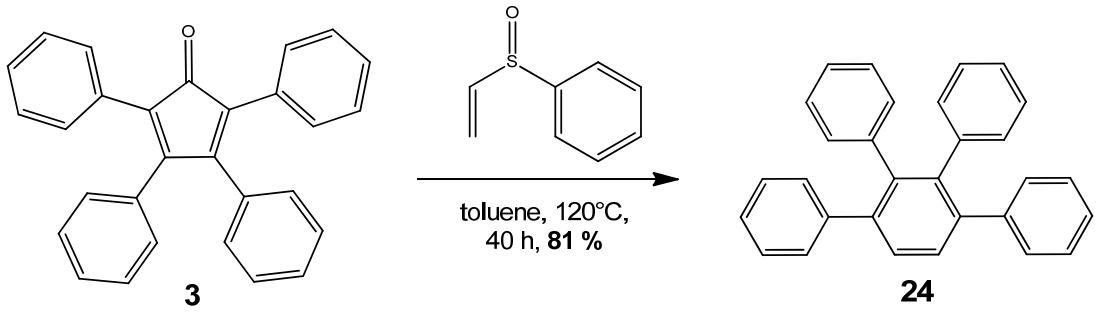

This reaction was performed following method B. Tetraphenylcyclopentadienone **3** (2.00 g, 5.20 mmol) and phenylvinylsulfoxide (1.19 g, 7.80 mmol, 1.5 eq) were dissolved in dry toluene and heated to reflux over 40 h. The reaction was stopped as soon as the purple color disappears. After cooling down to RT, the mixture was separated by column chromatography using pentane/CH_2Cl_2 1:1 as eluent.

One obtained 1.61 g (81 %) of the desired compound **24** as a white powder.

^{1}H-NMR: (360 MHz, $CDCl_3$): δ 7.51 (*s*, 2H, Ph), 7.08 – 7.18 (*m*, 10H, Ph), 6.89 – 6.96 (*m*, 6H, Ph), 6.78 – 6.84 (*m*, 4H, Ph).

^{13}C-NMR: (90.55 MHz, $CDCl_3$): δ 141.87 (2C, Ph), 140.88 (2C, Ph), 140.32 (2C, Ph), 139.87 (2C, Ph), 131.53 (4C, Ph), 129.89 (4C, Ph), 129.35 (2C, Ph), 127.51 (4C, Ph), 126.87 (4C, Ph), 126.14 (2C, Ph), 125.57 (2C, Ph).

EI-MS: m/z (% int): 382.4 ($M^{\bullet+}$, 100 %), 306.2 ($[M\text{-}Ph]^{\bullet+}$, 15 %).

4.1.16 tribenzo[fg,ij,rst]pentaphene

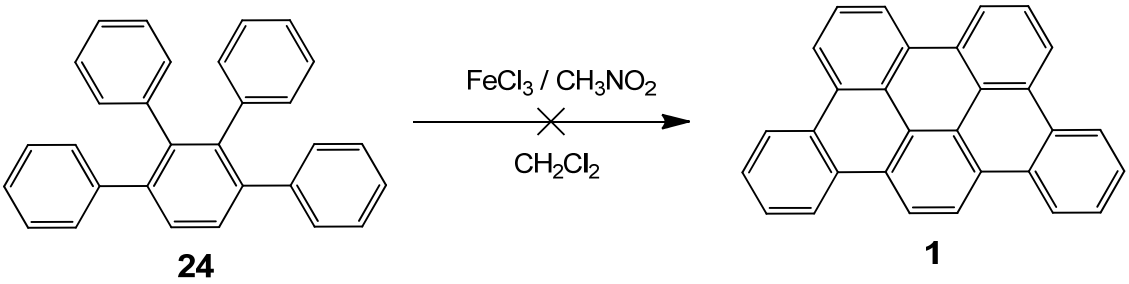

24 **1**

This reaction was performed following method D. $FeCl_3$ (11.45 g, 70.5 mmol, 18 eq.) was dissolved in CH_3NO_2 (35 mL) and cleaned with argon over 40 min. A solution of **24** (1.5g, 3.92 mmol) in dichloromethane (20 mL) was bubbled with argon over 30 min and then heated to 45°C. The $FeCl_3$ solution was added dropwise over 30 min and the reaction color turned from slight yellow over green to brown. After 45 min of reaction time, the mixture was cooled down to RT and quenched with MeOH. A brown substance precipitated. The mixture was cooled in the fridge overnight and filtered several times over Millipore. One obtains 4.01 g of insoluble black material. No NMR or MS could be measured due to its low solubility.

4.2 Elongated half-moon shaped DBPH derivative

4.2.1 2,7-dibromophenanthrene-9,10-dione

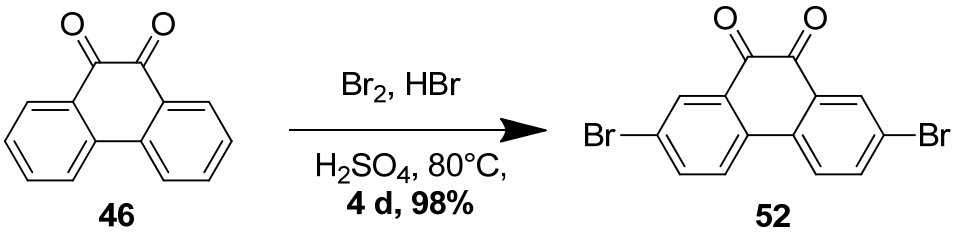

46 **52**

Method H. Phenanthrenequinone **46** (5.00 g, 24.0 mmol) was filled into Teflon®-sealed tubes with a security seal. A mixture of conc. H_2SO_4 (30 mL) and conc. HBr (30 mL), and a catalytic amount of elementary bromine was added. The reaction was stirred at 80°C for 4 days under inert atmosphere. An orange-brown solid appeared. The tubes have to be cooled down and shaken every 5 hours to homogenize the mixture.

After reaction completion the tube was cooled down to RT and the content carefully poured on ice. 50 mL 30 % aq. $Na_2S_2O_5$ was added. The aqueous layer was washed three times with DCM. The combined organic layers were washed with $NaHCO_3$ and water and dried over Na_2SO_4 and reduced in vacuo. The desired compound was obtained as a yellow-orange solid **52** in high yield (**98 %**) and was used without further purification.

^{1}H-NMR: (360 MHz, $CDCl_3$): δ 8.13 (*s*, 2H), 8.06 - 8.09 (*d*, 2H, $^3J_{HH}$=8.2 Hz), 7.64 - 7.69 (*d*, 2H, $^3J_{HH}$=8.2 Hz).

^{13}C-NMR: (90.55 MHz, $CDCl_3$): δ 178.82 (2C, C=O), 135.90 (2C, Ph), 133.42 (2C, Ph), 132.10 (2C, Ph), 132.08 (2C, Ph), 129.81 (2C, Ph), 127.37 (2C, Ph).

EI-MS: m/z (% int): 365.87 ($M^{\bullet+}$, 10 %), 337.87 ([M- 2 x CO]$^{\bullet+}$, 100 %).

4.2.2 5,10-dibromo-1,3-diphenyl-2*H*-cyclopenta[*l*]-phenanthren-2-one

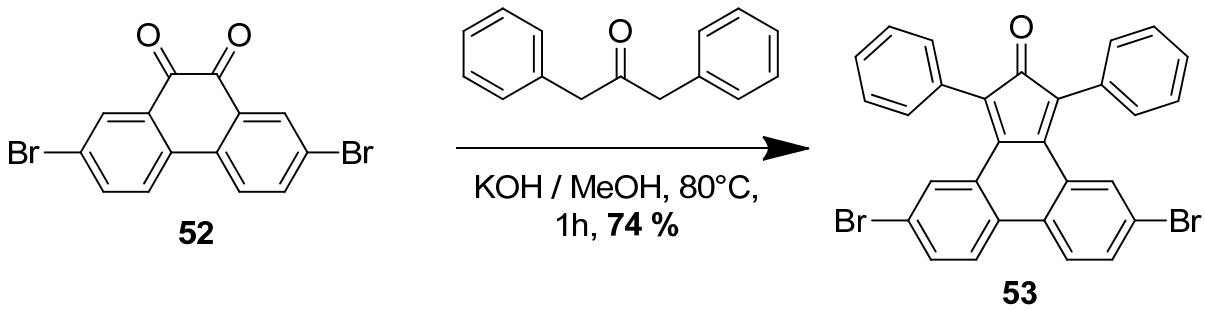

Method I. 2,7-dibromophenanthrene-9,10-dione **52** (6.00 g, 16.4 mmol) and 1,3-diphenylacetone (3.79 g, 18.0 mmol, 1.1 eq) in dry methanol was heated to reflux. More methanol was added until the complete dissolution of the starting materials to give a yellow solution (150 mL / mmol).

A solution of KOH in Methanol was added in one portion and the solution turns immediately brown. The mixture was stirred for 1h at reflux. After that, the mixture was cooled down to RT overnight. A green substance precipitates, which was filtered off by Büchner and washed with methanol.

One obtains 6.56 g (74 %) of compound **53** as a green solid which was used without further purification.

^{1}H-NMR: (360 MHz, $CDCl_3$): δ 7.87 (*s*, 2H), 7.33 – 7.42 (*m*, 12H), 7.08 – 7.13 (*m*, 2H).

^{13}C-NMR: (90.55 MHz, $CDCl_3$): δ 196.08 (C=O), 148.46 (2C, Cp), 134.11 (2C, Ph), 132.03 (2C, Ph), 131.83 (2C, Ph), 130.39 (2C, Ph), 129.96 (4C, Ph), 128.95 (4C, Ph), 128.66 (2C, Ph), 127.82 (2C, Ph), 127.68 (2C, Ph), 126.24 (2C, Cp), 119.31 (2C, Ph).

MALDI-ICR-MS (DCTB): m/z (% int): 539.96 ($M^{\bullet+}$, 100 %), 511.96 ($[M\text{-}CO]^{\bullet+}$, 50 %).

4.2.3 Synthesis of 6,11-dibromo-1,4-diphenyltriphenylene

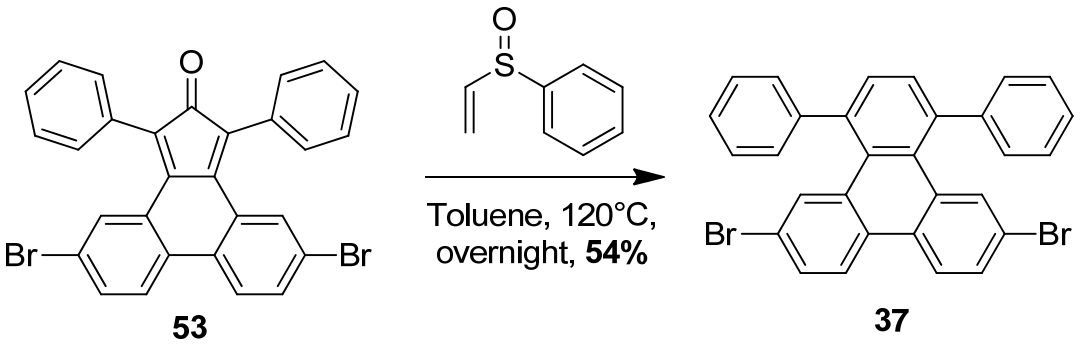

This reaction was performed following method B. Compound **53** (1.0 g, 1.85 mmol) and phenylvinyl sulfoxide (0.370 mL, 2.78 mmol) were dissolved in dry toluene (20 mL) in a Schlenk tube under inert atmosphere and under light exclusion to give a dark green suspension.

The mixture was stirred at 120°C overnight. The slightly yellow and transparent mixture was cooled down to RT (control the color!!). The organic solvents were removed in vacuo and the resulting yellow residue was separated by column chromatography (2x) using once Pentane / Ether 10:1 and for the second column pure pentane as eluent. One obtains 2.3 g (54 %) of the desired product **37** as a white powder.

^{1}H-NMR: (500 MHz, $CDCl_3$): δ 8.47 (*d*, 2H, $^{3}J_{HBr}$= 2.1 Hz), 7.55 (*d*, 2H, $^{3}J_{HH}$= 9.0 Hz), 7.54 (*s*, 2H), 7.37-7.45 (*m*, 10H), 7.19 (*dd*, 2H, $^{3}J_{HH}$= 9.0 Hz, $^{3}J_{HBr}$= 2.1 Hz).

^{13}C-NMR: (125.76 MHz, $CDCl_3$): δ 144.12 (2C, Ph), 139.24 (2C, Ph), 131.98 (2C, Ph), 131.72 (2C, Ph), 130.54 (2C, Ph), 130.43 (2C, Ph), 129.63 (4C, Ph), 129.52 (2C, Ph), 129.42 (4C, Ph), 129.21 (2C, Ph), 127.59 (2C, Ph), 126.14 (2C, Ph), 121.36 (2C, Ph).

MALDI-ICR-MS (DCTB): m/z (% int): 537.98 ($M^{\bullet+}$, 100 %), 457.06 ($[M\text{-}Br]^{\bullet+}$, 30 %), 378.14 ($[M\text{- }2 \times Br]^{\bullet+}$, 60 %).

4.2.4 1,4,6,11-tetraphenyltriphenylene

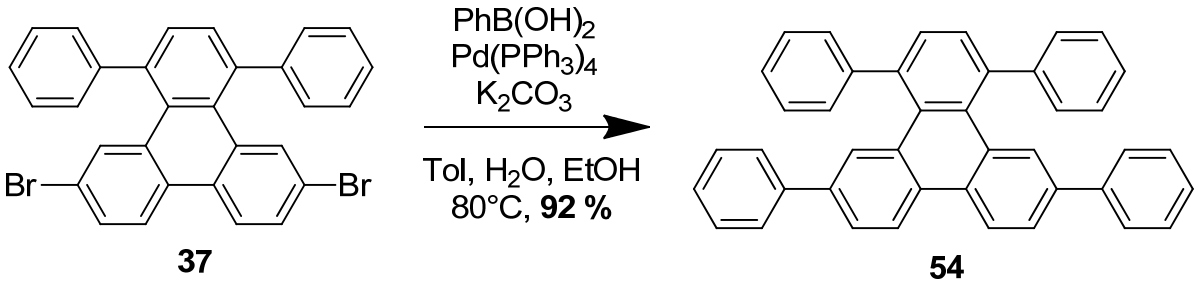

37 **54**

Method J. In a 75 mL Schlenk flask, 6,11-dibromo-1,4-diphenyltriphenylene **37** (45 mg, 0.084 mmol), phenylboronic acid (24.5 mg, 0.201 mmol, 2.2 eq.), tetrakis(triphenylphosphine) palladium(0) (1.9 mg, 1.67 µmol, 2 % mol), potassium carbonate (116 mg, 836 mmol, 10 eq.), are dissolved in a mix of toluene (9 mL), water (2 mL) and ethanol (2 mL). The reaction mixture was stirred at reflux for 3 days. After cooling down to RT, the mixture was extracted with water, dried over Na_2SO_4 and reduced in vacuo. One obtains 41 mg (92 %) of the desired product **54** as a yellowish powder.

^{1}H-NMR: (500 MHz, CD_2Cl_2): δ 8.75 (*s*, 2H), 7.76 (*d*, 2H, $^3J_{HH}$ = 8.8 Hz), 7.74 (*d*, 2H, $^3J_{HH}$ = 8.2 Hz), 7.73 (*d*, 2H, $^3J_{HH}$ = 8.0 Hz), 7.56 (*s*, 2H), 7.33 – 7.51 (*m*, 18H).

^{13}C-NMR: (90.55 MHz, CD_2Cl_2): δ 145.13 (2C, Ph), 141.23 (2C, Ph), 139.75 (2C, Ph), 139.64 (2C, Ph), 132.22 (2C, Ph), 131.45 (2C, Ph), 131.06 (2C, Ph), 130.60 (2C, Ph), 130.26 (2C, Ph), 130.15 (4C, Ph), 129.70 (4C, Ph), 129.44 (4C, Ph), 128.13 (2C, Ph), 127.77 (4C, Ph), 127.76 (2C, Ph), 125.08 (2C, Ph), 122.13 (2C, Ph).

EI-MS: m/z (% int): 532.21 ($M^{\bullet+}$, 100 %), 455.16 ($[M\text{-}Ph]^{\bullet+}$, 20 %).

4.2.5 Attempted synthesis of dibenzo-phenanthro-heptaphene

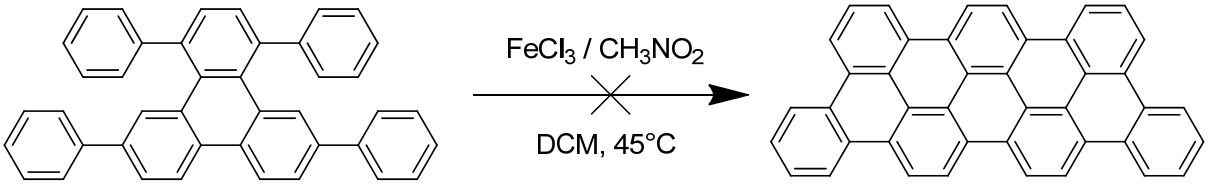

54 **55**

This reaction was performed following method D. $FeCl_3$ (256 mg, 1.58 mmol, 24 eq) was dissolved in CH_3NO_2 (1.5 mL) and cleaned with argon over 20 min. A solution of **54** (35 mg, 0.06 mmol) in dichloromethane (4 mL) was bubbled with argon over 30 min and then heated to 45°C. The $FeCl_3$ solution was added dropwise over 20 min. The solution turned dark green and then black. A black precipitate formed on the wall of the reaction vessel. The mixture quenched with MeOH was cooled in the fridge overnight and filtered several times over Millipore. One obtained 178 mg of insoluble black material.

No NMR or MS was obtained.

4.2.6 Synthesis of 6,11-bis(4-nonylphenyl)-1,4-diphenyltriphenylene

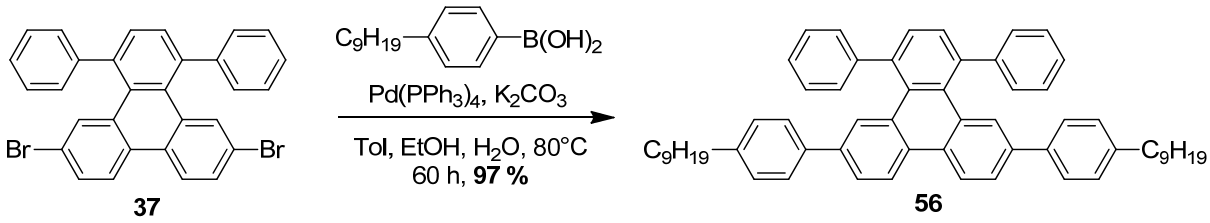

37 **56**

This reaction was performed following method J. In a 75 mL Schlenk flask, 6,11-dibromo-1,4-diphenyltriphenylene **37** (500 mg, 0.929 mmol), (4-nonylphenyl)boronic acid (553 mg, 2.23 mmol, 2.4 eq.), $Pd(PPh_3)_4$ (21.5 mg, 0.019 mmol, 2 %mol) and potassium carbonate (1.284 g, 9.29 mmol, 10 eq.) were dissolved in a mix of toluene (25 mL), water (5 mL) and ethanol (5 mL).

The mixture was refluxed for 60 h at 80°C. After cooling to RT, the mixture was washed with water. The combined organic layers were dried on $MgSO_4$ and reduced in vacuo. The resulting grey oil was poured over a short silica gel plug using a pentane / DCM 9:1 mixture as eluent.

One obtains 710 mg (**97 %**) of desired product **56** as colorless viscous oil.

^{1}H-NMR: (360 MHz, $CDCl_3$): δ 8.69 (*s*, 2H, Ph), 7.75 (*d*, 2H, $^3J_{HH}$ = 8.6 Hz, Ph), 7.73 (*d*, 2H, $^3J_{HH}$ = 8.6 Hz, Ph), 7.63 (*d*, 4H, $^3J_{HH}$ = 8.2 Hz, Ph), 7.53 (*s*, 2H, Ph), 7.26 – 7.52 (*m*, 10H, Ph), 7.18 (*d*, 4H, $^3J_{HH}$ = 7.2 Hz, Ph), 2.66 (*t*, 4H, $^3J_{HH}$ = 8.2 Hz, Ar-C*H*$_2$-C_8H_{17}), 1.64 (*tt*, 4H, $^3J_{HH}$ = 6.8 Hz, $^3J_{HH}$ = 6.8 Hz, Ar-CH_2-C*H*$_2$-C_7H_{15}), 1.29 (*m*, 24H, Ar-C_2H_4-C_6H_{12}-CH_3), 0.88 (*t*, 6H, $^3J_{HH}$ = 6.8 Hz, Ar-C_8H_{16}-C*H*$_3$).

^{13}C-NMR: (90.55 MHz, $CDCl_3$): δ 144.68 (C_q, 2C, Ph), 142.41 (C_q, 2C, Ph), 139.20 (C_q, 2C, Ph), 138.96 (C_q, 2C, Ph), 138.21 (C_q, 2C, Ph), 131.66 (C_q, 2C, Ph), 130.93 (C_q, 2C, Ph), 130.44 (CH, 2C, Ph), 129.63 (CH, 4C, Ph), 129.38 (C_q, 2C, Ph), 129.09 (CH, 4C, Ph), 128.92 (CH, 4C, Ph), 128.39 (CH, 2C, Ph), 127.13 (CH, 4C, Ph), 125.53 (CH, 2C, Ph), 124.52 (CH, 2C, Ph), 121.36 (CH, 2C, Ph), 35.67 (Ar-*C*H_2-C_8H_{17}), 31.90 (Ar-C_6H_{12}-*C*H_2-C_2H_5), 31.53 (Ar-CH_2-*C*H_2-C_7H_{15}), 29.58 (Ar-C_2H_4-*C*$_4H_8$-C_3H_7), 29.55 (Ar-C_2H_4-*C*$_4H_8$-C_3H_7), 29.38 (Ar-C_2H_4-*C*$_4H_8$-C_3H_7), 29.35 (Ar-C_2H_4-*C*$_4H_8$-C_3H_7), 22.69 (Ar-C_6H_{12}-*C*H_2-CH_3), 14.12 (Ar-C_8H_{16}-*C*H_3).

MALDI-ICR-MS (DCTB): m/z (% int): 784.50 ($M^{\bullet+}$, 100 %), 657.35 ([M-C_9H_{19}]$^{\bullet+}$, 20 %), 582.33 ([M- C_9H_{19} – Ph]$^{\bullet+}$, 40 %), 567.31 ([M- C_9H_{19} – Ph – CH_3]$^{\bullet+}$, 90 %), 455.18 ([M - 2 x C_9H_{19} - Ph]$^{\bullet+}$, 10 %).

4.2.7 Attempted synthesis of 5,16-dinonyl-dibenzophenanthroheptaphene

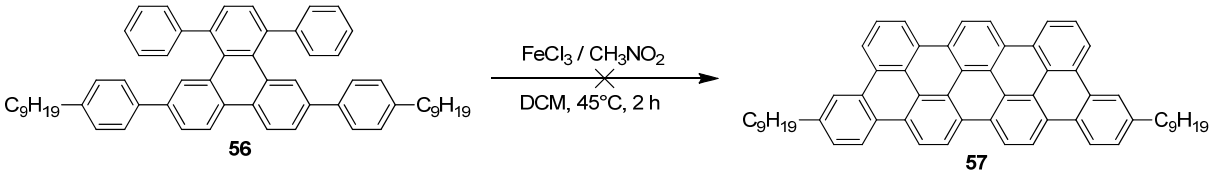

This reaction was performed following method D. $FeCl_3$ (3.471 g, 21.4 mmol, 24 eq, 3 eq per H to be removed) was dissolved in CH_3NO_2 (10 mL) and cleaned with argon over 30 min. A solution of **56** (700 mg, 0.892 mmol) in dichloromethane (60 mL) was bubbled with argon over 30 min and then heated to 45°C. The $FeCl_3$ solution was added dropwise over 20 min. The solution turned dark green and then black. The mixture was refluxed for 2h, followed by cooling to RT and quenching with MeOH.

The mixture was cooled in the fridge overnight and filtered several times over Millipore.

Only the partially oxidized compound **58** was obtained. The NMR spectra were not conclusive, the hydrogen labeled (a) below should have a displacement around 5 ppm due to the shielding of the aromatic ring below but could not be found on the ^{1}H-NMR spectrum.

MALDI-ICR-MS (DCTB): m/z (% int): 780.49 ($M^{\bullet+}$, 100 %), 668.37 ($[M\text{-}C_8H_{17}]^{\bullet+}$, 10 %), 578.33 ($[M\text{- }C_9H_{19} – Ph]^{\bullet+}$, 40 %), 555.25 ($[M\text{- 2 x }C_8H_{17}]^{\bullet+}$, 35 %), 465.20 ($[M - 2 \text{ x } C_9H_{19} - Ph]^{\bullet+}$, 30 %).

UV/VIS: (DCM, 10^{-6} M), λ_{max} [nm] = 306, 352, 372.

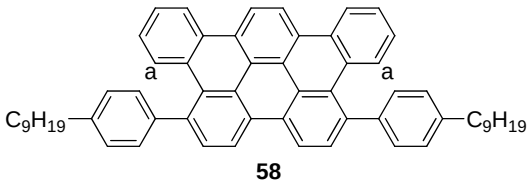

4.3 Triangular BBTO derivative

4.3.1 2,2''-dibromo-5'-(2-bromophenyl)-1,1':3',1''-terphenyl

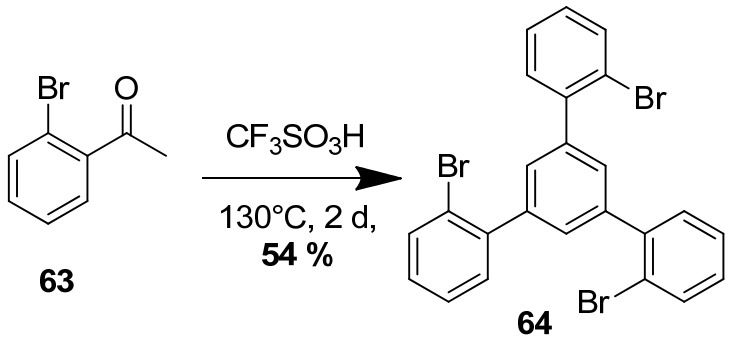

63 64

Method K. 2'-bromoacetophenone **63** (15.00g, 75.4 mmol) was filled into a Schlenk tube. Trifluoromethanesulfonic acid (1.13 g, 7.54 mmol, 10 %mol) was added in one portion and the mixture was stirred at 130°C over 2 days. The mixture was cooled down to room temperature and water was added.

The mixture was extracted with DCM. The combined organic layers were washed with water (2x 100 mL) and brine (2x 100 mL), dried over $MgSO_4$, filtered and dried *in vacuo*.

The crude product was adsorbed on silica and purified by column chromatography using pentane/DCM: 9/1 as eluent. One obtains 7.37 g (54 %) of the desired product **64** as an off-white powder.

^{1}H-NMR: (360 MHz, $CDCl_3$): δ 7.69 (*d*, 3H, $^{3}J_{HH}$ = 7.7 Hz, Ph), 7.51 (*s*, 3H, Ph), 7.46 (*d*, $^{3}J_{HH}$ = 7.3 Hz, Ph), 7.38 (*dd*, 3H, $^{3}J_{HH}$ = 7.7 Hz, $^{3}J_{HH}$ = 7.7 Hz, Ph), 7.22 (*dd*, 3H, $^{3}J_{HH}$ = 7.7 Hz, $^{3}J_{HH}$ = 7.7 Hz, Ph).

^{13}C-NMR: (90.55 MHz, $CDCl_3$): δ 142.12 (3C, Ph), 140.54 (3C, Ph), 133.36 (3C, Ph), 131.69 (3C, Ph), 129.78 (3C, Ph), 129.06 (3C, Ph), 127.59 (3C, Ph), 122.80 (3C, Ph).

EI-MS: m/z (% int): 542.3 ($M^{\bullet+}$, 20 %), 464.3 ($[M - Br]^{\bullet+}$, 5 %), 384.2 ($[M - 2 \times Br]^{\bullet+}$, 10 %), 302.4 ($[M - 3 \times Br]^{\bullet+}$, 30 %), 207.2 (100 %).

Crystallographic data of 64

Empirical formula	C24 H15 Br3
Formula weight	543.09
Temperature	150(2) K
Wavelength	0.71073 A
Crystal system, space group	Triclinic, P -1
Unit cell dimensions	a = 10.0652(7) A alpha = 104.603(5) deg.
	b = 11.0060(7) A beta = 109.816(5) deg.
	c = 11.6848(7) A gamma = 112.185(5) deg.
Volume	1014.60(11) A^3
Z, Calculated density	2, 1.778 Mg/m^3
Absorption coefficient	5.970 mm^-1
F(000)	528
Theta range for data collection	2.06 to 20.00 deg.
Limiting indices	-9<=h<=8, -10<=k<=10, 0<=l<=11
Reflections collected / unique	1826 / 1826 [R(int) = 0.0000]
Completeness to theta = 20.00	96.4 %
Refinement method	Full-matrix least-squares on F^2
Data / restraints / parameters	1826 / 0 / 244
Goodness-of-fit on F^2	0.978
Final R indices [I>2sigma(I)]	R1 = 0.0322, wR2 = 0.0748
R indices (all data)	R1 = 0.0420, wR2 = 0.0781
Largest diff. peak and hole	0.582 and -0.365 e.A^-3

Atomic coordinates (x 10^4) and equivalent isotropic displacement parameters (A^2 x 10^3) of **64**. U(eq) is defined as one third of the trace of the orthogonalized U_{ij} tensor.

	x	y	z	U(eq)
C(1)	-1514(7)	2113(6)	-1281(5)	27(1)
C(2)	-1505(7)	2066(6)	-108(6)	34(2)
C(3)	-2379(7)	2540(6)	400(6)	31(2)
C(4)	-3306(7)	3016(6)	-321(6)	33(2)
C(5)	-3351(7)	3079(6)	-1487(6)	28(1)
C(6)	-2426(7)	2644(6)	-1951(6)	31(2)
C(7)	-499(7)	1713(6)	-1792(5)	28(1)
C(8)	498(8)	2686(7)	-2111(6)	42(2)
C(9)	1488(9)	2406(9)	-2576(8)	59(2)
C(10)	1508(11)	1137(10)	-2731(9)	72(2)
C(11)	545(9)	161(8)	-2432(7)	56(2)
C(12)	-464(7)	436(7)	-1975(6)	35(2)
C(13)	-2348(8)	2462(6)	1670(6)	32(2)
C(14)	-3805(9)	1579(7)	1650(6)	42(2)
C(15)	-3803(9)	1436(7)	2773(7)	49(2)
C(16)	-2356(10)	2151(8)	3968(7)	49(2)
C(17)	-912(9)	3044(7)	4053(6)	42(2)
C(18)	-905(8)	3194(6)	2911(6)	36(2)
C(19)	-4233(7)	3715(6)	-2184(6)	29(1)
C(20)	-3988(7)	5062(6)	-1419(6)	37(2)
C(21)	-4698(8)	5747(7)	-2010(7)	43(2)
C(22)	-5664(8)	5123(8)	-3374(7)	45(2)
C(23)	-5958(8)	3817(7)	-4177(7)	43(2)
C(24)	-5254(7)	3101(6)	-3575(6)	34(2)
Br(1)	-1880(1)	-1071(1)	-1737(1)	46(1)
Br(2)	1137(1)	4443(1)	3078(1)	49(1)
Br(3)	-5854(1)	1214(1)	-4740(1)	51(1)

Bond lengths [Å]

C(1)-C(2)	1.381(8)
C(1)-C(6)	1.395(8)
C(1)-C(7)	1.489(8)
C(2)-C(3)	1.394(8)
C(2)-H(2)	0.9300
C(3)-C(4)	1.384(8)
C(3)-C(13)	1.498(8)
C(4)-C(5)	1.369(8)
C(4)-H(4)	0.9300
C(5)-C(6)	1.392(8)
C(5)-C(19)	1.486(8)
C(6)-H(6)	0.9300
C(7)-C(12)	1.384(8)
C(7)-C(8)	1.391(8)
C(8)-C(9)	1.377(9)
C(8)-H(8)	0.9300
C(9)-C(10)	1.371(11)
C(9)-H(9)	0.9300
C(10)-C(11)	1.359(10)
C(10)-H(10)	0.9300
C(11)-C(12)	1.388(9)
C(11)-H(11)	0.9300
C(12)-Br(1)	1.890(6)
C(13)-C(18)	1.400(9)
C(13)-C(14)	1.409(9)
C(14)-C(15)	1.361(9)
C(14)-H(14)	0.9300
C(15)-C(16)	1.375(10)
C(15)-H(15)	0.9300
C(16)-C(17)	1.365(10)
C(16)-H(16)	0.9300
C(17)-C(18)	1.387(8)
C(17)-H(17)	0.9300
C(18)-Br(2)	1.901(6)
C(19)-C(24)	1.395(8)
C(19)-C(20)	1.401(8)
C(20)-C(21)	1.375(9)
C(20)-H(20)	0.9300
C(21)-C(22)	1.360(9)
C(21)-H(21)	0.9300
C(22)-C(23)	1.358(9)
C(22)-H(22)	0.9300
C(23)-C(24)	1.407(9)
C(23)-H(23)	0.9300
C(24)-Br(3)	1.897(6)

Angles [°]

C(2)-C(1)-C(6)	118.3(5)
C(2)-C(1)-C(7)	122.1(5)
C(6)-C(1)-C(7)	119.4(5)
C(1)-C(2)-C(3)	121.1(5)
C(1)-C(2)-H(2)	119.5
C(3)-C(2)-H(2)	119.5
C(4)-C(3)-C(2)	118.5(5)
C(4)-C(3)-C(13)	121.9(5)
C(2)-C(3)-C(13)	119.5(5)
C(5)-C(4)-C(3)	122.2(5)
C(5)-C(4)-H(4)	118.9
C(3)-C(4)-H(4)	118.9
C(4)-C(5)-C(6)	118.1(5)
C(4)-C(5)-C(19)	121.6(5)
C(6)-C(5)-C(19)	120.1(5)
C(5)-C(6)-C(1)	121.6(5)
C(5)-C(6)-H(6)	119.2
C(1)-C(6)-H(6)	119.2
C(12)-C(7)-C(8)	116.8(5)
C(12)-C(7)-C(1)	124.8(5)
C(8)-C(7)-C(1)	118.4(5)
C(9)-C(8)-C(7)	122.0(6)
C(9)-C(8)-H(8)	119.0
C(7)-C(8)-H(8)	119.0
C(10)-C(9)-C(8)	119.7(7)
C(18)-C(13)-C(3)	123.2(5)
C(15)-C(14)-H(14)	119.2
C(13)-C(14)-H(14)	119.2
C(7)-C(12)-Br(1)	122.1(4)
C(11)-C(12)-Br(1)	116.6(5)
C(14)-C(13)-C(3)	120.4(5)
C(15)-C(14)-C(13)	121.6(6)
C(18)-C(13)-C(14)	116.3(5)
C(14)-C(15)-C(16)	120.3(7)
C(12)-C(11)-H(11)	119.7
C(7)-C(12)-C(11)	121.1(6)
C(14)-C(15)-H(15)	119.9
C(16)-C(15)-H(15)	119.9
C(10)-C(11)-C(12)	120.6(7)
C(10)-C(11)-H(11)	119.7
C(17)-C(16)-C(15)	120.6(6)
C(17)-C(16)-H(16)	119.7
C(15)-C(16)-H(16)	119.7
C(11)-C(10)-H(10)	120.1
C(9)-C(10)-H(10)	120.1
C(16)-C(17)-C(18)	119.4(6)
C(10)-C(9)-H(9)	120.1
C(11)-C(10)-C(9)	119.8(7)
C(8)-C(9)-H(9)	120.1
C(16)-C(17)-H(17)	120.3
C(18)-C(17)-H(17)	120.3
C(17)-C(18)-C(13)	121.7(6)
C(17)-C(18)-Br(2)	117.9(5)
C(13)-C(18)-Br(2)	120.4(4)
C(24)-C(19)-C(20)	116.2(5)
C(24)-C(19)-C(5)	124.8(5)
C(20)-C(19)-C(5)	118.9(5)
C(21)-C(20)-C(19)	121.9(6)
C(21)-C(20)-H(20)	119.1
C(19)-C(20)-H(20)	119.1
C(22)-C(21)-C(20)	120.1(6)
C(22)-C(21)-H(21)	120.0
C(20)-C(21)-H(21)	120.0
C(23)-C(22)-C(21)	121.2(6)
C(23)-C(22)-H(22)	119.4
C(21)-C(22)-H(22)	119.4
C(22)-C(23)-C(24)	118.9(6)
C(22)-C(23)-H(23)	120.6
C(24)-C(23)-H(23)	120.6
C(19)-C(24)-C(23)	121.7(6)
C(19)-C(24)-Br(3)	121.6(4)
C(23)-C(24)-Br(3)	116.6(4)

Anisotropic displacement parameters (A^2 x 10^3) of **64**. The anisotropic displacement factor exponent takes the form: $-2\pi^2$ [$h^2 a^{*2}$ U11 + ... + 2 h k a* b* U12]

	U11	U22	U33	U23	U13	U12
C(1)	32(3)	30(3)	26(3)	15(3)	14(3)	22(3)
C(2)	39(4)	40(4)	35(4)	18(3)	20(3)	30(3)
C(3)	40(4)	35(3)	25(3)	17(3)	16(3)	22(3)
C(4)	37(4)	43(4)	33(4)	19(3)	21(3)	30(3)
C(5)	28(3)	25(3)	31(4)	12(3)	12(3)	16(3)
C(6)	32(4)	33(3)	26(3)	13(3)	13(3)	16(3)
C(7)	25(3)	34(4)	23(3)	7(3)	12(3)	15(3)
C(8)	43(4)	38(4)	55(4)	22(3)	29(4)	23(3)
C(9)	64(5)	67(5)	79(5)	41(4)	54(5)	40(4)
C(10)	86(6)	91(7)	104(7)	56(6)	76(6)	68(6)
C(11)	61(5)	57(5)	71(5)	29(4)	41(4)	40(4)
C(12)	32(4)	43(4)	35(4)	14(3)	17(3)	25(3)
C(13)	43(4)	28(3)	35(4)	12(3)	22(4)	26(3)
C(14)	56(5)	52(4)	34(4)	18(3)	26(4)	37(4)
C(15)	56(5)	49(4)	51(5)	22(4)	34(5)	26(4)
C(16)	84(6)	50(4)	44(5)	31(4)	46(5)	42(5)
C(17)	63(5)	42(4)	30(4)	19(3)	23(4)	32(4)
C(18)	47(4)	30(3)	42(4)	20(3)	26(4)	24(3)
C(19)	26(3)	35(4)	32(4)	17(3)	18(3)	18(3)
C(20)	39(4)	38(4)	39(4)	18(3)	17(3)	25(3)
C(21)	52(4)	30(4)	69(6)	27(4)	39(4)	29(4)
C(22)	50(4)	58(5)	49(5)	37(4)	24(4)	38(4)
C(23)	49(4)	45(4)	42(4)	24(4)	20(3)	29(4)
C(24)	37(4)	40(4)	31(4)	16(3)	19(3)	22(3)
Br(1)	49(1)	40(1)	54(1)	24(1)	24(1)	26(1)
Br(2)	47(1)	47(1)	47(1)	19(1)	21(1)	20(1)
Br(3)	60(1)	48(1)	37(1)	11(1)	16(1)	33(1)

Hydrogen coordinates (x 10^4) and isotropic displacement parameters (A^2 x 10^3) of **64**.

	x	y	z	U(eq)
H(2)	-906	1713	350	41
H(4)	-3921	3302	-2	39
H(6)	-2415	2710	-2726	37
H(8)	497	3551	-2007	51
H(9)	2140	3075	-2783	71
H(10)	2178	944	-3041	86
H(11)	562	-698	-2535	67
H(14)	-4793	1082	848	50
H(15)	-4784	852	2734	59
H(16)	-2361	2024	4724	59
H(17)	59	3549	4870	51
H(20)	-3326	5505	-486	44
H(21)	-4518	6638	-1476	52
H(22)	-6131	5599	-3764	54
H(23)	-6614	3403	-5109	51

Torsion angles [°]

C(6)-C(1)-C(2)-C(3)	-0.2(8)
C(7)-C(1)-C(2)-C(3)	175.6(5)
C(1)-C(2)-C(3)-C(4)	2.1(9)
C(1)-C(2)-C(3)-C(13)	179.6(5)
C(2)-C(3)-C(4)-C(5)	-2.1(9)
C(13)-C(3)-C(4)-C(5)	-179.5(5)
C(3)-C(4)-C(5)-C(6)	0.1(8)
C(3)-C(4)-C(5)-C(19)	-174.5(5)
C(4)-C(5)-C(6)-C(1)	2.0(8)
C(19)-C(5)-C(6)-C(1)	176.7(5)
C(2)-C(1)-C(6)-C(5)	-2.0(8)
C(7)-C(1)-C(6)-C(5)	-177.8(5)
C(8)-C(7)-C(12)-Br(1)	-174.5(4)
C(1)-C(7)-C(12)-Br(1)	5.7(8)
C(16)-C(17)-C(18)-Br(2)	-179.7(5)
C(14)-C(13)-C(18)-C(17)	0.6(8)
C(8)-C(7)-C(12)-C(11)	1.1(9)
C(1)-C(7)-C(12)-C(11)	-178.7(6)
C(3)-C(13)-C(18)-C(17)	-177.0(5)
C(14)-C(13)-C(18)-Br(2)	-179.0(4)
C(8)-C(9)-C(10)-C(11)	0.3(12)
C(9)-C(10)-C(11)-C(12)	0.2(12)
C(3)-C(13)-C(18)-Br(2)	3.4(8)
C(4)-C(5)-C(19)-C(24)	-135.7(6)
C(1)-C(7)-C(8)-C(9)	179.3(6)
C(7)-C(8)-C(9)-C(10)	-0.2(11)
C(6)-C(5)-C(19)-C(24)	49.8(8)
C(4)-C(5)-C(19)-C(20)	47.2(8)
C(6)-C(5)-C(19)-C(20)	-127.3(6)
C(21)-C(22)-C(23)-C(24)	0.4(10)
C(20)-C(19)-C(24)-C(23)	1.8(8)
C(5)-C(19)-C(24)-C(23)	-175.4(5)
C(20)-C(19)-C(24)-Br(3)	-175.0(4)
C(19)-C(20)-C(21)-C(22)	-0.4(9)
C(20)-C(21)-C(22)-C(23)	0.5(10)
C(5)-C(19)-C(24)-Br(3)	7.9(8)
C(22)-C(23)-C(24)-C(19)	-1.6(9)
C(24)-C(19)-C(20)-C(21)	-0.8(8)
C(5)-C(19)-C(20)-C(21)	176.5(5)
C(22)-C(23)-C(24)-Br(3)	175.2(5)
C(16)-C(17)-C(18)-C(13)	0.7(9)
C(6)-C(1)-C(7)-C(8)	47.0(7)
C(12)-C(7)-C(8)-C(9)	-0.5(9)
C(4)-C(3)-C(13)-C(14)	59.7(8)
C(6)-C(1)-C(7)-C(12)	-133.2(6)
C(2)-C(1)-C(7)-C(8)	-128.7(6)
C(2)-C(1)-C(7)-C(12)	51.1(8)
C(2)-C(3)-C(13)-C(14)	-117.6(6)
C(18)-C(13)-C(14)-C(15)	-0.7(8)
C(3)-C(13)-C(14)-C(15)	177.0(6)
C(4)-C(3)-C(13)-C(18)	-122.8(6)
C(2)-C(3)-C(13)-C(18)	59.9(8)
C(13)-C(14)-C(15)-C(16)	-0.5(10)
C(14)-C(15)-C(16)-C(17)	1.9(10)
C(10)-C(11)-C(12)-C(7)	-1.0(10)
C(10)-C(11)-C(12)-Br(1)	174.9(6)
C(15)-C(16)-C(17)-C(18)	-2.0(9)

4.3.2 (5''-(4'-(trimethylsilyl)-[1,1'-biphenyl]-2-yl)-[1,1':2',1'':3'',1''':2''',1''''-quinquephenyl]-4,4''''-diyl)bis(trimethylsilane)

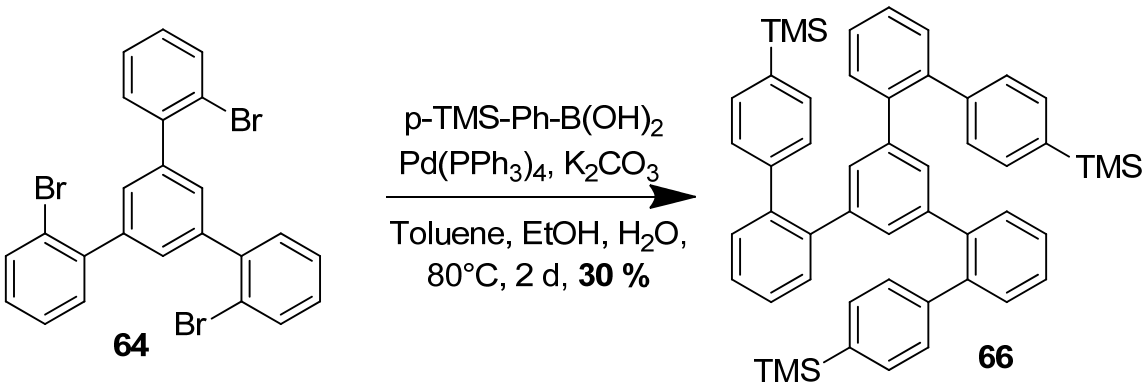

This reaction was performed similar to method J. In a Schlenk flask, 2,2"-dibromo-5'-(2-bromophenyl)-1,1':3',1"-terphenyl **64** (3.1 g, 5.70 mmol), 4-(trimethylsilyl)phenylboronic acid (3.98 g, 20.52 mmol, 3.6 eq), potassium carbonate (7.88 g, 57.0 mmol, 10 eq) and tetrakis(triphenylphosphine) palladium(0) (198 mg, 0.171 mmol, 3 % mol) were dissolved in a mix of toluene (100 mL), water (20 mL) and ethanol (20 mL).

The reaction mixture was stirred at reflux (80 °C) for 2 days. After cooling down to RT, the mixture was extracted with water, dried over Na_2SO_4 and reduced *in vacuo*.

The mixture was separated by column chromatography on silica gel using PE/DCM: 6/1 as eluent. One obtains 1.29 g (30 %) of the desired product **66** as a white powder.

^{1}H-NMR: (360 MHz, $CDCl_3$): δ 7.52 (*d*, 6H, $^3J_{HH}$ = 7.3 Hz, Ph), 7.40 (*dd*, 3H, $^3J_{HH}$ = 7.3 Hz, $^3J_{HH}$ = 7.3 Hz, Ph), 7.36 (*dd*, 3H, $^3J_{HH}$ = 7.3 Hz, $^3J_{HH}$ = 7.3 Hz, Ph), 7.13 – 7.27 (*m*, 3H, Ph), 7.10 (*d*, 6H, $^3J_{HH}$ = 7.3 Hz, Ph), 6.70 – 6.77 (*m*, 6H, Ph), 0.32 (*s*, 27H, Ar-TMS).

^{13}C-NMR: (90.55 MHz, $CDCl_3$): δ 142.23 (3C, Ph), 140.86 (3C, Ph), 140.68 (3C, Ph), 140.62 (3C, Ph), 138.28 (3C, Ph), 133.06 (6C, Ph), 130.59 (3C, Ph), 130.41 (3C, Ph), 130.10 (3C, Ph), 129.79 (6C, Ph), 127.45 (3C, Ph), 127.43 (3C, Ph), -0.88 (TMS).

EI-MS: m/z (% int): 750.4 ($M^{\bullet+}$, 100 %).

4.3.3 1,3,5-tris(4''-iodo-2'-biphenyl)benzene

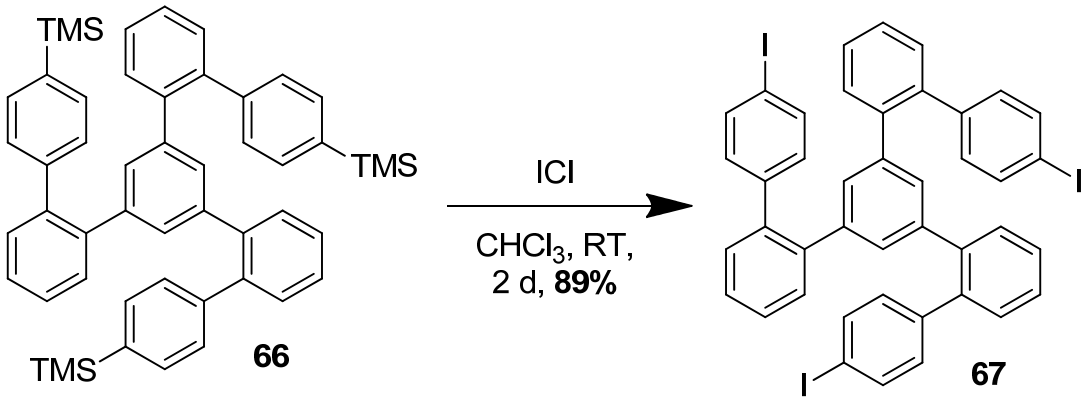

Method L. (5''-(4'-(trimethylsilyl)-[1,1'-biphenyl]-2-yl)-[1,1':2',1'':3'',1''':2''',1''''-quinquephenyl]-4,4''''-diyl)bis(trimethylsilane) **66** (5.38 g, 7.19 mmol) was dissolved in chloroform (2.4 L) and iodine monochloride (4.20 g, 25.9 mmol, 3.6 eq.) was added. The mixture was agitated over 2 days at RT. The reaction was quenched by adding saturated aqueous sodium disulfite (200 mL).

The organic layer was washed with water thrice and dried over Na_2SO_4. The mixture was concentrated to 100 mL and MeOH was added in order to precipitate the desired product which was filtered off by Büchner. One obtains 5.86 g (89 %) of the triiodo-compound **67** as a bright white powder.

^{1}H-NMR: (360 MHz, $CDCl_3$): δ 7.63 (*d*, 6H, $^3J_{HH}$ = 8.3 Hz), 7.30 - 7.40 (*m*, 9H), 6.85 (*m*, 3H), 6.73 (*d*, $^3J_{HH}$ = 8.3 Hz, 6H), 6.67 (*s*, 3H).

^{13}C-NMR: (90.55 MHz, $CDCl_3$): δ 141.34 (3C, Ph), 140.77 (3C, Ph), 140.20 (3C, Ph), 139.54 (3C, Ph), 137.18 (6C, Ph), 132.15 (6C, Ph), 130.67 (3C, Ph), 130.05 (3C, Ph), 129.94 (3C, Ph), 128.03 (3C, Ph), 127.75 (3C, Ph), 92.38 (3C, Ar-I).

EI-MS: m/z (% int): 912.0 ($M^{\bullet+}$, 100 %), 786.1 ($[M\text{-}I]^{\bullet+}$, 10 %), 658.2 ($[M\text{- 2 x I}]^{\bullet+}$, 40 %).

4.3.4 Synthesis of „1,3,5-tris-terphenylbenzene“

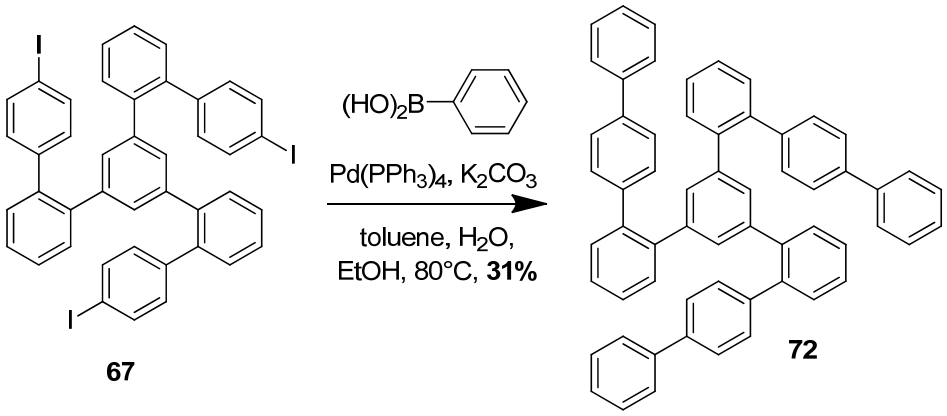

This reaction was performed similar to method J. In a 75 mL Schlenk flask, 1,3,5-tris(4''-iodo-2'-biphenyl)benzene **67** (100 mg, 0.110 mmol), phenylboronic acid (48 mg, 0.395 mmol, 3.6 eq.), tetrakis(triphenylphosphine) palladium(0) (3.8 mg, 3.29 µmol, 0.03 %mol), potassium carbonate (151 mg, 1.10 mmol, 10 eq.), are dissolved in a mix of toluene (15 mL), water (3 mL) and ethanol (3 mL). The reaction mixture was stirred at reflux for 2.5 days. After cooling down to RT, the mixture was extracted with water, dried over Na_2SO_4 and reduced in vacuo.

The residue was dissolved in pentane and poured over a short silica gel plug using pentane as eluent. One obtains the desired compound **72** (26 mg, 31 %) as a white powder.

EI-MS: m/z (% int): 762.3 ($M^{\bullet+}$, 100 %).

4.3.5 Attempted synthesis of benzo[*o*]bistriphenyleno-ovalene

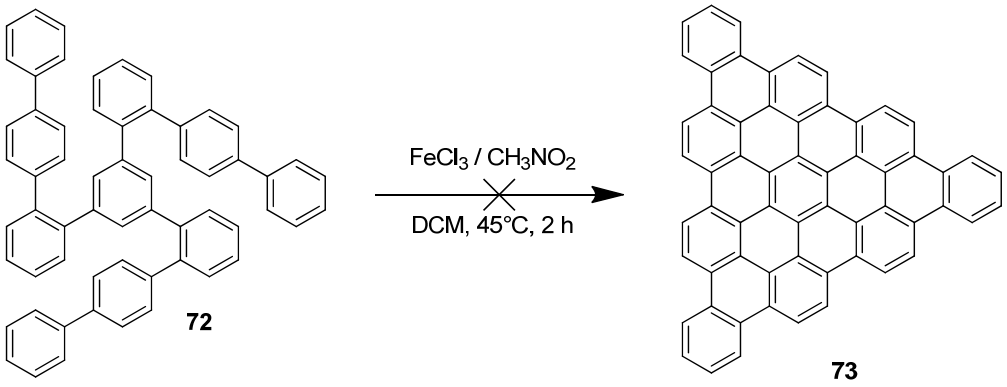

This reaction was performed following method D. $FeCl_3$ (298 mg, 1.84 mmol, 54 eq) was dissolved in CH_3NO_2 (1.0 mL) and cleaned with argon over 20 min. A solution of **72** (26 mg, 0.035 mmol) in dichloromethane (2 mL) was bubbled with argon over 30 min and then heated to 45°C. The $FeCl_3$ solution was added dropwise over 20 min. The solution turned dark green and then black. A black precipitate formed on the wall of the reaction vessel. After heating for 2 h, the mixture was cooled do RT and quenched by MeOH. After storing in the fridge overnight and several filtrations over Millipore®, one obtained 198 mg of insoluble black material.

No NMR or MS was obtained.

4.3.6 Synthesis of compound 75

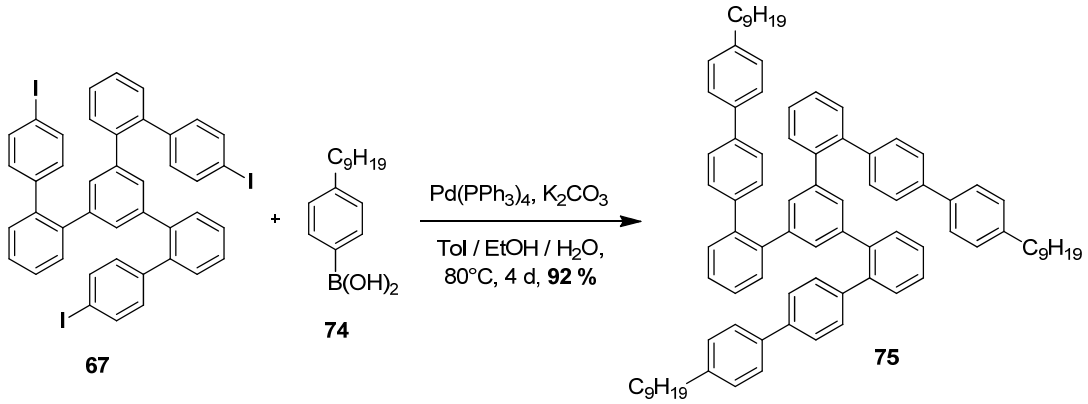

This reaction was performed similar to method J. In a 75 mL Schlenk tube, 4,4""-diiodo-5"-(4'-iodo-[1,1'-biphenyl]-2-yl)-1,1':2',1":3",1"':2"',1""-quinquephenyl **67** (600 mg, 0.658 mmol), (4-nonylphenyl)boronic acid **74** (588 mg, 2.367 mmol), $Pd(PPh_3)_4$ (22.80 mg, 0.020 mmol) and K_2CO_3 (909 mg, 6.58 mmol) were dissolved in a mixture of 20 mL of toluene, 5 mL of water and 5 mL of ethanol (ratio 5:1:1). The mixture was refluxed for 4 days.

After cooling down to RT, the mixture was washed with water; the organic phase was dried over $MgSO_4$ and reduced in vacuo. The crude mixture was poured over a short silica gel plug using PE/DCM 9:1 as eluent. One obtains 691 mg of the desired compound **75** (92 %) as colorless viscous oil.

^{1}H-NMR: (360 MHz, CD_2Cl_2): δ 7.29 – 7.36 (*m*, 12H, Ph), 7.20 – 7.28 (*m*, 9H, Ph), 7.17 (*d*, 6H, $^3J_{HH}$ = 7.7 Hz Ph), 6.99 (*d*, 3H, $^3J_{HH}$ = 7.7 Hz, Ph), 6.90 (*d*, 6H, $^3J_{HH}$ = 7.7 Hz, Ph), 6.80 (*s*, 3H, Ph), 2.67 (*t*, 4H, $^3J_{HH}$ = 7.7 Hz, Ar-C*H*$_2$-C_8H_{17}), 1.67 (*tt*, 4H, $^3J_{HH}$ = 6.8 Hz, $^3J_{HH}$ = 6.8 Hz, Ar-CH_2-C*H*$_2$-C_7H_{15}), 1.21 – 1.41 (*m*, 24H, Ar-C_2H_4-C_6H_{12}-CH_3), 0.88 (*t*, 6H, $^3J_{HH}$ = 6.8 Hz, Ar-C_8H_{16}-C*H*$_3$).

^{13}C-NMR: (90.55 MHz, CD_2Cl_2): δ 142.80 (C_q, 3C, Ph), 141.85 (C_q, 3C, Ph), 141.25 (C_q, 3C, Ph), 141.10 (C_q, 3C, Ph), 140.86 (C_q, 3C, Ph), 139.55 (C_q, 3C, Ph), 138.54 (C_q, 3C, Ph), 130.98 (CH, 3C, Ph), 130.88 (CH, 6C, Ph), 130.62 (CH, 3C, Ph), 130.18 (CH, 3C, Ph), 129.47 (CH, 6C, Ph), 127.90 (CH, 3C, Ph), 127.75 (CH, 3C, Ph), 127.35 (CH, 6C, Ph), 127.01 (CH, 6C, Ph), 36.24 (Ar-*C*H_2-C_8H_{17}), 32.51 (Ar-C_6H_{12}-*C*H_2-C_2H_5), 32.23 (Ar-CH_2-*C*H_2-C_7H_{15}), 30.19 (Ar-C_2H_4-*C*$_4H_8$-C_3H_7), 30.07 (Ar-C_2H_4-*C*$_4H_8$-C_3H_7), 29.96 (Ar-C_2H_4-*C*$_4H_8$-C_3H_7), 29.94 (Ar-C_2H_4-*C*$_4H_8$-C_3H_7), 23.28 (Ar-C_6H_{12}-*C*H_2-CH_3), 14.49 (Ar-C_8H_{16}-*C*H_3).

MALDI-ICR-MS: m/z (% int): 1140.74 ($M^{\bullet+}$, 100 %), 923.55 ([M-Ph-C_9H_{19}-CH_3]$^{\bullet+}$, 20 %).

4.3.7 Synthesis of the tri-alkyl substituted DBPO

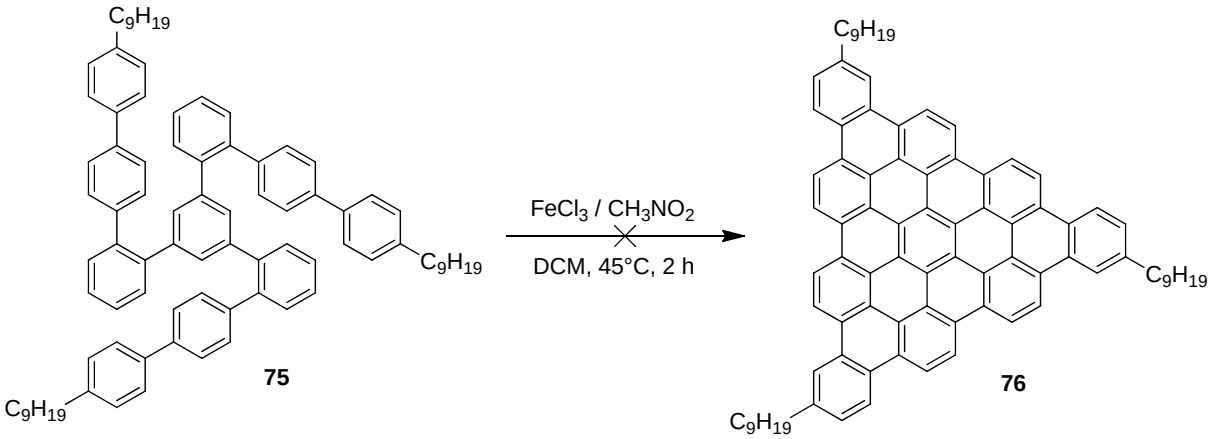

This reaction was performed following method D. $FeCl_3$ (5.294 g, 32.6 mmol, 24 eq, 3 eq per H to be removed) was dissolved in CH_3NO_2 (15 mL) and cleaned with argon over 30 min. A solution of **75** (690 mg, 0.604 mmol) in dichloromethane (50 mL) was bubbled with argon over 30 min and then heated to 45°C. The $FeCl_3$ solution was added dropwise over 20 min. The solution turned dark green and then black. The mixture was refluxed for 2h, followed by cooling to RT and quenching with MeOH.

The mixture was cooled in the fridge overnight and filtered several times over Millipore®. The brown residue is dissolved in 1 L of DCM and extracted with water. One obtains probably only the partially oxidized compound **77**, even if the MALDI shows the fully oxidized compound. This is probably due to the ionization energy of the MALDI-LASER. The NMR spectra were not conclusive.

MALDI-ICR-MS: m/z (% int): 1122.61 ($M^{\bullet+}$, 100 %), 1009.48 ($[M - C_8H_{17}]^{\bullet+}$, 25 %), 996.48 ($[M - C_9H_{19}]^{\bullet+}$, 20 %), 896.35 ($[M - C_9H_{19} - C_7H_{15}]^{\bullet+}$, 20 %), 883.34 ($[M - C_9H_{19} - C_8H_{17}]^{\bullet+}$, 20 %), 769.20 ($[M- 2 \times C_9H_{19} – C_7H_{18}]^{\bullet+}$, 15 %), 756.19 ($[M- 2 \times C_9H_{19} - C_8H_{17}]^{\bullet+}$, 10 %).

UV/VIS: (DCM, 10^{-6} M), λ_{max} [nm] = 393, 484.

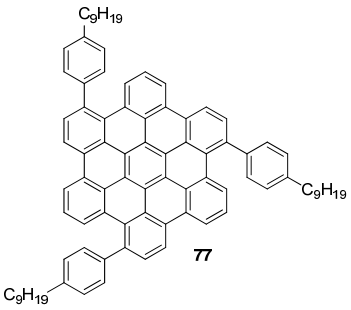

4.4 Perfluorinated sidechain

4.4.1 1,2-di(but-3-enyl)benzene

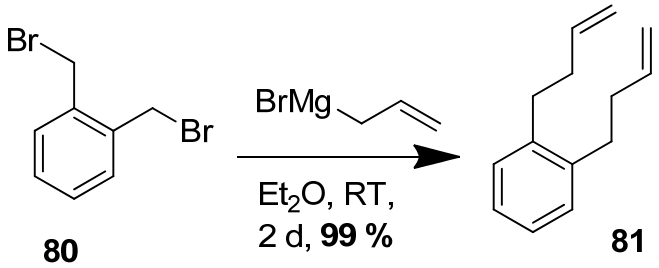

Method M. α-α'-bromo-*o*-xylene **80** (2.00 g, 7.58 mmol) was dissolved in Diethyl ether (10 mL) in a Schlenk tube. Allylmagnesium bromide 1M in Et_2O (16.67 mL, 16.67 mmol, 2.2 eq) was added slowly (1 mL/h) to the mixture using an automatic injector. After the end of the addition period the reaction was stirred at RT during 2 days.

Subsequent to hydrolysis with water and half concentrated H_2SO_4 until no precipitate was observed, the organic layer was separated and the water phase extracted thrice with Et_2O.

The combined organic layers were washed with water, aqueous $NaHCO_3$, dried over Na_2SO_4, filtered and reduced in vacuo.

One obtains 1.40 g (99 %) of the desired compound **81** as a pale yellow, very volatile oil. The compound was used without further purification.

^{1}H-NMR: (360 MHz, $CDCl_3$): δ 7.15 (*m*, 4H, Ph), 5.56 – 5.59 (*m*, 2H, Ph-C_2H_4-C*H*-CH_2), 5.07 (*d*, 2H, $^3J_{HH(trans)}$= 17.3 Hz, Ph-C_3H_5-C*H*$_2$), 5.00 (*d*, 2H, $^3J_{HH(cis)}$= 10.0 Hz, Ph-C_3H_5-C*H*$_2$), 2.72 (*t*, 4H, $^3J_{HH}$= 8.2 Hz, Ar-C*H*$_2$-C_3H_5), 2.34 (*dt*, 4H, $^3J_{HH}$= 8.2 Hz, $^3J_{HH}$= 7.7 Hz, Ar-CH_2-C*H*$_2$-C_2H_3).

^{13}C-NMR: (90.55 MHz, $CDCl_3$): δ 139.4 (2C, Ph), 138.1 (2C, Ph-C_2H_4-*C*H-CH_2), 129.0 (2C, Ph), 126.0 (2C, Ph), 114.8 (2C, Ph-C_3H_5-*C*H_2), 35.2 (2C, Ph-CH_2-*C*H_2-C_2H_3), 32.0 (2C, Ph-*C*H_2-C_3H_5).

EI-MS: m/z (% int): 186.0 ($M^{\bullet+}$, 100 %).

4.4.2 1,2-bis(5,5,6,6,7,7,8,8,9,9,10,10,10-tridecafluoro-3-iododecyl)benzene

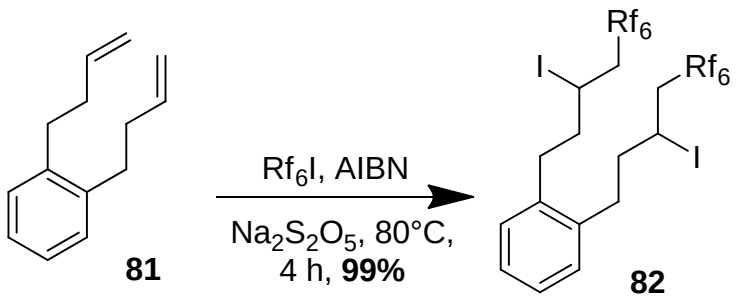

Method N. 1,2-di(but-3-enyl)benzene **81** (500 mg, 2.68 mmol) was added into a Schlenk tube and heated to 50°C. A 30% solution of Sodium metabisulfite (0.5 mL) and perfluorohexyliodide (1.62 mL, 2.8 eq) were added. Under a positive stream of argon, AIBN (17.6 mg, 0.04 eq) was added and the mixture heated to 80°C. The reaction was followed by GC/MS and ^{1}H-NMR. After 2 h of reaction time, a second (0.04 eq) portion of AIBN was added and the mixture stirred for another 2 h at 80°C.

After cooling down to RT, water was added and the obtained suspension was extracted with ether (emulsions!!). The combined organic layers were washed with water, dried over Na_2SO_4 and reduced in vacuo.

One obtains the desired compound **82** (2.88 g, 99 %) as pale pink oil. It was used without further purification.

^{1}H-NMR: (360 MHz, $CDCl_3$): δ 7.19 (*m*, 4H, Ph), 4.34 – 4.44 (*m*, 2H, Ph-C_2H_4-C*H*I-CH_2-Rf_6), 2.86 – 3.08 (*m*, 4H, Ph-C*H*$_2$-C_3H_5I-Rf_6), 2.68 – 2.84 (*m*, 4H, C_3H_5I-C*H*$_2$-Rf_6), 2.03 – 2.14 (*m*, 4H, Ph-CH_2-C*H*$_2$-C_2H_3I-Rf_6).

^{13}C-NMR: (90.55 MHz, CD_2Cl_2): δ 140.13 (2C, Ph), 129.77 (2C, Ph), 126.74 (2C, Ph), 107.9 – 121.66 (Rf_6), 41.63 (Ph-C_3H_5I-*C*H_2-Rf_6), 41.44 (2C, Ph-CH_2-*C*H_2-C_2H_3I-Rf_6), 35.01 (2C, Ph-*C*H_2-C_3H_5I-Rf_6), 19.78 (2C, Ph-C_2H_4-*C*HI-CH_2-Rf_6).

EI-MS: m/z (% int): 1078.2 ($M^{\bullet+}$, 5 %), 951.4 ([M-I]$^{\bullet+}$, 10 %), 823.4 ([M – 2 x I]$^{\bullet+}$, 70 %), 462.9 ([M-C_3H_5I-Rf6]$^{\bullet+}$, 100 %), 105.1 ([M - 2 x C_3H_5I-Rf6]$^{\bullet+}$, 95 %).

4.4.3 1,2-bis(5,5,6,6,7,7,8,8,9,9,10,10,10-tridecafluoro-decyl)benzene

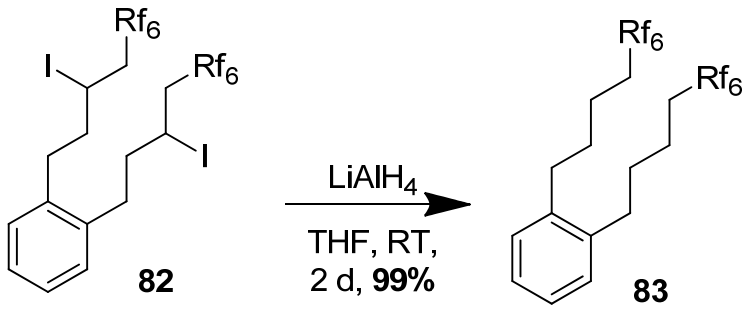

Method O. Lithium aluminum hydride (0.119 g, 3.49 mmol, 2.4 eq. resp. to **7**) was put in a 75 mL Schlenk flask and dry THF (10 mL) was syringed in. Compound **82** (1.57 g, 1.456 mmol) was dissolved in THF (10 mL) and was carefully added to the $LiAlH_4$ slurry.
After 2 days at RT, the mixture was quenched with water, 15% NaOH and again with water. The crude mixture was filtered on a porous frit and the filtrate was extracted with ether. The combined organic layers were washed with water, dried over Na_2SO_4 and reduced in vacuo. One obtains 1.44 g (99 %) of the desired compound **83** as pale yellow oil.

^{1}H-NMR: (360 MHz, CD_2Cl_2): δ 7.05 (*m*, 4H, Ph), 2.48 – 2.72 (*m*, 4H, Ph-C*H*$_2$-C_3H_6-Rf_6), 1.90 – 2.13 (*m*, 4H, C_3H_6-C*H*$_2$-Rf_6), 1.11 – 1.69 (*m*, 8H, Ph-CH_2-C_2*H*$_4$-CH_2-Rf_6).
^{13}C-NMR: (90.55 MHz, CD_2Cl_2): δ 140.30 (2C, Ph), 129.94 (2C, Ph), 126.92 (2C, Ph), 104.20 – 121.43 (Rf_6), 34.05 (2C, Ph-*C*H_2-C_3H_6-Rf_6), 32.79 (2C, Ph-CH_2-*C*H_2-C_2H_4-Rf_6), 31.30 (Ph-C_3H_6-*C*H_2-Rf_6), 20.82 (2C, Ph-C_2H_4-*C*H_2-CH_2-Rf_6).
EI-MS: m/z (% int): 826.2 ($M^{\bullet+}$, 50 %), 464.8 ($[M\text{-}C_3H_5Rf_6]^{\bullet+}$, 100 %).

4.4.4 (4-bromo-1,2-phenylene)dimethanol

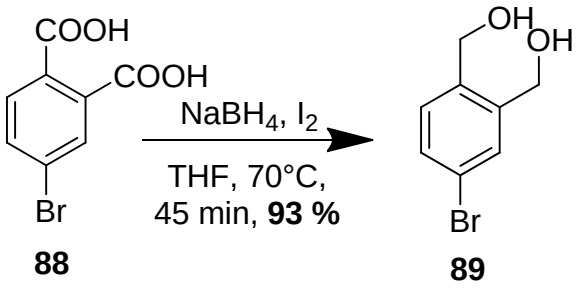

88 **89**

Method P. In a 250 mL round bottom flask a suspension was created using 48 mL of distilled THF and $NaBH_4$ (3.05 g, 81 mmol) and stirred for 15 minutes. 4-Bromophthalic acid **88** (5.00 g, 20.4 mmol) was dissolved in 36 mL of distilled THF and added dropwise, with stirring, to the $NaBH_4$ suspension. I_2 (10.2 g, 40.2 mmol) was dissolved in 30 mL distilled THF and added dropwise, with stirring, to the suspension.

The solution was then refluxed for approximately 45 minutes. After cooling to room temperature, the THF was removed via rotary evaporation, yielding a white solid. The solid was completely dissolved using a sufficient volume of 10% NaOH. The solution was then acidified to a pH of approximately 5-6 using 2 M HCl. The solution was transferred to a 500 mL separatory funnel and extracted into ethyl acetate. The ethyl acetate was rinsed with three 25 mL portions of 3 M NH_3, 40 mL 12% $NaHSO_3$, and 50 mL saturated NaCl, respectively, draining each aqueous phase before the next was added.

The product solution was dried over Na_2SO_4 and decanted into a round bottom flask. The ethyl acetate was removed via rotary evaporation, yielding an oily product. The oily substance was placed under high vacuum, inducing the precipitation of **89** as a white solid in good yield (93 %).

^{1}H-NMR: (360 MHz, $CDCl_3$): δ 7.49 (*s*, 1H, Ph), 7.42 (*d*, 1H, $^3J_{HH}$ = 8.2 Hz, Ph), 7.19 (*d*, 1H, $^3J_{HH}$ = 8.2 Hz, Ph), 4.65 (*s*, 2H, C*H*$_2$), 4.63 (*s*, 2H, C*H*$_2$), 2.90 (*br s*, 2H, Ph-CH_2-O*H*).

^{13}C-NMR: (90.55 MHz, $CDCl_3$): δ 141.5 (Ph), 138.1 (Ph), 132.4 (Ph), 131.4 (Ph), 131.2 (Ph), 122.3 (Ph), 63.4 (Ph-*C*H_2OH), 62.8 (Ph-*C*H_2OH).

EI-MS: m/z (% int): 245.18 ($M^{\bullet+}$, 100 %).

4.4.5 4-bromo-1,2-bis(bromomethyl)benzene

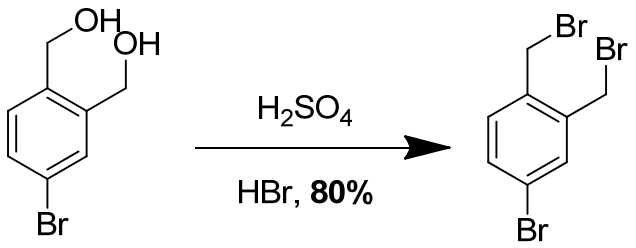

89 **90**

Method Q. Starting material **89** (4.1 g, 18.9 mmol) was placed in a 500 mL round bottom flask. To the flask was added dropwise with stirring, 100 mL 48% HBr and 35 mL concentrated H_2SO_4. The reaction mixture was heated to 60-70 °C for 2 hours. After heating, the flask was placed the refrigerator to cool overnight. The purple colored liquid was decanted from the greenish solid (desired product). The solid was filtered and washed with cold, distilled water and a ~10% NH_3 solution. One obtains 5.39 g of desired product **90** as a white powder (80 %).

^{1}H-NMR: (360 MHz, $CDCl_3$): δ 7.51 (*s*, 1H, Ph), 7.42 (*d*, 1H, $^3J_{HH}$ = 8.2 Hz, Ph), 7.22 (*d*, 1H, $^3J_{HH}$ = 8.2 Hz, Ph), 4.59 (*s*, 2H, CH_2), 4.57 (*s*, 2H, CH_2).

^{13}C-NMR: (90.55 MHz, $CDCl_3$): δ 138.61 (Ph), 135.63 (Ph), 133.99 (Ph), 132.64 (Ph), 132.53 (Ph), 123.13 (Ph), 29.05 (Ph-*C*H_2-Br), 28.76 (Ph-*C*H_2-Br).

EI-MS: m/z (% int): 344.0 ($M^{\bullet+}$, 20 %), 264.0 ([M-Br]$^{\bullet+}$, 100 %), 184.0 ([M - 2 x Br]$^{\bullet+}$, 90 %).

4.4.6 4-bromo-1,2-di(but-3-en-1-yl)benzene

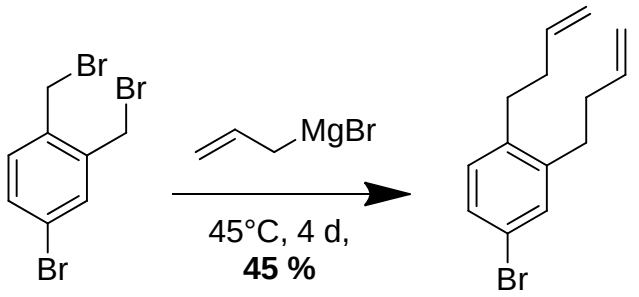

90 **91**

This reaction was performed similar to method M. Starting material **90** (5.4 g, 15.72 mmol) was dissolved in diethyl-ether in a 250 mL three-necked flask. Allylmagnesium bromide (24.6 mL, 1M in Et_2O) was added slowly (2 mL/h) over 5 hrs to the mixture using an addition funnel. The reaction was stirred at reflux during 5 days and followed by GC/MS.

Subsequent to hydrolysis with water (150 mL), the organic layer was separated and the water phase extracted thrice with Et_2O (3 x 150 mL).

The combined organic layers were washed with water, aqueous $NaHCO_3$, dried over Na_2SO_4, filtered and carefully reduced *in vacuo*.

The mixture was purified by column chromatography using pentane as eluent (Rf ~0.8).

One obtains 1.87 g (45 %) of product **91** as a pale yellow, very volatile oil.

^{1}H-NMR: (360 MHz, $CDCl_3$): δ 7.48 (s, 1H, Ph), 7.20 (d, 1H, $^3J_{HH}$ = 8.2 Hz, Ph), 7.07 (d, 1H, $^3J_{HH}$ = 8.2 Hz, Ph), 5.80 – 5.94 (*m*, 2H, Ph-C_2H_4-C*H*-CH_2), 4.99 – 5.13 (*m*, 4H, Ph-C_3H_5-C*H*$_2$), 2.81 (*t*, 2H, $^3J_{HH}$= 6.8 Hz, Ar-C*H*$_2$-C_3H_5), 2.76 (*t*, 2H, $^3J_{HH}$= 6.8 Hz, Ar-C*H*$_2$-C_3H_5), 2.35 – 2.46 (*m*, 4H, Ar-CH_2-C*H*$_2$-C_2H_3).

^{13}C-NMR: (90.55 MHz, $CDCl_3$): δ 138.67 (Ph), 135.69 (Ph), 134.04 (2C, Ph-C_2H_4-*C*H-CH_2), 132.71 (Ph), 132.70 (Ph), 132.59 (Ph), 123.19 (Ph), 115.89 (2C, Ph-C_3H_5-*C*H_2), 29.85 (Ph-*C*$_2H_4$-C_2H_3), 29.81 (Ph-*C*$_2H_4$-C_2H_3), 29.12 (Ph-*C*$_2H_4$-C_2H_3), 28.83 (Ph-*C*$_2H_4$-C_2H_3).

EI-MS: m/z (% int): 265.97 ($M^{\bullet+}$, 100 %), 185.07 ([M-Br]$^{\bullet+}$, 95 %), 131.09 ([M-Br-C_4H_7]$^{\bullet+}$, 5 %).

4.4.7 4-bromo-1,2-bis(5,5,6,6,7,7,8,8,9,9,10,10,10-tridecafluoro-3-iododecyl)benzene

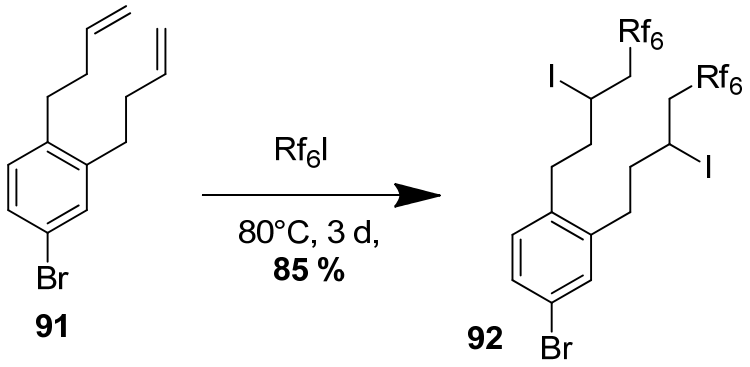

This reaction was performed similar to method N. Starting material **91** (1.87 g, 7.05 mmol) was added into a 50 mL three-necked flask and heated to 50°C. A 30 % solution of sodium metabisulfite (500 µl) and perfluorohexyliodide (10.06 g, 3.2 eq) were added. Under a positive stream of argon, AIBN (0.06 eq) was added and the mixture heated to 80°C. The reaction was followed by GC/MS and NMR.

After 2, 4, 6 and 8h, another portion of AIBN (4 x 0.06 eq) were added and the mixture stirred overnight. On the next day 2 other portions of AIBN and 0.07 eq of Rf_6I were added. The next morning, the reaction was cooled down

Water (250 mL) was added and the obtained suspension was extracted with ether (3 x 50 mL). The combined organic layers were washed with water, dried over Na_2SO_4 and carefully reduced *in vacuo*. One obtains 6.97 g (85 %) of the desired compound **92** as yellowish oil which turns slightly pink upon storage in the fridge. It was used without further purification.

^{1}H-NMR: (360 MHz, $CDCl_3$): δ 7.32 (s, 1H, Ph), 7.28 (d, 1H, $^3J_{HH}$ = 8.3 Hz, Ph), 7.06 (d, 1H, $^3J_{HH}$ = 8.3 Hz, Ph), 4.31 – 4.45 (*m*, 2H, Ph-C_2H_4-C*H*I-CH_2-Rf_6), 2.68 – 3.05 (*m*, 8H, Ph-C*H*$_2$-C_3H_5I-Rf_6, C_3H_5I-C*H*$_2$-Rf_6), 1.98 – 2.11 (*m*, 4H, Ph-CH_2-C*H*$_2$-C_2H_3I-Rf_6).

4.4.8 4-bromo-1,2-bis(5,5,6,6,7,7,8,8,9,9,10,10,10-tridecafluoro-decyl)benzene

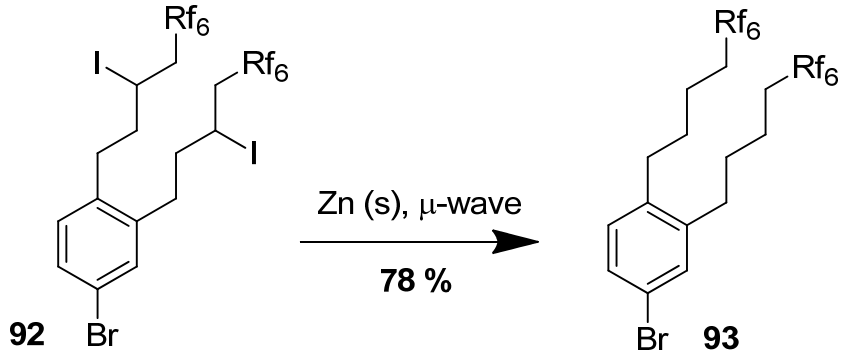

Method R. Starting material **92** (2.32 g, 2.00 mmol) and zinc powder (289 mg, 4.42 mmol, 2.2 eq) were put in a microwave reactor tube. The tube was then purged with argon. Water (72 µl, 4.02 mmol, 2 eq) and THF (20 mL) were syringed in and the tube was sealed.
The tubes were heated to 180°C for 2 x 25 min in a microwave reactor. The content of the tube was extracted with 3 x 100 mL of pentane. The combined organic layers were washed with a 10 % solution of sodium thiosulfate, dried on $MgSO_4$, filtered and reduced *in vacuo*.
One obtains 4.24 g (78 %) of the desired product **93** as a colorless liquid.

^{1}H-NMR: (360 MHz, $CDCl_3$): δ 7.22 (*s*, 1H, Ph), 7.20 (*d*, 1H, $^3J_{HH}$ = 7.9 Hz, Ph), 6.95 (*d*, 1H, $^3J_{HH}$ = 7.9 Hz, Ph), 2.48 – 2.69 (*m*, 4H, Ph-C*H*$_2$-C_3H_6-Rf_6), 1.90 – 2.12 (*m*, 4H, Ph-CH_2-C*H*$_2$-C_2H_4-Rf_6), 1.50 – 1.68 (*m*, 4H, C_3H_6-C*H*$_2$-Rf_6), 1.39 – 1.49 (*m*, 4H, Ph-C_2H_4-C*H*$_2$-CH_2-Rf_6).
^{13}C-NMR: (90.55 MHz, $CDCl_3$): δ 141.77 (1C, Ph), 138.38 (1C, Ph), 132.08 (1C, Ph), 131.02 (1C, Ph), 129.44 (1C, Ph), 120.04 (1C, Ph), 107.63 – 119.30 (12C, Rf_6), 32.25 (1C, Ph-*C*H_2-C_3H_6-Rf_6), 31.97 (1C, Ph-*C*H_2-C_3H_6-Rf_6), 31.04 (1C, Ph-CH_2-*C*H_2-C_2H_4-Rf_6), 30.80 (1C, Ph-CH_2-*C*H_2-C_2H_4-Rf_6), 30.61 (2C, Ph-C_3H_6-*C*H_2-Rf_6), 20.38 (1C, Ph-C_2H_4-*C*H_2-CH_2-Rf_6), 20.34 (1C, Ph-C_2H_4-*C*H_2-CH_2-Rf_6).
EI-MS: m/z (% int): 906.2 ($M^{\bullet+}$, 30 %), 542.9 ([M-$C_3H_5Rf_6$]$^{\bullet+}$, 30 %), 182.9 ([M - 2x $C_3H_5Rf_6$]$^{\bullet+}$, 100 %).

4.5 Other reactions

4.5.1 (5''-(3'-(trimethylsilyl)-[1,1'-biphenyl]-2-yl)-[1,1':2',1'':3'',1''':2''', 1''''-quinquephenyl]-3,3''''-diyl)bis(trimethylsilane)

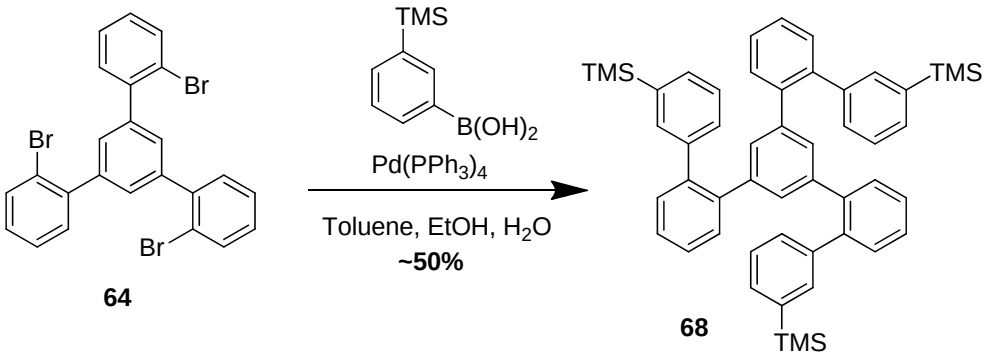

This reaction was performed similar to method J. In a 70 mL Schlenk-flask, **64** (150 mg, 0.276 mmol), 3-TMS-phenylboronic acid (177 mg, 0.911 mmol), tetrakis(triphenylphosphine) palladium(0) (9.57 mg, 8.29 µmol) and potassium carbonate (382 mg, 2.76 mmol) are dissolved in a mixture of toluene (30 mL), ethanol (7 mL) and water (7 mL).

The reaction mixture was stirred at 80°C for 3 days. After cooling down to RT, the organic layer was washed with water, dried over $MgSO_4$ and reduced *in vacuo*. One obtains 95 mg (46 %) of desired product **68**.

^{1}H-NMR: (360 MHz, CD_2Cl_2): δ 7.42 (d, 3H, $^3J_{HH}$ = 7.3 Hz), 7.29 – 7.38 (m, 6H), 7.19 – 7.26 (m, 6H), 7.11 – 7.19 (m, 3H), 6.87 (d, 3H, $^3J_{HH}$ = 7.3 Hz), 6.66 (s, 3H), 6.61 (d, 3H, $^3J_{HH}$ = 7.3 Hz), 0.15 (s, 27H, TMS).

^{13}C-NMR: (90.55 MHz, $CDCl_3$): δ 141.51 (3C, Ph), 141.37 (3C, Ph), 140.91 (3C, Ph), 140.86 (3C, Ph), 140.85 (3C, Ph), 135.55 (3C, Ph), 131.91 (3C, Ph), 131.18 (3C, Ph), 130.80 (3C, Ph), 130.67 (3C, Ph), 130.42 (3C, Ph), 127.77, 127.76 (3C, Ph), 127.68 (3C, Ph), -0.92 (9C, TMS).

EI-MS: m/z (% int): 750.5 ($M^{\bullet+}$, 100 %).

V. REFERENCES

[1] www.intel.com

[2] G. E. Moore, *IEEE IEDM Tech. Dig.*, **1975**, 11

[3] M. Pope, C. E. Swenberg, *Electronic Processes in Organic Crystals and Polymers*, **1999**, 2nd ed., *Oxford University Press*, Oxford.

[4] H. Inokuchi, *Org. Electronics*, **2006**, *7*, 62

[5] A. Tsumura, H. Koezuka, T. Ando, *Appl. Phys. Lett.*, **1986**, *49*, 1210 – 1212

[6] S. M. Sze, *Semiconductor Devices: Physics and Technology*, **1985**, *6*, 216, *507*, Wiley, New York.

[7] V. Subramanian, *IEE Trans. Comp. Pack. Tech.*, **2005**, *28*, 742

[8] L. Torsi, A. Dodabalapur, *Anal. Chem., A-Pages,* **2005**, *77*, 380

[9] H. E. Katz, X. M. Hong, A. Dodabalapur, R. Sarpeshkar, *J. Appl. Phys*., **2002**, *91*, 1572 – 1576

[10] M. Muccini, *Nature Materials*, **2006**, *5*, 605 – 613

[11] M. Kitamura, T. Imada, Y. Arakawa, *Jpn. J. Appl. Phys.*, **2003**, *42*, 2483 – 2487

[12] H. E. A. Huitema, G. H. Gelinck, J. B. P. H. van der Putten, K. E. Kuijk, C. M. Hart, E. Cantatore, D. M. de Leeuw, *Adv. Mater.*, **2002**, *14*, 1201 – 1204

[13] Z. Wang, J. Yuan, J. Zhang, R. Xing, D. Yan, Y. Han, *Adv. Mater.*, **2003**, *15*, 1009 – 1012

[14] M. Halik, H. Klauk, U. Zschieschang, G. Schmid, W. Radlik, W. Weber, *Adv. Mater.*, **2002**, *14*, 1717 – 1722

[15] H. Sirringhaus, T. Kawase, R. H. Friend, T. Shimoda, M. Inbasekaran, W. Wu, E. P. Woo, *Science*, **2000**, *290*, 2123 – 2126

[16] S. Yamaguchi, C. Xu, T. Okamoto, *Pure Appl. Chem.*, **2006**, *78*, 721 – 730

[17] Y. Kunugi, K. Takimiya, K. Yamane, K. Yamashita, Y. Aso, T. Otsubo, *Chem. Mater*, **2003**, *15*, 6 – 7

[18] C. D. Dimitrakopoulos, P. R. L. Malenfant, *Adv. Mater.*, **2002**, *14*, 99 – 117

[19] A. Facchetti, *Materials Today*, **2007**, *10*, 28 – 37

[20] H. Ishii, K. Sugiyama, E. Ito, K. Seki, *Adv. Mater.*, **1999**, *11*, 605 – 625

[21] C. R. Newman, C. D. Frisbie, D. A. da Silva Filho, J.-L. Brédas, P. C. Ewbank, K. R. Mann, *Chem. Mater.*, **2004**, *16*, 4436 – 4451

[22] H. Usta, C. Risko, Z. Wang, H. Huang, M. K. Deliomeroglu, A. Zhukhovitsky, A. Facchetti, T. J. Marks, *J. Am. Chem. Soc.*, **2009**, *131*, 5586 – 5608

[23] J. Locklin, M. E. Roberts, S. C. B. Mannsfeld, Z. Bao, *J. Macromol. Sci. Polym. Rev.*, **2006**, *46*, 79 – 101

[24] X. Cheng, Y.-Y. Noh, J. Wang, M. Tello, J. Frisch, R.-P. Blum, A. Vollmer, J. P. Rabe, N. Koch, H. Sirringhaus, *Adv. Funct. Mater.*, **2009**, *19*, 2407 – 2415

[25] T. J. Richards, H. Sirringhaus, *J. Appl. Phys.*, **2007**, *102*, 094510

[26] Y. Zhang, X. Cai, D. Qi, Y. Bian, J. Jiang, *J. Phys. Chem. C*, **2008,** *112*, 14579 – 14588

[27] T. B. Singh, F. Meghdadi, S. Günes, N. Marjanovic, G. Horowitz, P. Lang, S. Bauer, N. S. Sariciftci, *Adv. Mater.*, **2005**, *17*, 2315 – 2320

[28] Z. Rang, A. Haraldsson, D. M. Kim, P. P. Ruden, M. I. Nathan, R. J. Chesterfield, C. D. Frisbie, *Appl. Phys. Lett.*, **2001** *79*, 2731

[29] H. Klauk, D. J. Gundlach, J. A. Nichols, T. N. Jackson, *IEEE Trans. Electron Dev.*, **1999**, *46 (6)*, 1258 – 1263

[30] G. Horowitz et al., *Synth. Met.*, **1991**, *41*, 1127

[31] D. J. Carswell, J. Ferguson, L. E. Lyons, *Nature*, **1954**, *173*, 736

[32] V. C. Sundar, J. Zaumseil, V. Podzorov, E. Menard, R. L. Willett, T. Someya, M. E. Gershenson, J. A. Rogers, *Science*, **2004**, *303*, 1644 - 1646

[33] I. N. Hulea, S. Russo, A. Molinari, A. F. Morpurgo., *Appl. Phys. Lett.*, **2006**, *88*, 113512

[34] N. Stingelin-Stutzmann, E. Smits, H. Wondergem, C. Tanase, P. Blom, P. Smith, D. de Leeuw, *Nature Materials*, **2005**, *4*, 601 – 606

[35] A. L. Briseno, R. J. Tseng, M.-M. Ling, E. H. L. Falcao, Y. Yang, F. Wudl, Z. Bao, *Adv. Mater.*, **2006**, *18*, 2320 – 2324

[36] F. Würthner, R. Schmidt, *ChemPhysChem*, **2006**, *7*, 793

[37] Y. Y. Lin, D. J. Gundlach, S. F. Nelson, T. N. Jackson, *IEEE Trans. Electron Dev. Lett.*, **1997**, *18*, 606 – 608

[38] H. Klauk, M. Halik, U. Zschieschang, G. Schmid, W. Radlik, W. Weber, *J. Appl. Phys.*, **2002**, *92*, 5259 – 5263

[39] R. A. Laudise, Ch. Kloc, P. G. Simpkins, T. Siegrist, *J. Cryst. Growth*, **1998**, *187*, 449 – 454

[40] C. R. Kagan, A. Afzali, T. O. Graham, *Appl. Phys. Lett.*, **2005**, *86*, 193505

[41] H. Meng, M. Bendikov, G. Mitchell, R. Helgeson, F. Wudl, Z. Bao, T. Siegrist, C. Kloc, C.-H. Chen, *Adv. Mater.*, **2003**, *15*, 1090 – 1093

[42] J. E. Anthony, J. S. Brooks, D. L. Eaton, S. R. Parkin, *J. Am. Chem. Soc.*, **2001**, *123*, 9482 – 9483

[43] M. M. Payne, S. R. Parkin, J. E. Anthony, C.-C. Kuo, T. N. Jackson, *J. Am. Chem. Soc.*, **2005**, *127*, 4986 – 4987

[44] C. Huang, H. E. Katz, J. E. West, *J. Appl. Phys.*, **2006**, *100*, 114512

[45] C. A. Lee, D. W. Park, S. H. Jin, I. H. Park, J. D. Lee, and B.-G. Park, *Appl. Phys. Lett.*, **2006**, *88*, 252102

[46] S. Kobayashi, T. Nishikawa, T. Takenobu, S. Mori, T. Shimoda, T. Mitani, H. Shimotani, N. Yoshimoto, S. Ogawa, Y. Iwasa, *Nature Materials*, **2004**, *3*, 317 – 322

[47] B. H. Hamadani, D. A. Corley, J. W. Ciszek, J. M. Tour, and D. Natelson, *Nano Lett.*, **2006**, *6*, 1303 – 1306

[48] K. Tsukagoshi, K. Shigeto, I. Yagi, Y. Aoyagi, *Appl. Phys. Lett.*, **2006**, *89*, 113507

[49] A. Salleo, M. L. Chabinyc, M. S. Yang, R. A. Street, *Appl. Phys. Lett.*, **2002**, *81*, 4383

[50] A. Facchetti, M.-H. Yoon, T. J. Marks, *Adv. Mater.*, **2005**, *17*, 1705 – 1725

[51] M. Pratontep et al., *Synth. Meth.*, **2004**, *146*, 387

[52] F. Garnier, A. Yassar, R. Hajlaoui, G. Horowitz, F. Deloffre, B. Servet, S. Ries, P. Alnot, *J. Am. Chem. Soc.*, **1993**, *115*, 8716 – 8721

[53] M. Mushrush, A. Facchetti, M. Lefenfeld, H. E. Katz, T. J. Marks, *J. Am. Chem. Soc.*, **2003**, *125*, 9414

[54] A. Pron, P. Rannou, *Prog. Polym. Sci.*, **2002**, *27*, 135

[55] A. Assadi, C. Svensson, M. Willander, O. Inganäs, *Appl. Phys. Lett.*, **1988**, *53*, 195

[56] I. G. Hill, A. Kahn, *Proc. SPIE*, **1998**, *3476*, 168

[57] D. M. DeLongchamp, S. Sambasivan, D. A. Fischer, E. K. Lin, P. Chang, A. R. Murphy, J. M. J. Fréchet, V. Subramanian, *Adv. Mater.*, **2005**, *17*, 2340 – 2344

[58] H. Klauk, T. N. Jackson, *Solid State Technol.*, **2000**, *43*, 63

[59] S. Goettling, J. Brill, N. Fruehauf, J. Pflaum, E. Margallo-Balbás, *Proc. SPIE*, **2005**, *5940*, 594010

[60] J. Lee, J. H. Kim, S. Im, *J. Appl. Phys.*, **2004**, *95*, 3733 – 3736

[61] L. A. Majewski, R. Schroeder, M. Grell, P. A. Glarvey, M. L. Turner, *J. Appl. Phys.*, **2004**, *96*, 5781 – 5787

[62] Y. Iino, Y. Inoue, Y. Fujisaki, H. Fujikake, H. Sato, M. Kawakita, S. Tokito, H. Kikuchi, *Jpn. J. Appl. Phys.*, **2003**, *42*, 299 – 304

[63] L. A. Majewski, R. Schroeder, M. Grell, *Adv. Mater.*, **2005**, *17*, 192 - 196

[64] C. D. Dimitrakopoulos, S. Purushothaman, J. Kymissis, A. Callegari, J. M. Shaw, *Science*, **1999**, *283*, 822 - 824

[65] F.-Y. Yang, K.-J. Chang, M.-Y. Hsu, C.-C. Liu, *J. Mater. Chem.*, **2008**, *18*, 5927

[67] M. G. Debije, J. Piris, M. P. de Haas, J. M. Warman, Z. Tomovic, C. D. Simpson, M. D. Watson, K. Müllen, *J. Am. Chem. Soc.*, **2004**, *126*, 4641 – 4645

[68] D. de Leeuw et al., *Synth. Meth.*, **1997**, *87*, 53

[69] L.-L. Chua, *Nature*, **2005**, *434*, 194

[70] M.-H. Yoon, C. Kim, A. Facchetti, T. J. Marks, *J. Am. Chem. Soc.*, **2006**, *128*, 12851 – 12869

[71] A. Facchetti, M. Mushrush, H. E. Katz, T. J. Marks, *Adv. Mater.*, **2003**, *15*, 33 – 38

[72] A. Facchetti, M. Mushrush, M.-H. Yoon, G. R. Hutchison, M. A. Ratner, T. J. Marks, *J. Am. Chem. Soc.*, **2004**, *126*, 13859 – 13874

[73] J. R. Ostrick, A. Dodabalapur, L. Torsi, A. J. Lovinger, E. W. Kwock, T. M. Miller, M. Galvin, M. Berggren, H. E. Katz, *J. Appl. Phys.*, **1997**, *81*, 6804 – 6808

[74] T. Uchida, H. Akamatu, *Bull. Chem. Soc. Jpn.*, **1961**, *34*, 1015

[75] Y. Sakamoto, T. Suzuki, M. Kobayashi, Y. Gao, Y. Fukai, Y. Inoue, F. Sato, S. Tokito, *J. Am. Chem. Soc.*, **2004**, *126*, 8138 – 3140

[76] D. Schlettwein, D. Woehrle, E. Karmann, U. Melville, *Chem. Mater.*, **1994**, *6*, 3 - 6

[77] J. Kastner et al., *Solid State Sciences*, H. Kuzmany et al. (ed.), **1993**, Springer – Verlag, New York

[78] R. C. Haddon, A. S. Perel, R. C. Morris, T. T. M. Palstra, A. F. Hebard, R. M. Fleming, *Appl. Phys. Lett.*, **1995**, *67*, 121

[79] C. Waldauf, P. Schilinsky, M. Perisutti, J. Hauch, C. J. Brabec, *Adv. Mater.*, **2003**, *15*, 2084 – 2088

[80] T. D. Anthopoulos, F. B. Kooistra, H. J. Wondergem, D. Kronholm, J. C. Hummelen, D. M. de Leeuw, *Adv. Mater.*, **2006**, *18*, 1679 – 1684

[81] J. A. Letizia, S. Cronin, R. Ponce Ortiz, A. Facchetti, M. A. Ratner, T. J. Marks, *Chem. Eur. J.*, **2010**, *16*, 1911 – 1928

[82] Images copyright© of their respective owners (www.merck.com)

[83] Images copyright© of their respective owners (www.cope.gatech.edu)

[84] Images copyright© of their respective owners (www.uni-bonn.de)

[85] Images copyright© of their respective owners (www.polyic.de)

[86] W. Helfrich, W. G. Schneider, *Phys. Rev. Lett.*, **1965**, *14*, 229

[87] M. Pope, H. P. Kallmann, P. Magnante, *J. Chem. Phys.*, **1963**, *38*, 2042

[88] S. A. van Slyke. C. W. Tang, *Appl. Phys. Lett.*, **1987**, *51*, 913 – 915

[89] J. H. Burroughes, D. C. C. Bradley, A. R. Brown, R. N. Marks, K. Mackay, R. H. Friend, P. L. Burns, A. B. Holmes, *Nature*, **1990**, *347*, 539 – 541

[90] M. A. Baldo, M. E. Thompson, S. R. Forrest, *Nature*, **2000**, *403*, 750 – 753

[91] A. P. Kulkarni, C. J. Tonzola, A. Babel, S. A. Jenekhe, *Chem. Mater.*, **2004**, *16*, 4556 – 4573

[92] J. G. C. Veinot, T. J. Marks, *Acc. Chem. Res.*, **2005**, *38*, 632 – 643

[93] A. L. Burin, M. A. Ratner, *J. Phys. Chem. A*, **2000**, *104*, 4704 – 4710

[94] D. F. O'Brien, M. A. Baldo, M. E. Thompson, S. R. Forrest, *Appl. Phys. Lett.*, **1999**, *74*, 442 – 444

[95] M. A. Baldo, S. Lamansky, P. E. Burrows, M. E. Thompson, S. R. Forrest, *Appl. Phys. Lett.*, **1999**, *75*, 4 – 6

[96] C. W. Tang, S. A. VanSlyke, C. H. Chen, *J. Appl. Phys.*, **1989**, *65*, 3610 – 3616

[97] R. G. Kepler, *Phys. Rev.*, **1960**, *119*, 1226

[98] E. H. Martin, J. Hirsch, *Solid State Commun.*, **1969**, *7*, 783

[99] J. M. Warman, A. M. van de Craats, *Mol. Cryst. Liq. Cryst.*, **2003**, *396*, 41

[100] G. Horowitz, *Adv. Mater.*, **1998**, *10*, 365

[101] A. Babel, S. A. Jenekhe, *J. Am. Chem. Soc.* **2003**, *125*, 13656

[102] X. Zhang, S. A. Jenekhe, *Macromolecules*, **2000**, *33*, 2069

[103] S. A. Jenekhe, S. Yi, *Appl. Phys. Lett.*, **2000**, *77*, 2635

[104] H. Antoniadis, M. A. Abkovitz, B. R. Hsieh, *Appl. Phys. Lett.*, **1994**, *65*, 2030

[105] Images copyright© of their respective owners (www.samsung.com)

[106] Images copyright© of their respective owners (www.visionox.com)

[107] Images copyright© of their respective owners (www.sony.com)

[108] V. Palermo, P. Samori, *Angew. Chem. Int. Ed.*, **2007**, *46*, 4428 – 4432

[109] F. J. M. Hoeben, P. Jonkheijm, E. W. Meijer, A. P. H. J. Schenning, Chem. Rev., 2005, 105, 1491 – 1546

[110] A. C. Grimsdale, K. Müllen, *Angew. Chem. Int. Ed.*, **2005**, *44*, 5592 – 5629

[111] O. Aebischer, *Thesis Nr. 1575*, University of Fribourg, **2007**

[112] V. Palermo, S. Morelli, C. Simpson, K. Müllen, P. Samori, *J. Mater. Chem.*, **2006**, *16*, 266 – 271

[113] P. Jonkheijm, P. van der Schroot, A. P. H. J. Schenning, *Science*, **2006**, *313*, 80 - 83

[114] M. Surin, P. Leclere, S. deFeyter, M. M. S. Abdel-Mottaleb, F. C. de Schryver, O. Henze, W. J. Feast, R. Lazzaroni, *J. Phys. Chem. B*, **2006**, *110*, 7898 – 7908

[115] M. Kastler, W. Pisula, D. Wasserfallen, R. Pakula, K. Müllen, *J. Am. Chem. Soc.*, **2005**, *17*, 4286 – 4296

[116] P. Herwig, C. W. Kayser, K. Müllen, G. W. Spiess, *Adv. Mater.*, **1999**, *8*, 510 – 513

[117] A. Fechtenkötter, N. Tchebotareva, M. D. Watson, K. Müllen, *Tetrahedron*, **2001**, *57*, 3769 – 3783

[118] C.-Y. Liu, A. Fechtenkötter, M. D. Watson, K. Müllen, A. J. Bard, *Chem. Mater.*, **2003**, *15*, 124 – 130

[119] S. Ito, M. Wehmeier, J. D. Brand, C. Kübel, R. Epsch, J. P. Rabe, K. Müllen, *Chem. Eur. J.*, **2000**, *6*, 4327 – 4342

[120] B. Alameddine, *Thesis Nr. 1440*, University of Fribourg, **2004**

[121] Y. Ruiz-Morales, *J. Phys. Chem. A*, **2002**, *106*, 11283 – 11308

[122] L. Schmidt-Mende, A. Fechtenkötter, K. Müllen, E. Moons, R. H. Friend, J. D. MacKenzie, *Science*, **2001**, *293*, 1119 – 1122

[123] S. P. Brown, I. Schnell, J. D. Brand, K. Müllen, H.-W. Spiess, *J. Am. Chem. Soc.* **1999,** *121*, 6712 – 6718

[124] T. Kawase, T. Oshawa, T. Enomoto, M. Oda, *Chem. Lett.*, **1994**, 1333 – 1336

[125] S. Grimme, *J. Comput. Chem.*, **2006**, *27*, 1787–1799

[126] X. Feng, V. Marcon, W. Pisula, M. R. Hansen, J. Kirkpatrick, F. Grozema, D. Andrienko, K. Kremer, K. Müllen, *Nature Materials*, **2009**, *8*, 421 – 426

[127] P. Tondo, *planned Thesis*, University of Fribourg, **2010**

[128] S. Adimurthy, G. Ramachandraiah, P. K. Ghosh, A. V. Bedekar, *Tetrahedron Lett.*, **2003**, *44*, 5099 – 5051

[129] K. Rajesh, M. Somasundaram, R. Saiganesh, and K. K. Balasubramanian, *J. Org. Chem.*, **2007**, *72*, 5867 – 5869

[130] F. Dewhurst, P. K. J. Shah, *J. Chem. Soc. (C)*, **1969**, 1503 – 1504

[131] M. Hanif, P. Lu, M. Li, Y. Zheng, Z. Xie, Y. Ma, D. Li, J. Li, *Polym. Int.*, **2007**, *56*, 1507 – 1513

[132] C.-S. Tuan, Z.-W. Tsai, S.-S. Hsu, H.-B. Cheng, Y.-F. Cheng, S.-J. Chang, *U.S. Pat. Appl.*, **20050176952**

[133] G. D. Dennis, D. Edwards-Davis, L. D. Field, A. F. Masters, T. Maschmeyer, A. J. Ward, I. E. Buys, P. Turner, *Aust. J. Chem.*, **2006**, *59*, 135 – 146

[134] X. Feng, J. Wu, V. Enkelmann, K. Müllen, *Org. Lett.*, **2006**, *8*, 1145 – 1148

[135] E. Lindner, C. S. Ayasse, K. Eichele, M. Steimann, *Organometallics*, **2002**, *21*, 4217 – 4225

[136] B. R. Steele, M. Micha-Screttas, C. G. Screttas, *Tetrahedron Lett.*, **2004**, *45*, 9537 – 9540

[137] Z.-G. Wang, B.-H. Zhou, Y.-F. Chen, G.-D. Yin, Y.-T. Li, A.-X. Wu, L. Isaacs, *J. Org. Chem.* **2006**, *71*, 4502 – 4508

[138] D. A. Guthrie, J. D. Tovar, *Org. Lett.*, **2008**, *10*, 4323 – 4326

[139] J. D. Dunitz, A. Gavezzotti, *Chem. Soc. Rev.*, **2009**, *38*, 2622 – 2633

[140] T. Yatsunami, A. Yazaki, S. Inoue, H. Yamamoto, M. Yokomoto, J. Nomiyama, S. Noda, *European Patent*, **EP0343560A2**

[141] M. B. Pangborn, M. A. Giardello, R. H. Grubbs, R. K. Rosen, F. J. Timmers, *Organometallics*, **1996**, *15*, 1518 - 1520

VI. ANNEX

I. TASK

See 'Projekt Dimerberechnung PAH Grimme – Jenny'

II. METHODOLOGY

A. Methods

Energies have been calculated and geometries have been optimized with the dispersion corrected density functional theory (DFT-D) from ref. [1] that has been described before in ref. [2]. In this approach the total DFT energy E_{KS-DFT} is augmented by an empirical dispersion correction E_{disp},

$$E_{DFT-D} = E_{KS-DFT} + E_{disp}.$$

E_{disp} is given by

$$E_{disp} = -s_6 \sum_{i=1}^{N_{at}-1} \sum_{j=i+1}^{N_{at}} \frac{C_6^{ij}}{R_{ij}^6} f_{dmp}(R_{ij}).$$

Here, N_{at} is the number of atoms in the system, C_6^{ij} denotes the dispersion coefficient for atom pair ij, s_6 is a global scaling factor that only depends on the functional used, R_{ij} is an interatomic distance, and $f_{dmp}(R_{ij})$ is a damping function to avoid near-singularities for small R and reduce electron correlation double-counting effects [1]. DFT-D and related methods are reviewed in [3]. Large Gaussian AO basis sets of heavily polarized triple-ζ quality [4] are employed. Density fitting techniques, also called resolution-of-the-identity (RI) approximation, were used throughout to speed up DFT GGA computations [5, 6] roughly by a factor of 10-20 at insignificant extra inaccuracy. All results have been obtained with a slightly modified version of the Turbomole program package [7]. The Gaussian AO basis sets are taken from the Turbomole library [8]. SCF convergence criterion for increment of total energy $< 10^{-7}$ and increment of one-electron energy $< 10^{-4}$ au. Geometry convergency criterion for total SCF-energy is 10^{-7} and for maximum norm of SCF-energy gradient is 10^{-3} au. For the quadrature of exchange correlation terms, the multiple grid m4 has been specified. All other computational parameters have been chosen as their default values.

B. Procedure

First monomers of the polyaromatic compounds $C_{30}H_{16}$ (1), $C_{56}H_{22}$ (2), $C_{42}H_{20}$ (3), $C_{60}H_{24}$ (4), $C_{42}H_{18}$ (5) were optimized. Starting structures of compounds 1 (tribenzo[b,n,pqr]perylene) and 5 (hexabenzo[bc,ef,hi,kl,no,qr]coronene) were taken from the NIST database [9]. Compounds 2, 3, and 4 were built with a modelling program [10]. The resulting total energies are taken as reference for the dimer energies.

The potential energy surface of the dimer has been explored with rigid monomers. For fully stacked dimers, the interplane distance has been varied from 6.1 to 7.5 a.u. in steps of 0.1 a.u. At a fixed separation of 6.3307 a.u. (the experimental interlayer spacing of graphene), the two monomers were displaced in-plane in two directions: from 0.0 to 4.5 a.u. in steps of 0.5 a.u. along the molecular axes starting from the fully stacked structure of the dimers of compounds 1, 2, and 3; from 0.0 to 4.5 a.u. along the long and from -4.5 to 4.5 a.u. along the short molecular axis in steps of 0.5 a.u. starting from the 180 degrees rotated structure of the dimers of compounds 1 and 3 (configuration 1/3c).

The structures corresponding to the local minima of the potential energy surfaces were fully energy minimized.

III. RESULTS

A. Tribenzo[b,n,pqr]perylene ($C_{30}H_{16}$) and $C_{42}H_{20}$

Both tribenzo[b,n,pqr]perylene and $C_{42}H_{20}$ are practically planar. The mean distance of the carbon atoms from the rms plane amounts to 0.1 and 1.4 pm for tribenzo[b,n,pqr]perylene and $C_{42}H_{20}$, respectively (see Tab. I).

The fully stacked dimers have a potential energy minimum at 6.9 a.u. interplane distance, with interaction energies of -21.2 and -32.4 kcal mol^{-1} for rigid tribenzo[b,n,pqr]perylene and $C_{42}H_{20}$, respectively.

The potential energy surfaces for the stacked dimer of rigid tribenzo[b,n,pqr]perylene starting from the fully stacked and the 180 degrees rotated (configuration 1c) structures are shown in Fig. 1. The intermolecular interaction energy varies from –28.8 to –16.0 kcal mol^{-1} for parallel and from –29.9 to –18.5 kcal mol^{-1} for antiparallel dimers. For the parallel displaced structure (left side of Fig. 1), the potential energy minimum corresponds

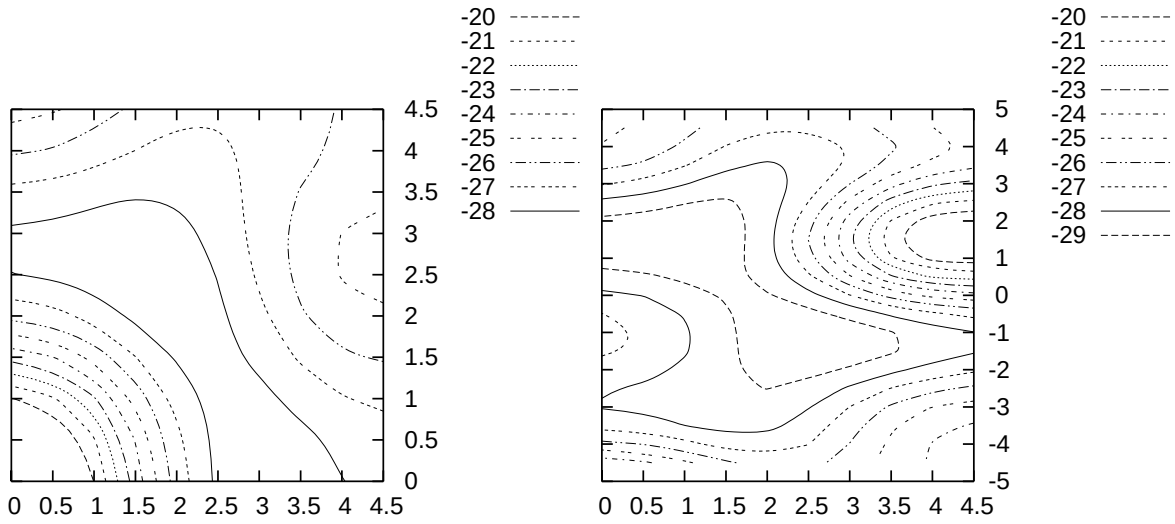

FIG. 1: B97-D/TZV(d,p) potential energy surface of the stacked dimer of rigid tribenzo[b,n,pqr]perylene: parallel (left) and antiparallel (right) displaced. The origin on the left corresponds to the fully stacked, the origin on the right to 180 degrees rotated structure (configuration 1c). Displacement along the long molecular axis refer to the abcissa (R_1), the short molecular axis to the ordinate (R_2). Contours in kcal mol^{-1}, axes in a.u. The interplane spacing (R_e) is 6.3307 a.u.

to a displacement of about 3 a.u. irrespective of the direction, i.e. along each molecular axis or inbetween. For smaller displacements the energy increases steeply with the energy maximum at the fully stacked structure about 13 kcal mol^{-1} above the minimum. For larger in-plane displacements the energy increases more smoothly to local maximum values about 4 kcal mol^{-1} above the minimum and to saddle point values about 2 kcal mol^{-1} above the minimum inbetween.

For the antiparallel (180 degrees rotated) displaced structure (right side of Fig. 1), the potential energy minimum corresponds to smaller displacements up to 2 a.u. out of the maximally overlapping structure (configuration 1c). Displacements are not equivalent for all directions, but displacements along the short molecular axis with larger overlap of the monomers (positive R_2 direction) are energetically favoured over equally large displacements with smaller overlap of the monomers (negative R_2 direction). The structure with maximal overlap of the monomers is not an energy maximum now and only 3 kcal mol^{-1} above the potential energy minimum. The potential energy maximum corresponds to displacements of about 4 and 2 a.u. along the long and short molecular axes (in R_1 and R_2 directions),

respectively, with an 11 kcal mol^{-1} higher energy than the potential energy minimum. Alltogether, large in-plane displacements correspond to small energy variations on the order of thermal energies, i.e. the molecules are almost freely mobile in the dimer.

The dissociation energies and geometrical data of stationary tribenzo[b,n,pqr]perylene dimers found are given in Tab. I, the corresponding structures are displayed in Fig. 2. The fully stacked structure (1f) could only be obtained by imposing C_{2v} symmetry and has a dissociation energy of –21.5 kcal mol^{-1}. Optimization without symmetry constrains leads to structure 1g with the monomers rotated by 18 degrees, thus structure 1f is not a local minimum. All freely (i.e. without symmetry constrain) optimized structures have dissociation energies in the range from –28.2 to –30.8 kcal mol^{-1}. The three structures with the lowest energies, 1b, 1d, and 1i, are antiparallel displaced dimers (in structure 1i the displacement along the short molecular axis of structure 1d is reversed). The parallel displaced structure found with the lowest energy (1e) is 1.5 kcal mol^{-1} higher in energy than the lowest energy structure. Parallel displaced structures with a displacement only along the short (1a) or long (1j) molecular axis are another 0.7 or 0.1 kcal mol^{-1} higher in energy, respectively. An antiparallel displaced structure with a displacement only along the long molecular axis could not be identified as minimum of the potential energy. Optimization starting from an antiparallel dimer displaced along the long molecular axis resulted in structure 1d. Starting from an antiparallel dimer displaced along the short molecular axis in positive direction gave structure 1h, where the monomers are rotated by 173 (instead of 180) degrees.

The interplanar distance (R_e) of the fully optimized dimers in Tab. I is the average distance of the carbon atoms in one monomer from the rms plane through the carbon atoms of the other monomer. For the freely optimized dimers, R_e varies from 325 to 341 pm. A rough but not strict correlation between R_e and the dissociation energy (D_e) is observed. In particular, the most strongly bound dimer 1i has also the shortest interplanar distance. The mean distance of the carbon atoms in one monomer from the rms plane of the same monomer (Δz) is a measure for the deformation the monomers experience upon formation of the dimer. It varies from 2.0 to 10.6 pm for parallel and from 4.3 to 8.0 pm for antiparallel displaced dimers, in comparison to the Δz value of 0.1 pm for isolated tribenzo[b,n,pqr]perylene. The largest deformations occur for the two rotated dimers 1g and 1h with $\Delta z = 14.5$ and 17.0 pm, respectively. To estimate the displacements along the long (R_1) and short (R_2) molecular axes, the difference vector between the centers of the

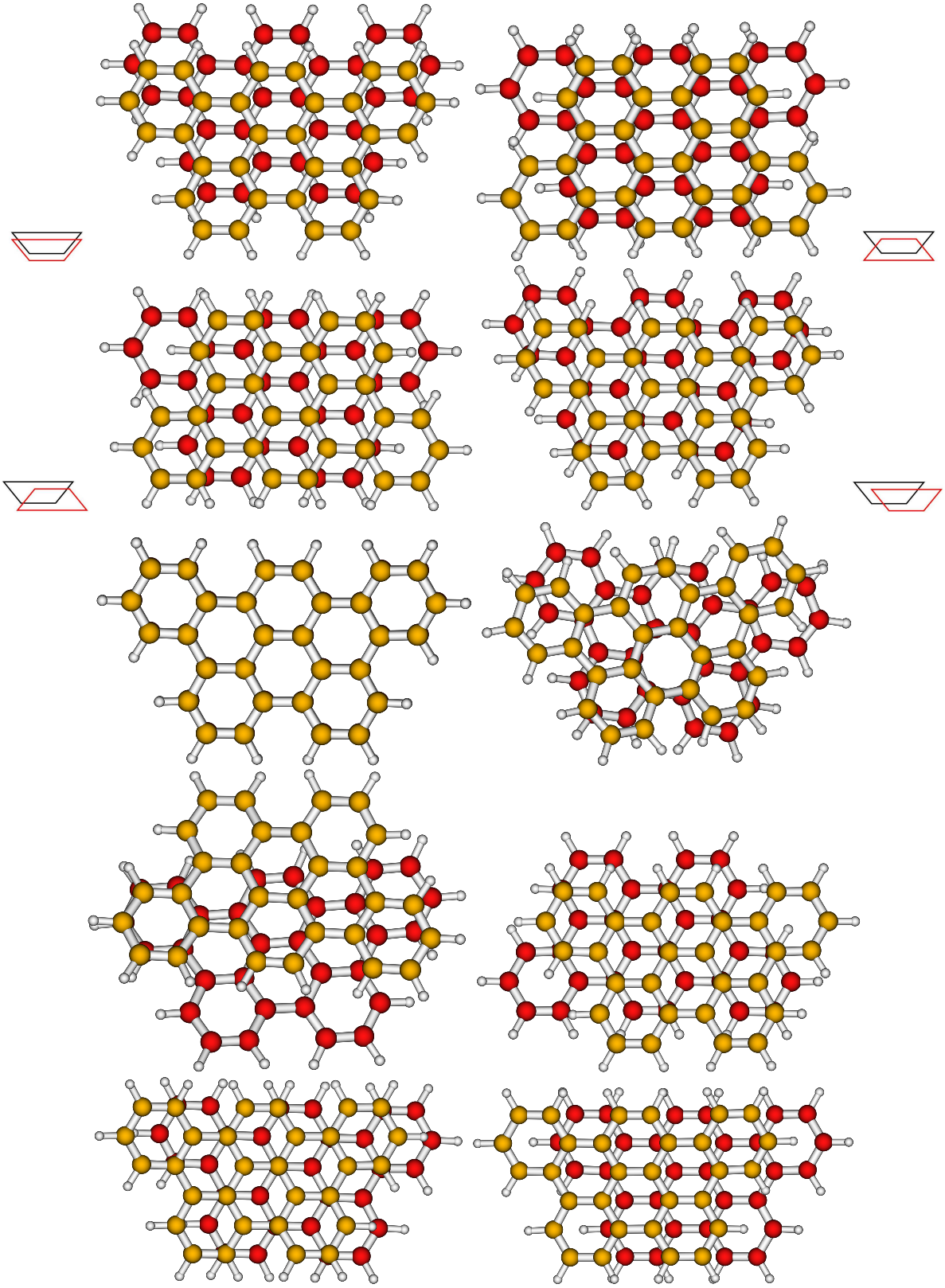

FIG. 2: B97-D/TZV(d,p) optimized structures of tribenzo[b,n,pqr]perylene dimers 1a, 1b, (top from left to right) 1d, 1e, (2nd row from left to right) 1f, 1g, (3rd row from left to right) 1h, 1i, (4th row from left to right) 1j, and 1j' (bottom).

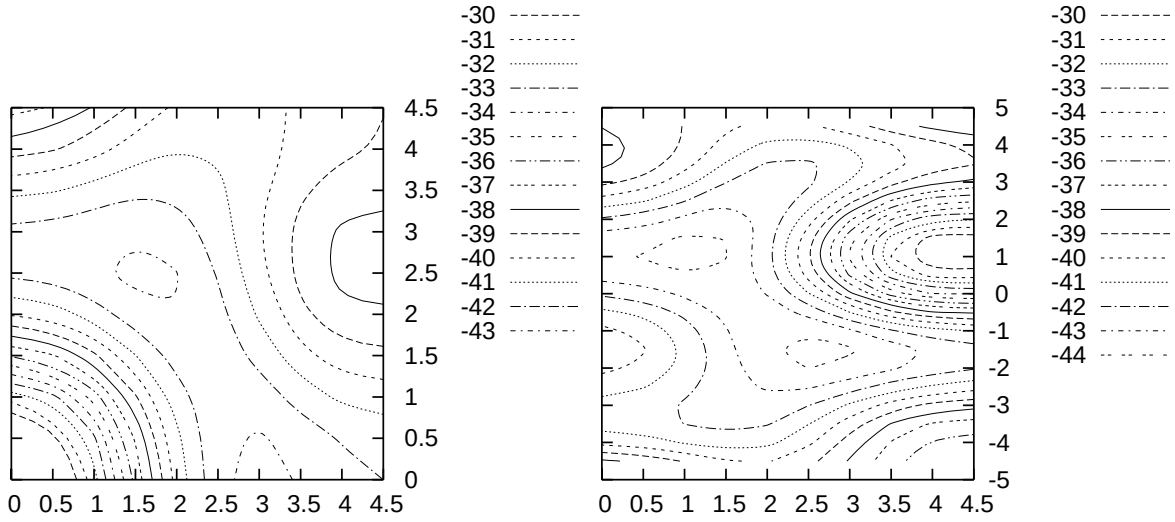

FIG. 3: B97-D/TZV(d,p) potential energy surface of the stacked dimer of rigid $C_{42}H_{20}$: parallel (left) and antiparallel (right) displaced. The origin on the left corresponds to the fully stacked, the origin on the right to 180 degrees rotated structure (configuration 3c). Displacement along the long molecular axis refer to the abcissa (R_1), the short molecular axis to the ordinate (R_2). Contours in kcal mol^{-1}, axes in a.u. The interplane spacing (R_e) is 6.3307 a.u.

carbon atoms in the two monomers is projected into the rms plane of one of the monomers. (The length of the projection of the same difference vector onto the normal of the rms plane equals R_e.) As long molecular axis, (the projection of) the direction of a C-C bond vector (into the same rms plane) is taken. Since all the geometrical data depend on which of the monomers is chosen for their calculation, two values are given for those structures, where the monomers are not equivalent (1a and 1e). The minimum energy structure of the antiparallel displaced tribenzo[b,n,pqr]perylene dimer (1i) is displaced along the long molecular axis by about 148 pm and along the short molecular axis by about 74 pm, the by 0.1 kcal mol^{-1} higher in energy (i.e. practically isoenergetic) structure 1d has R_1 and R_2 values of 54 and –84 pm, respectively. The minimum energy structure of the parallel displaced tribenzo[b,n,pqr]perylene dimer (1e) is displaced along the long molecular axis by about 72 pm and along the short molecular axis by about 141 pm. Parallel displaced dimers with a displacement only along the short (1a) or long molecular axis (1j) are displaced by 153 and 168 pm, respectively.

The shape of the potential energy surface for the stacked dimer of rigid $C_{42}H_{20}$ (Fig. 3) closely resembles that of the dimer of rigid tribenzo[b,n,pqr]perylene (Fig. 1), but the

dissociation energies are increased. The dissociation energy varies between –43.4 and –26.1 kcal mol^{-1} for parallel and from –44.4 to –28.7 kcal mol^{-1} for antiparallel dimers. For the parallel displaced structure on the left of Fig. 3, the fully stacked structure again corresponds to the energy maximum 17 kcal mol^{-1} above the minimum at relative displacements of 3 a.u. The local energy maxima at larger in-plane displacements are now about 6 kcal mol^{-1} above the minimum and the heigth of the saddle points inbetween is 3 kcal mol^{-1}. For the antiparallel displaced structure on the right of Fig. 3, two almost isoenergetic local minima occur at displacements out of the maximally overlapping structure of 1 a.u. along both long and short molecular axes and of 2.5 a.u. along the long and of –1.5 a.u. (opposite direction to other minimum) along the short molecular axis. The global maximum of the PES corresponds to displacements of 4 a.u. along the long and 1 a.u. along the short molecular axis and is almost 16 kcal mol^{-1} higher in energy. The maximally overlapping structure is by 2 kcal mol^{-1} above the minimum energy structure.

The dissociation energies and geometrical data of stationary $C_{42}H_{20}$ dimers found are given in Tab. I, the corresponding structures are displayed in Fig. 4. Comparing to the dissociation energies of the tribenzo[b,n,pqr]perylene dimers, dissociation energies of the corresponding $C_{42}H_{20}$ dimers are increased by a factor of 1.5. In particular, the energetic sequences of the $C_{42}H_{20}$ and the tribenzo[b,n,pqr]perylene dimers are (almost) the same. Lowest energies have the antiparallel displaced structures 3i (–45.5 kcal mol^{-1}), 3d (–45.3 kcal mol^{-1}), and the 180 degrees rotated structure 3c (–44.6 kcal mol^{-1}). The lowest energy parallel displaced structure 1e (–44.1 kcal mol^{-1}) is by 1.4 kcal mol^{-1} higher in energy than the lowest energy structure found, but by 0.1 kcal mol^{-1} more stable than the antiparallel displaced structure 1h with displacement only along the short molecular axis, which could now (in contrast to the tribenzo[b,n,pqr]perylene dimer) be optimized without rotation of the monomers. Parallel displaced structures with displacements only along the short (3a) and long molecular axes (3j) are by 1.0 and 0.4 kcal mol^{-1} higher in energy than the lowest energy parallel displaced structure 1e, respectively. The fully stacked structure 3f again could only be obtained by imposing C_{2v} symmetry, while unrestrained optimization starting from a fully stacked dimer results in structure 3g with the monomers rotated by 10 degrees.

The interplane spacings of the $C_{42}H_{20}$ dimers are by 1 to 2 pm smaller than those of the corresponding tribenzo[b,n,pqr]perylene dimers. The mean distances of the carbon atoms from the rms plane are increased compared to the value of 1.4 pm for the isolated $C_{42}H_{20}$, to

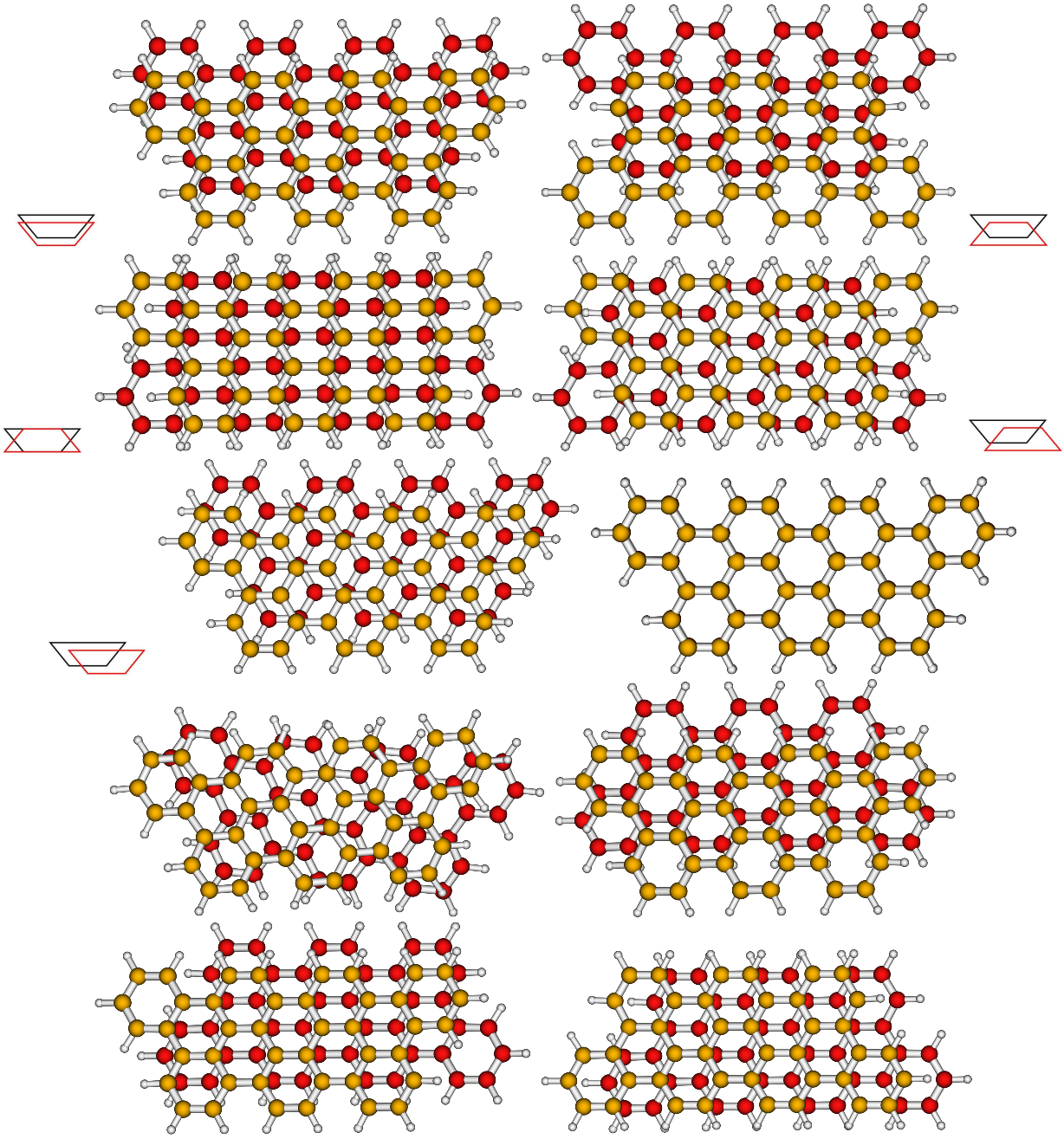

FIG. 4: B97-D/TZV(d,p) optimized structures of $C_{42}H_{20}$ dimers 3a, 3b, (top from left to right) 3c, 3d, (2nd row from left to right) 3e, 3f, (3rd row from left to right) 3g, 3h, (4th row from left to right) 3i, and 3j (bottom).

between 2.6 and 8.3 pm for parallel and between 5.7 and 12.3 pm for antiparallel displaced dimers. The largest deformation of the monomers occurs with 15.6 pm for the rotated dimer 3g. The R_1/R_2 values for the displacements of the $C_{42}H_{20}$ parallel displaced dimers 3a, 3e, 3f, 3j, 3j', and antiparallel displaced dimers 3d and 3i resemble their counterparts for the

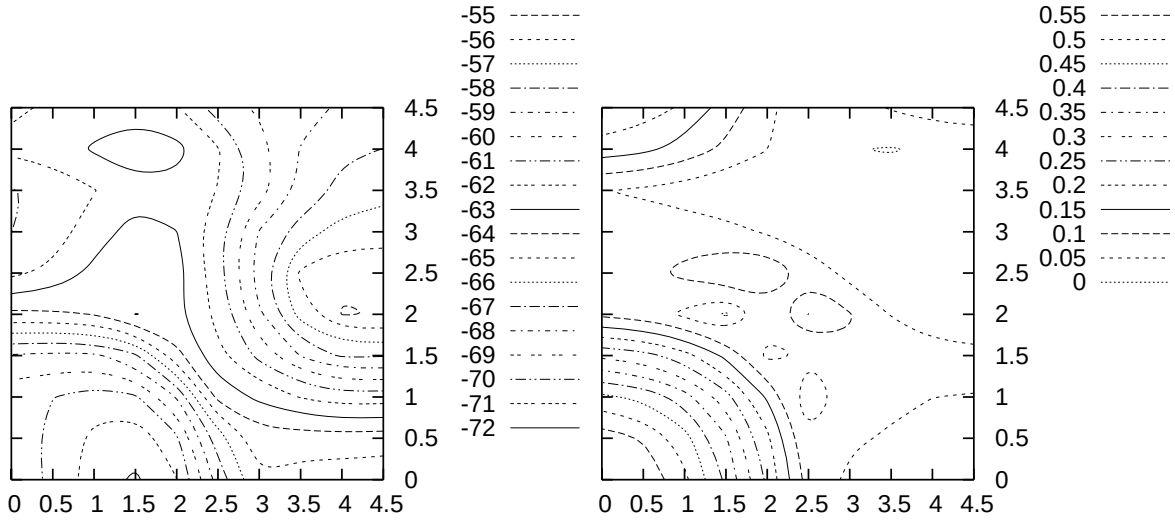

FIG. 5: B97-D/TZV(d,p) potential energy surface (left) and HOMO-LUMO gap (right) of the stacked dimer of rigid $C_{56}H_{22}$. The origin corresponds to the fully stacked structure. Displacement along the long molecular axis refer to the abcissa (R_1), the short molecular axis to the ordinate (R_2). Contours on the left in kcal mol^{-1} and on the right in eV, axes in a.u. The interplane spacing (R_e) is 6.3307 a.u.

tribenzo[b,n,pqr]perylene dimers, but the absolute R_1 and R_2 values differ. This difference is most pronounced for the 1b and 3b dimers and a consequence of the flatness of the potential energy surfaces in terms of in-plane displacements and rotation, reflecting the limitation of characterizing the various configurations by single minimum energy structures.

B. $C_{56}H_{22}$

The mean distance of the $C_{56}H_{22}$ carbon atoms from the rms plane is 0.3 pm (see Tab. I). The molecule is essentially planar.

The potential energy minimum of the fully stacked dimer of rigid $C_{56}H_{22}$ occurs at 6.4 a.u., i.e. at an 0.5 a.u. smaller interplane distance as rigid tribenzo[b,n,pqr]perylene or $C_{42}H_{20}$ dimers, with an interaction energy of –69.6 kcal mol^{-1}.

The potential energy surface for the parallel displaced dimer of rigid $C_{56}H_{22}$ (left side of Fig. 5) has its global minimum at an displacement of 1.5 a.u. along the long molecular axis. The fully stacked structure is 2.7 kcal mol^{-1} higher in energy. Displacement only along the short molecular axis leaves the energy roughly constant for 1 a.u. and then increases it to a

maximal value 8.6 kcal mol^{-1} higher than the fully stacked structure at 3.5 a.u. displacement. A local minimum appears at 2 and 4 a.u. displacement in R_1 and R_2 direction, but at 9 kcal mol^{-1} above the global minimum of the potential energy surface.

The unusual shape of the $C_{56}H_{22}$ dimer potential energy surface, i.e. the steep increase around the global minimum and the incommensurabilty between its shape and the geometric structure of the monomers, is related to the unusual electronic structure. The isolated $C_{56}H_{22}$ monomer has a HOMO-LUMO gap of 6 mH (Tab. I), and it decreaces to values below 1 mH for the parallel displaced dimer with the minimum of 0.006 mH at R_1 and R_2 values of 3.5 and 2.5 a.u., respectively. At $R_1 = 1.5$ and $R_2 = 2.0$ a.u. and $R_1 = 3.5$ and $R_2 = 4.0$ a.u., negative HOMO-LUMO gap of –0.3 and –0.1 mH, respectively, are obtained. This does not only lead to severe convergence problems of the SCF procedure, but also renders the approach questionable to describe the electronic structure by a singlet state. In any case, we will continue to describe the results for the structures obtained by full geometry optimization based on singlet states in the following.

The dissociation energies and geometrical data of stationary $C_{56}H_{22}$ dimers found are given in Tab. I, the corresponding structures are displayed in Fig. 6. Lowest energy structure is the parallel displaced structure 2d, where the monomers are displaced by 100 pm along the long molecular axis. The parallel displaced structure 2a, where the monomers are displaced along the short molecular axis, and the fully stacked structure 2f could only be obtained by imposing C_{2h} and D_{2h} symmetry, respectively. Unrestrained optimization leads to structure 2d in both cases. The fully stacked structure is by 4.2 kcal mol^{-1} higher in energy than the lowest energy structure 2d, the parallel displaced structure 2a by 14.7 kcal mol^{-1}. The parallel displaced structure 2e is by 9.1 kcal mol^{-1} higher in energy than the lowest energy structure 2d, the 44 degrees rotated structure 2c by another 4.8 kcal mol^{-1}. The optimization of the 90 degrees rotated structure 2b is still running (energy change 0.0000002, MAX geom. grad. 0.0002094 a.u., D_e = –57.50 kcal mol^{-1}).

The interplane distance of the lowest energy structure 2d (324 pm) is slightly larger than that of the parallel displaced structure 2e, but smaller than those of the parallel displaced structure 2a, the fully stacked structure 2f, and all tribenzo[b,n,pqr]perylene and $C_{42}H_{20}$ dimers. The distortion of the monomers in the lowest energy structure 2d is larger than for the parallel displaced structures 2a and 2e, fully stacked structure 2f, and for the isolated $C_{56}H_{22}$. For the strongly distorted (> 30 pm) monomers of the rotated dimer 2c, the

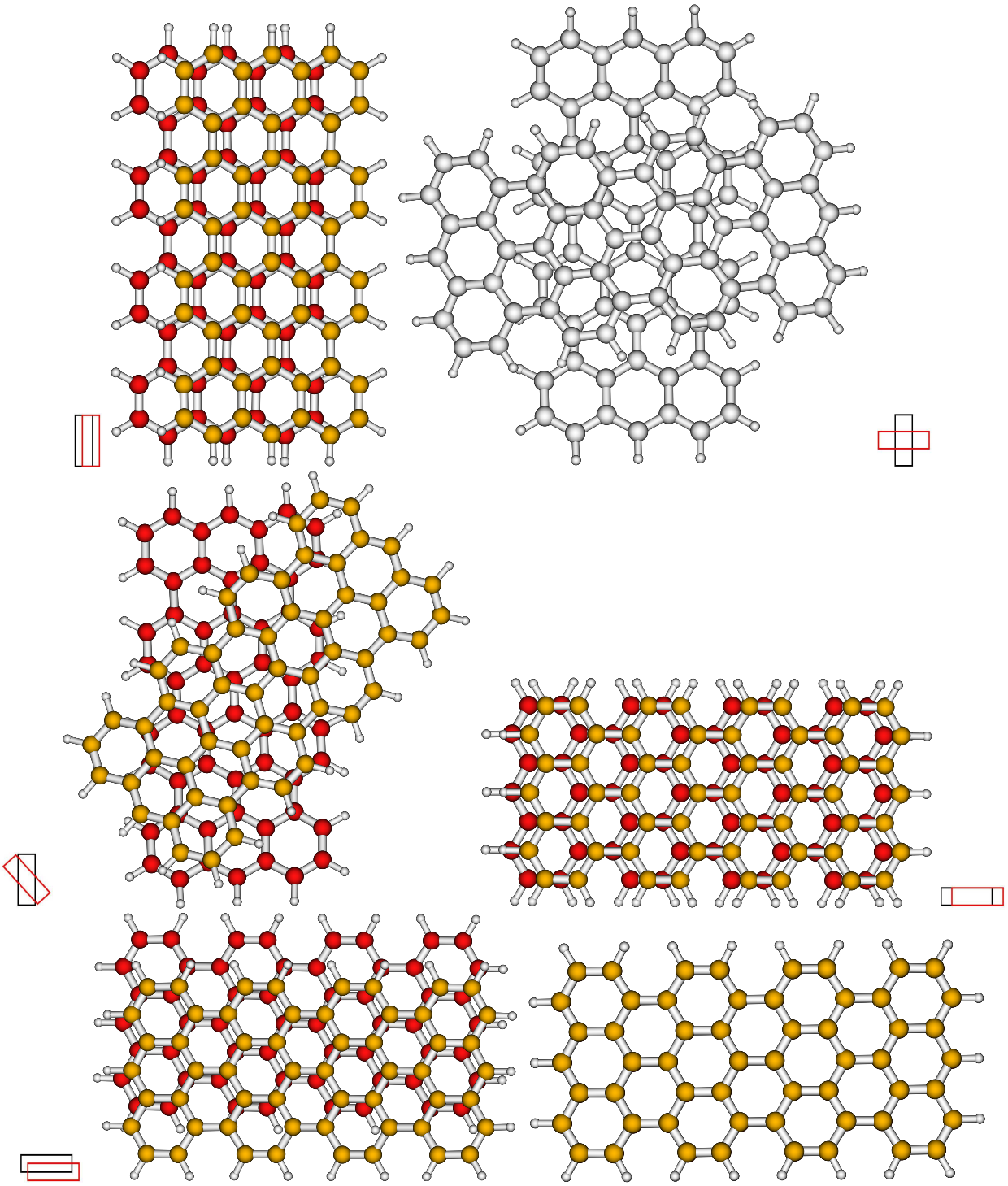

FIG. 6: B97-D/TZV(d,p) optimized structures of $C_{56}H_{22}$ dimers 2a, (2b), (top) 2c, 2d, (middle from left to right) 2e, and 2f (bottom from left to right).

interplanar distance R_e is not meaningful since it underestimates the actual atom-atom distance between the monomers.

C. $C_{60}H_{24}$ and Hexabenzo[bc,ef,hi,kl,no,qr]coronene ($C_{42}H_{18}$)

The mean distance of the $C_{60}H_{24}$ carbon atoms from the rms plane is 0.7 pm (see Tab. I). The molecule is essentially planar. The mean distance of the hexabenzo[bc,ef,hi,kl,no,qr]coronene carbon atoms from the rms plane is 12.4 pm (see Tab. I). The molecule is distorted as a consequence of the phenanthrene interaction between adjacent peripheral benzene rings.

The potential energy minima of the fully stacked dimer of rigid $C_{60}H_{24}$ and hexabenzo[bc,ef,hi,kl,no,qr]coronene occur at 6.8 a.u., i.e. at an 0.1 a.u. smaller interplane distance as rigid tribenzo[b,n,pqr]perylene or $C_{42}H_{20}$ dimers, with interaction energies of –51.6 and –35.6 kcal mol^{-1}, respectively.

The structures of the stationary $C_{60}H_{24}$ dimers obtained are displayed in Fig. 7, the corresponding dissociation energies and geometrical data are given in Tab. I. Optimization of the fully stacked structure 4f (energy change 0.0004662, MAX geom. grad. 0.0006348 a.u., D_e = –53.09 kcal mol^{-1}) and a structure 4g with monomers rotated from a fully stacked structure (energy change 0.0001187, MAX geom. grad. 0.0002929 a.u., D_e = –67.12 kcal mol^{-1}) are still running. The 180 degrees rotated structure 4d is by 1 kcal mol^{-1} higher in energy than the parallel displaced structure 4a. The parallel displaced structure 4b/c could only optimized by imposing C_s symmetry and is by 1.7 kcal mol^{-1} higher in energy than structure 4a.

The deformation of the monomers is larger than the value of the isolated $C_{60}H_{24}$ for both dimers: 3.2 pm for the parallel displaced structure 4a, 5.2 pm for the parallel displaced structure 4b/c, and 21.4 pm for the 180 degrees rotated structure 4d. The interplane spacing is 330 pm for the parallel displaced structure 4a and 333 pm for the parallel displaced structure 4b/c. R_1 now stands for displacement along, R_2 for displacement perpendicular to a C-C bond. The parallel displaced structure 4a is displaced by 156 pm along a C-C bond, the parallel displaced structure 4b/c is displaced by 140 pm perpendicular to a C-C bond, and the 180 degrees rotated structure 4d is displaced by 124 pm perpendicular to a C-C bond.

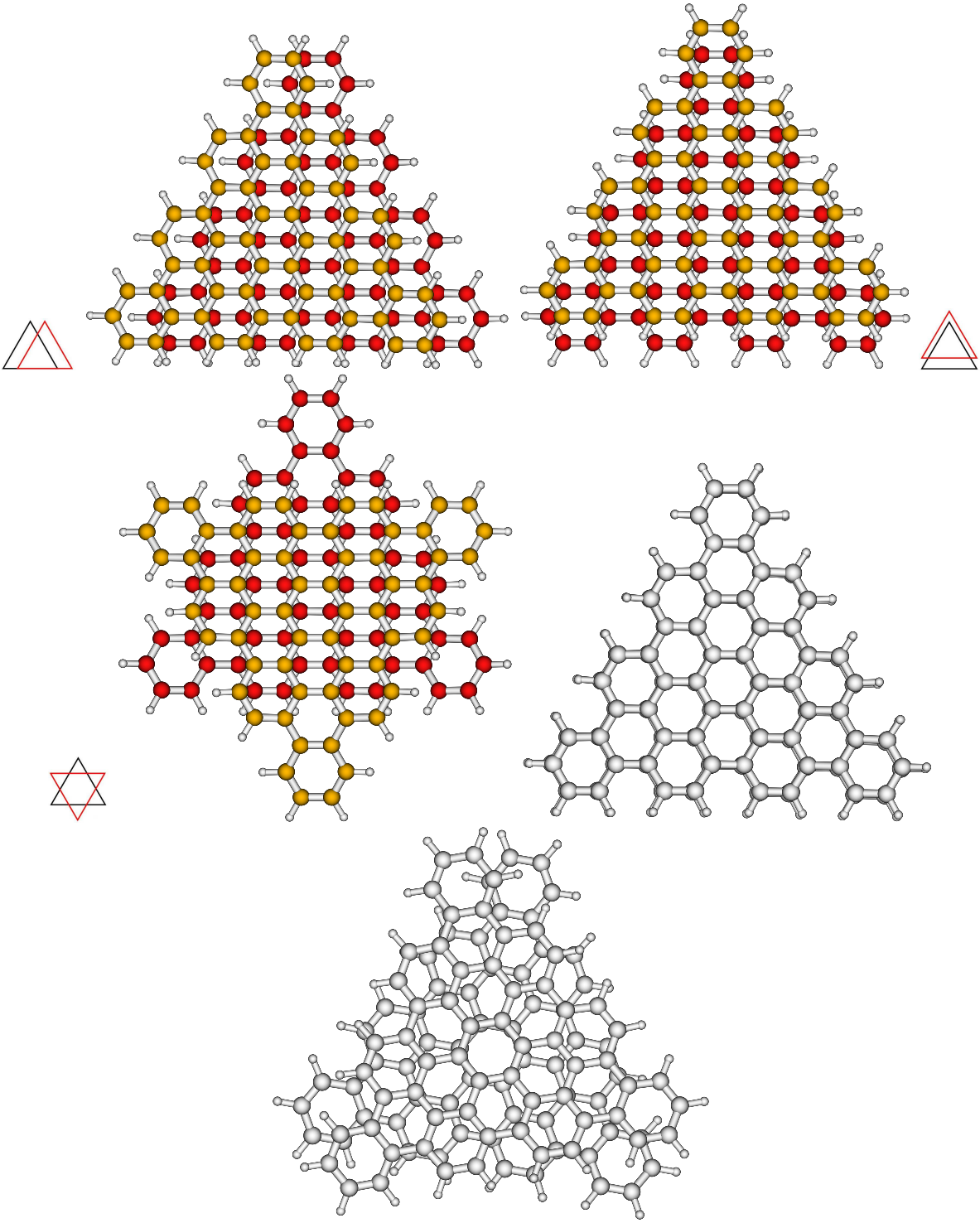

FIG. 7: B97-D/TZV(d,p) optimized structures of $C_{60}H_{24}$ dimers 4a, 4b/c, (top from left to right) 4d, (4f), (middle from left to right) and (4g) (bottom).

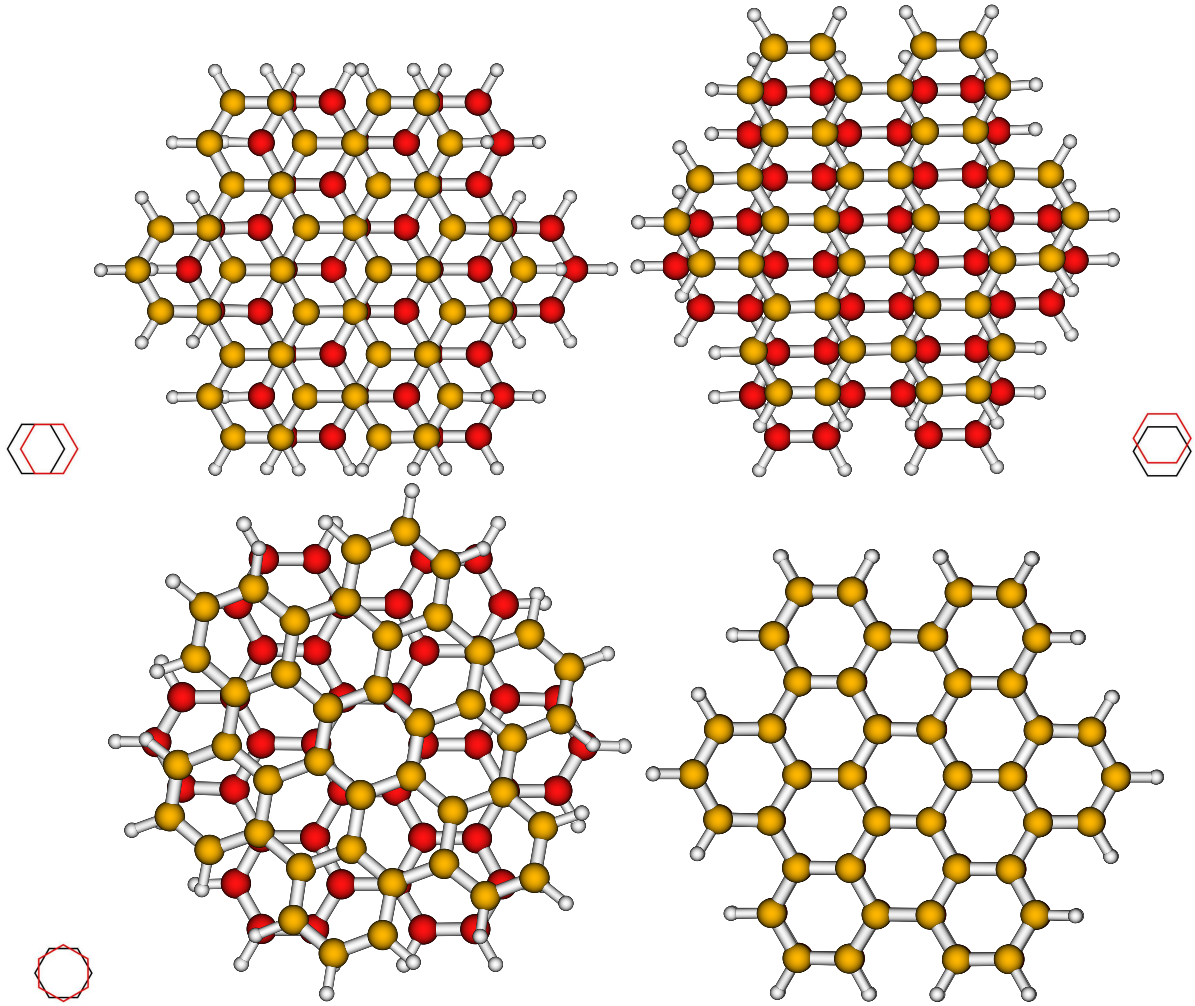

FIG. 8: B97-D/TZV(d,p) optimized structures of hexabenzo[bc,ef,hi,kl,no,qr]coronene dimers 5a, 5b/c, (top from left to right) 5d, and 5f (bottom from left to right).

The structures of three stationary hexabenzo[bc,ef,hi,kl,no,qr]coronene dimers are displayed in Fig. 8, the corresponding dissociation energies and geometrical data are given in Tab. I. The lowest energy has the parallel displaced dimer 5a, where the displacement is along two opposite edges of the hexagon. The parallel displaced dimer with the displacement perpendicular to two opposite edges of the hexagon (5b/c) has an 1.7 kcal mol^{-1} higher dissociation energy. It has almost the same energy as dimer 5d with 36 degrees rotated monomers. The fully stacked structure (5f) could only be obtained by imposing D_{3d} symmetry and has an 9 kcal mol^{-1} higher energy than the minimum energy structure. Optimization without symmetry leads to structure 5d with the monomers rotated.

The interplane distance of the two parallel displaced dimers is 332 pm, the rotated

dimer has a separation of 339 pm, and the fully stacked dimer of 359 pm. While in the latter two dimers the distortion of the monomers is larger compared to the isolated hexabenzo[bc,ef,hi,kl,no,qr]coronene, for the two parallel displaced dimers the mean distance of the carbon atoms from the rms plane is reduced. In the parallel displaced dimer 5a the monomers are displaced by 154 pm along, in the parallel displaced dimer 5b/c by 144 pm perpendicular to a C-C bond.

IV. SUMMARY AND OUTLOOK

Stacked dimers of five polyaromatic compounds have been calculated with dispersion-corrected density functional theory, resulting in a series of structures and an energetic ranking (see Fig. 9). Configurations of stacked dimers of polyaromatic hydrocarbons (PAH) are readily classified by two in-plane displacements and a relative rotation. The potential energy surface in these three coordinates is flat, so that a separation of structures into different binding modes is not straightforward. Generally, the contour of the PAH determines the shape and the size of the PAH its roughness of the potential energy. In the stacked dimer of rectangular $C_{56}H_{22}$, the HOMO-LUMO gap is sensitive to in-plane displacement of the monomers, leading to configurations with splitting below 1 mH. As the HOMO-LUMO gap of $C_{56}H_{22}$ alone is 6 mH, it remains open whether the ground state is not better described by a triplet state.

For an interpretation of the derived structures it might be useful to examine the electrostatic potential of the monomers and to perform an energy decomposition analysis (EDA) of the intermolecular interaction energies. Finally, single point energy calculations on the optimized structures at the SCS-MP2 [11] and B2-PLYP-D [12] levels with a larger basis set could validate the energetic ranking.

[1] S. Grimme, *J. Comput. Chem.*, 2006, **27**(15), 1787–1799.

[2] S. Grimme, *J. Comput. Chem.*, 2004, **25**(12), 1463–1473.

[3] S. Grimme, J. Antony, T. Schwabe, and C. Mück-Lichtenfeld, *Org. Biomol. Chem.*, 2007, **5**, 741–758.

[4] A. Schäfer, C. Huber, and R. Ahlrichs, *J. Chem. Phys.*, 1994, **100**(8), 5829–5835.

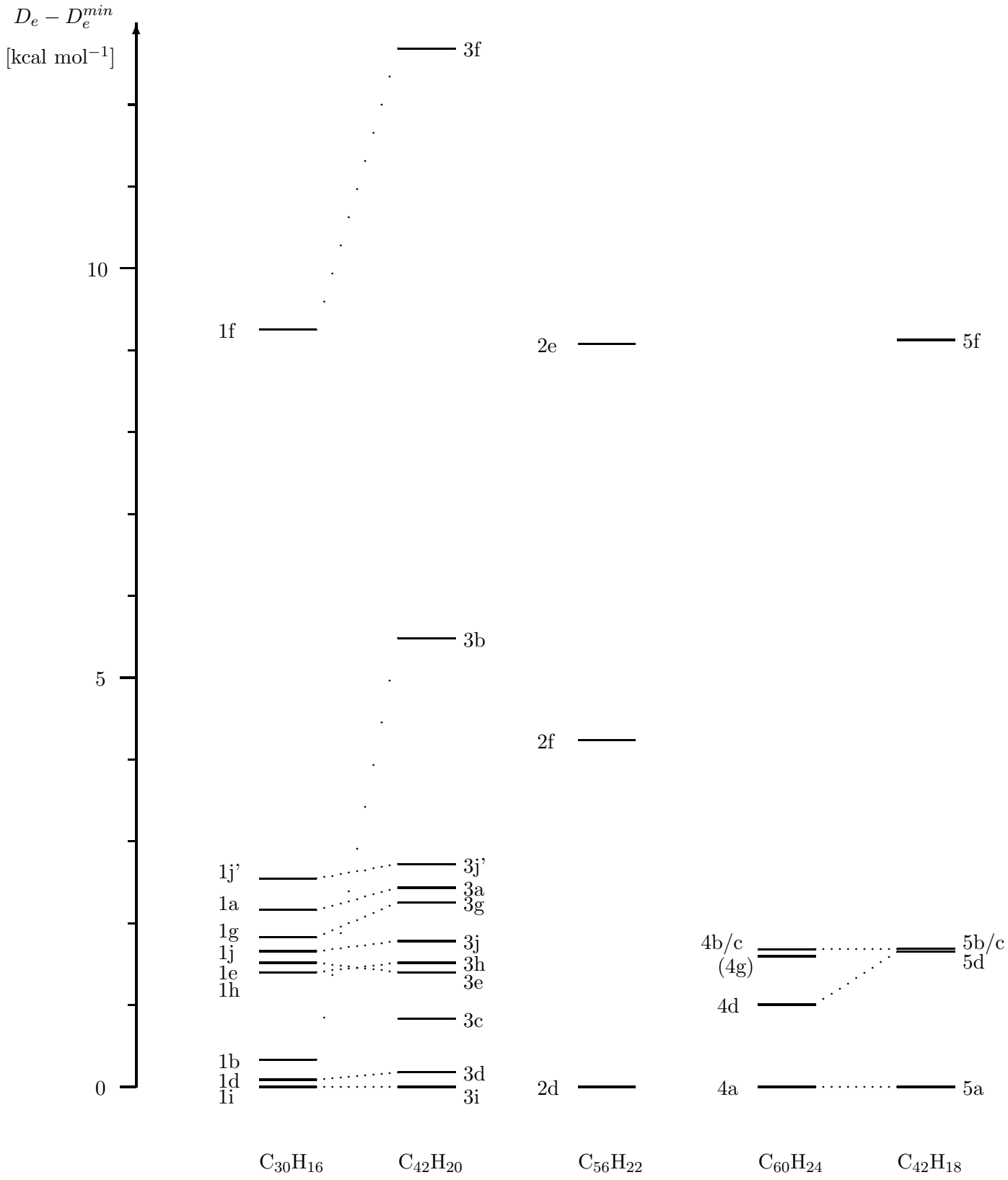

FIG. 9: Relative B97-D/TZV(d,p) dissociation energies (kcal mol^{-1}) for B97-D/TZV(d,p) energy minimized dimers of tribenzo[b,n,pqr]perylene ($C_{30}H_{16}$), $C_{42}H_{20}$, $C_{56}H_{22}$, $C_{60}H_{24}$, and hexabenzo[bc,ef,hi,kl,no,qr]coronene ($C_{42}H_{18}$).

[5] K. Eichkorn, O. Treutler, H. Öhm, M. Häser, and R. Ahlrichs, *Chem. Phys. Lett.*, 1995, **240**(4), 283–289.

[6] K. Eichkorn, O. Treutler, H. Öhm, M. Häser, and R. Ahlrichs, *Chem. Phys. Lett.*, 1995, **242**(6), 652–660.

[7] Turbomole Version 5.9 Program Package for *ab initio* Electronic Structure Calculations; http://www.cosmologic.de/QuantumChemistry/main_qChemistry.html, 2006.

[8] The basis sets are available from the Turbomole homepage via the FTP Server Button; http://www.cosmologic.de/QuantumChemistry/ftpServer.html.

[9] NIST Standard Reference Database Number 69, June 2005 Release; http://webbook.nist.gov/chemistry/.

[10] Pcmodel version 9.1; http://www.serenasoft.com/.

[11] S. Grimme, *J. Chem. Phys.*, 2003, **118**(20), 9095–9102.

[12] S. Grimme, *J. Chem. Phys.*, 2006, **124**(3), 034108.

TABLE I: B97-D/TZV(d,p) energy[a] (kcal mol^{-1}), interplanar distance (R_e), mean distance of carbon atoms from rms plane (Δz), and displacements along the long (R_1) and short (R_2) molecular axes (pm)[b] for dimers of polyaromatic compounds.

	a	b	c	d	e	f	g	h[c]	i[d]	j[e]	j'[e]
1:	Tribenzo[b,n,pqr]perylene ($C_{30}H_{16}$) Δz = 0.1 pm[f], 95 mH = 2.59 eV[g]										
D_e	–28.61	–30.44	[h]	–30.69	–29.26	–21.52[i]	–28.94	–29.37	–30.77	–29.12	–28.23
R_e	334/334	330	[h]	328	334/332	366[i]	341	331	325	333	332
Δz	5.8/2.1	4.3	[h]	6.1	8.7/8.0	2.0[i]	14.5	17.0	6.6	10.6	3.5
R_1	0/0	0		54	72/72	0	98[j]	8[k]	148	168	234
R_2	153/154	–80		–84	141/146	1	11[j]	151[k]	74	7	2
2:	$C_{56}H_{22}$ Δz = 0.3 pm[f], 6 mH = 0.17 eV[g]										
D_e	–62.38[l]		–63.20	–77.08	–68.01	–72.85[m]					
R_e	331[l]		289/292	324	321	339[m]					
Δz	2.3[l]		36.6/32.3	7.3	6.2	4.7[m]					
R_1	0		65/141	100	91	0					
R_2	140		142/51	0	211	0					
3:	$C_{42}H_{20}$ Δz = 1.4 pm[f], 78 mH = 2.13 eV[g]										
D_e	–43.03	–39.98	–44.63	–45.28	–44.06	–32.77[i]	–43.21	–43.94	–45.46	–43.68	–42.74
R_e	332/332	326	330	328	330/330	363[i]	340	329	325	333	329
Δz	8.3/5.7	12.3	6.4	6.2	7.2/4.6	2.6[i]	15.6	5.7	7.2	4.1	4.4
R_1	0/0	0	0	60	77/77	0	115[n]	90	142	157	272
R_2	150/150	–273	–58	–60	141/141	1	5[n]	165	92	0	1
4:	$C_{60}H_{24}$ Δz = 0.7 pm[f], 80 mH = 2.19 eV[g]										
D_e	–68.71		–67.03[o]		–67.71						

R_e	330	333/333^o	298	
Δz	3.2	5.2/3.6^o	21.4	
$R_1{}^p$	156	0/0	8	
$R_2{}^q$	3	140/141	124	

5: Hexabenzo[bc,ef,hi,kl,no,qr]coronene ($C_{42}H_{18}$) Δz = 12.4 pm^f, 91 mH = 2.47 eV^g

D_e	–45.66	–43.97	–44.01	–36.53^r
R_e	332	332	339	359^r
Δz	11.3	7.6	14.8	17.3^r
$R_1{}^p$	154	0	7	0
$R_2{}^q$	0	144	3	0

^{a}Energy referred to relaxed monomers ^{b}Two values given for non-equivalent monomers ^{c}1/3b with displacement along short molecular axis reversed ^{d}1/3d with displacement along short molecular axis reversed ^{e}1/3a with displacement only along long instead of short molecular axis ^{f}Mean distance of carbon atoms from rms plane ^{g}HOMO-LUMO gap ^{h}Optimization starting from a maximally overlapping 180 degrees rotated structure leads to structure 1b ^{i}Fully stacked (sandwich) structure obtained by imposing C_{2v} symmetry (optimization with C_1 symmetry leads to structure 1/3g) ^{j}Monomers rotated by 18 degrees ^{k}Monomers rotated by 173 degrees ^{l}Parallel displaced structure obtained by imposing C_{2h} symmetry (optimization with C_1 symmetry leads to structure 2d) ^{m}Fully stacked (sandwich) structure obtained by imposing D_{2h} symmetry (optimization with C_1 symmetry leads to structure 2d) ^{n}Monomers rotated by 10 degrees ^{o}Parallel displaced structure obtained by imposing C_s symmetry (optimization with C_1 symmetry leads to structure 4a) ^{p}Displacement along a C-C bond ^{q}Displacement perpendicular to a C-C bond ^{r}Fully stacked (sandwich) structure obtained by imposing D_{3d} symmetry (optimization with C_1 symmetry leads to structure 5d)

VII. CURRICULUM VITAE

Personal details

Last Name	**Schindler**
First Name	**Mauro** Kevin
Title	**M.Sc.**
Address	rue Georges – Jordil 3
Town	CH - 1700 Fribourg
Date of birth	29.02.1980
Place of origin	Röthenbach i.E. (BE)
Martial status	Married
Nationality	Swiss

Languages

German	Native tongue
French	Native tongue
English	Fluent
Luxemburgish	Fluent
Italian	Basic knowledge

Education

08.2006 – 05.2010:	PhD student, organic / analytical chemistry**, Univ. of Fribourg (CH)**
10.2001 – 06.2006:	Bachelor / Master of Science in Chemistry, **Fribourg (CH)**
08.1996 – 06.2000:	High-school, „Kollegium Heilig Kreuz“, **Fribourg (CH)**
08.1995 – 07.1996:	Secondary school „Orientierungsschule Freiburg“, **Fribourg (CH)**
08.1993 – 07.1995:	Secondary school, “Collège du Château”, **Payerne (CH)**
01.1993 – 07.1993:	Primary school, “Collège Henri Nans“, **Aups (F)**
10.1988 – 12.1992:	Primary school, “Schule an den Linden“, **Rödermark (D)**
07.1987 – 10.1988:	Primary school, “Primarschule Rain”, **Ittigen (CH)**

Internships / Professional experience

07.2009 – 05.2010:	**Airfield manager (Part time), Fribourg Regional Aerodrome**
07. – 09.2004:	**R & D, Firmenich SA, La Jonction, Geneva (CH)**, 10 weeks
07. – 10.2003:	**R & D, Ecolab & Co OHG, Düsseldorf (D)**, 3 months
01. – 10.2001:	**Debtor accountant / Assistant to the CFO, Carbagas, Gümligen (CH),** 9 months
09. – 10.2000:	**Emergency medicine assistant, Aarberg Hospital, Aarberg (CH)**, 1 month
1996 – 1999:	**R & D, Blösch AG, Grenchen (CH),** 4 x 2 months

Diplomas

06.2006: **Master of Science (M.Sc.) in chemistry, Master thesis in advanced organic synthesis. Courses in: advanced synthetic tools, analytics, polymers, advanced materials science & technology**

12.2005: **Bachelor of Science (B.Sc.) in chemistry**

10.2004: Second propaedeutic diploma, chemistry

07.2002: First propaedeutic diploma, chemistry

06.2000: High school degree in natural sciences

Present positions

- **PhD student**, organic chemistry, analytics
- **Responsible for the internal analytical service**: HPLC-MS and MS^n
- Measurement of GC/MS, HPLC-MS, MS^n and solid-state-NMR spectra for the chemical and biochemical departments as well as **external clients**
- **Teaching assistant**:
  - **Responsible** for the organization and the supervision of practical works in organic chemistry and analytical chemistry for 2^{nd} year undergraduate students in chemistry, biochemistry and pharmacy
  - **Lectures** (with **exercises**) in analytical chemistry for 2^{nd} year undergraduate students in chemistry, biochemistry and pharmacy
  - Private chemistry lessons for high-school students
  - **Supervision** of high-school students for the „Schweizer Jugend Forscht“– program

Specific knowledge

^{1}H-, ^{13}C-, ^{19}F-NMR, SS-NMR, MAS-NMR, GC/MS, HPLC, UV/VIS, fluorescence, IR/RAMAN, SEM, DSC, XRF, electrochemical methods, advanced organic synthesis, organometallic synthesis, Sonogashira- / Suzuki- / Heck- / Kumada- crosscouplings, synthesis under inert atmosphere

Computational knowledge

Windows / MacOS / WWW / Microsoft Office / Outlook / Lotus
ChemOffice / E-Notebook / HyperChem / ISIS Draw
Micrografx Picture Publisher / Macromedia Dreamweaver

Memberships

Since 2009:	Royal Society of Chemistry, Associate Member, AMRSC
Since 2008:	Of@UNIFR, Officers – Society of the University of Fribourg
Since 2007:	American Chemical Society
Since 2007:	Aero - Club Switzerland
Since 2006:	ABC – Suisse, Association of specialists for NBC prevention
Since 2006:	Swiss Officers Society
Since 2005:	Swiss Chemical Society
Since 2005:	Swiss Young Chemists Forum
Since 2005:	Choir „L'Accroche – Choeur Ensemble Vocal Fribourg"
Since 2002:	Choir of the University of Fribourg, member of the board 2003 - 2005

Hobbies

Flying (PPL, private pilot license) / motorbike / photography / badminton / swimming / music (singing, French horn) / politics / reading / cooking / travel

Army

Rank:	Specialist officer (captain), since 10.2005
Function:	NBC-prevention officer / protection & security-officer responsible for 700 men
10.2006:	Technical course for NBC – prevention officers, Spiez (CH), 3.5 weeks
2004 – 2005:	Section chief, responsible for 15 men (lance corporal)